Proceedings of The International Symposium on

"The Role of Remote Sensing for The Environmental Issues in Arid and Semi-Arid Regions"

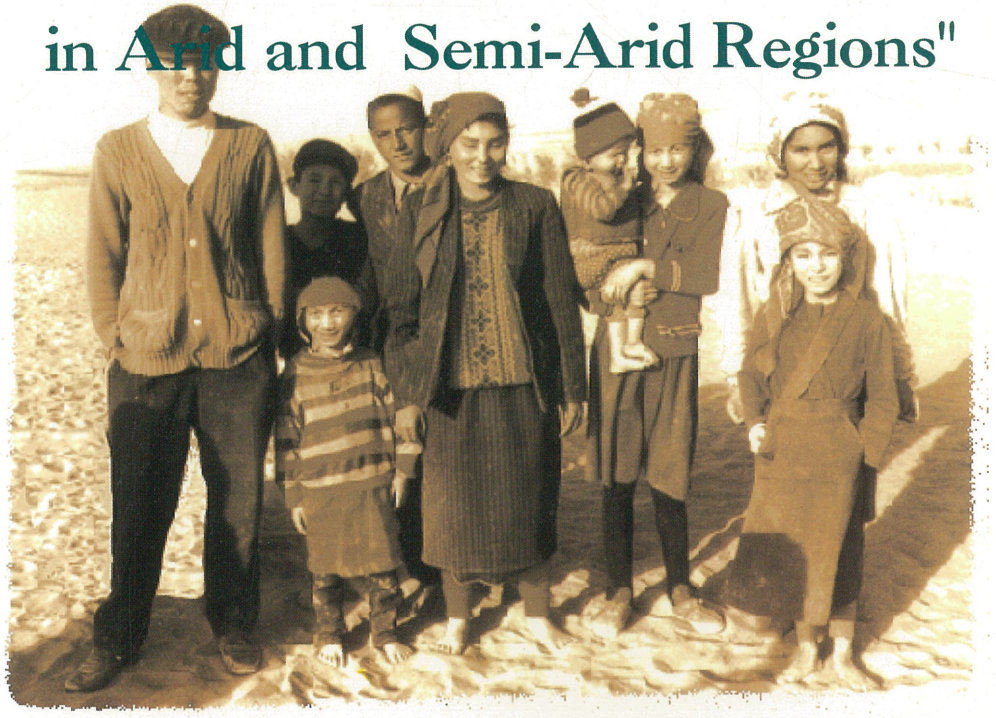

January 29-31, 1997

Center for Environmental Remote Sensing,
Chiba University, Japan

CEReS

Edited by Shizuo Shindo and Akihiko Kondoh

Published by
Center for Environmental Remote Sensing(CEReS), Chiba University
1-33 Yayoi-cho, Inage-ku, 263 Japan
Fax: +81-43-290-3857

The CEReS International Symposium on The Role of Remote Sensing for the Environmental Issues in Arid and Semi-Arid Regions

29-31 January, 1997
Chiba University

CEReS
Center for Environmental Remote Sensing
Chiba University, Japan

CONTENTS

Application of a High Spectral Resolution Vegetation Index For Estimating Percent Cover, Leaf Area Index, and Evapotranspiration in Arid Environments

Christopher D. Elvidge

Desert Research Institute, University of Nevada System on assignment at the
National Oceanic and Atmospheric Administration
National Geophysical Data Center, Solar-Terrestrial Physics Division
3100 Marine Street, Boulder, Colorado 80303 USA
Fax: 303-497-6513
Email: cde@ngdc.noaa.gov

Abstract

Airborne spectroradiometer data of arid land vegetation was acquired of three sites in the western USA. The data were used to generate values for a derivative green vegetation index (DGVI) which measures the amplitude of the chlorophyll red edge feature. DGVI values were found to be highly correlated to measures of percent cover, Leaf Area Index (LAI) and annual evapotranspiration (ET). The results indicate that high spectral resolution satellite remote sensing will be very useful for monitoring and characterizing arid land vegetation.

1. Introduction

Vegetation indices are mathematical transforms designed to assess the spectral contribution of vegetation to multispectral observations. The most widely used green vegetation indices are formed with data from discrete red and near infrared (NIR) bands. These vegetation indices operate by contrasting intense chlorophyll pigment absorptions in the red against the high reflectivity of plant materials in the NIR. The value of red versus NIR vegetation indices lies in the potential use of the vegetation index values to estimate vegetation parameters such as percent cover, transpiration rate, and Leaf Area Index.

It has been observed that variations in the spectral properties of background rock and soil materials can have adverse affects on vegetation indices, especially at low levels of vegetation cover. There are three main types of rock-soil affects on vegetation indices, listed here in their general order of prominence: 1) Albedo Affect: The brightness of the background materials can have a pronounced impact on the vegetation index values

derived using ratio based formulas (Huete et al., 1985; Elvidge and Lyon, 1985), with bright backgrounds producing lower vegetation index values and dark backgrounds producing higher vegetation index values. The albedo affect on green vegetation indices can be demonstrated through simple linear mixing of pure vegetation and rock-soil spectra (Elvidge and Lyon, 1985). 2) Red-NIR Slope Affect: Variations in the slope from red to NIR reflectance in background materials (rock, soil, litter) can produce variations in vegetation index values (Elvidge and Lyon, 1985). Most background materials have slightly higher reflectance in NIR wavelengths than in the red region. This produces a positive slope from red to NIR. However, there are considerable variations in this red to NIR slope for different background materials. And 3) Non-Linear Mixing Affect: NIR light transmitted through plant canopies can be either absorbed or reflected by substrate materials. For plant canopies with bright backgrounds there can be a measurable enhancement of the NIR light reflecting from a plant canopy with a bright background relative to a dark background (Huete et al., 1985), creating a non-linear spectral mixing situation (Roberts et al. 1993). This third affect acts in an opposite sense to the first affect, raising vegetation index values slightly for plant canopies with bright backgrounds.

In analyzing the three adverse effects of background variations on vegetation indices, we have hypothesized that a green vegetation index derived from a continuous set of narrow bands across the chlorophyll red edge feature, would be capable of reducing the first two listed adverse background effects (albedo and red to NIR slope) on vegetation index performance. It is known that the albedo affect is induced by band ratioing. By making direct measurements of the amplitude of the chlorophyll red edge without the use of band ratios, the background albedo affect can be eliminated. The red to NIR slope affect should be minimized by restricting the red to NIR wavelength range to the chlorophyll red edge and the immediately adjacent bands.

Studies by Elvidge et al. (1993) revealed that the presence of trace quantities of green vegetation (~5% green cover) can be detected in high spectral resolution data from NASA's Airborne Visible-Infrared Imaging Spectrometer (AVIRIS). These results were based on the persistence of the chlorophyll red edge feature, from 0.7 to 0.75 um, at low levels of green vegetation cover. However, these results were obtained using tree covered plots with relatively uniform soil background. Elvidge and Chen (1995) developed a high spectral resolution green vegetation index, using first to measure the amplitude of the chlorophyll red edge (Figure 1). Elvidge and Chen successfully demonstrated the superiority of the narrow band vegetation index by analyzing reflectance spectra of a plant canopy with a variety of rock-soil backgrounds. By successively removing leaf material Elvidge and Chen (1995) demonstrated that the detection limits for green vegetation with high spectral resolution observations is in the range of 3-5 % green vegetation cover. Traditional vegetation indices have difficulty confirming the presence of vegetation with less than 10-20% green cover.

In this paper we present results obtained from airborne spectra indicating the potential use of high spectral resolution observations for the estimation and temporal tracking of green cover, evapotranspiration, and leaf area index in arid environments.

2. Methods

High spectral resolution reflectance spectra were acquired over arid land sites using an Analytical Spectral Devices - Personal Spectrometer (PS-2). This instrument acquires spectra in the 0.4 to 1.0 um region with 4 nm bandpasses (full width half maxima) with 1.4 nm sampling interval. The instrument head mounted in the bottom of the aircraft fuselage and was operated from inside the cockpit. The instrument calibrated to record reflectance spectra by acquiring measurements of a white calibration panel prior to takeoff. All spectra were completed within 20-30 minutes of takeoff under clear sky conditions. Airborne spectra were acquired from an altitude of approximately 60 meters above the ground surface. At this altitude the field of view of the sensor was ~ 27 meters in diameter.

Spectra were acquired at five sites in the Goshute Valley, Nevada; eleven sites in the Owens Valley, California; and eight sites along the Colorado River south of Blythe, California. From three to five spectra were acquired at each site. Figure 2 shows the three study sites on a map outline of the western USA.

The sites flown were selected based on the availability of ground truth data on the vegetation or rates of evapotranspiration. The sites in the Goshute Valley and Blythe each had an Bowen ratio meteorological station. The airborne spectral measurements were acquired of the vegetation surrounding the Bowen ration station towers. Date from the Bowen ratio stations provide estimates of the annual evapotranspiration in mm of water. Percent cover estimates for the Goshute Valley sites were made using a point count measurements in the field along randomly oriented line transects. Leaf point counts were used to estimate LAI along permanent transects flown in the Owens Valley. Percent cover estimates for the Blythe sites were made using gridded point counts made on the aerial photographs acquired at the time of the spectral data acquisition.

The DGVI calculation was performed by integrating the first derivative values obtained from the reflectance spectra from 680 to 754 nm. The first derivative value at 650 nm was subtracted from the each of the integrated values, providing a local baseline correction.

3. Results

Figure 3 shows sample reflectance spectra obtained from the airborne measurements. DGVI values were highly correlated to vegetation cover, ET and LAI. The relationship between DGVI and vegetation cover was found to be log-linear (Figure 4), as was the relationship between DGVI and LAI (Figure 5). DGVI values were linearly related to ET (Figure 6).

4. Conclusion

A growing body of research indicates that high spectral resolution remote sensing of the chlorophyll red-edge provides significant advantage over traditional broad band remote sensing for the detection and monitoring of the low levels of green vegetation present in arid lands. While such measurements are currently restricted to airborne or field surveys, satellite remote sensing with high spectral resolution is nearly a reality. In 1997 NASA will launch the first spaceborne imaging spectrometer designed for Earth observations (LEWIS). It is anticipated that there will a proliferation of such systems in the coming decades.

5. References

Elvidge, C.D., Chen, Z., and Groeneveld, D.P. (1993) Detection of trace quantities of green vegetation in 1990 AVIRIS data. Remote Sensing of Environment, v. 44, p. 271-279.

Elvidge, C.D. and Lyon, R.J.P. (1985) Influence of rock and soil spectral variation on the assessment of green biomass. Remote Sensing of Environment, v. 17, p. 265-279.

Elvidge, C.D. and Chen, Z., 1995, Comparison of broad-band and narrow-band red and near-infrared vegetation indices. Remote Sensing of Environment, v. 54, p. 38-48.

Huete, A.R., Jackson, R.D., Post, D.F., 1985, Spectral response of a plant canopy with different soil backgrounds. Remote Sensing of Environment, v. 17, p. 37-53.

Roberts, D.S., Smith, M.O., Adams, J.B., 1993, Green vegetation, nonphotosynthetic vegetation and soils in AVIRIS data. Remote Sensing of Environment, v. 44, p. 255-269.

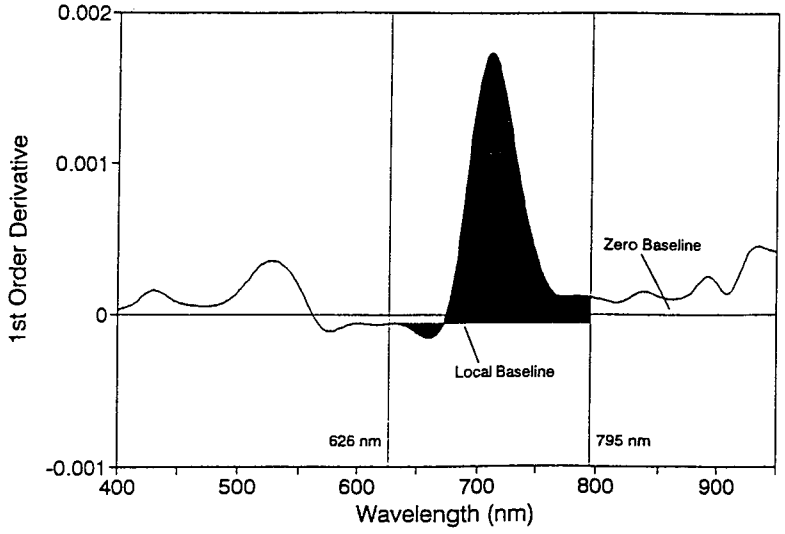

Figure 1. The Derivative Green Vegetation Index is calculated by integrating first derivative values across the chlorophyll red edge.

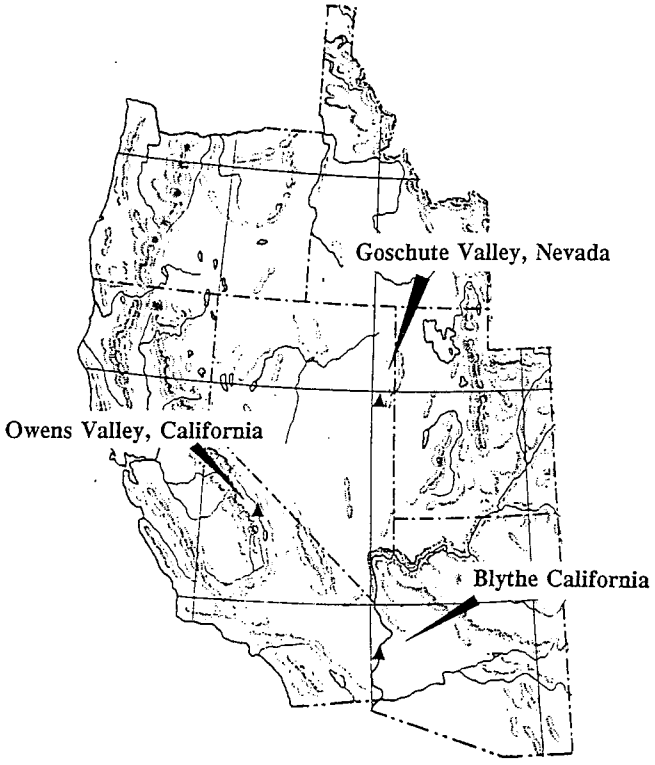

Figure 2. Sketch map of the western USA showing the three study sites.

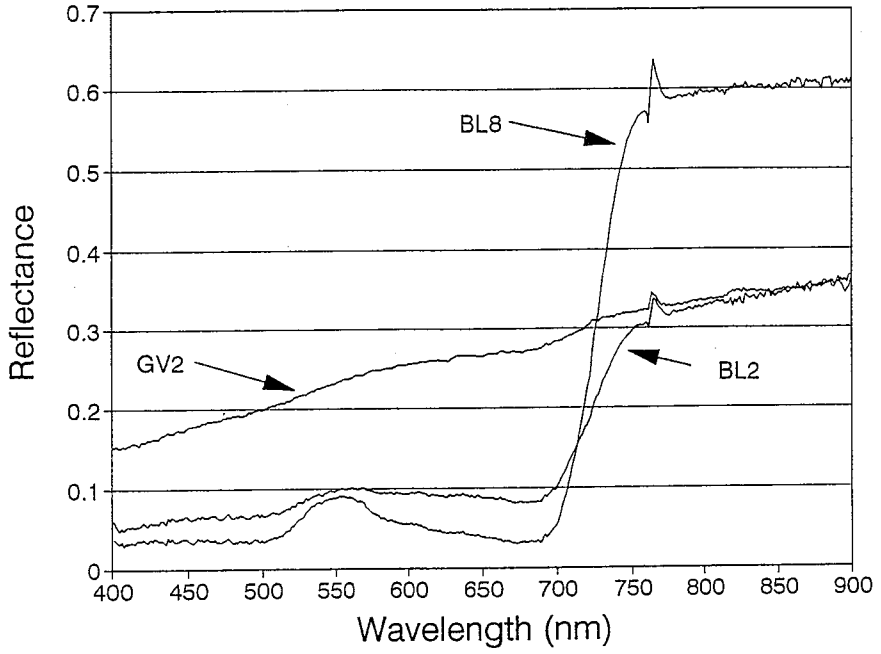

Figure 3. Sample reflectance spectra from the airborne measurements. BL8 = Uncut alfalfa crop at Blythe. BL2 = Salt cedar - mesquite area at Blythe. GV2 = Desertscrub in Goshute Valley.

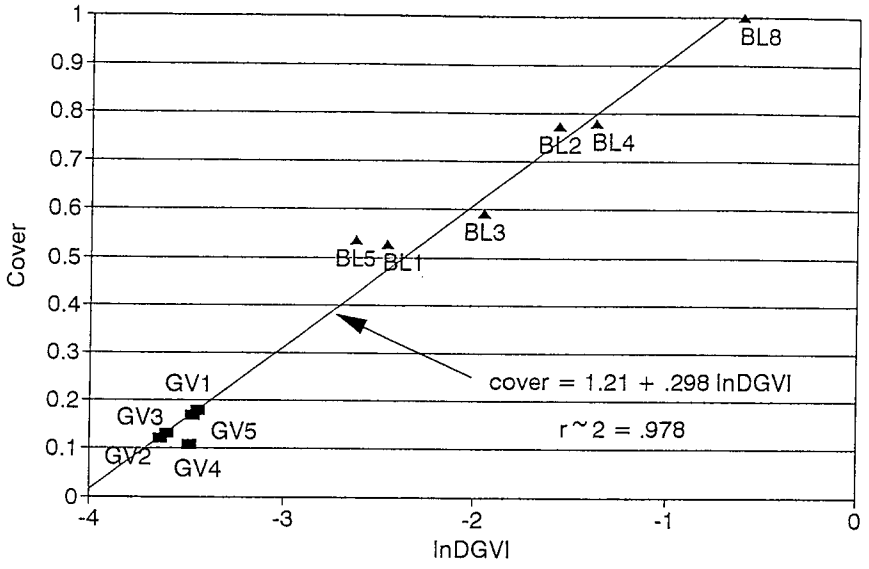

Figure 4. DGVI values versus cover for Goshute Valley and Blythe sites.

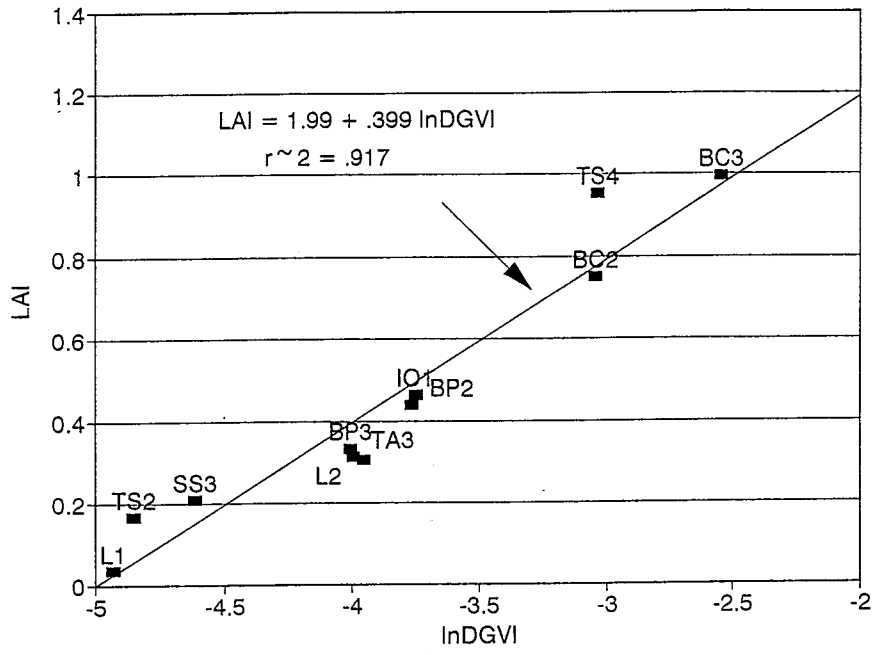

Figure 5. DGVI values versus Leaf Area Index (LAI) for eleven sites in the Owens Valley.

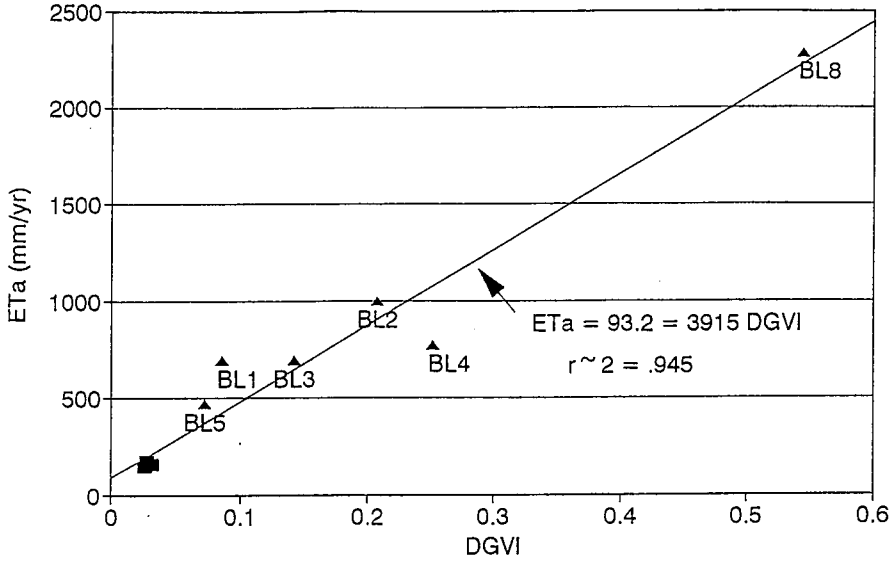

Figure 6. DGVI versus evapotranspiration (ET) for Goshute Valley and Blythe sites.

ENVIRONMENTAL MONITORING AND NATURAL RESOURCE MANAGEMENT IN INDIAN ARID REGION USING SPACE INFORMATICS

R.B. Singh

**Department of Geography, Delhi School of Economics,
University of Delhi, Delhi-110007, INDIA
Fax : 91-11-7257336 or 91-11-7257312**

ABSTRACT

The advancement of space informatic technology in India since 1980s in general and establishment of Regional Remote Sensing Research Centres of Department of Space in particular have already had a significant contribution on desert monitoring and natural resource management in Indian Arid Region. The communication revolution initiated through INSAT of satellites are now providing climatic and meteorological information over the India enabling scientists to provide more accurate weather forecasting which is very essential for disaster prone arid regions. Subsequently, the satellite remote sensing data generated by IRS-1B LISS-II and IRS-1C LISS-III series of satellites has been assisting to promote sustainable resource development strategies at the micro-levels. Such initiatives are based on continuous environmental monitoring of land and water resources including meteorological parameters using space informatic technology.

INTRODUCTION

In recent years, environmental degradation has attracted attention to policy makers at global and national levels. This has become an issue for further regional and international negotiations as it cuts across political boundaries, Recognising the integral and interdependent nature of the earth, our home, the Earth summit held at Rio in 1992 identified 27 principles on general rights and obligations for environmental protection. The rapid increase in anthropogenic activities combined with the poor management of natural resources are posing severe threat to vulnerable arid geosystem in India. Largely it is true that ecologically marginal regions of India are also economically and socially marginal. For development of such regions like arid and semi-arid areas require multi-

dimensional and integrated resource management strategies in order to promote sustainable development by ensuring livelihood security, capacity building and involvement of indigenous knowledge initiatives.

Environmental diversity in arid and semi-arid regions (Fig.1) is reflected by geographical environment, socio-economic conditions, traditional culture, population growth and poverty. Environmental degradation particularly land and water constitutes a major threat to the livelihood of millions of people in marginal areas. For tackling such complex issues, it is necessary to promote effective environmental monitoring and forecasting by making a state-of-the-art inventory of existing space informatic technology, natural resources information and data base and make them accessible to researchers willing to undertake scientific studies. It is necessary to establish Geographic Information System including remote sensing as Decision Support System for short and long term studies to improve our understanding of environmental processes (Singh, 1994)..

STATE OF ENVIRONMENTAL MONITORING IN ARID REGION

Desertification is a major problem which threatens the food supply and is a cause of human sufferings in the arid areas of India. The region is facing the severe problem and manifested in the overcultivation, overgrazing, deforestation and mismanagement of the irrigated farming. Sand dune encroachment and falling productivity of the land is a major cause of concern. Poor land use is presently crippling the ecological balance of the region. Biotic resources are severely pressurised by increasing livestock population. The biological characteristics of plants is adversely changing. The soil erosion and removal of vegetation are the two main physical characteristics of desertification. Water-table lowering is progressing at an alarming rate and farmers require deepening of wells each year. At some sites, the farmers are on the verge of abandoning the cultivation altogether. Excessive exploitation of the groundwater and poor or no replenishment year round to the aquifer, is threatening the entire local ecosystem (Singh, 1994)..

Dryland farming in the study area, inherently posses serious threat to land conservation. The plant growth, being less, varies from year to year in response to the fluctuations in the rainfall. Soil is bare and prone to wind and water erosion during five to six months each year. The choice of crop is restricted to drought-tolerant crops and the rotation of food crops with leguminous crops and vegetation is found to be uneconomic. Soil erosion is the prominent problem, being most extensive in areal coverage. Expansion of cultivated land and excessive grazing of village common lands and grazing lands are the

two main cause of soil erosion in the district. Dust storms are a common feature of summers. Consistent overgrazing and expansion of net sown area has appeared in the form of extinction of some grasses and shrubs. The land use changes that are happening play a crucial role in the aggravation of the ecological problems. Land, which was earlier left abandoned for eco-friendly purposes such as regaining the depleted nutrients and fertility, is facing tough utilization competition. Farmers are not more interested in fallow system as they require more and more land for cultivation and, therefore, take the fallow lands for perpetual cultivation. Grazing lands and pastures are also experiencing decrease in areas. It resulted into intensive exploitation of those lands. Cash crop cultivation on the expanded land demand the most intensive use. Nutrient and fertility depletion occurred immediately. Secondly, the bare surface became prone to soil erosion which again resulted into fertility depletion. Sand dunes without vegetation are reactivated by repeated human interferences in the form of cultivation and grazing. Movement of sand dunes threatens the cultivated lands as sand dunes encroach upon the surrounding fields (Fig. 2).

In recent year, environmental degradation particularly land and water problems have attained worst proportions. Out of total country soil degraded area of 187.7 mha (57.1 per cent of the geographical area), 149 mha is due to water erosion and 13.5 mha attributable to wind erosion. The area affected is being concentrated in semi-arid and arid regions which occupy 95.7 and 31.7 mha or 30 and 10 per cent of the country's area respectively (Singh and Chauhan, 1994).. In the Indira Gandhi Canal Command Area, the increasing anthropogenic activities are responsible for the massive sand drifting and deposition problem resulting in the formation of barchan dunes of 1.5 to 6.5 m height, sand ridges of 0.9 to 2.9 m height and sand sheets of 150 to 450 cm thickness on the adjoining agricultural lands and engineering structures. The rate of sand movement in these areas varies from 4 to 40 m/year and the soil loss ranges between 2525 to 3452 t/ha/year. The soil loss by water generally varies from 5 to 25 tones per ha and sand transport from one field to another in sandy desert averages between 120 to 450 tones/ha. It has been estimated that 0.16 to 1545 t/sq km soil is annually lost from the Bandi river. The accelerated water erosion has removed 0.2 to 53.5 g/1 sediments in the hilly terrain of the Aravallis and 1.0 to 453.6 g/1 in the lower reaches of the Luni river basin. The Aravallis are facing severe problems of deforestation and environmental degradation. The forest cover of in the Aravalli hill region continuously declined and reached a level as low as 6.34 per cent as per the satellite imagery of 1990-92 in the Aravalli region of Rajasthan which constitutes more than 84 per cent of the total hill part. The recent data

shows that of the 237 development blocks in the Rajasthan state, 198 are facing alarming decline of water table. Rajasthan being second state so far as the mineral deposits are concerned, it ranks fifth in the production. Illegal mining is going upto 60 per cent in some of the areas, resulting environmental degradation as those involved in illegal mining have no obligations towards EIA procedure.

According to an estimate, western Rajasthan is expected to face drought every 2.5 years. Such frequent occurrence of droughts creates environment of desertification. During 1971-72, there was an increasing trends of dust storms. Whenever rainfall falls steeply, there is a sharp rise in the occurrence of dust storms. It has a considerable significance in the soil erosion and desertification process. It also speeds up the process of their formation. The process of desertification is further accelerated by overgrazing on the pasture lands due to lack of fodder during droughts. Ministry of Agriculture of Government of India has implemented drought - prone areas programme for drought management. (Singh, 1990) (Fig. 3). Such complex environmental situations require application of space informatics for continuous natural resource monitoring in order to promote sustainable development.

SPACE INFORMATICS AS DECISION SUPPORT SYSTEM

Environmental monitoring require to analyze phenomena, processes and their interactions throughout space and time. Information has to be considered in its attribute dimension (variables), spatial dimension (spatial units of measurement), temporal dimension (dynamic process and change). Geographic Information System are offering such capabilities as they integrated attribute, spatial and temporal dimensions. Geographic Information System should be developed as a decision support system which is a system designed to support :- the analysis of decision problems,

- determination and evaluation of alternative decisions,
- selection of a particular decision (or rejection in given conditions), and
- monitoring of the execution of selected decision and suggesting corrective actions.

In general, governmental Decision Support Systems (DSS) can be easily interlinked with Geographical Information System which required access to large data bases containing data from censuses, surveys, inventories of natural resources using space informatics (Table 1 and Fig. 4). The following data base problems should be resolved :

- which data are needed for the system (electronic documents, drawings, maps),
- which data can be obtained from existing sources,
- which data bases must be created and how to collect row data,

- access to external data base (on-line, off-line),
- conversion of data in paper documents to electronic format,
- unification of data formats and access methods,
- interfaces between data bases (DBMS) and other modules of DSS,
- data verification and data integrity control.

Table 1 Principles of Decision Support System

Major Issues	Attributes
Spatial Data	- Space/Geographic Data
	- Spatial Data Sources : Conventional & Remote Sensing
	- Global Positioning System (GPS)
	- Coordinate Systems and Map Projections
Non-spatial Data	- Demographic/Census Data
	- Socio-economic data
	- Other data
Digital Representation	- Low-level Data Structures
	- High-level Data Structures
	- Data Capture
	- Database management
	- Digital Terrain Modeling
	- Three Dimensional GIS
Functional Issues	- Cartographic Modeling & Thematic Mapping
	- Spatial & Non-spatial Data Integration
	- Spatial Analysis Methods : Overlay etc.
	- Spatial Query Language (SQL)
	- GIS & Spatial DSS
	- Knowledge-based Approaches
Display Issues	- Visualization
	- Generalization of Spatial Databases
	- Object Oriented GIS
Operational Issues	- Evaluation & Implementation
	- Distributed Heterogeneous Spatial Databases
	- Spatial Data Exchange and Standardization
	- Inter-operability of Spatial & Attribute Data
	- Legal Aspects

The generic and specific characteristics of software architecture are very important for developing decisions support system which is an assembly of cooperating software modules. The components of a DSS are developed using many software technologies (RDBMS, GIS, Expert Systems, Natural Language Processing, Multimedia, etc. The major components of a DSS are : data base management, document repository manage-

ment, embedded expert systems, simulation models base and user interface modules.

NEW OPPORTUNITIES IN APPLICATION OF SPACE INFORMATICS

With launching operational remote sensing satellites IRS-1A (1988) and 1B (1991) and setting up of information systems like NNRMS, NRIS, RRSSCs and NRDMS, about 350 national/regional level remote sensing application projects (Fig. 5) have been conducted in India. The successful launch of second generation and indigenously built IRS-1C satellite on 28th December, 1995 in India has provided tremendous opportunities for applying space informatics in areas of environmental monitoring and natural resources management in arid and semi-arid regions. Browse data for PAN and LISS - III are being generated for users. The IRS-1C marks a major milestone in the India's satellite remote sensing programme by contributing to National Natural Resources Management System with better resolution, coverage and revisit in order to provide invaluable data on environmental resources. The IRS-1C surveys the whole earth surface in just 24 days. The IRS-1C satellite has three types of advanced imaging sensors. The Panchromatic Camera (PAN) provide very high spatial resolution data of 5.8 m and a ground swath of 70 km. The PAN camera can be steered to ± 26 degrees which in turn increases revisit capability to 5 days . Linear Imaging and Self Scanning (LISS-III) Sensor provides multispectral data collected in four bands. The Wide Field Sensor (WiFS) collects data in two spectral bands (Table 2). All the three cameras are operating in real time over Indian ground station visibility circle two or three times a day (NRSA, 1995)

Table 2 Characteristics of IRS-1C Sensors

Sensors	Spatial Resolution (M)	Grand Swath (Km)	Bands/Regions (Microns)
PAN	5.8	70	Visible Region 0.50 - 0.75
LISS-III			
Visible and Infra-red	23.5	141	0.52 - 0.59 0.62 - 0.68
Shortwave Infra-red	70.5	148	1.55 - 1.70
WiFS	188	810	Visible Region 0.62 - 0.86 Near Infra-red 0.77- 0.86

Space informatic technology is being increasingly used mainly to improve data acquisition, storage and presentation; enhance precision and quality; accelerate pace of

survey, interpretation and presentation of data; incorporate comparability over time and space. Local-specific action plans for sustainable development thus generated for priority watersheds/blocks (the size of about 10,000 ha) are essentially recommended for optimum management of land and water resources. The contents of the action plans to illustrate, involve identification of sites for :

- water harvesting through ponds and check dams, and soil conservation,
- afforestation, agro-forestry and agro-horticulture,
- fuelwood and fodder development,
- mining and necessary conservation measures.

CONSTRAINTS IN DEVELOPMENT OF SPACE INFORMATICS

The space informatic technology is very expensive in India. There is lack of digitized data and trained personnel. There is little GIS infrastructure at the micro-level. The GIS maps do not have large enough scale. Traditional data gathering agencies follow different systems, and do not provide digitized data. Thus, both duplication and expensive, data conversion are unavoidable. Largely GIS projects have been carried out for the project report and demonstration stage. There is a lack of an umbrella organisation which looks after related projects in holistic perspective at arid region. There is little understanding among decision makers in the management of the space informatics for government programmes.

CONCLUSIONS

The restoration of ecological balance in arid regions requires check on desert extension, intensification of desertification, degradation of natural resources such as forests, grazing lands, soil water aquifers, incidence of floods and droughts etc. There is an urgent need for regenerating arid regions particularly the Aravalli hill region by introducing Joint Forest management programme which is becoming key sustainable forest management strategy in India. Satellite photograph has facilitated mapping and distribution of dunal, inselberg and pediment areas. The geological and related environmental studies have been carried out from block and white and coloured satellite imageries. The emerging application of GIS provides further help in monitoring environmental issues and planning sustainable development strategies in arid region of India. The appropriate space informatic technology and its hardware and software requirements should be identified on the bases of experiences of several institutions. The establishment of space information database as

a multi-disciplinary project at one place involving relevant organisations in order to promote technology transfer and exchange of Arid Information System at national level is an urgent requirement. At micro-level, existing data base available at various institutions should be taken into consideration for standardization identifying key sectors like meteorological, hydrological, geographical, paleoclimatic, geological, biospheric, land uses, anthropogenic and socio-cultural aspects. Subsequently satellite and geo-spatial data of low cost as well as user friendly format should be provided to various micro-levels resource monitoring projects. High resolution satellite data and low resolution satellite data should complied and integrated in a multi-temporal data base to support regional and local projects in arid regions.

REFERENCES

National Remote Sensing Agency (NRSA), 1996 : *IRS-1C. Sensors; Interface,* Vol. 7, No. 1, Hyderabad.

Singh, R.B. , 1984, "Spatial Perspective on Population and Resource in Arid Environment : A Case Study of Western Rajasthan, Eds. H.G. Mensching and R.C. Sharma, *Resource Management in Drylands*, New Delhi, Rajesh Pub., pp. 206-214.

Singh, R.B. 1990, "Drought - Prone Areas in India : Regional Planning Issues and Resource Management Strategy", Ed. A. Kumar, *Planning Development and Disparities in Rural India*, New Delhi, Commonwealth Pub, pp. 323-342.

Singh, R.B. 1994, *Space Technology for Disaster Monitoring and Mitigation in India*, INCEDE Report No. 3, University of Tokyo, pp. 1-58.

Singh, R.B. 1994, "Desert Region in India : Resource Management Issues and Research Strategy", Eds. T. Miyazaki and A.Tsunekawa, *Towards Solving the Global Desertification Problem*, Tsukuba, Nat. Inst. for Environmnetal Studies, pp. 1-18.

Singh, R.B. and Chauhan, G.S, 1994, "Land use Pattern, Land Degradation Hazard and sustainability in the Indian Desert Region", Eds P. Singh et al. *Agroforestry Systems for Degraded Lands*, New Delhi, Oxford and IBH Pub., pp. 13-19.

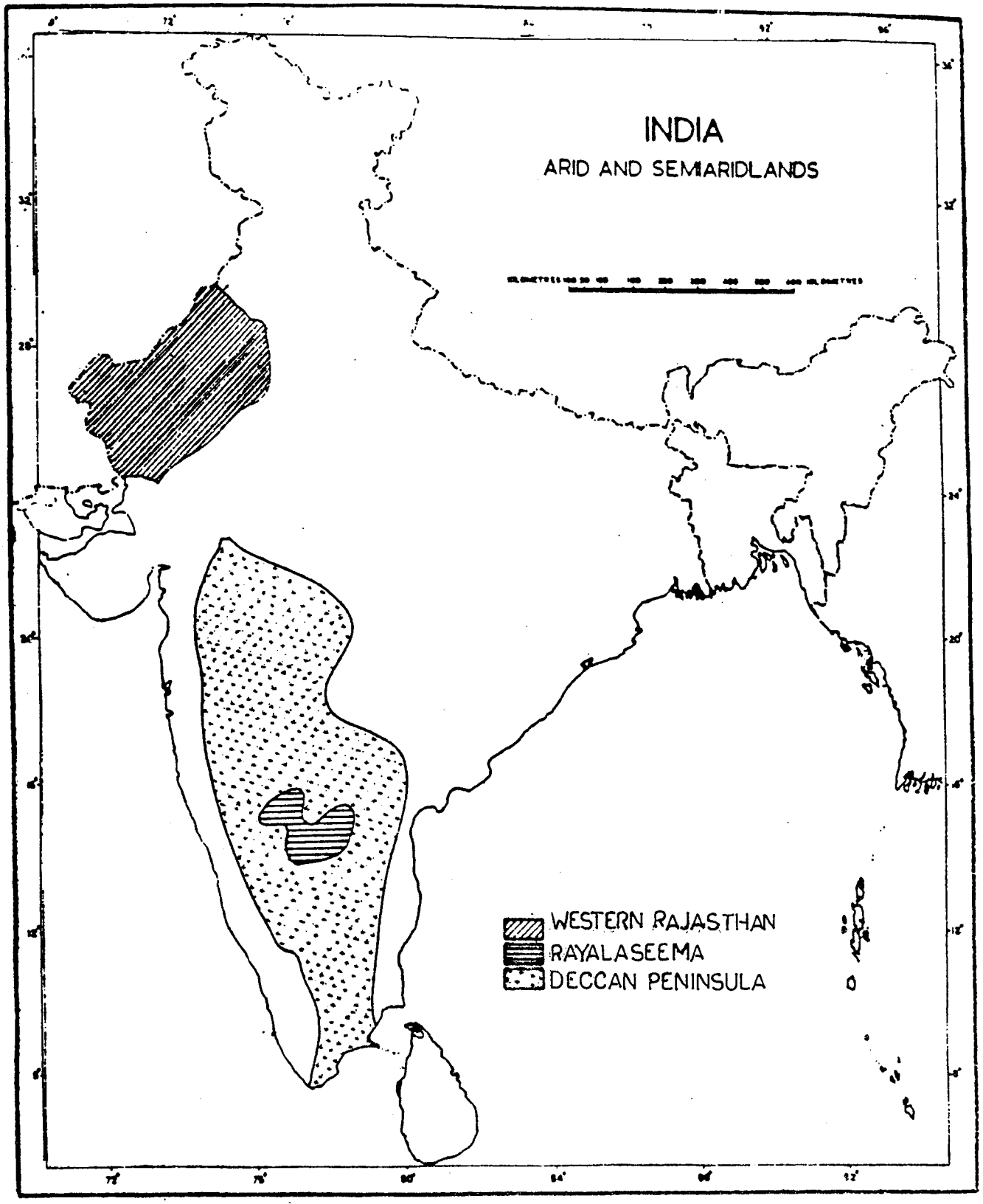
INDIA
ARID AND SEMIARIDLANDS
WESTERN RAJASTHAN
RAYALASEEMA
DECCAN PENINSULA

FIG.1

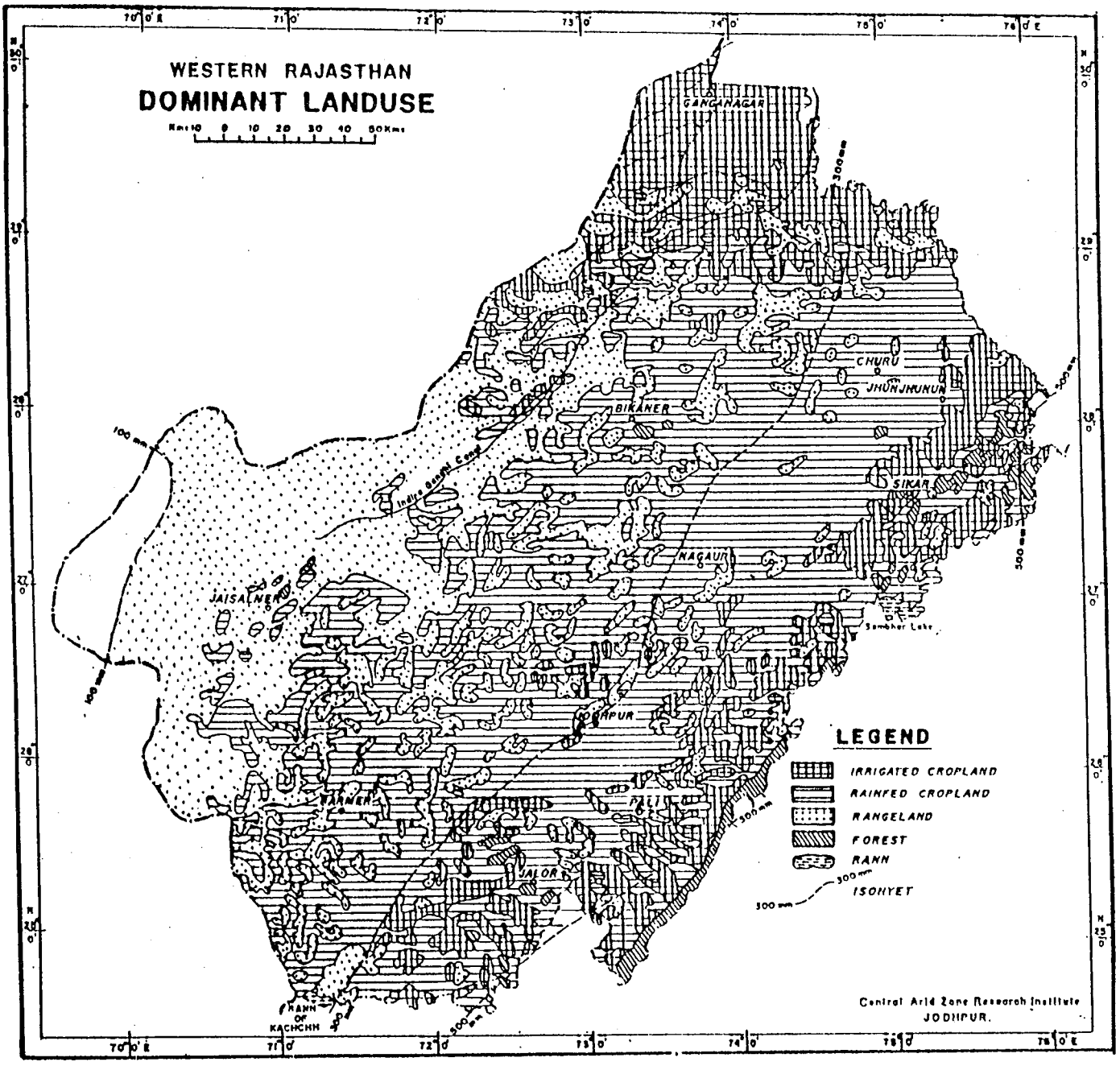
WESTERN RAJASTHAN
DOMINANT LANDUSE
GANGANAGAR
CHURU
JHUNJHUNUN
BIKANER
SIKAR
NAGAUR
JAISALMER
JODHPUR
BARMER
PALI
JALOR
RANN OF KACHCHH
LEGEND
IRRIGATED CROPLAND
RAINFED CROPLAND
RANGELAND
FOREST
RANN
ISOHYET
Central Arid Zone Research Institute
JODHPUR.

FIG. 2

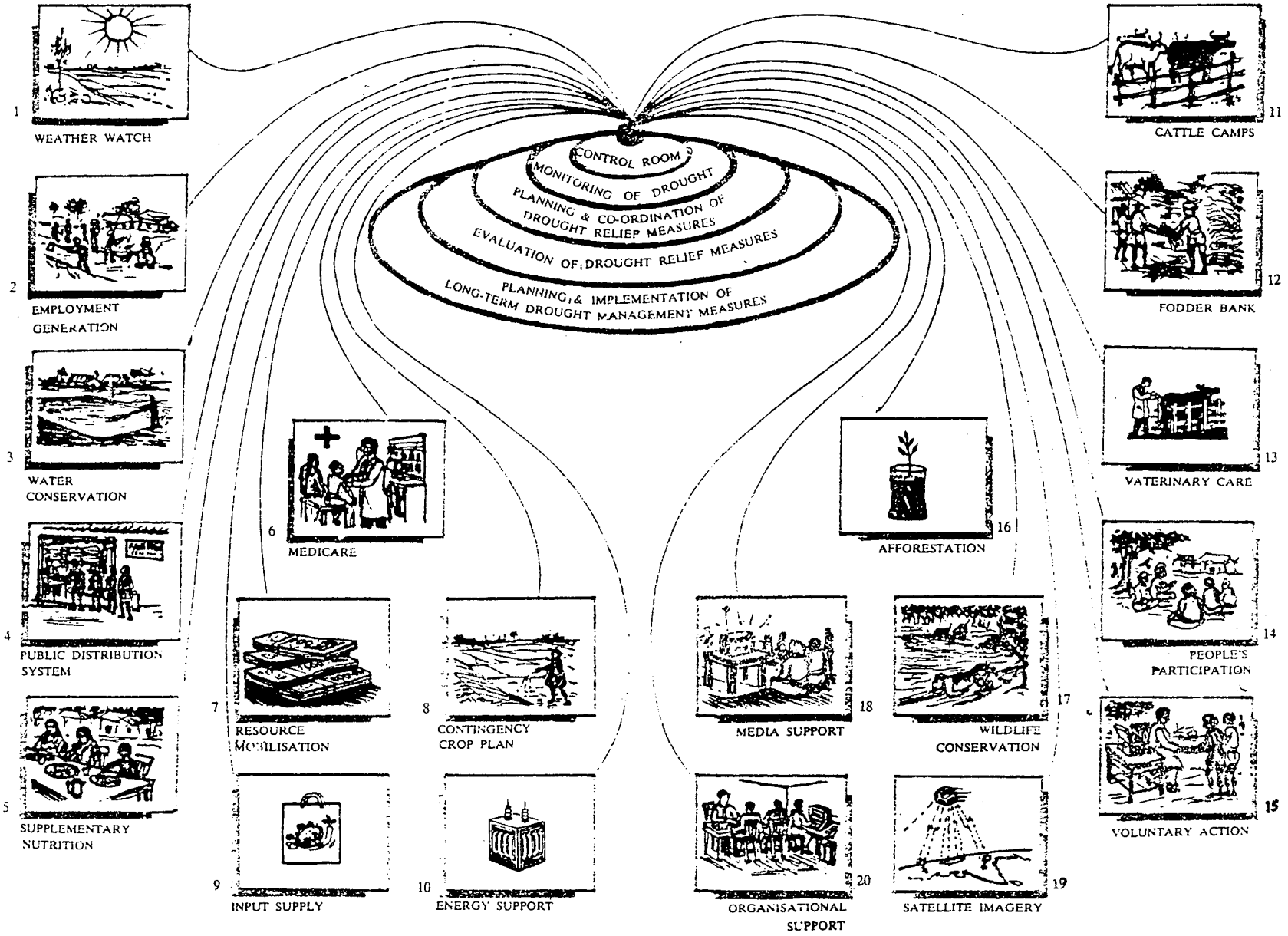

Figure 3 : A Conceptual Model of Drought Management

INFORMATION PROCESSING STEPS

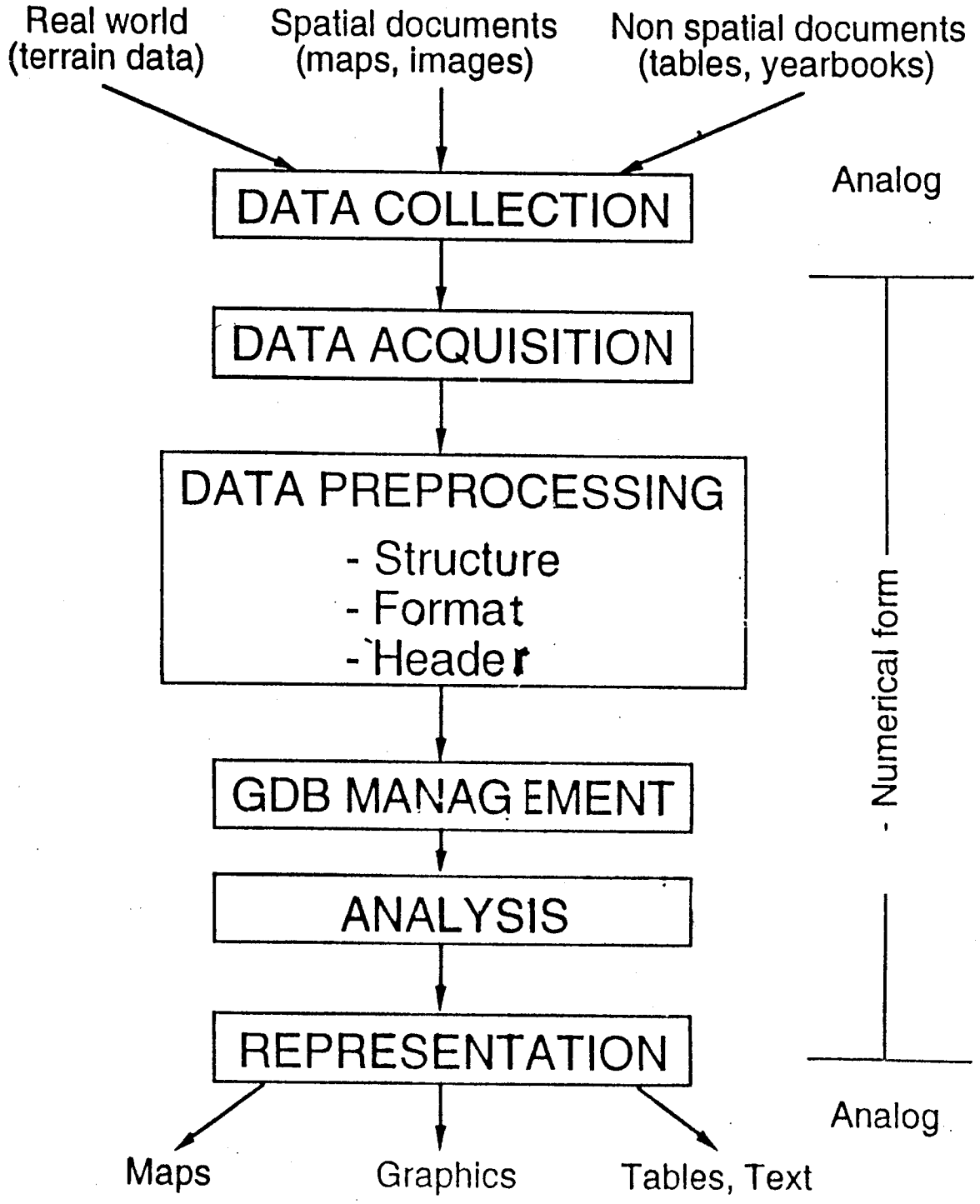

FIG.4

FLOW CHART SHOWING METHODOLOGY FOR MAPPING LAND USE/LAND COVER THROUGH VISUAL INTERPRETATION TECHNIQUES

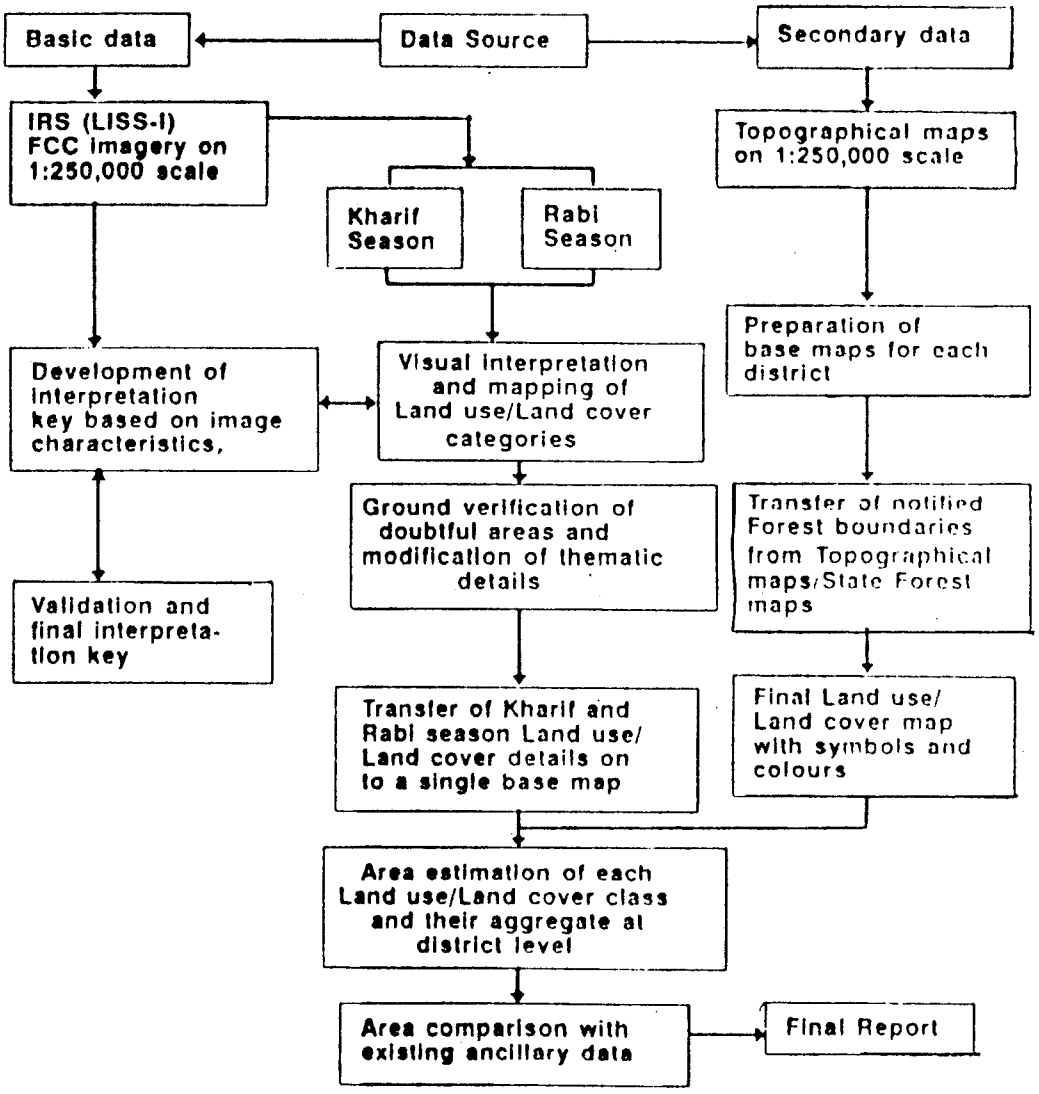

FIGURE 5

USE OF REMOTE SENSING FOR ASSESSMENT AND MAPPING DESERTIFICATION ON A REGIONAL LEVEL

Nikolai Kharin
Centre on Problems of Ecology and Forest Productivity
Russian Academy of Science
Moscow, Russia

Abstract

Desertification maps on their scales are divided into four classes : large scale (1 : 100,000 and larger), medium scale (1 :250,000-1 : 500,000), small scale (1 : 1,000,000-1:2,500,000), very smallscale (1:5,000,000 and smaller).

Desertification maps contain information on types of land degradation, desertification classes, desertification aspects and other criteria dealing with assessment of land degradation. A set of desertification criteria has been developed on the basis of regional approach for Central Asia. They include quantitative data on biological producrtivity, wind and water erosion, soil salinization, human pressure on environment etc.

Methodology of mapping includes field study, photo interpritation of aerial and space photos, reconnaissance from helicopter and literature survey. Combination of these methods depends upon map scale and general specification of project.

Methodology was tested in Central Asia, Mongolia, Libya and Mali.

Key words : Desertification, Vegetation, Erosion,Land use/cover, Photo interpretation.

USE OF REMOTE SENSING FOR ASSESSMENT AND MAPPING DESERTIFICATION ON A REGIONAL LEVEL

Nikolai Kharin

UN Convention to Combat Desertification (CCD) considers desertication as a process of global dimension (United Nartions Convention, 1994). More than 100 countries of the world with population of 250 million are affected by desertification. CCD promotes several new approaches in desertification control. Creation of a system of desertification monitoring at

national,regional and global levels is a part of these activities. Use of new technologies, in particular remote sensing and GIS could provide politicians, decision makers and planners with operative information on desertification status within countries and regions.

Our practical experience includes use of remote sensing for thematic mapping in Central Asia, Mongolia, Libya and Mali (N.G.Kharin et al.,1991, N.G.Kharin,1991, N.G.Kharin et al.,1994).

Various concepts and methodologies are used for assessment and mapping desertification. Desertification maps (maps of land degradation) can be compiled at different scales (large, medium, small and very small).Criteria for the assessment of desertification coud be regional, subregional, national and local. Above that, in different regions desertification process has its own features depending on physical environment and socio - economic conditions. Is it possible to develop a standard methodology for the assessment and mapping desertification ?

Our practical activity on desertification mapping testifies to the possibility of realization of this idea on a regional level.

Classification of desertification maps.The main types of land degradation are the following : degradation of the vegetative cover, wind and water erosion, salinization of irrigated farmlands, soil crusting and compaction, technogenic desertification, zoogenic desertification. In Central Asia to them belong :waterlogging of desert rangelands and soil salinization due to drop of the Aral Sea level.

Maps of land degradation are divided into four classes depending upon their scales :

- large scale maps (1 : 100 000 and larger)
- medium scale maps (1 : 250 000 - 1 : 500 000)
- small scale maps (1 : 1000 000 - 1 : 2500 000)
- very small scale maps (1: 5000 000 and smaller)

Zero level of assessment. Different scales of rating can be used by the assessment of desertification :

Table 1

Possible scales of assessment

Without changes	Slight	Moderate	Severe	Very severe
Zero level	Slight	Moderate	Severe	
	Slight	Moderate	Severe	

Five point rating is used when a zero level is unknown and a status of desert environment at definite time is taken as a zero level. Four point rating is used when a zero level is known. The three point rating could be used when relable data on a zero level are absent,the map scale is very small and the territory to be mapped is very large.

Desertification criteria. A set of criteria was used by the assessment of desertification conducted by the author in Central Asia These criteria could be used as a basis for further development of the assessment methods in desertification study in other countries of Asia.

Table 2

Criteria for the assessment of desertification

Scales			
Large	Medium	Small	Very small
Degradation of the vegetative cover			
Change of species composition, plant cover,loss of biological productivity in absolute figures	Change of dominants and subdominants,plant cover, loss of biological productivity in absolute figures	Change of dominants,dynamics of plant communities,plant cover, loss of biological productivities,%	Dynamics of plant cover, loss of biological productivity,%, per cent of nude soil
Wind erosion			
Sod cover,%, ratio of shrub and herb cover, area covered with barkhans and deflation hollows, volume of soil blown out, MT/year	Per cent of area covered with moving sands, per cent of area covered with vegetation, volume of soil blown out, MT/year	Per cent of area covered with moving sands, per cent of area covered with vegetation	Per cent of area covered with moving sands
Water erosion			
Type of erosion,number of gullies per 1 lin km,loss of top soil, cm, depth of gullies	Type of erosion, loss of top soil, %, per cent of area covered with gullies, vegetative cover,%	Type of erosion,per cent of eroded area, vegetative cover,%	Type of erosion, per cent of eroded area

Salinization of irrigared farmlands

Type of salinization,dense residue, g/l, toxic salt content,location of salt layers in soil profile, new soil formations,loss of yield of agricultural crops MT/ha, seasonal salt accumulation MT/ha	Type of salinization,dense residue g/l, toxic salt content, loss of yield of agricultural crops MT/ha,	Type of salinazation, dense residue g/l, loss of yield of agricultural crops, %	Type of salinization,loss of yield of agricultural crops,%

Methodology of mapping could vary dipending on the map scale. Sources of information are given in table 3. Panchromatic photos were used by desertification study in Central Asian deserts because of the higher optical contrast of landscape features in the visible spectral band. Faulse colour and infrared films gave better results by interpretation of cultural landscapes and vegetation of river vallies. NDVI was used by desertification study in Mali.

Table 3

Map scales	Sources of information						
	Field survey	Selected field work	Aerial photos	Space photos	Thematic maps	Literature	Reconnaisance from helicopter
Large	+		+				
Medium		+	+	+	+		+
Small		+		+	+	+	+
Very small				+	+	+	+

Desertification monitoring. Decision makers and managers need information on dryland status in each country. The transfer of information from sectorial sources to decision makers is a continuing ongoing process. The problem can be solved by application of remote sensing and other modern technologies.

To realize this idea a Desertification Monitoring Network (DMN) should be established. Countries signed the CCD will set up National Monitoring Centres (NMC). For example, National Action Programme to Combat Desertification in Turkmenistan (1996) envisages setting up NMC which will be responsible for collection, processing and distribution of information about land degradation.Remote sensing will play an important role in activity of NMC. Desertification maps will be compiled annually on the basis of low resolution imagery. High resolu tion space photos will also be used for mapping selective key areas.

DMC will function if a standard methodology is developed. The main guidelines of this methodology should include :

- Criteria of assessment
- Standard scele of maps
- Standard format and content of reports
- Standard data sets
- Standard hardware and softawre
- Standard format of database.

A methodology proposed by N.G. Kharin et al (1990) could be used as a basis for setting up NMC in countries of Asia.These NMCs will function in the frame of joint DMN.

BIBLIOGRAPHY

1. Kharin N.G. et al. Arid centre on collection and processing of remote sensing information. Concept, hardware and software. Desert Research Inst., Ashkhabad,1990.112 p. (In Russian)
2. Kharin N.G. Gobi and the man. Ylym Publ.,Ashkhabad,1991.100 p. (In Russian).
3. Kharin et al.Methodologie par l'evaluation et cartographie dela desertification au Sahel. Noosphere Publ., Ashkhabad, 1991.60 p.
4. Kharin et al. Map of human induced land degradation in the Aral Sea basin. Desertification Control Bulletin, 1994, N 23, p. 24 - 28.
5. National Action Programme to Combat Desertification in Turkmenistan. Desert Research Institute/UNEP,Ashkhabad,1996.106 p.
6. United Nations Convention to Combat Desertification in Those Countries Experiencing Serious Drought and/or Desertification, Particularly in Africa.UNEP,1994. 71 p. Kharin.

Testing of Instant Aero Survey

Yoshiaki Honda, Koji Kajiwara
CEReS, Chiba University
1-33 Yayoi-cho, Inage-ku, Chiba, 263 JAPAN
E-mail : yhonda@rsir.cr.chiba-u.ac.jp
FAX : +81-43-290-3857

ABSTRACT

When physical value is calculated from satellite data, it is very important to make a comparison between satellite data and ground truth data. Therefore, ground truth data is quite important. Many spectral data are collected using spectral meters on the ground level. But some parts of ground are very difficult to take spectral information of their surfaces. For example, Forest, wetland and agricultural land are difficult to take spectral information.

Instant Aero Surveying system with spectral meter has been developed to make spectral information of forest, wetland and agricultural land. A remote control helicopter was applied to this system.

1. System

We integrated with a remote control helicopter, spectral meter, micro-computer, GPS receiver, CCD camera and. The integrated system is shown in Figure 1. Remote helicopter was made by Organ needle co. Its payload is 11kg in ground height. When it is used over 1500m, its payload is 6kg due to low air pressure. The weight of our observing system is less than 6kg. Therefore, our system is available even over 1800m, high land area.

Our spectral meter has 2 channels. One channel is for sample observing. Another one is for white reference. Reflectance ratio is always calculated from these 2 values. It is not necessary to take a white reference measurement by sample channel during observing. This characteristic is very important to develop this system. If it is needed to make a white reference measurement by sample channel, it is impossible to make less than 6 kg and short observing time a observing module.

This system can collect reflectance data, image and GPS positioning data on the same time (each 1 second). All data except image data is collected in micro computer. This computer has 40 MB flash memory. Remote control helicopter can fly for 20 minutes. It is flying over 100 - 150m height from operator. Its ability is more high flight. But 150m is limitation of operator's eye.

This system can give us 30 - 50m accuracy of position. It is good enough for NOAA AVHRR data analysis. For more high resolution data (LANDSAT, SPOT ADEOS etc.), high accuracy positioning data is needed. In the near future, we will apply DGPS mode to positioning. In that case, accuracy of positioning is less than 3 m.

2. Test in field

This system was tested in Nagano pref. and Mongolia. Mongolia is almost high land area over 1400m. We had 5 flights in Mongolia. 1st flight is over slight dense grassland area. Figure 2 shows landscape of 1st test flight. 2-3 flights are over slight dense grassland with low trees. Figure 3 shows landscape of 2-3 test flight area. 4-5 flights are over middle dense grassland. Figure 4 shows landscape of 4-5 flights area.

When spectral data is detected from 1 - 2 m height, 1st test area is too low dense vegetation. 2-3 test area has low trees. Therefore, 1 - 2 m height measurement can not cover wide view of spectral meter. It is impossible to collect average information from such land cover.

Our system can collect average spectral data from such land cover areas. Because view area can be controlled by remote control helicopter flight height. If skillful operator control a helicopter, helicopter flight is very stable. Figure 5 shows result of spectral data of 2nd flight.

3. Conclusion

This system can take spectral information of canopy of forest, surface of water, wetland, agricultural land. The cost of ordinal aero experiment is too expensive. Therefore such measurement can not be standard information of ground truth. Much standard ground truth information is needed to process satellite data for physical values. This system is invaluable.

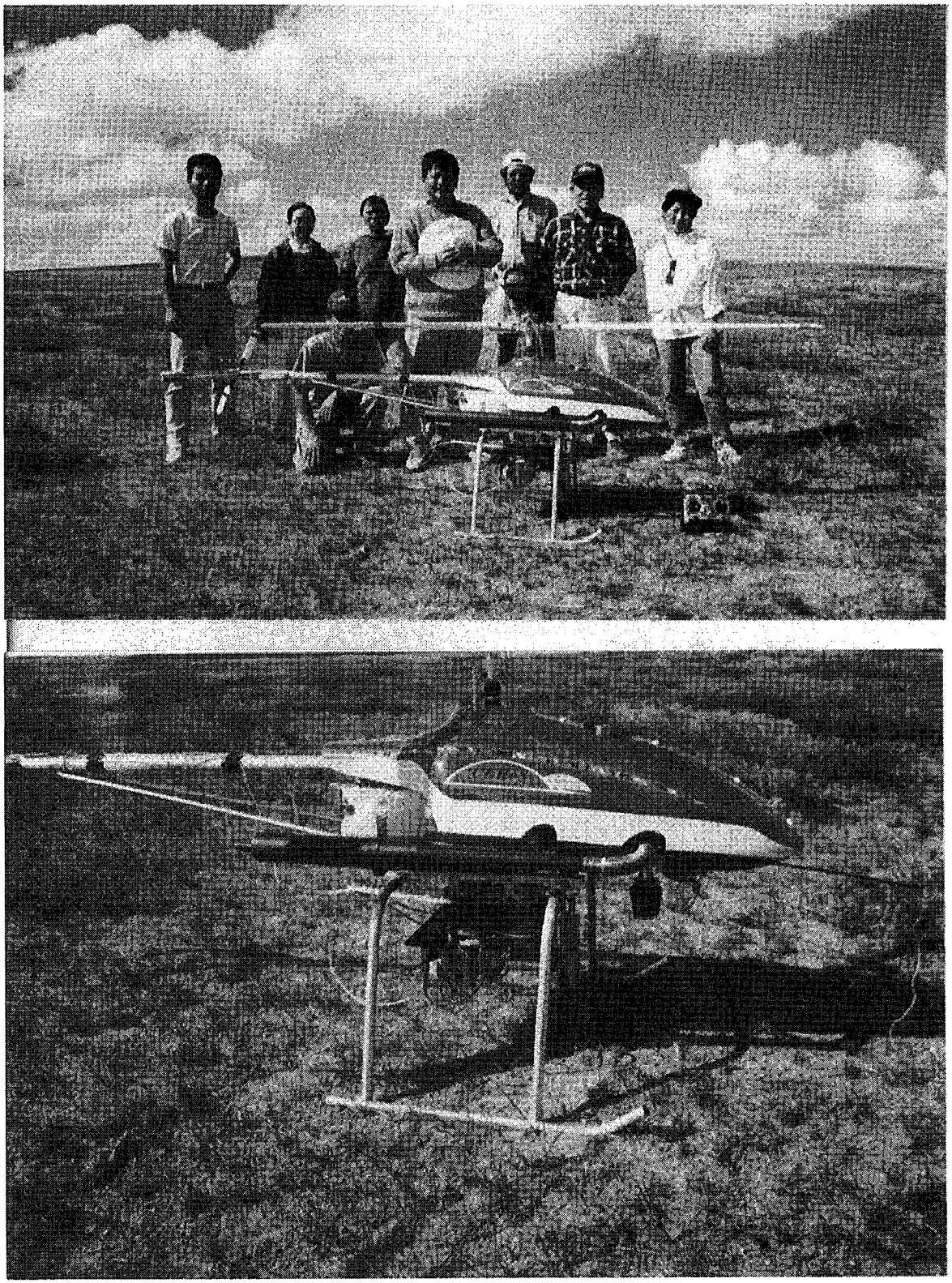

Figure 1 Integrated system

Figure 2 Landscape 1

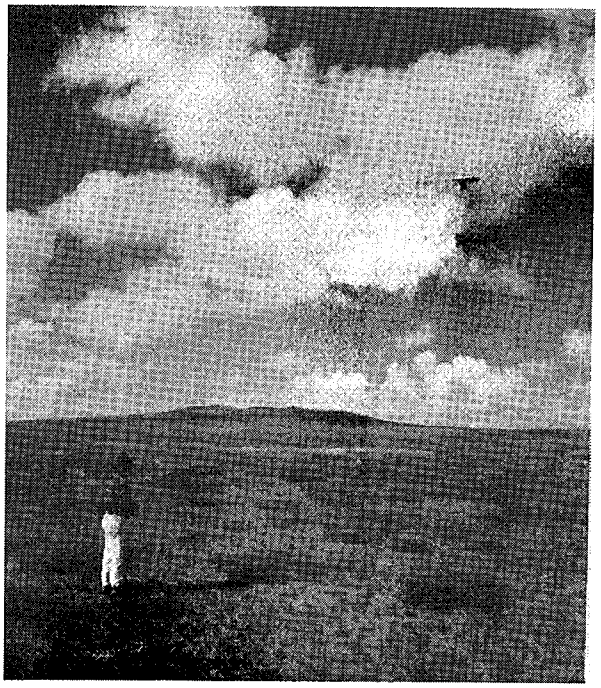

Figure 3 Landscape 2-3

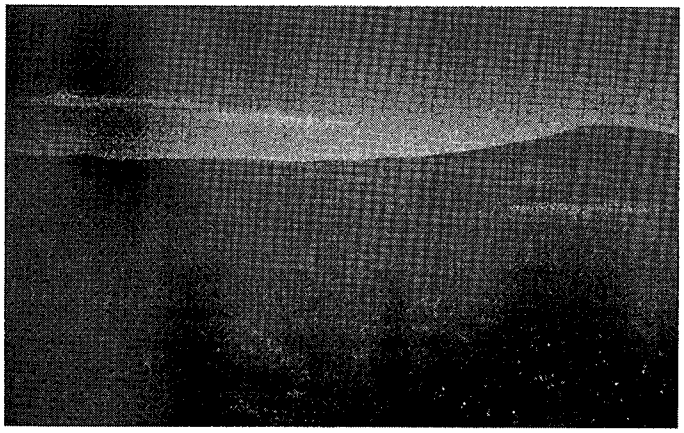

Figure 4 Landscape 4-5

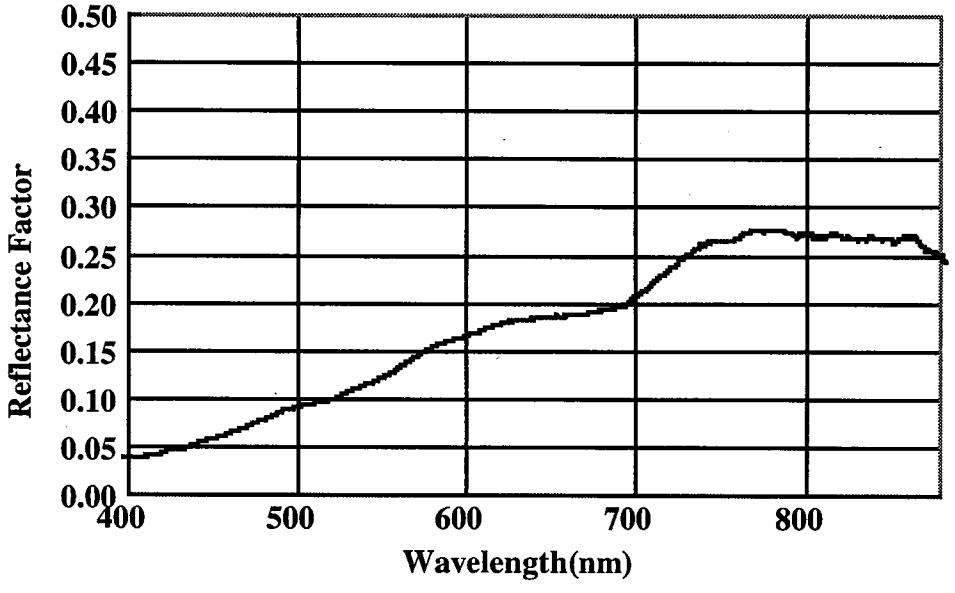

Figure 5 Reflectance

Review of Wildfire Observations in Mongolia During April and May of 1996 With Data From the DMSP Operational Linescan System

Christopher D. Elvidge*

Desert Research Institute, University of Nevada System on assignment at the
National Oceanic and Atmospheric Administration
National Geophysical Data Center, Solar-Terrestrial Physics Division
3100 Marine Street, Boulder, Colorado, 80303 USA
Fax: 303-497-6513
Email: cde@ngdc.noaa.gov

Abstract

A review of the nighttime fires of Mongolia observable with the Defense Meteorological Satellite Program (DMSP) Operational Linescan System (OLS) reveals major fires in the north-central, northeast and far eastern sections of the country started occurred intermittently from mid-April to mid-May, 1996. Time period with the most extensive sets of fires observable with DMSP-OLS data include April 12-14, 20, 22, 26-28 and May 13, 20-21.

1. Introduction

In reviewing the literature, the earliest report describing the observation of fire using a satellite sensor acquiring daily - global earth observations occurred when Croft (1973) described observing fires at night in Africa using "photographs" generated from the Defense Meteorological Satellite Program (DMSP) Operational Linescan System (OLS) visible band data. Croft (1978) was later able to use digital OLS data to observe fires, city lights and gas flares. The first systematic inventory of fires with OLS data was accomplished by Cahoon et al. (1992) who manually digitized fire points from film produced from nighttime OLS orbits over Africa. More recently algorithms for the detection of fires using digital OLS data have been developed (Elvidge et al., 1996a). In this paper we review a set of fire observations made in Mongolia during the devastating fire season of April and May of 1996.

2. The DMSP Operational Linescan System

The DMSP maintains a constellation of two satellites in sun-synchronous, near-polar orbit at altitudes of approximately 833 km, an inclination of 98.8 degrees, and an orbital period of 102 minutes. One satellite is in a dawn - dusk orbit, the second in a day - night orbit. The DMSP platforms are three axis stabilized, with roll, pitch, and yaw variations kept to within +/- 0.01 degrees. This stability is unique compared to other polar orbiting systems such as Landsat or the NOAA Polar Orbiting Environmental Satellites.

The NOAA National Geophysical Data Center (NGDC) serves as DoD's archive of data for the DMSP sensors. The U.S. Air Force Global Weather Central has sends DMSP data tapes to NGDC daily. The DMSP archive was established in March of 1992, and began receiving data on a daily basis in September of 1992 and has operated continuously since that time.

The Operational Linescan System (OLS) is an oscillating scan radiometer designed for cloud imaging with two spectral bands (VIS and TIR) and a swath of 3000 km. There are two spatial resolution modes in which data can be acquired. The full resolution data, having nominal spatial resolution of 0.56 km, is referred to as "fine". On board averaging of five by five blocks of fine data produces "smooth" data with a nominal spatial resolution of 2.7 km. Most of the data received by NOAA-NGDC is in the smooth spatial resolution mode. The "VIS" bandpass straddles the visible and near-infrared (VNIR) portion of the spectrum with a full-width-half-maximum (FWHM) of 0.58 - 0.91 um. The TIR band has a FWHM of 10.3 - 12.9 um. NGDC OLS geolocation accuracy for the OLS data is +/- one pixel using physically based orbital mechanics and terrain correction algorithms.

The identification of fires in OLS data relies on detecting areas of active visible and near infrared emission on the planet surface at night, when solar illumination is absent. The VIS band signal is intensified at night using a photomultiplier tube (PMT), making it possible to detect faint VNIR emission sources Elvidge, 1996b). The PMT system was implemented to facilitate the detection of clouds at night using moonlight. With sunlight eliminated, the light intensification results in a unique data set in which city lights, gas flares, and fires can be observed. Because of the long wavelength of the OLS's thermal band, the VIS band is far superior for the detection of fires.

3. Mongolian Fire Observations

Nighttime DMSP-OLS visible band imager of Mongolia acquired with data from satellite F-12 was visually inspected for evidence of fires. This data is summarized in Table 1. Because of the high latitude and width of Mongolia, the country was generally obse /able on two OLS orbits, with the earlier orbit covering eastern and central Mongolia and the later orbit covering western and central Mongolia. As the date of image acquisition approached the summer solstice, the data are increasingly contaminated by sunlight, particularly west of nadir. Observations were not possible on all dates due to missing data.

TABLE 1

Fires of Mongolia Observed With DMSP-OLS Data In 1996
Time = GMT, North = N, East = E, West = W, Central = C

Date		Time	Comment	Time	Comment
April	1	1225	missing data	1407	missing data
	2	1213	quiet	1355	quiet
	3	1201	quiet	1343	quiet
	4	1149	fires NE	1331	missing data
	5	1136	missing data	1318	missing data
	6	1124	quiet	1306	missing data
	7	1254	fire NE	1436	quiet W
	8	1242	fire NE	1424	quiet W
	9	1230	fire NE	1412	fire NE
	10	1218	fire NE	1400	fire NE
	11	1206	fire NE	1348	fire NE and NC
	12	1335	many fires NE and NC		
	13	1323	many fires NE and NC		
	14	1311	many fires NE and NC		
	15	1259	missing data		
	16	1247	fires NC	1429	fires NC
	17	1235	fires NC	1417	fires NC
	18	1222	fires NC	1404	missing data
	19	1210	fires recede NC	1352	new fires NC
	20	1158	quiet NC new fires FE	1340	many fires NC
	21	1146	fire FE	1328	missing data
	22	1316	many fires NC and NE		
	23	1304	fires recede NC and expand FE		
	24	1252	fires NC and FE		
	25	1239	fires NC and FE	1421	fires NC (FE not visible)
	26	1227	fires NE and FE	1409	many fires NE and FE
	27	1215	fires NE large fires FE	1357	many fires NC and FE
	28	1203	large fires FE	1345	many fires NC and FE
	29	1333	fires receding		
	30	1139	quiet	1321	quiet

TABLE 1 - Continued

Fires of Mongolia Observed With DMSP-OLS Data In 1996
Time = GMT, North = N, East = E, West = W, Central = C Date

		Time	Comment	Time	Comment
May	1	1309	fire NE		
	2	1256	missing data		
	3	missing data			
	4	1232	fires FE	1414	quiet W
	5	1220	quiet E	1402	fire NC
	6	missing data			
	7	1325	fire NC		
	8	missing data			
	9	missing data			
	10	1301	fires NE		
	11	1249	fires NE	1431	fires NC (NE not visible)
	12	1237	quiet E	1419	fires NC (NE not visible)
	13	1225	quiet E	1407	many fires NC
	14	missing data			
	15	1200	solar glare	1342	fires NC
	16	missing data			
	17	1318	quiet		
	18	1306	quiet		
	19	1254	quiet	1436	fires NC
	20	1242	fires NE	1424	many fires NC (E not visible)
	21	1229	quiet	1411	many fires NC
	22	missing data			
	23	1347	fires NC		
	24	1335	fire FE		
	25	1323	quiet		
	26	missing data			
	27	missing data			
	28	1246	quiet	1428	quiet W
	29	1234	quiet	1416	quiet W
	30	1404	fires NC		
	31	1210	sunlight	1352	quiet

4. Conclusion

A series of distinct periods of quiet and active outbursts of fires can be observed in DMSP-OLS data acquired during the April and May fires season in Mongolia during 1996. Time period with the most extensive sets of fires observable with DMSP-OLS data include April 12-14, 20, 22, 26-28 and May 13, 20-21. Quiet periods include April 1-9, 29-30 and May 17-18, 25, 28-29, 31. Because the OLS data is only useful for detection of fires at night, derivation of a more complete fire record would require addition of daytime.

5. References

Cahoon, D.R. Jr., Stocks, B.J., Levine, J.S., Cofer, W.S. III, O'Neill, K.P., 1992, Seasonal distribution of African savanna fires. Nature, v. 359, p. 812-815.

Croft, T.A., 1973, Burning waste gas in oil fields. Nature, v. 245, p. 375-376.

Croft, T.A., 1979, The brightness of lights on Earth at night, digitally recorded by DMSP satellite. Stanford Research Institute Final Report Prepared for the U.S. Geological Survey.

Elvidge, C.D., Kroehl, H.W., Kihn, E.A., Baugh, K.E., Davis, E.R., Hao, W.M., 1996a, Algorithm for the retrieval of fire pixels from DMSP Operational Linescan System data. Global Biomass Burning, MIT Press, In Press.

Elvidge, C.D., Baugh, K.E., Kihn, E.A., Kroehl, H.W., Davis, E.R., 1996b, Mapping city lights with nighttime data from the DMSP Operational Linescan System. Photogrammetric Engineering and Remote Sensing, In Press.

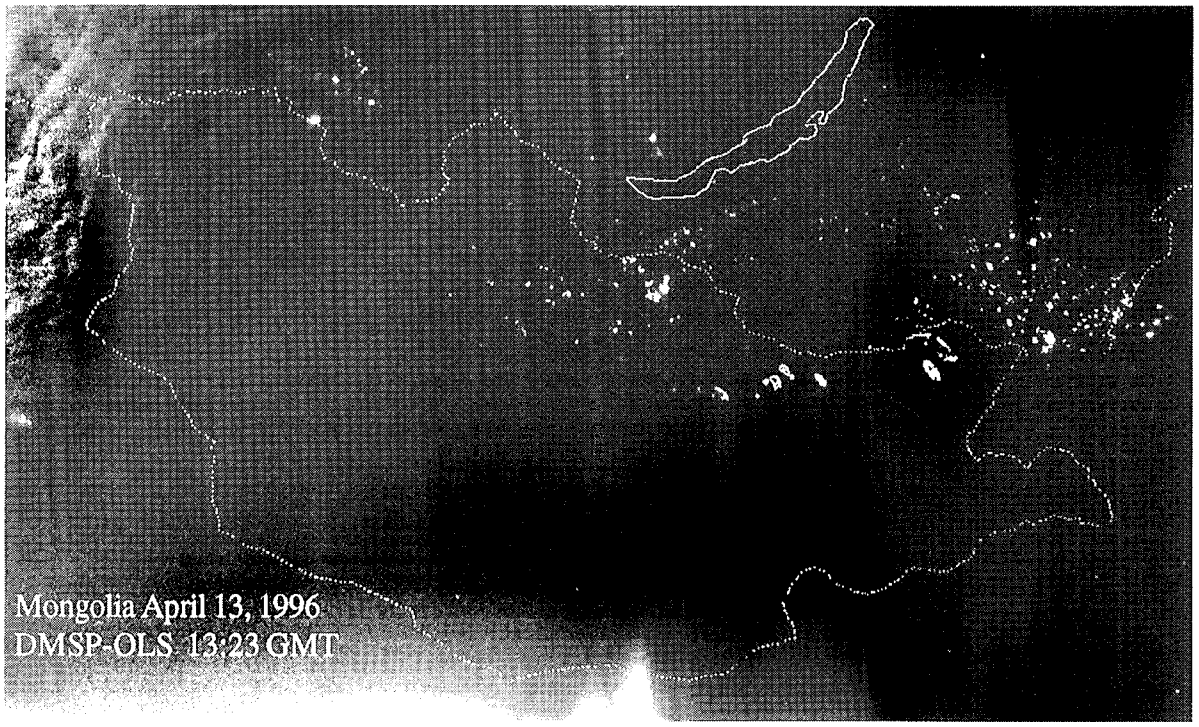

Figure 1. Fires observed in north-central and north-east Mongolia at night using DMSP-OLS data acquired April 11, 1996 at 13:23 GMT. Note fire rings in north-east.

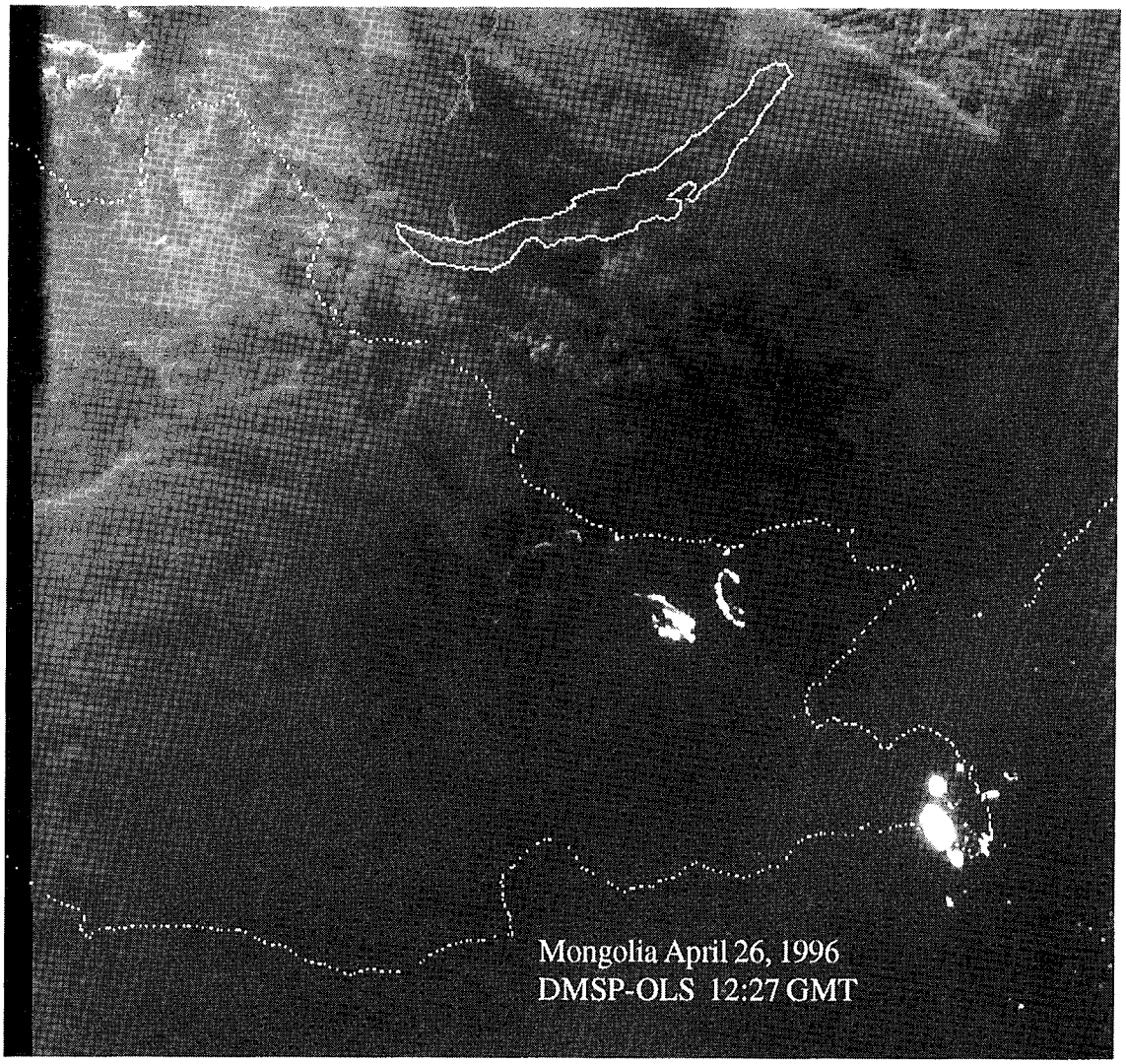

Figure 2. Fires observed at night in north-east and far-eastern Mongolia using DMSP-OLS data acquired April 26, 1996 at 12:27 GMT. Note fire ring in north-east.

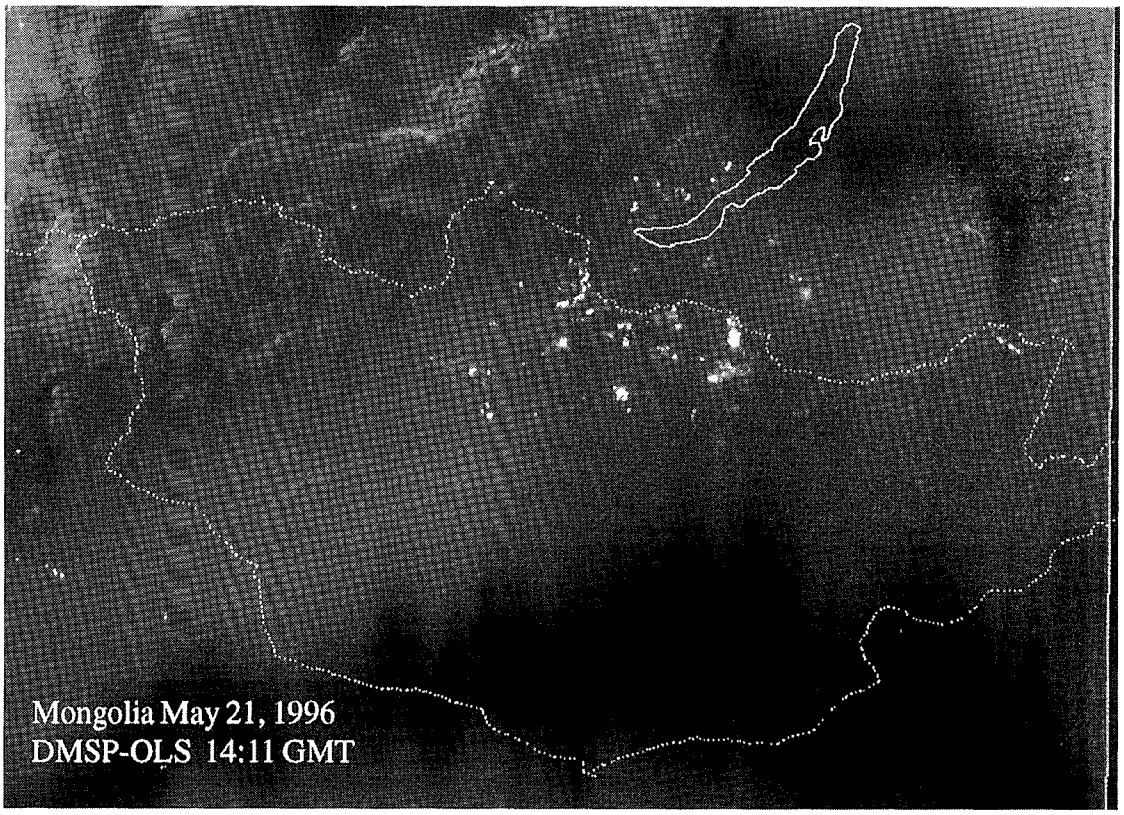

Figure 3. Fires observed at night in north-central Mongolia using DMSP-OLS data acquired May 21, 1996 at 14:11 GMT.

Archeologic Site Mapping and the Image Processing in the Semi-arid Mongolian Grassland

Isao Akojima(*)

*Environmental Geography,Faculty of Human Culture and Social Sciences,
Yamagata University
1 Kojirakawa-cho,Yamagata city,990,Japan
Fax:+81-236-28-4212(c/o Jinbun-Gakubu)
Email:akojima@human.kj.yamagata-u.ac.jp

Abstract

One of the interesting problems for the conservation of Mongolian steppe land is the survey of the recent and the ancient cultivated field. The traditional food production in the Mongolian grass land has been the nomad of sheep that is a tender and sustainable way for grass land. But in the last several decades the large scale cultivation has been done by machine under the Russian support. The stripes of wheat field is being used alternately every other year. Some fields are not used now. It is one of the serious problems whether the large scale cultivation by machine is sustainable or not. The image from the satellite may be useful for detecting the change of large scale cultivation which was begun in the 1960's. We are now starting to survey on the ground and on the satellite image. And we are feeling the necessity of the help of middle scale air photo.

And the another subject is the recent findings of some evidences of the ancient cities and the cultivated field. That needs the more large scale air-photo and the near-ground sensing technology. I want to report some easy image-processing methods for the help of archeologic site mapping.

1. Avraga Palace, the capital of the Early Mongolian Age and the trace of cultivation in the Suujiin Plain, East Central of the Mongolia (Figures and Photos No.1-10).

By the archeologic investigation of the Gorvan Gol Project 1990-94, the site of avragin burgas was concluded as the site of the city at the beginning of Mongolian age when the Chingis Khane was living and as the site of holy place of all the past Khanes later. The remnants of the city were found in the dry steppe.

The plan of the city was mapped by hand. The stereo-graphic pair of Fig.4 is drawn from the survey map. Three differnt street pattern of the city, the remmnant of low wall in the north west side of the city and the remnant of the shallow channel outside of the wall were recognized.

The plant mark may be closely related with the micro relief of the site like a example of Nos.6

and 8. Photo 5, a pair of stereo-graph in 16 colors in CRT screen, is a false relief map made from the mono-chrome air photo. The relief image of Photo 5 shows the difference of brightness of the land (the dryness or poorness of the soil). The method will save the old or dim photos.

Line picture of fig.7 is made by stressing the edge of the plant or shadow mark of the photo 6.

The mapping methods of No.5 and 7 may help the rapid survey of archeologic site in the field, because the drawing of the outline is the first of all of the mapping work.

Trace of rectangular field pattern is found from the air in the lower part of the Suujiin basin (Photo 10), but it is not recognizable on the ground .

2. Kharaholin(Kharakhorum), the Capital of the Ancient Mongolian Empire and the trace of the cultivation, West Central of the Mongolia (Figures and Photos No.11-13).

The details of the capital city of the Mongolian Empire during the 13th to 14th century become evident by the recent investigation (Shiraishi,1996). Trace of field pattern was found in the north inside of the city wall. As the height of the wall is less than 2 meters, Shiraishi(1996) thinks that the wall of the city was not made for the defence to the enemy but to the animals.

Cultivation is also confermed in the picture in the beginning of this century in nomadic Mongolia (Photo 14).

Maps and photos

1 Studied spots A: Avragin Burgas site in the Suujiin Plain
K: Kharaholin (Kharakhorum Capital site)

2 LANDSAT/TM image to show the Suujiin Plain from "Gurvan Gol" Report,p.53.
TM image,Sept.24,1994 was processed by Sakata and others,Tokai Univ. Research and Information Center. D: Delgerkhaan, T: Tossn nuul, AB: Avragin Burgas site, Б : baruun Saarly river, З :Zoon Saarly river, A :Avrag river K : Kherlen River

3 Plant mark of the Avragin Burgas site in the dry steppe of the Suujiin Plain.
The photo was taken by helicopter from the north to the south. Photos 3,6 and 8 are from "Gurvan Gol" Report(1994).

4 A pair of stereo-graph to show the topography and the plan of the Early Mongolian City.
The stero-pair were computed from the contour lines of the survey map.
The survey of the base map was done by Katoh Sinpei, Tsurumaru T., Shiraishi N., Katoh Sinji, Miyake T., Furuya T. and Akojima I. on foot. The remnant of crank shaped channel outside the bank is not shown.

5 Stero-pair to show the plant mark and the plan of the archeologic site.
The brightness (dryness or poorness of the soil) in 16 colore grades in CRT screen is made from mono-chrome air photo. The color grades in this print is not same as the image in the CRT screen.

6 Stero-pair of photo showing the remnants of the ancient city blocks.
Some holes may be the excavating holes made by Mongolian archeologist during 1960's.

7 Edge line map made from the Photo 6.

8 Plant mark on the mound of the largest boulding in the ancient palace.

9 Surveyed map of the same site as photo 8. Contour interval is 0.1 meter.

10 Rectangle plan of "former cultivated field(?) by Chinese during the 19th C.(?) " in the lower part of the Suujiin basin.
Light colored part in the right half is the denuded part by the recent cultivation.

11 Old and new field patterns near the Kharakhorum site.
More than three field patterns are superimposed in the recent cultivation.
Black line was added to show the plan of low wall of the Mongolian Empire Capital and the small rectangle is the wall of temple made after the destruction of the capital during the 16th century. Photo by the Mongolian parmission.

12 Field pattern inside of the city wall.

13 Plan of the Kharakhorum site newly surveyed by Shiraishi(1996).

14 Mongolian cultivation in the beginning of the 20th century.
This picture is copied by hand from the famous painting of "A day of Mongolia---Spring" (Sharav?, 1915). The original picture is in the Central Museum of Fine Arts, Ulaanbator.

Acknowledgement

The autor want to express the thanks to Prof. Katoh S., Furuya T.,Chiba Univ., Tsurumaru T., Sapporo Gakuin Univ. and other menbers of the Gorvan Gol Project for their help in the field, and to Mr.Shiraishi,N., Niigata Univ. and Mr. Purevdorj T., Mongol State Univ.(now in Chiba Univ.), for their helpful informations.

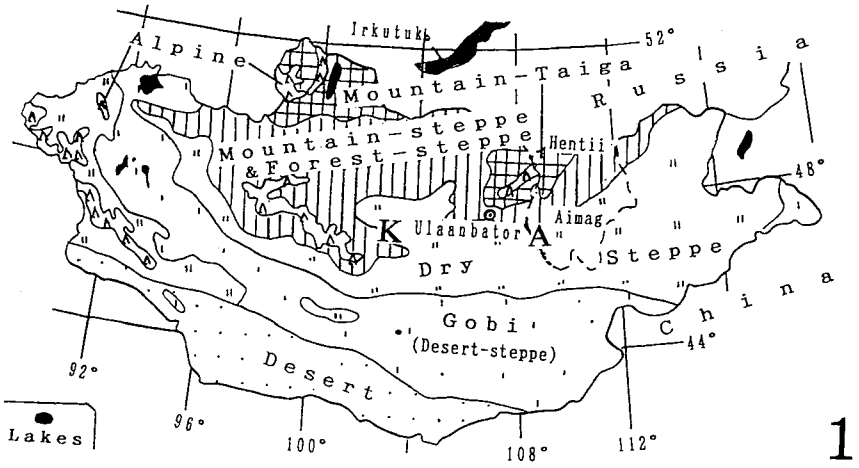
Irkutuk
52°
Alpine
Mountain-Taiga
R u s s i a
Mountain-steppe
& Forest-steppe
Hentii
48°
K
Ulaanbator
A
Aimag
Dry
Steppe
C h i n a
Gobi
(Desert-steppe)
44°
92°
Desert
96°
100°
108°
112°
Lakes

1

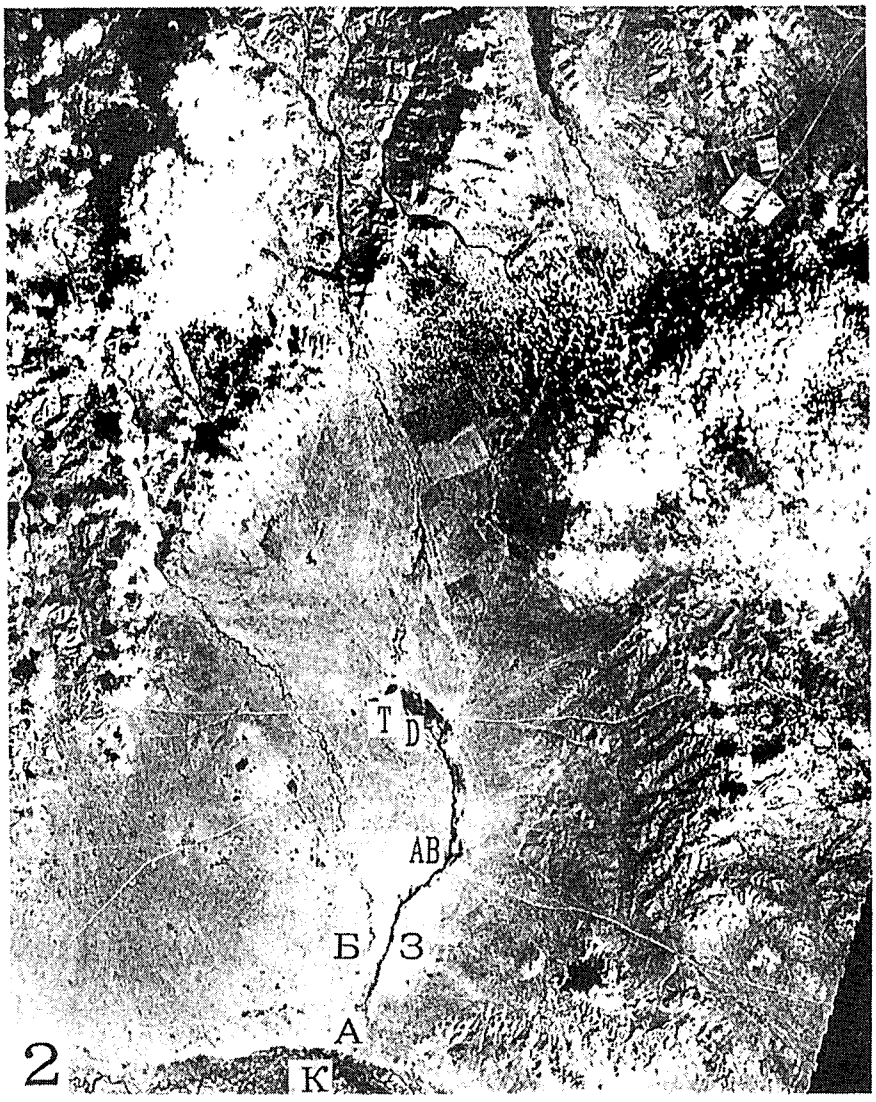
T
D
AB
Б
З
A
K

2

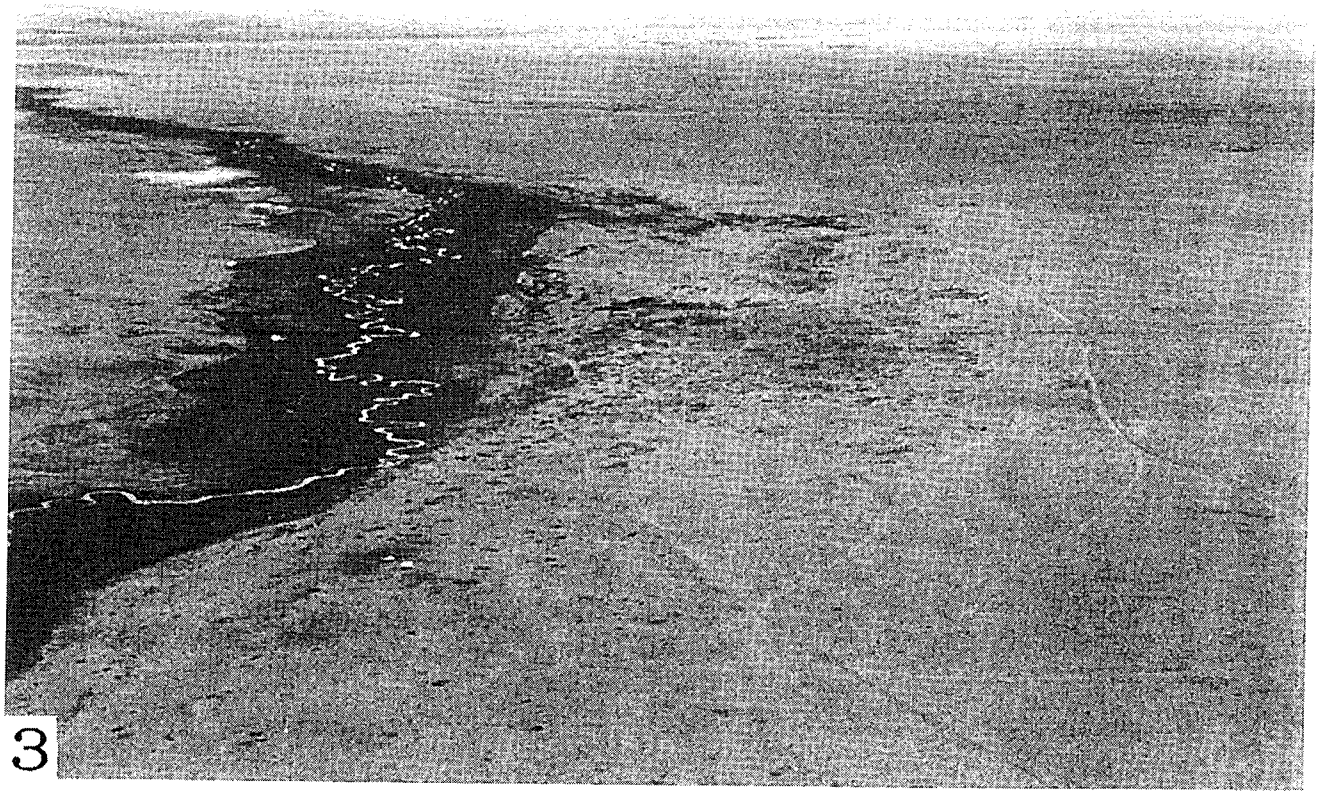

3

North

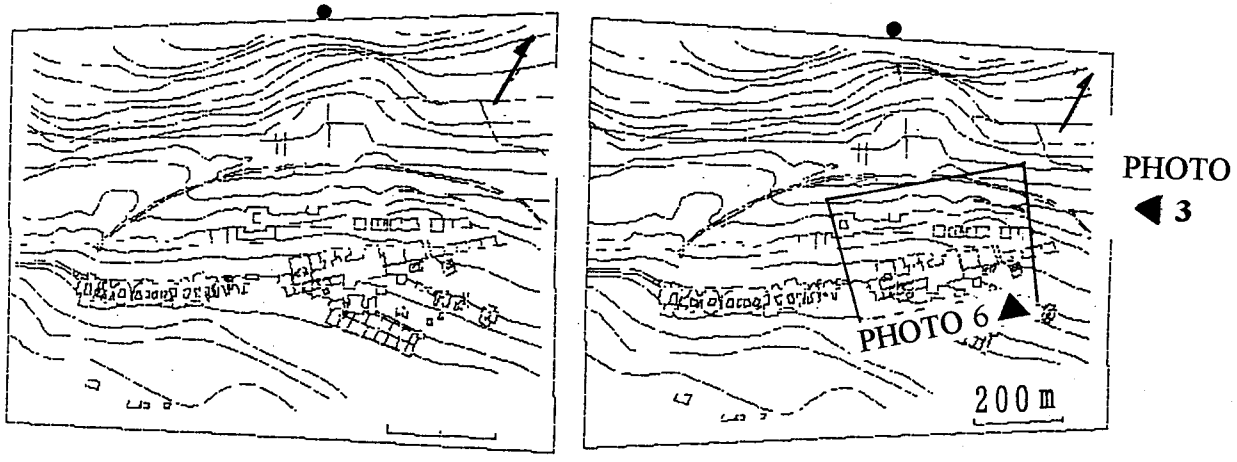

PHOTO ◀ 3

4

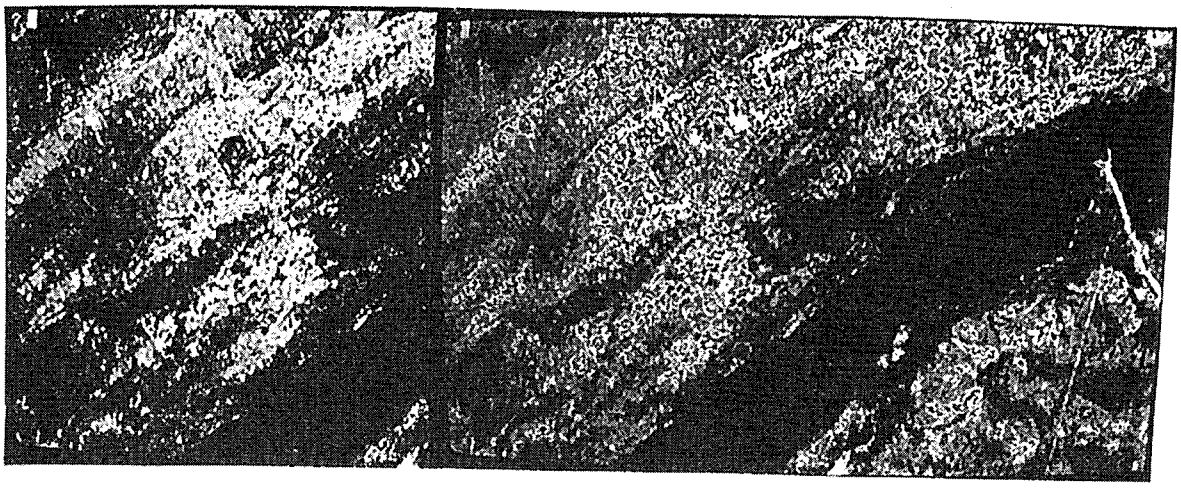

5

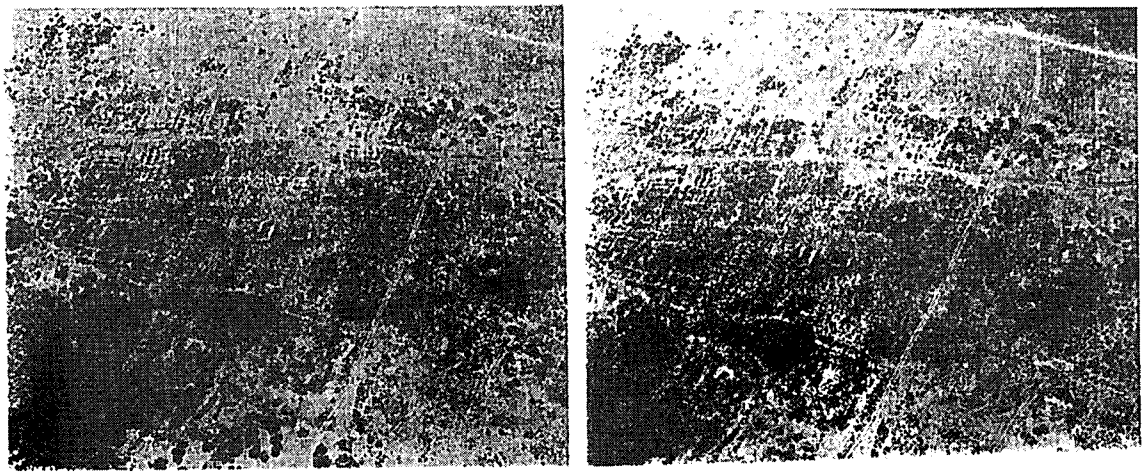

6

7

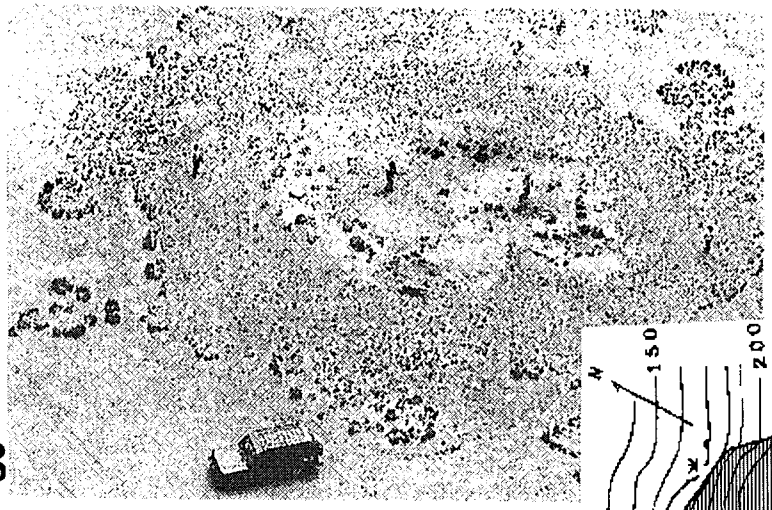

8

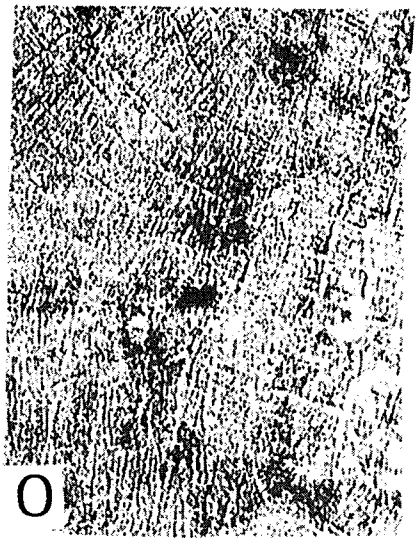

10

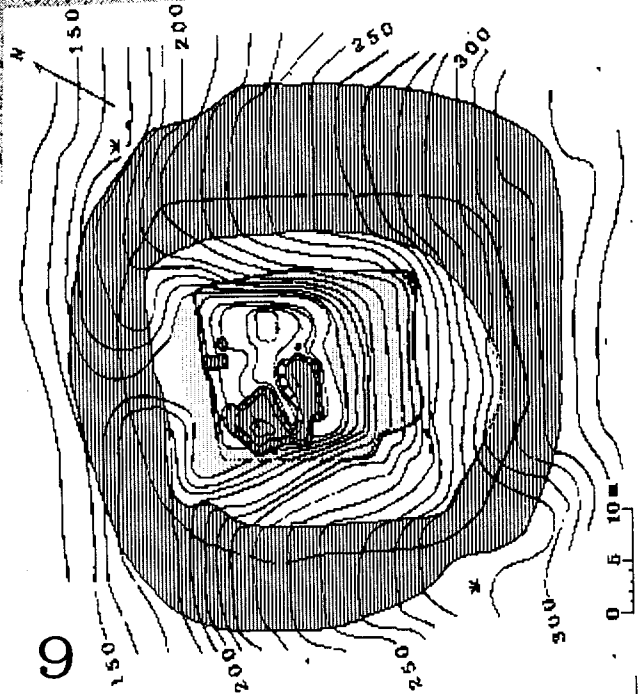

9

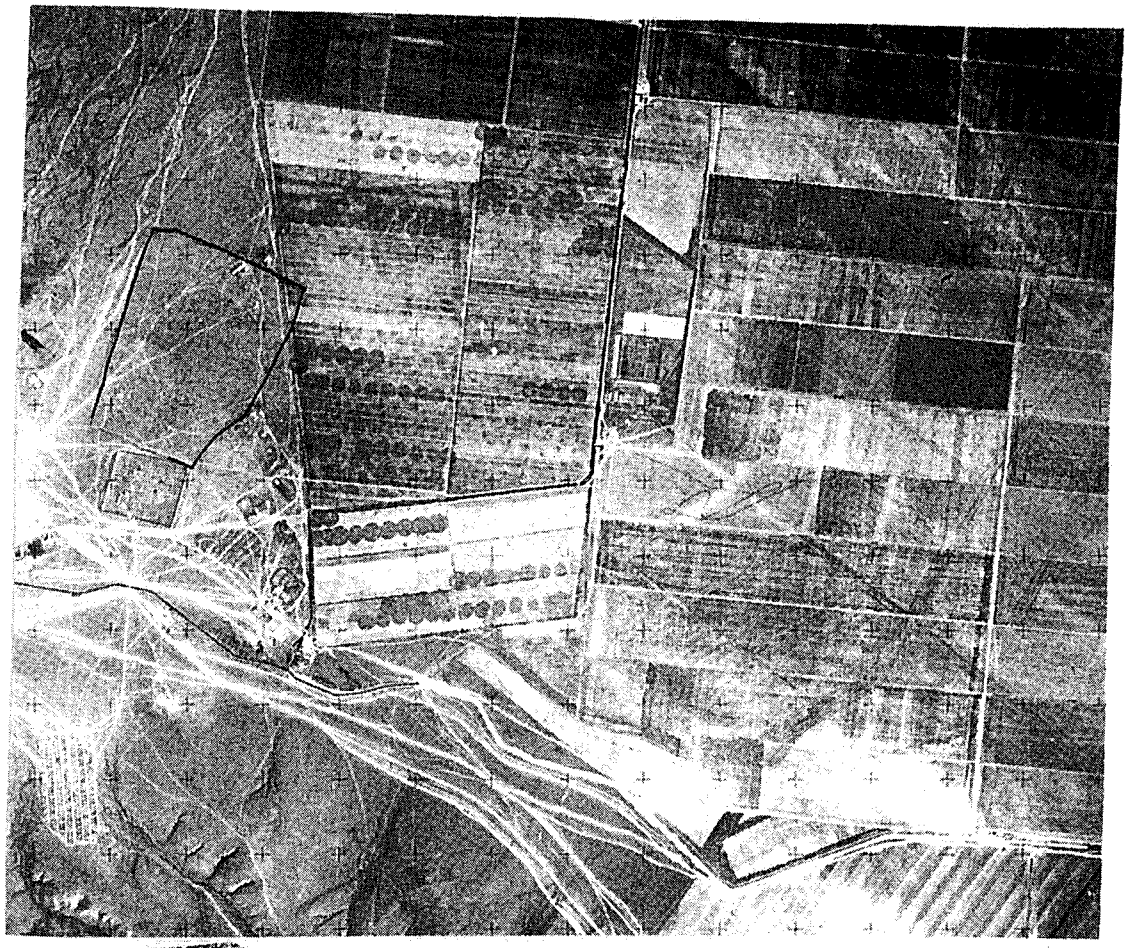

11

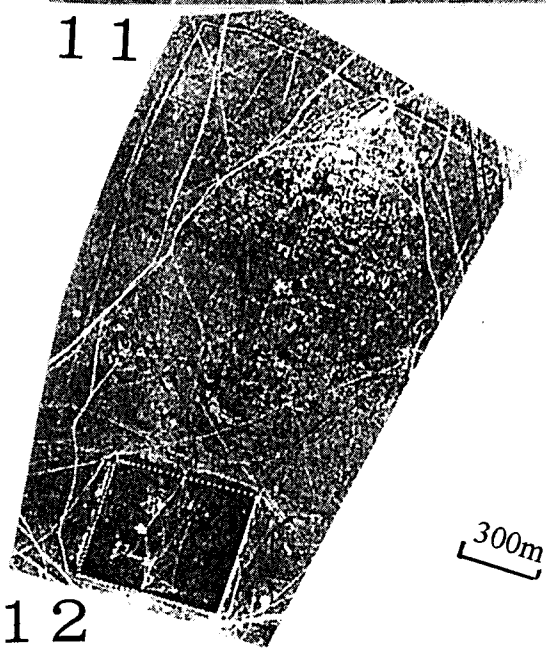

12

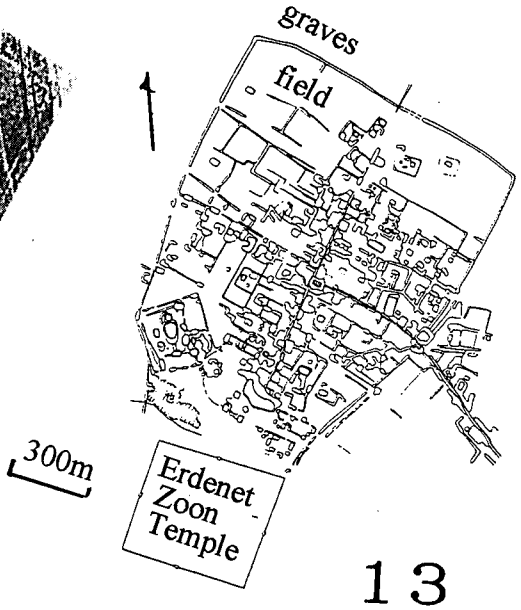

13

Shiraishi(1996).

14 Mongolian cultivation in the beginning of the 20th century.

References

Akojima,I.(1993) "Some examples of image processing in the semi-arid Mongolian steppe. Ann. Tohoku Geographical Association, 45-2, pp.144－146

Mongolian Academy of Sciences and the Yomouri Shinbun,Japan(1994) "A report on the joint investigation under the Mongolian and Japanese, Gurvan Gol , Historic Relict Probe Project 1991-1993.", 85ps

Shiraishi,N.(1996) "A preliminary report of archaeological survey at the Kharakhorum site, Mongolia." The Japanese Sea Rim Studies Annual Report, Institute of Modern Socio-Cultural Studies of Niigata Univ., 3, pp.125－130

Seasonal and Diurnal Changes of Atmosphere-Land Interaction over Mongolia

Shin Miyazaki and Tetsuzo Yasunari[1]
Adyasuren Tsohiogiin [2]

ABSTRACT

The Eurasian Continent is the largest continent on the earth which consists of various kinds of climates and surface conditions such as tropical rain forest,humid temperate climate,desert,steppe,glass land,taiga,tundra and so on. The surface condition which is including vegetation of Eurasian Continent plays very important role in the formation of global climate. Mongolia is one of the largest plateau in Eurasian Continent and plays a great role in dry air mass formation and structure change of Baiu front(Kato,1985,1987),which is one of the most important phenomena in Asian Monsoon region. Therefore it is very important to investigate the characteristics of climate over Mongolia to clarify its role on the global climate.

The purpose of this study is to investigate characteristics of seasonal and diurnal change of surface meteorological elements and surface heat balance. These are very important factor to understand atmosphere-land interaction and air mass formation over Mongolia. Thus,surface meteorological observation has been carried out from 30 September of 1993 up to now,to study the diurnal and seasonal variation of surface meteorological elements by using AANDERA Automatic Weather Station(AWS) in the Baruunkharaa (48°55′N,106°4′E)in the Northern part of Mongolia.

The results are summarized as follows: Some abrupt changes of surface meteorological elements are recognized in transitional seasons simultaneously in Baruunkharaa in the Northern part of Mongolia by analyzed AWS data from late September 1993 to mid-November 1994. Abrupt decrease of T(air temperature(20 °C)),q(specific humidity(2g/kg)) and abrupt increase of albedo occurred in mid-November 1994,which suggest that abrupt decrease of T and q might be related to surface snow cover. From mid-November to mid-February there might be stable snow cover(albedo was more than 0.5) on the surface. In this period T was below -15 °C and net radiation expressed negative value and diurnal range of q was small(1g/kg) which is likely to small evaporation caused by little water vapor. In mid-March 1994 abrupt increase of T(20 °C),q(2g/kg) occurred and after this period diurnal range of specific humidity became larger(2g/kg) than winter. After this period afternoon decrease of q which can be related entrainment caused by grown mixed layer become dominant responded to large sensible heat flux. In mid-June 1994 abrupt increased of q(5 g/kg) occurred. After this period diurnal range of q became larger(5g/kg) and diurnal range of potential temperature became smaller and latent heat flux became main component of heat balance. These results suggests that in the summer season large amount of precipitation may contribute to grow the vegetation and increase of soil moisture and evaporation from the surface. In early September abrupt decrease of q(5g/kg) occurred and diurnal range of q became small(2g/kg) same as spring. Although the afternoon decrease of q wasn't encountered and sensible heat flux was smaller than spring which implies that there was not enough growth of mixed layer to raise entrainment.

1 Introduction

The Eurasian Continent is the largest continent on the earth with has various kinds of climates and surface conditions,e.g. tropical rain forest,humid temperate climate,desert,steppe,glass land,taiga,tundra

[1]Institute of Geoscience,University of Tsukuba

[2]Ministry of Nature and Environment,Mongolia

and so on. The surface condition includes vegetation of Eurasian Continent plays very important role in formation of global climate. Mongolia is one of the largest plateau in Eurasian Continent.

The structure change in the Baiu front in China and the northward shift of the polar front in the Eurasia seems to be response to heating from the ground in the semiarid region from Takla Makan to North China including Mongolian Plateau.(Kato,1985,1987) Baiu front is one of the most important phenomena in Asian Monsoon region. Therefore it is very important to investigate the characteristics of climate over Mongolia to clarify the its role in effect of global climate.

The purpose of this study is to investigate characteristics of seasonal and diurnal change of surface meteorological elements and surface heat balance. They are very important factor to understand atmosphere-land interaction over Mongolia.

2 Observation of surface meteorological elements and energy balance

2.1 The Observation Site

The Baruunkharaa observation site (48°55′N,106°4′E) is located on the typical topographic Mongolian Plateau ,about 150 km north of Ulaanbatar Capital in the northern part of Mongolia. The altitude of the site is 806.9m above sea level. The Hanghai Mountains of altitude of 2000 $\sim$ 4000 m are located about 500 km south west of the site. The Hentei Mountains of altitude of 1800 $\sim$ 2800 m are located about 180 km south east of the site. The Burengiun Mountains of altitude of 1500 $\sim$ 2000 m are located about 100 km north west of the site. A stream, Hara River runs from south to north about 500 m east of the site. The site is located center of Baruunkharaa village. Several two or three storied structure are surrounded about 50 m around the site ,which is satisfied with standard of Hydorometeorological Research Institute of Mongolia. The population of Baiangol sum is about 6000.

2.2 Method of Surface Meteorological Elements Observation

The automatic weather station (AANDERA 2704)has been used for long-term monitoring surface meteorological elements . It consists of 3-cups anemometer, a resistance thermometer,hygroscopic humidiometer,two pyranometer(downward and upward solar radiation) for measuring surface meteorological elements. Air temperature,relative humidity and wind speed were measured at 1m and 4m and the downward and upward solar radiation were measured at 4m above the ground surface. This system has been operated by solar cell power module and data have been recorded automatically by a data logging system every 30 minutes from October 1993. Wind speed was measured as a 30-minutes average but another surface meteorological elements were measured as an instantaneous value. The stored data were collected by a portable personal computer once three months. In the following analysis the Local Standard Time(LST;GMT+8 hours) was used.

2.3 Method of Surface Energy Balance Calculation

Surface heat balance is calculated by bowen ratio method as follows.

1. Soil Heat Flux

$$G = c_R Rn \tag{1}$$

G and c_R are soil heat flux(Wm^{-2}) and emprical constant(=0.1),respectively.(Brutseart,1992)

2. Latent Heat of Evaporation(Kondo et al,1994)

$$l = 2.50 \times 10^6 - 2400T \tag{2}$$

3. Bowen Ratio(Kondo et al,1994)

$$Bo = \frac{c_p(T_1 - T_4)}{l(q_1 - q_4)} \tag{3}$$

Bo,c_p,T_1,T_4,q_1,q_4 are bowen ratio,specific heat of air at constant pressure(=1005($Jkg^{-1}K^{-1}$),air temperature at 1m and 4m(K),specific humidity at 1m and 4m(kg/kg),respectively.

4. The Rate of Evaporation(Kondo et al,1994)

$$E = \frac{Rn - G}{l(Bo + 1)} \tag{4}$$

E is rate of evaporation($kgm^{-2}s^{-1}$).

5. The Rate of Evaporation(Kondo et al,1994)

$$H = Bo \times lE \tag{5}$$

H is sensible heat flux(Wm^{-2}).

3 Seasonal and Diurnal Changes of Surface Meteorological Elements

3.1 Seasonal Change

Figure 1 shows time series of 11 day-running mean values of air temperature and specific humidity from October 1993 to September 1994. In the mid-November 1993 11day-running mean values of air temperature decreased about 20 °C and specific humidity also decreased about 2 g/kg during several days. In the mid-March 1994 11day-running values of air temperature increased about 20 °C and specific humidity increased about 2g/kg during a week. In the mid-June 1994 11day-running mean values of specific humidity increased about 5 g/kg during several days . In the later August 1994 11day-running mean values of specific humidity decreased 5 g/kg during several days . Air temperature and specific humidity varied with the same phase except the beginning and end of summer season. Increase and decrease of specific humidity at the beginning and the end of summer season might be related air mass exchange.

Figure 2 shows time series of daily precipitation from October 1993 to September 1994. In Barunkharaa most of precipitation occurred in summer season from June to August.

Figure 3 shows time series of 11days running mean values of global solar radiation from October 1993 to September 1994. In early June 1994 downward solar radiation suddenly decreased by 10 MJ/day. The difference between downward and upward solar radiation was very small value less than 5 MJ/day from November to middle of February. Except this season the difference was more than 10 MJ/day. The

small difference between downward and upward solar radiation indicates that albedo was high value as follows.

Figure 4 shows time series of 11days running mean values of air temperature and albedo from October 1993 to September 1994. In middle of November 1993 albedo suddenly increased by 0.4 to 0.9. In middle of February 1994 albedo decreased by 0.4 to 0.3. The abrupt increase of albedo and the abrupt decrease of air temperature were occurred simultaneously but the abrupt decrease of albedo and abrupt increase of air temperature occurred with one month lag. It was speculated that the transition from autumn to winter was related to cold air mass and snow cover but transition from winter to spring was occurred by surface heating about one month after snow cover was despaired.

3.2 Diurnal Change

To clarify seasonal march of diurnal cycle of potential temperature and specific humidity which is likely to express the surface Bowen ratio,we showed that the plot of (θ,q) of hourly data of decadal mean values from October 1993 to September 1994 in Fig. 5. In the all seasons the diurnal range of potential temperature was about 15 K except in the summer. In the winter from middle of November to middle of March the diurnal range of specific humidity was about 1g/kg. In the spring from later March to early June the diurnal range of specific humidity was about 2 g/kg . In the summer from middle of June to later August the diurnal range of potential temperature was about 10 K and the diurnal range of specific humidity was 4 g/kg. In the autumn from early September to early November the diurnal range of specific humidity was about 2 g/kg. In winter the diurnal range of specific humidity was smaller than another seasons which might be related that water vapor was very little and evaporation from the surface might be small and most of available energy might become sensible heat flux. In spring as the potential temperature increased ,the specific humidity increased in the morning. Although in the afternoon as the potential temperature increased ,the specific humidity decreased. It is likely to response that as the mixed layer grew,the entrainment of dry air become dominant and the soil surface become very dry. In summer diurnal range of potential temperature was smaller than another seasons and the diurnal range of specific humidity was the largest values of the all seasons,which suggest that the evaporation from the surface was very large and latent heat flux might be main component of surface heat balance. In autumn the diurnal range of both potential temperature and specific humidity were same as spring but there were no afternoon decrease of specific humidity,which implies that there was not enough growth of mixed layer to raise entrainment.

4 Seasonal Change of Surface Heat Balance

Figure 6 shows time series of 11days running mean values of heat balance components from October 1993 to September 1994. From mid-November 1993 to mid-February 1994 net radiation expressed negative values correspond to high albedo values and low air temperature. This suggests that in this period the surface stable snow cover affected to high albedo values and incoming radiation was smaller than outgoing radiation. The negative values of net radiation might be affected to keep low air temperature. In March and April 1994 sensible heat flux was small and almost same values as latent heat flux. In early May 1994 the sensible heat flux increased and become larger than latent heat flux. In the mid-June 1994 latent heat flux increased and become larger than sensible heat correspond to abrupt specific humidity increase. It seems that the large values of the latent heat flux in the summer season might be related with surface vegetation and evaporation. In the August 1994 the latent heat flux and sensible heat flux were shown same values.

5 Conclusion

The results are summarized as follows: Some abrupt changes of surface meteorological elements are recognized in transitional seasons simultaneously in Baruunkharaa in the Northern part of Mongolia by analyzed AWS data from late September 1993 to mid-November 1994. Abrupt decrease of T(air temperature(20 °C)),q(specific humidity(2g/kg)) and abrupt increase of albedo occurred in mid-November 1994,which suggest that abrupt decrease of T and q might be related to surface snow cover. From mid-November to mid-February there might be stable snow cover(albedo was more than 0.5) on the surface. In this period T was below -15 °C and net radiation expressed negative value and diurnal range of q was small(1g/kg) which is likely to small evaporation caused by little water vapor. In mid-March 1994 abrupt increase of T(20 °C),q(2g/kg) occurred and after this period diurnal range of specific humidity became larger(2g/kg) than winter. After this period afternoon decrease of q which can be related entrainment caused by grown mixed layer become dominant responded to large sensible heat flux. In mid-June 1994 abrupt increased of q(5 g/kg) occurred. After this period diurnal range of q became larger(5g/kg) and diurnal range of potential temperature became smaller and latent heat flux became main component of heat balance. These results suggests that in the summer season large amount of precipitation may contribute to grow the vegetation and increase of soil moisture and evaporation from the surface. In early September abrupt decrease of q(5g/kg) occurred and diurnal range of q became small(2g/kg) same as spring. Although the afternoon decrease of q wasn't encountered and sensible heat flux was smaller than spring which implies that there was not enough growth of mixed layer to raise entrainment.

Rreferences

[1] Kato,K., 1985: On the abrupt change in the structure of the Baiu front over China Continent in late May of 1979.J. Meteoro. Soc. Japan,63,20-36.

[2] Kato,K., 1987: Air mass transformation over the semiarid region around North China and abrupt change in the structure of the Baiu front in early summer.J. Meteoro. Soc. Japan,65,737-750.

[3] Brutseart 1982: Evaporation into the Atmosphere ,Kluwer Academic Publishers,299pp.

[4] Kondo et al 1994: Meteorology of hydrological environment - surface water balance and heat balance,Asakura Shoten,348pp.

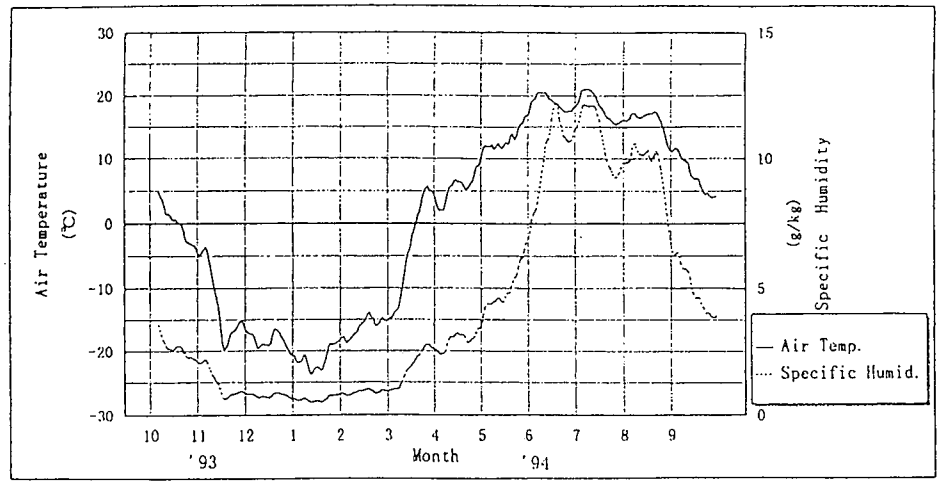

fig1 Time series of 11 days running mean values of air temperature and specific humidty from October 1993 to September 1994

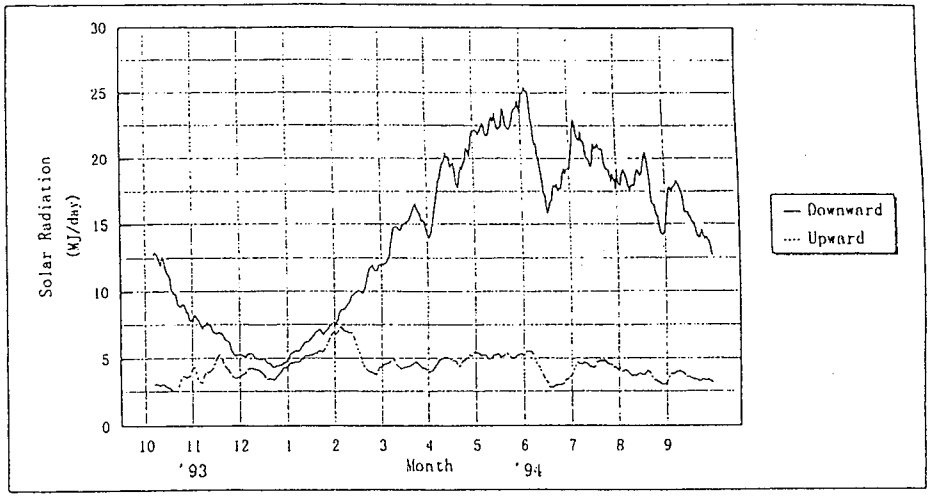

fig3 Time series of 11 days running mean values of global solar radiation from October 1993 to September 1994

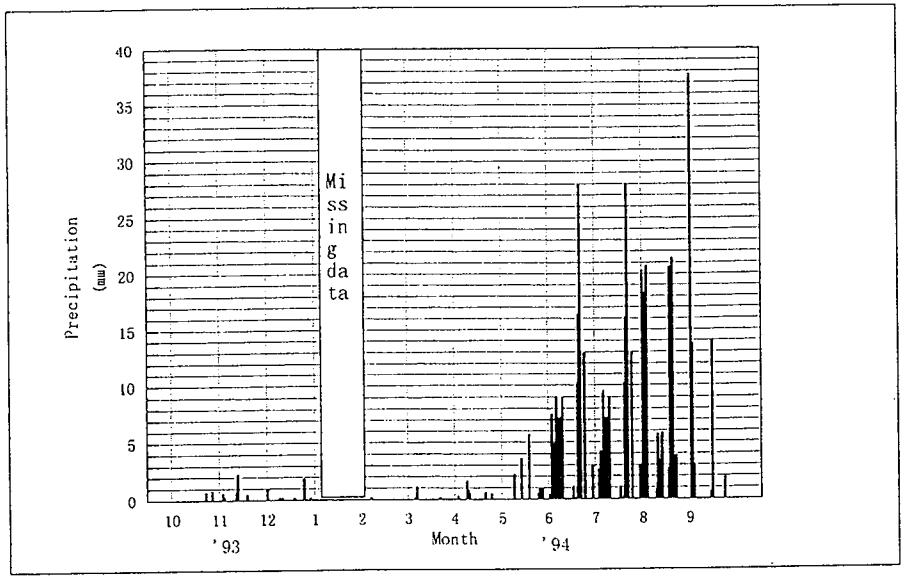

fig2 Time series of daily precipitation from October 1993 to September 1994

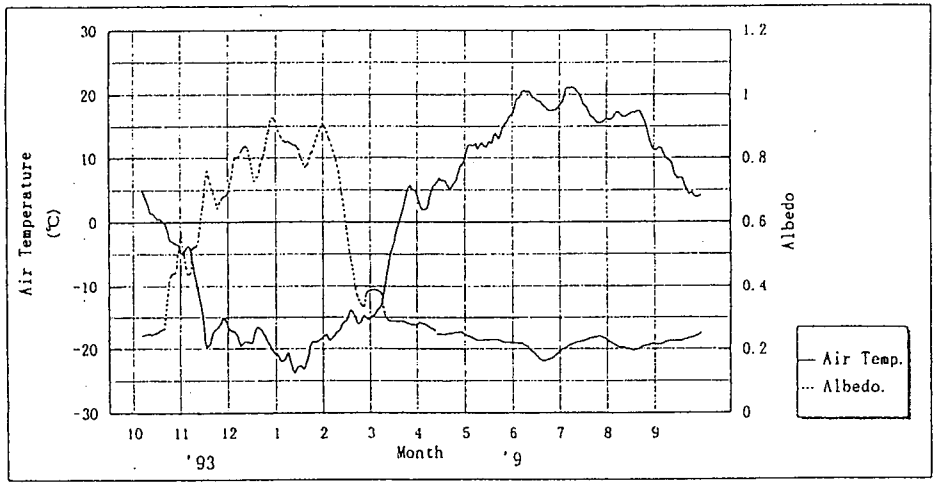

fig4 Time series of 11 days running mean values of air temperature and albedo from October 1993 to September 1994

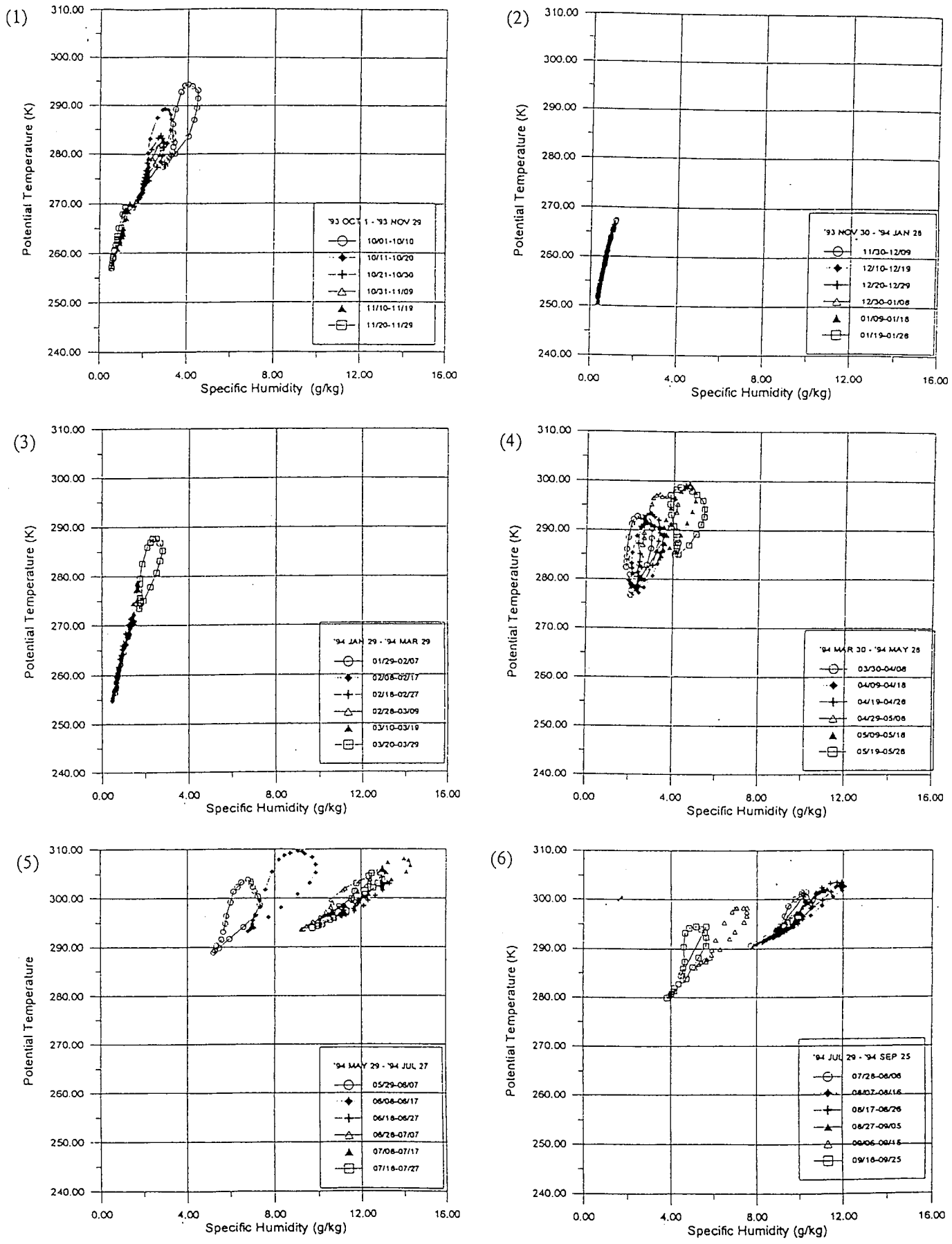

fig5 Plot of (θ ,q) of hourly data of decadal mean values (1)'93 10/1-11/29 (2)'93 11/30-'94 1/28 (3)'94 1/29-3/29 (4)'94 3/30-5/28 (5)'94 5/29-7/27 (6)'94 7/29-9/25

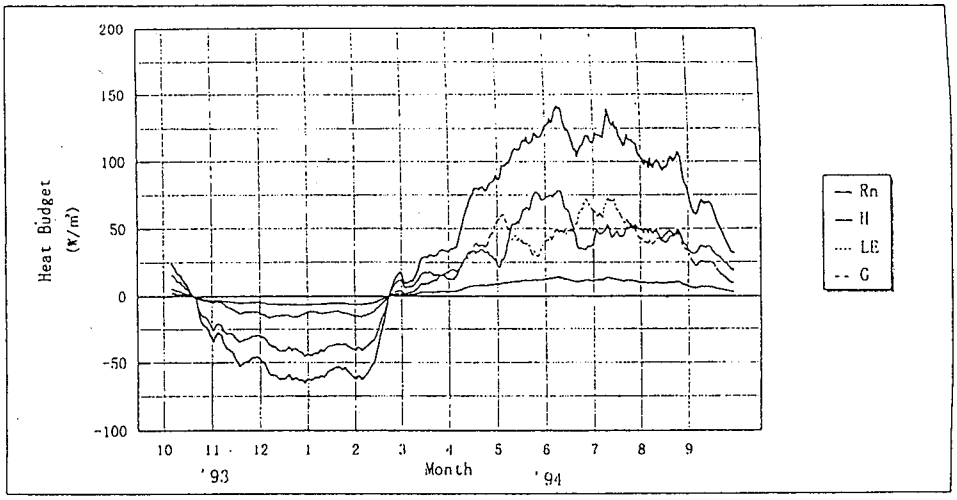

fig6 Time series of 11 days running mean values of heat balance component from October 1993 to September 1994

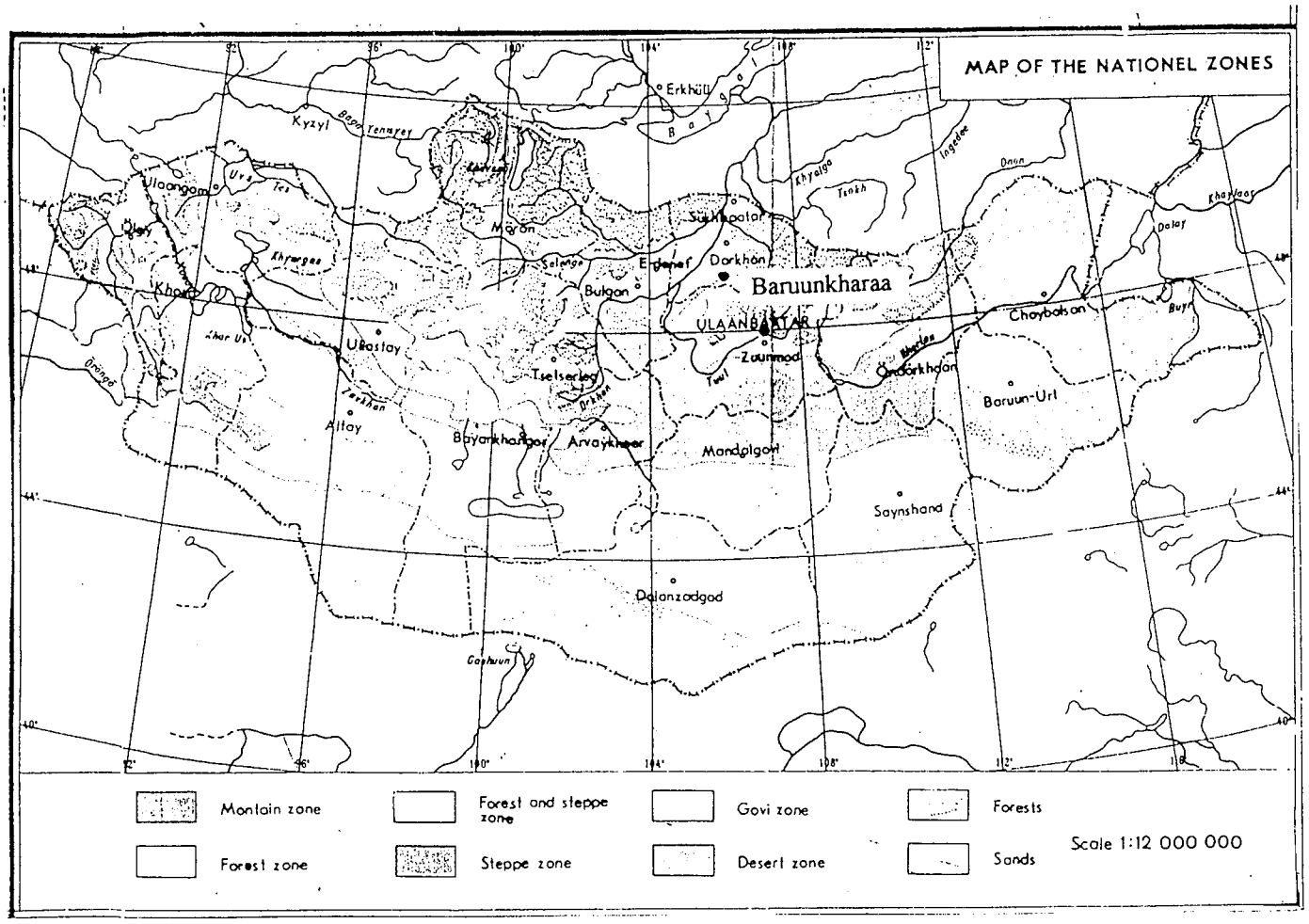

The location map of observation point.(Mongolian Atlas)

Investigation of Hydrological Change in Closed Lake of Arid and Semi-Arid Regions

Yasunori Nakayama(*), Sotaro Tanaka(*), Toshiro Sugimura(*),
Kunihiko Endo(**) and Yuzou Suga(***)

*Remote Sensing Technology Center of Japan
1-9-9 Roppongi, Minato-ku, Tokyo 106 Japan
Fax:+81-3-5561-9542
Email:nakayama@restec.or.jp, tanaka@restec.or.jp,
sugimura@restec.or.jp
**Department of Earth Science, Nihon University
3-25-40 Sakurajosui, Setagaya-ku, Tokyo 156 Japan
Fax:+81-3-3290-5451
Email:endo@chs.nihon-u.ac.jp
***Hiroshima Institute of Technology
2-1-1 Miyake, Saeki-ku, Hiroshima 731-51 Japan
Fax:+81-829-22-5204
Email:ysuga@ds5.cc.it-hiroshima.ac.jp

Abstract

This paper describes a method for the investigation of hydroogical change in closed lake by using satellite data, bathymetric map, and meteorological observation data. The changes for the last about 30 years in water balance of Aral Sea and Lake Balkhash were analyzed in detail. The effect of human activities in the change of Aral Sea, and both effects of human activities and natural climate variation in the change of Lake Balkhash were presumed.

1. Introduction

The water area in closed lakes which are locating in arid land of the Asian and African continents are changing by the influence of the environmental change within their drainage area. Especially, most of these lakes have been rapidly changed for the last about 30 years. Authors showed that the human activities and the climate variation along the inflow river had the effect on the remarkable change of the water area in lakes based on the results of the investigation for change situation using satellite data (Nakayama *et al.* 1994, 1995, 1996). However, the precise examination for the effect of human activities or natural variation to the change of closed lake and its drainage area is necessary to analyze satellite data with ground survey data in detail.

In this paper, the remarkable change in the water volume for Aral Sea and Lake Balkhash of central Asia was firstly described by the analysis of multi-temporal satellite data with the

bathymetric map, and next, the hydrological change was reported on comparing these results with the variation of meteorological observation data.

2. Analysis method

2.1 Water balance of closed lake

Our previous investigation using satellite data showed that the water area with about $66x10^3km^2$ of Aral Sea and the one with about $18x10^3km^2$ of Lake Balkhash at 1960 had shrunk to about 67% and 89% respectively for about 30 years afterwards. On the other hand, the decrease in inflow volume caused by the consumption of river water was grasped because the irrigation field along inflow river enlarged (Nakayama *et al.* 1994).

The change of lake have been generally described by means of the variation in water level in the previous study. However, the more detailed investigation at the viewpoint of water balance is possible by analyzing the relationship among the changes of water volume, inflow/outflow and evaporation in lake.

The water balance in closed lake is described as follows;

$$\Delta QL=PL-EL+R+GL \qquad (1)$$

where ΔQL is change volume of lake water, R is inflow volume from the surface, PL and EL are the calculated precipitation and the estimated evaporation in water area using meteorological observation data respectively, and GL is inflow/outflow volume of underground water. Water volume QL is calculated by water area A from analyzed satellite data and bathymetric map based on ground survey. Then, $\Delta QL(=QL_1-QL_2)$ is given by the changed water volume of lake for the period of object years. PL and EL are estimated as

$$PL=A \times P \qquad (2)$$

$$EL=A \times E \qquad (3)$$

where E is estimated by using P and A. GL of equation(1) is difficult to observe in actuality. In this analysis, we defined the changes of precipitation, evaporation and inflow volume of surface only affected the change of water volume on the assumption that GL was unchangeable.

2.2 Data and analysis procedure

The analyzed results for the changes in water area of lake and vegetation area along inflow rivers from satellite data and other sources had been reported (Nakayama *et al.* 1994, 1995, 1996). This paper described the estimation of changes in water volume and water level, and

analysis of water balance in lakes by using the images detected water area change from satellite data and bathymetric map. The flow of this analysis is shown in figure 1.

A bathymetric map of Aral Sea produced by the former USSR and a corrected bathymetric map of Lake Balkhash based on the utilized document (Kurata *et al.* 1994) were used. The isobathymetric lines from each map were converted to digital isobathymetric images with 250m x 250m mesh type through the digitizing process. These images were registered to geographical corrected satellite images with conformal conical projection by using GCPs. Thus, the water level and volume in each lake were calculated, and its changes were investigated in detail by comparing the isobathymetric images at the object years.

The evaporation based on Penman method (Kondo, 1994) and the calculation of precipitation in lake were carried out using the water area data from satellite image and the meteorological observations from datasets of World Monthly Surface Station Climatology by National Center for Atmospheric Research (NCAR) (Spangler, 1990).

Finally, the changes of water balance in Aral Sea and Lake Balkhash based on equation (1) were discussed with referring to the graphs described the relationship among the changes of lake water volume, evaporation, precipitation on lake area and inflow volume from surface. Moreover, Authors mentioned the relationship between lake change and environmental change at a continental scale through the comparative analysis of meteorological observations.

3. Change in water volume of Aral Sea and Lake Balkhash

The changes in water volume of Aral Sea and Lake Balkhash analyzed with satellite data, bathymetric map and other maps were described in figure 2. The solid line and broken line show the change ration of each year to 1960 of water volume and area respectively, because their changes before 1960 indicated little.

The water area in Aral Sea and Lake Balkhash shrank to about 57% and 89% respectively, and these respective volume decreased to under 25% and about 83%. The change in volume of Lake Balkhash indicated comparatively gradual decrease as well as the shrinkage in water area. Especially, the change was a little within the last a few years. However, it was clarified that the water volume of Aral Sea had become less than a quarter due to more amount of water loss than that of the assumption by the water area change. It is considered that the difference between both basins, which are the complicated relief of bottom of Aral Sea in contrast with the shallow and gradual one of Lake Balkhash, affects each change situation. The images for water depth of Aral Sea and Lake Balkhash composed of satellite data in land and shades corresponding to depth in lake are shown in Figure 3 and 4 respectively. These show that the depth distribution is largely different in the east and the west of the inland in Aral Sea, that is, the deep geographical features in lake of the west side contrasts with the shallow one of the east side.

The above results mentioned that the analysis using actual water volume is important to investigate the change in water balance of closed lake in detail.

4. Change in water balance of Aral Sea and Lake Balkhash

4.1 Water balance of Aral Sea

Figure 5 shows the water balance of Aral Sea based on equation (1) using satellite data, bathymetric map, geographical information data and meteorological observations. The water volume and inflow from the surface indicate the rapid decrease in contrast with a little change in precipitation and evaporation on the lake. On the other hand, the inflow from surface had shown remarkable decrease from the latter half of 1970's to beginning of 1980's, which became the tendency of gradual decrease since then. Therefore, it is presumed that most of decrease in lake water volume was caused by the decrease of inflow from the surface, if the change in inflow/outflow of underground is comparatively constant.

The precipitation in the drainage area of last about 40 years showed the tendency of almost unchanged or a little increase in the same manner as that of unchanged or a little rising in temperature. In the above points of view with the fact of the increase in the irrigated field along inflow rivers, it was clarified that the shrinkage of Aral Sea was most of the artificial effect and few effect by natural variation.

4.2 Water balance of Lake Balkhash

Figure 6 shows the water balance of Lake Balkhash based on equation (1) using satellite data, bathymetric map, geographical information data and meteorological observations. In contrast with the gradual decrease of water volume, a little change in precipitation for the last about 30 years, and decrease until the first half of 1970's and a little increase since then in the evaporation are indicated. Moreover, the tendency of decrease in inflow water became more gradual after the latter half of 1970's as compared with before then. Because the precipitation in the drainage area for the last about 40 years is the tendency of unchanged and the temperature is that of a little rise, it is assumed that these phenomena affect the change in evaporation.

In consideration of the above results with the fact for the expansion in the irrigated field along inflow rivers, it is assumed that the human activities until the first half of 1970's and natural variation of the gradual temperature rise with the artificial one after that affect the change in hydrological environment.

5. Conclusion

In this report, the change in water volume for the closed lakes of Aral Sea and Lake Balkhash in arid and semi-arid region were firstly calculated by analyzing the satellite images of water area change with bathymetric map and geographical information data. Next, the hydrological changes in both lakes were examined by the investigation of the water balance

referring to the meteorological observations. Based on the results, authors were able to investigate the detailed change situation in lake water volume, and detected the remarkable decrease in the volume of Aral Sea in especial. According to the above mentions, it is considered that the investigation of water volume is important to examine the water balance of closed lake in arid and semi-arid regions. Moreover, the change in Aral Sea affected by human activities and the change of Lake Balkhash affected by human activities with natural variation were presumed through the actual investigation of water balance.

The change in closed lake responds to the environmental change within the drainage area intensively, because a lot of various lakes, whose drainage areas are close with each other, distributed in arid and semi-arid regions of continents. Therefore, it can be considered that the change situation in closed lake has the possibility to used for an index of the change in drainage area, and it becomes effective information for the environmental change of arid and semi-arid regions. The continuous investigation for changes in closed lake with the landcover and snow cover within their drainage area is important to monitor the environmental change of arid and semi-arid regions.

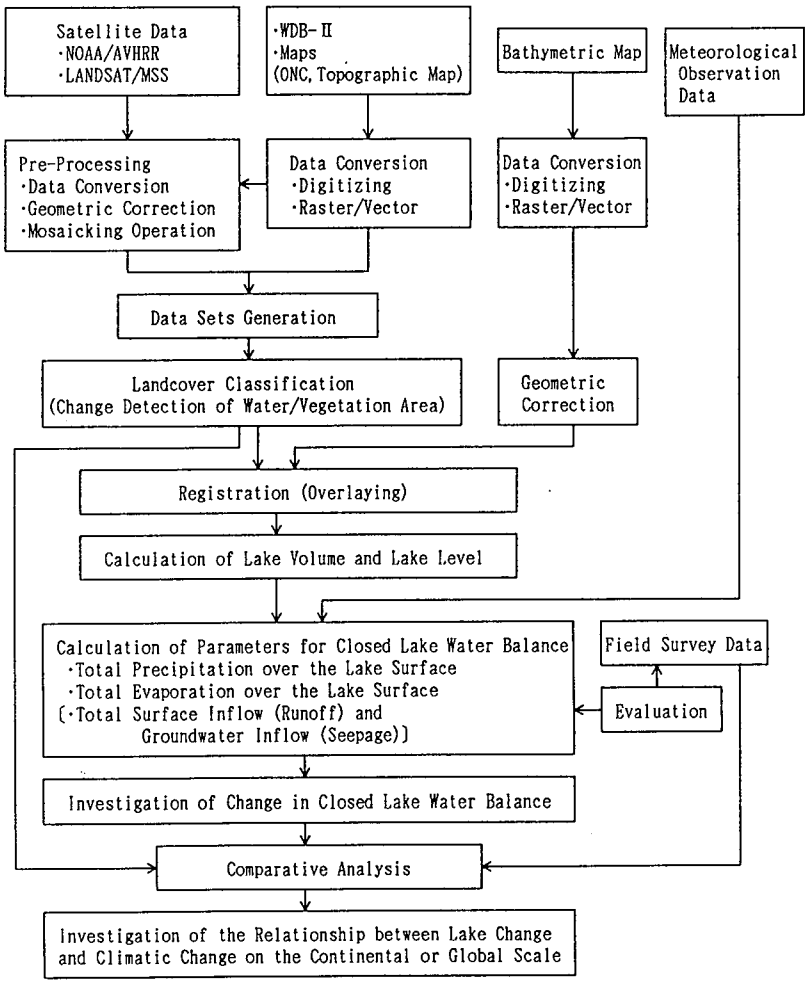

Figure 1. A flow chart for investigation of the change in the water balance of closed lake by satellite data, Bathymetric map and other sources.

Acknowledgments

Authors would like to thank Dr. A. Kondo of Chiba University for his helpful suggestions and providing materials on the calculation for evaporation, and Prof. S. Horiuchi of Nihon University for his comments. We are thankful to Mr. Y. Hirosawa and the Institute of Technology of Shimizu Corporation, who have provided a bathymetric map of Aral Sea.

References

Kondo,A., 1994, "Comparison of the evapotranspiration in monsoon Asia estimated from different methods", *J.Hydrol.*, Vol.24, pp.11-30.

Kurata,A. *et al.*, 1994, "Compact-size edition of data book of world lake environments: a survey of the state of world lakes", International Lake Environment Committee Foundation(ILEC), pp.505-512.

Nakayama,Y., Tanaka,S., Endo,K., and Suga,Y., 1993, "A changes of Aral Sea's water area by satellite data", *Proceeding of IGARSS'93*, Vol.1, pp.194-196.

Nakayama,Y., Tanaka,S., Endo,K., and Suga,Y., 1994, "MOnitoring water and vegetation area changes in aril lands studied with satellite data", *Journal of Arid Land Studies*, Vol.4, pp.21-38.

Nakayama,Y., Tanaka,S., Endo,K., and Suga,Y., 1995, "Monitoring changes of Aral Sea and its vicinity with satellite data", *Journal of The Remote Sensing Society of Japan*, Vol.15, pp.54-69.

Spangler,W.M.L., and Jenne,L., 1990, "World montjly surface station climatology", Natonal Center for Atmospheric Research.

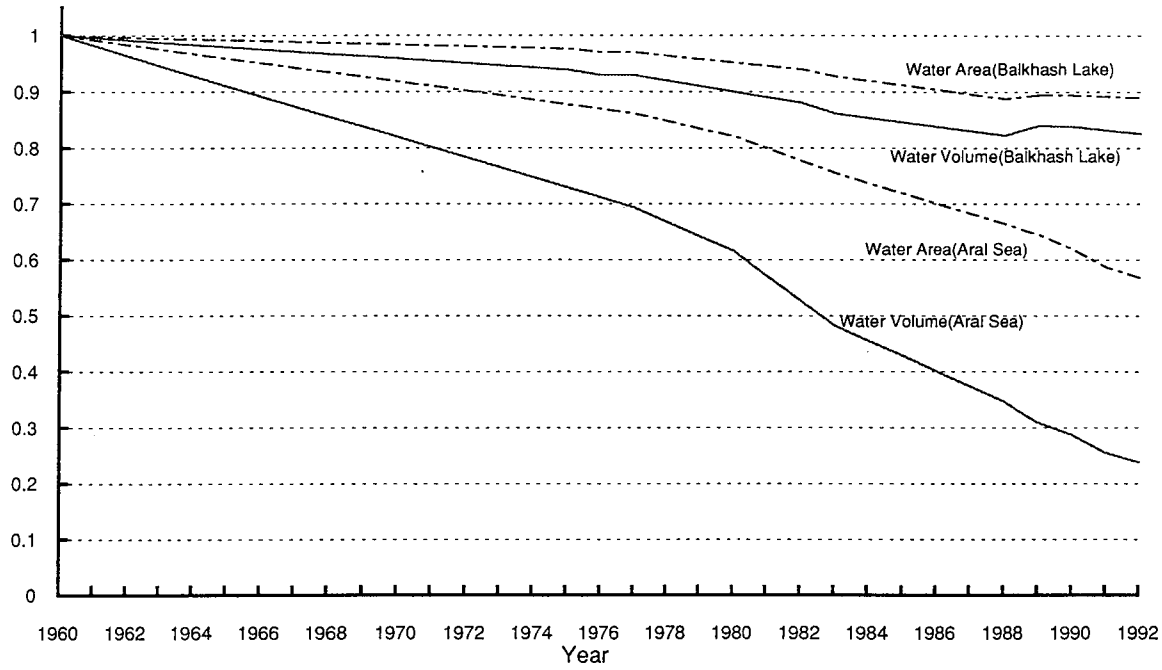

Figure 2. Changes in water volume and area of Aral Sea and Lake Balkhash. The solid line and broken line show the change ration of each year to 1960 of water volume and area respectively.

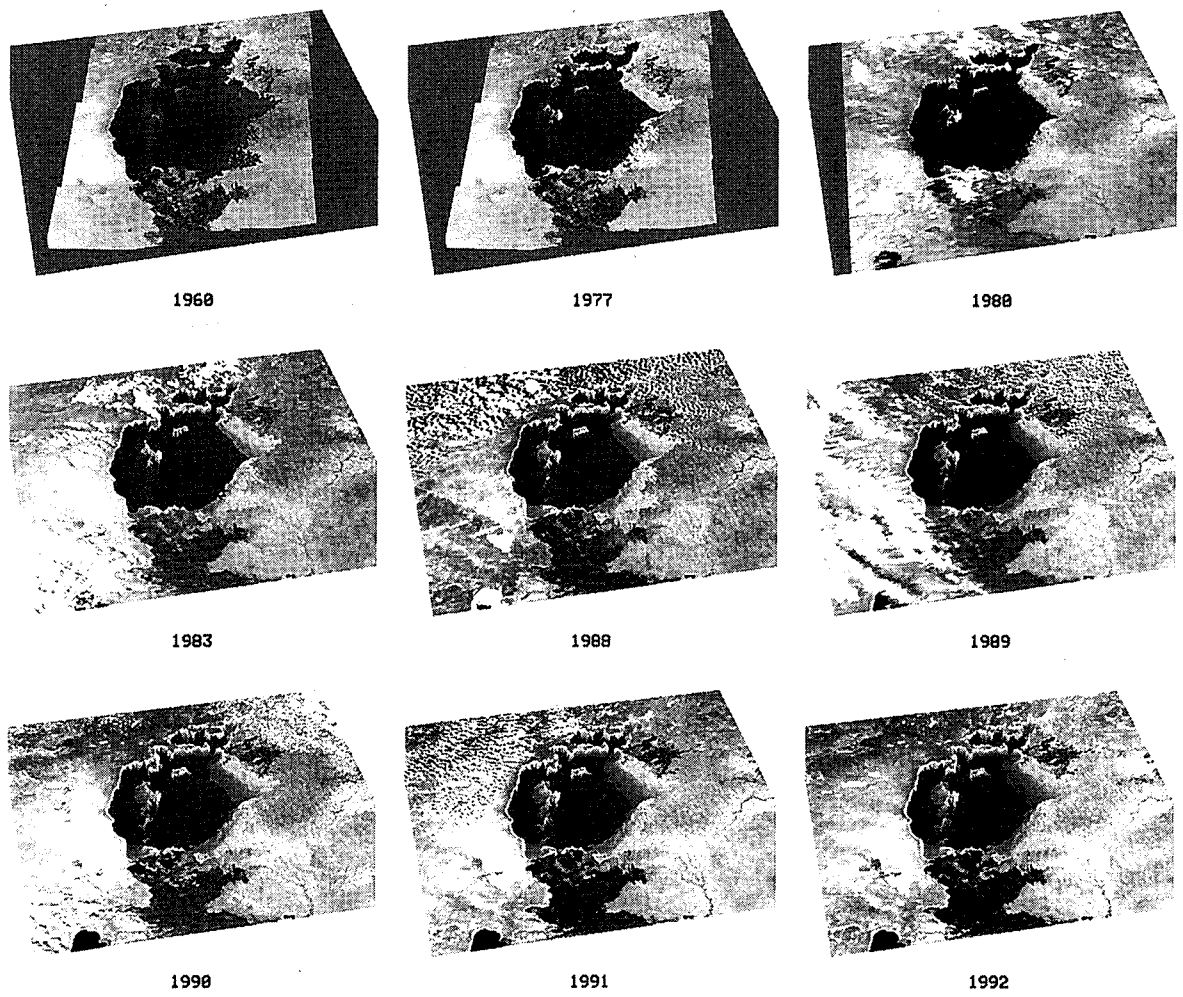

Figure 3. Change situation in water depth of Aral Sea from 1960 to 1992 based on satellite data and bathymetric map. Each image consists of satellite data in land and shading image based on bathymetric map.

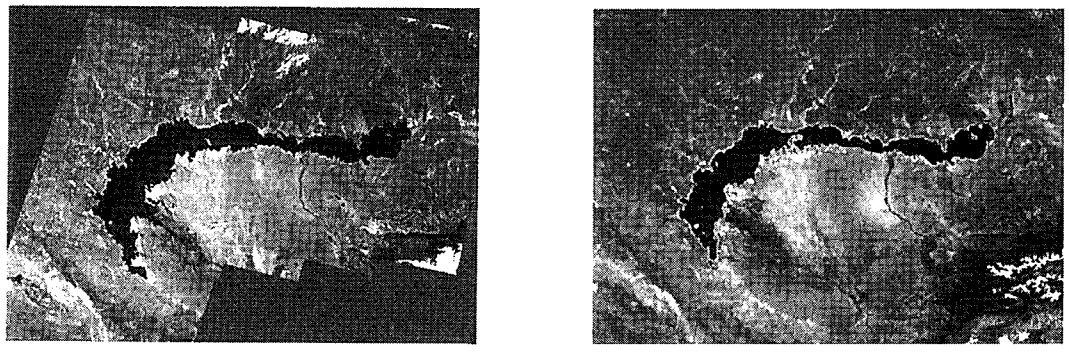

Figure 4. Change situation in water depth of Lake Balkhash at 1960 and 1992 based on satellite data and bathymetric map. Each image is similar to that of Aral Sea.

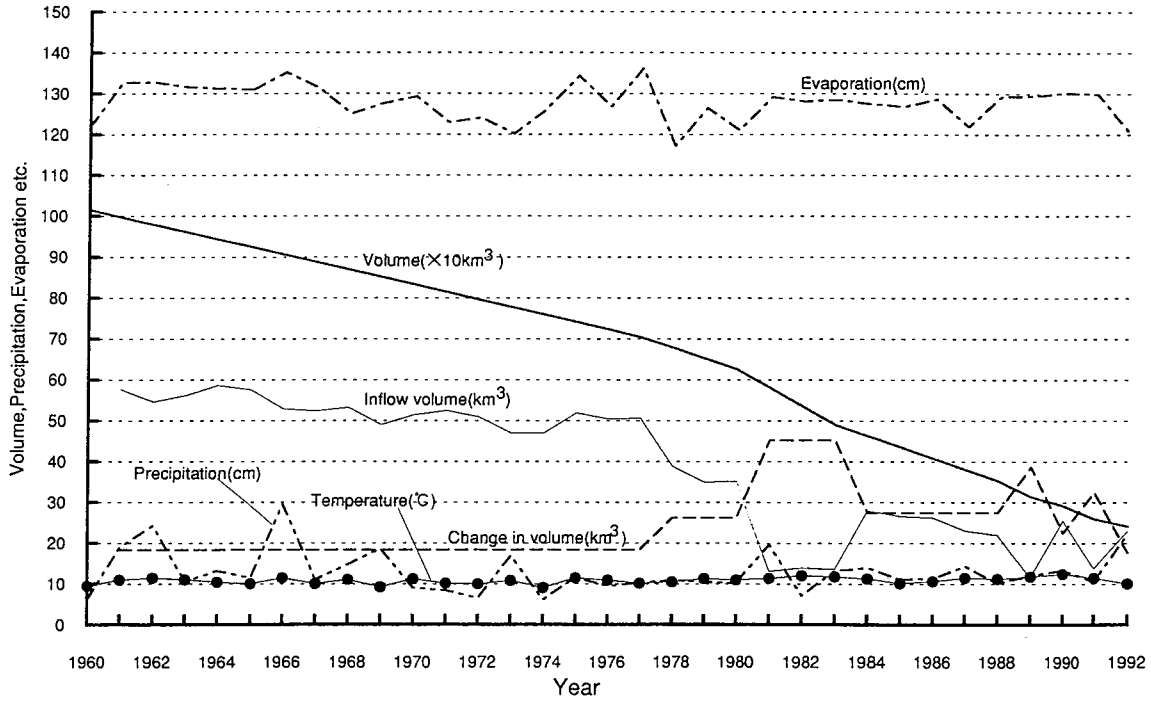

Figure 5. Change in water balance of Aral Sea.

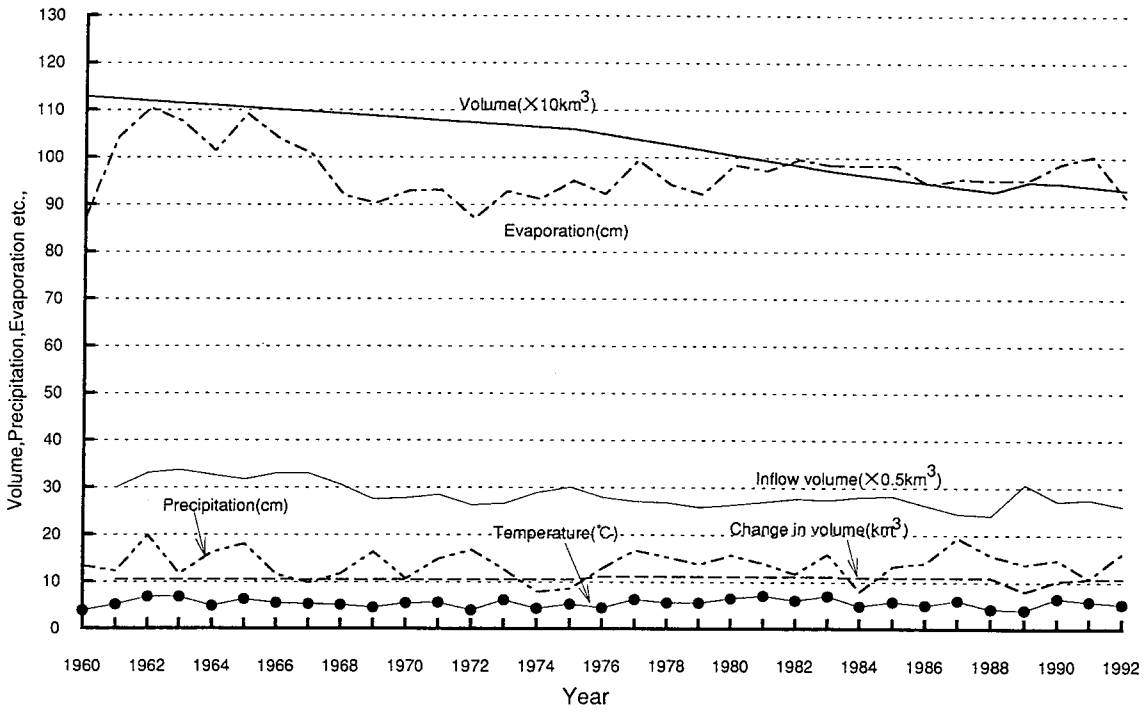

Figure 6. Change in water balance of Lake Balkhash.

Several Landscape Ecological Concepts on the Aral Sea Crisis Revealed by Remote Sensing

Yukihiro Morimoto (*), Atsuo Morimura (**) and Natalia Ogar (***)

* Laboratory of Landscape Architecture and Conservation,
Faculty of Agriculture, Osaka Prefecture University
1-1, Gakuen-cho, Sakai, Osaka, 593 Japan
Fax: +81-722-52-0341
Email: yuki@center.osakafu-u.ac.jp

** Division of Agriculture, Osaka Prefecture University Graduate School
1-1, Gakuen-cho, Sakai, Osaka, 593 Japan
Fax: +81-722-52-0341
Email: morimura@envi.osakafu-u.ac.jp

***Institute of Botany and Phytointroduction, National Academy of Sciences
Alma-Ata, Kazakhstan
Fax: +7-3272-617938
Email: envirc@kazmail.asdc.kz

Abstract

Characteristics and problems of the Aral Sea desertification caused by an irrigation policy was discussed from the view point of landscape ecology. (1) General concepts of vegetation distribution including geobotanical zoning, (2) landscape mosaics in delta vegetation, (3) relationship between traditional and modern land use and natural condition, and (4) vegetation changes caused by massive irrigation in the arid areas of Middle Asia. A time sequential animation of GVI, vegetation maps made from NOAA LAC and SPOT HRV data sets were very powerful for the study.

Key words: the Aral Sea, desertification, arid areas, landscape ecology, vegetation change, remote sensing, sustainable land use, vegetation monitoring.

1.Introduction

An exploitative irrigation policy of the former Soviet Union, which supports cotton and rice production in Middle Asia has led to the drastic contraction of the Aral Sea. In addition to this sensational fact, the large amount of irrigated lands are going to reduce productivity because of salinization. This phenomenon is called the Aral Sea desertification. We must

distinguish the terms desertification and desert. A desert is a natural ecosystem found in arid areas in which ecological conditions continue to change on a daily, seasonally, and yearly basis in a natural way. Desertification, on the other hand, means a drastic decline of biological productivity or a decrease in biological diversity. It is necessary, therefore, to know what the natural fluctuations are, in order to distinguish them and assess the human impact on them.

It goes without saying that irrigation agriculture was not planned for the purpose of destroying nature. Managing to create an enormous income from irrigated agriculture was a brilliant success. However, the contraction of the Aral Sea and some other consequences brought by irrigation had been treated as trifling matters by the authorities until the 1970s. The development seems to have been planned mainly from the view point of rapid construction. Careful consideration to sustainability was not given to the extensive project. Rice production in crop rotation, however, seems to have been planned for leaching salinized soils. Rice is a main crop producted in the irrigation system of Kazakhstan, but the production is maintained by an enormous amount of water, more than 3,000 mm/y (Watanabe et. al. 1996).

After 1980, cotton production in Uzbekistan began, as did rice production in Kazakhstan because of salinization. This demonstrate that large scale agriculture need to be based on landscape ecology in order to achieve sustainability.

We are going to present a natural structure of the vegetation distribution in this area and show the types of changes that are now taking place by means of remote sensing and ground truth.

2.General recognition using GVI animation

The irrigated areas in Middle Asia stretches along rivers and big canals. Syr-Dar`ya and Am-Dar`ya rivers of Aral Sea basin and Ili river for Balkhas lake are the main sources for irrigation.

As the precipitation is around 100 mm/yr., biological productivity in the arid area of the Middle Asia in natural conditions is very low. In addition, nomadism had been the main land utilization until the 1950's when this large scale irrigation project started. We notice , however, that desert does not mean simple and uniformly low productivity. Due to the abundant solar radiation, the potential for the productivity of plants through irrigation is greater in the Aral Sea region than in Japan (Otsuki et. al. 1996). Even in a natural ecosystem, great mountain ranges capture precipitation, and big rivers flow down from the mountains to the desert area. I believe that large *Phragmites* communities at the deltas of these rivers and lakes may have contributed to the motive for the irrigation agriculture.

An animation of weekly Global Vegetation Index (GVI) data set could show the characteristics of the seasonal change of the vegetation activity. Two completely different and contrastive type of vegetation exist in the arid area. One is spring-type vegetation which depends on on-the-spot precipitation. *Artemisia terrae-albae* is the most common small shrub species in such environment. The height of the plant is determined by quantity of spring rainfall, and it turns brown and is dormant in summer. It is the climatic climax community. The other is summer-type vegetation which depends on underground water and river water. This is the wetlands vegetation which consists of a series along ground water level; Phragmites australis communities in the most wet environment, riverside forest called Tugai, grassland of Calamagrostis epigeios , Tamarix spp. et. al. including medicinal plant, Glyceyrriza . These trees and plants had been supporting the life of nomads including their tent house called a 'Yulta'.

3. GVI assisted geobotanical zoning

Vegetation types and their distribution have been studied in depth by N. Ogar and others, however remote sensing data can assist the study in various aspects. only by field expeditions. Weekly GVI images can offer important informations on the determination of the geobotanical zoning. Vegetation types are affected by geology, topography and regions, and satellite images of low spatial resolution are expected to show comprehensive landscapes of the region.

The principal component image created from NDVI of weekly GVI for four seasons, temperature and a near infrared channel could effectively assist in the geobotanical zoning. And the reliability of the result was verified by reclassification of sampled pixels in each zone using the maximum likelihood method. Factor analysis for the species composition of each zone showed the importance of ground water condition and surface geology.

Thus we are able to create a large scale landscape ecological zoning map of the arid areas of Middle Asia. This map shows that conditions in the desert become more severe from Balkhas lake through the Aral Sea to the Caspian Sea.

4. Mosaics of delta vegetation shown by SPOT HRV

In springtime, flooding occurs in the delta area due to snow melting on the mountain. This is essential seasonal dynamics for the vegetation of the deltas; submergence, leaching salinity and flushing silty soil down to the lake. Dynamic processes such as the destruction of vegetation, the scattering of seeds and the regeneration of the plant community occur naturally. SPOT HRV images of the lli delta show us mosaics of the patch regeneration of

the plant communities. That means the natural vegetation in a delta consists of disturbance dependent plant species, and a difficulty with the ground truth in high resolution images taken some years before.

Reservoir dam construction in the Balkhas Lake basin has caused a kind of desertification of the Ili delta. This is not only due to the use of water for irrigation, but to flooding regulations.

5. Extensive irrigation agriculture and traditional land use

Traditional land use in the past had close ties to natural conditions. The environment of the Silk Road and colonies including famous trading cities such as Samalkand and Tashkent offers suitable conditions for oasis agriculture. That is, the environment is neither a mountainous zone nor a desert lowland. As in Uzbekistan, oasis agriculture at the foot of a mountain range can capture rainfall. Thus, traditional cotton and silk worm production had been sustainable in Uzbekistan. In Kazakhstan, however, nomadism had been the most suitable and sustainable land use in arid areas because of the lack of such an environment.

On the other hand, wetland were chosen for large scale irrigation agriculture where an appropriate drainage system, the most important countermeasure against salinization, is difficult to construct. Even under natural conditions with flooding, some parts of a delta are covered with Solonchak and Takyr soils where biomass is very limited. These condition are clarified with a color synthesis image of NOAA LAC which consists of visible range (blue), infrared (green) and thermal range (red, reverse). We can distinguish salinized soils from clouds which are almost inevitable for large areas.

6. Saksawool and barbecue

The riverside forest has a large standing mass per unit area, but only occupies a limited lowland in the vast desert region. Here we must mention Saksawool, which depends on little precipitation and comparatively deep underground water. It is a drought tolerant, C4, and large shrub which has the largest biomass in the area. There are two species, namely *Haloxylon persicum* and *H. aphyllum*, the former preferring sandy condition. The height and density of the Saksawool woodlands are mainly determined by the ground water level. They form sparse communities of less than 1 m in height under dry conditions. However, closed stands around the irrigated farms sometimes reach 6 m in height.

We can clearly see the examples around the Bereke farm near the Bakanas in the Balkhas basin by means of a false color composite image of SPOT HRV. Along the drainage line,

which is a geologically old river flow, on activated Saksawool community can be recognized. This is thought to be a temporal stage in a change to a Tsugai forest.

On the other hand, a main dinner entree of the nomads is barbecue of mutton called Shashrik. The charcoal of Saksawool is the best fuel for cooking, and its usage and regeneration were considered to be in a balance before the 1950s. But it has been on a remarkable decrease. One of the reasons for this is the shortage and the rise in price of oil and coal after the dissolution of the Soviet Union. Saksawool woodlands, once distributed widely in the former Aral Sea shore region, have mostly been cut down already. We can see some experiments with afforestation in the Saksawool woodland, but they have not been a sufficient success.

7. Invasion by plants on the exsiccated sea bed of Aral

It has been said by journalist that the exsiccated sea beds are covered with only salty sand and silty clay. However, through the use of SPOT HRV images and careful ground truth, information about the exsiccated sea beds proved this statement to be an exaggeration. Moving sand dunes, which were caused by overpasturing, are in existence only around villages.

On the exsiccated sea bed of the Aral Sea, invasion and plant succession are now occurring on a very dynamic basic. Pioneer plants here are the annual hyper halophytes: *Atriplex fominii*, *Salicornia europaea*, *Suaeda arcuata*. Sometimes, a very large plant community on a salt swamp is established during the initial decade, but then it declines as the environment changes. The invasion of *Tamarix* spp. occurs in the early stage and endures for a comparatively long time. As a results, we can clearly notice belts of vegetation in the classified Satellite image using three channels and an NDVI channel of SPOT HRV. Plant succession along the process from a salt swamp to a dry land occurs according to the soil properties and other conditions. There are three main directions ; namely halophyte, meadow and psammophyte directions (Ogar 1995).

It is an astonishing fact that we can see vegetation even on the exsiccated sea bed in this extremely dry region. We must add, however, that we could not find any Saksawool which is the most important species for the environment.

8. Trade off relationship

Some ecologists do not recommend rice production in such arid areas. It is true in one sense, however, that rice requires almost the same habitat as *Phragmites* and rice production may be a natural land utilization. This means that rice paddies are in a trade off relationship

with natural wetlands. The NDVI images in summer from NOAA LAC show large irrigated farms and natural wetlands clearly, and prove that the area of irrigated farms reaches up to one sixth of the wetlands in the Ili River basin. The proportion is far smaller than that for the Aral region. This may be the main reason why the Balkhas area has fewer problems with cultivation, and in a sense, with the nature conservation of wetlands which is a treasure chest of wild life.

Wetlands conservation, revegetation of the Tsugai forest, and the Saksawool woodlands are needed for the restoration and the conservation of natural productivity and biodiversity in the arid desert areas of Middle Asia.

9. References

Kobayashi, T., Morimura, A., Temirbekov S. and Morimoto, Y. (1995), "Ecofunctional analysis of dryland vegetation - structure, mechanism and their changes", *Proc. of the Forum on Caspian, Aral and Dead Sea*, UNEP/IETC, 79-91

Morimoto, Y., Morimura, A., Kobayashi, T. and Ogar, N.(1995), "Vegetation dynamics in arid area of the Central Asia with special reference to the irrigation", Jour. Jap. Soc. Irrigation, Drainage and Reclamation Engineering, 64(10),1013-1016.(in Japanese)

Ogar, N. (1995), "Anthropogenic dynamics of vegetation of the Central Asia", *Proc. of the Forum on Caspian, Aral and Dead Sea*, UNEP/IETC, 73-78

Ohte, N., Oki, T. and Morimoto, Y., "A strategy for estimation of water budget in the Aral Sea basin by atmospheric water balance", *Proc. of the Forum on Caspian, Aral and Dead Sea*, UNEP/IETC, 101-113

Otsuki, K., Oue, H. and Tsutsui, H.(1996), "Climatological features and agricultural productivity in the Aral Sea Basin", *J. Jap. Soc. Irrigation, Drainage and Reclamation Engineering*, 64(10), 1007-1011.(in Japanese)

Plisak, R. P. and Ogar, N. (1989), "Productivity and structure of desert zone meadows", Alma-Ata, Nauka, pp. 186, (in Russian)

Watanabe, T., Ogino, Y., Takaishi, H. and Shimizu, K., "Irrigation management in paddy-based rotational cropping systems in the Aral Sea basin" , *J. Jap. Soc. Irrigation, Drainage and Reclamation Engineering*, 64(10), 1003-1006.(in Japanese)

Monitoring Reforestation in Northeast Thailand using the NETVIS

NAGATA Yoshikatsu(*), KONO Yasuyuki(**),
TAKEDA Shinya(***) and YOSHIDA Kengo(****)

*Media Center, Osaka City University
3-3-138, Sugimoto, Sumiyoshi, Osaka 558, Japan
Fax: +81-6-690-2736 / +81-6-605-3379
Email: nagata@media.osaka-cu.ac.jp
**Center for Southeast Asian Studies, Kyoto University
46 Shimo-adachi-cho, Yoshida, Sakyo, Kyoto 606-01, Japan
Fax: +81-75-753-7350
Email: kono@cseas.kyoto-u.ac.jp
***Faculty of Agriculture, Kyoto University
Oiwake-cho, Kita-shirakawa, Sakyo, Kyoto 606-01, Japan
Fax: +81-75-753-6372
Email: takedas@kais.kyoto-u.ac.jp
****Reforestation and Extension Project in the Northeast of Thailand (JICA-REX)
P.O.Box 81, Khon Kaen 40000, Thailand
Fax: +66-1-954-2539 / +66-43-370-061

Abstract

The area of forest in Northeast Thailand decreased by about 30% of the area of the region in 30 years from 1961. To prevent further loss of forest, many reforestation projects have progressed significantly in the last decade. However, forest areas estimated from satellite images continue to decline and do not reflect recent expansion of tree plantations. This is partly due to the difficulty of distinguishing newly planted forest land from idle land and upland fields by remote sensing.

This study aims at monitoring and mapping recent reforestation in Northeast Thailand based on the results of a questionnaire survey, available databases and national statistics, as a preparatory step to combining remote sensing technology with various types of field survey. NETVIS, an integrated GIS developed by the authors, which incorporates the Village Database and agricultural statistics as its primary data, is applied to this study.

1. Background

According to the statistics published by the Royal Forest Department (RFD), Thailand, the area of forest in Northeast Thailand decreased by about 30% of the area of the region in 30 years from 1961 (RFD, 1985; 1994). To prevent further loss of forest, many reforestation projects have progressed significantly in the last decade. Besides those run by the RFD, other governmental organizations such as the Community Development Department (CDD), the Department of Agricultural Extension (DOAE) and the Forestry Industry Organization (FIO) and NGOs typified

by the Population and Community Development Association (PDA) have their own projects (Akaha, 1994).

In recent years, in projects run by RFD alone, hundreds of millions of seedlings of various tree species have been distributed and planted every year in Northeast Thailand (Yoshida, 1996). However, forest areas estimated from satellite images continue to decline and do not reflect the new planting. This is partly due to the difficulty of distinguishing newly planted forest land from idle land and upland fields by remote sensing. Therefore, this study aims at monitoring and mapping recent reforestation in Northeast Thailand based on non-remote-sensing data, including results of a questionnaire survey, available databases and national statistics, as a preparatory step to combining remote sensing technology with various types of field survey.

2. Data Used

2.1 Questionnaire Survey

To collect information on the present status of tree plantation on private and public lands, a questionnaire survey was carried out in four provinces, Yasothon, Buriram, Maha Sarakham and Nong Bua Lamphu, from among nineteen provinces in Northeast Thailand in cooperation with the RFD and the REX (the Reforestation and Extension Project in the Northeast of Thailand). The questionnaire was distributed to every village headman in the four provinces at the beginning of June, 1996. It covered: 1) eucalyptus plantation as a whole, 2) eucalyptus plantation in the past five years, 3) eucalyptus forest cut last year, 4) tree plantation other than eucalyptus as a whole, and 5) tree plantation other than eucalyptus in the past five years. Each item had sub-items for a) public land, b) private land, and c) total. After filling out the questionnaire, village headmen sent it by mail to Maha Sarakham Nursery Center, one of four nursery centers of the REX, or brought it to a district office. Headmen were questionnaired in about 5,300 villages in total and about 23% of them replied.

2.2 Village Level Socio-economic Conditions

Village Databases (*Ko Cho Cho Song Kho*) for 1986, 1988, 1990 and 1992 were already incorporated in NETVIS and are referred to in this study. These databases cover a wide range of information, including basic information on population and households, infrastructure, production environment, education, and hygiene (Nagata, 1996a; 1996b).

3. Present Tree Plantation

3.1 Eucalyptus Plantations on Private Lands

The average area of eucalyptus plantations on private lands does not significantly differ between provinces and is presently 6 to 8 ha per village, of which 50% was planted during the last five years (1991 - 1995). Assuming that the average area of eucalyptus plantations per village is 6.4 ha (= 40 *rai*), the total area of eucalyptus plantations on private lands in Northeast Thailand is estimated to be 0.18 million ha, which is equal to 2% of the total agricultural land. Eucalyptus plantations

in the Northeast were mainly established from the mid-1980s, and thus their area increased by 0.2% of the total agricultural land per year during the last decade.

3.2 Non-eucalyptus Tree Stands on Private Lands

Areas of tree stands other than eucalyptus per village are 6 to 8 ha in Buriram and Maha Sarakham provinces and more than 16 ha in Yasothon and Nong Bua Lamphu Provinces. The area newly planted during the last five years does not differ significantly between provinces and is about 3 ha per village. Estimated areas of tree stands other than eucalyptus in the three provinces other than Nong Bua Lamphu in 1991 coincide closely with the areas of "fruit trees and tree crops" in *Agricultural Statistics of Thailand* (Office of Agricultural Economics).

3.3 Tree Stands on Public Lands

The average area of community forests in the four provinces is 24 ha, of which 4 ha was newly planted during the last five years, with half of newly planted trees being eucalyptus. It is remarkable that the average area of community forest in Yasothon is as large as 40 ha, of which 30% is recently planted eucalyptus.

4. Distribution of Eucalyptus Plantations

4.1 Method of Analysis

Two factors are hypothetically assumed to determine the distribution of eucalyptus plantations. These are land availability and labor availability. Land availability is assumed to be quantified in terms of the scale of cassava farm holding, because cassava is the dominant field crop in the Northeast and is in the process of being replaced by eucalyptus plantations. The questionnaire-surveyed districts are classified into three types based on the average scale of cassava farm holding: large (1.6 ha or over), medium (0.8 to 1.6 ha) and small (less than 0.8 ha). Labor availability is assumed to be quantified in terms of the proportion of the total labor population that is working away from the village. The districts are also classified into three types from this viewpoint: high (one-third or more), medium (one-fifth to one-third) and low (less than one-fifth). With these criteria, all the surveyed districts in the Northeast were classified into nine types, and the average area of eucalyptus plantations in each type was calculated.

4.2 Results

The results show a clear correlation between the area of eucalyptus plantations and the scale of cassava farm holding. Expansion of eucalyptus plantations is concentrated in areas with large cassava farm holdings. This indicates that many of the lands planted with eucalyptus were formerly cassava fields, and this trend is expected to continue in the future. On the other hand, no correlation can be found between eucalyptus plantation and labor availability. This indicates that there are various reasons why villagers work away from their home villages. A lack of diversity in local working opportunities is one reason for a high proportion of working away, because the proportion is comparatively high in areas of monoculture of rice.

5. Conclusions

The major conclusions of this study are 1) it is estimated that 2 % of agricultural land in Northeast Thailand is occupied by eucalyptus plantations at present; and 2) many of the present eucalyptus plantations occupy former cassava fields.

Remote sensing data is expected to provide more detailed information on reforestation, which could substantiate statistical analysis like that described here. If the technology to distinguish tree species becomes established, it will bring revolutionize every stage of the reforestation projects.

Acknowledgments

This study was supported by the REX project. We wish to express our gratitude to all the parties concerned.

Note

This report is a revised and combined edition of (Nagata *et al.*, 1996a) and (Nagata *et al.*, 1996b).

References

Akaha, Takeshi, 1994, "Study on Institutionalization of Collaborative Systems to Promote Social Forestry in Thailand" (in Japanese), *A Study on the Development of a System for Identification, Registration and Utilization of Specialists in Education Required for International Co-operation Volume 1*, pp. 127-248.

Nagata, Yoshikatsu, 1996a, "Development of the Northeast Thailand Village Information System (NETVIS) based on the Village Database" (in Japanese), *Theory and Applications of GIS*, 4(1), pp. 19-26.

Nagata, Yoshikatsu, 1996b, "Mapping the Village Database: The Spread of Economic Growth to Rural Areas of Northeast Thailand", *Southeast Asian Studies*, 33(4), pp. 138-156.

Nagata, Y.; Yoshida, K.; Takeda, S. and Kono, Y., 1996a, "Application of NETVIS to the Evaluation of a Reforestation Project in Northeast Thailand", *Proceedings of the 17th Asian Conference on Remote Sensing*, pp. E.3.1-6.

Nagata, Y.; Kono, Y.; Takeda, S.; Yoshida, K.; Monton J. and Somchai M., 1996b, "Monitoring and Mapping Reforestation in Northeast Thailand: An Application of the Northeast Thailand Village Information System (NETVIS)", *Proceedings of the FORTROP'96* (forthcoming).

Royal Forest Department (RFD), Thailand, 1985, *Forestry Statistics of Thailand 1985*.

Royal Forest Department (RFD), Thailand, 1994, *Forestry Statistics of Thailand 1994*.

Yoshida, Kengo, 1996, *Tohoku Tai Zorin Fukyu Keikaku 1996 Nendo Dai 2 Shihanki Gyomu Hokokusho (Progress Report of the REX Project, the Second Quarter of Fiscal Year 1996)* (in Japanese).

Human Dimensions in the Oases in the Arid Regions in China

Masatoshi YOSHINO
Institute of Geography
Aichi University
Toyohashi, Japan

1. Introduction

There are two directions of interaction between human activities and climatic environment in the arid regions. Namely, climates affect the human activities and in an opposite way, human activities do climatic environment. Desertification is one of the most typical phenomena among the problems related to these interactions.

Taking examples in the Taklimakan desert in Xinjiang, China, the present paper deals with the present conditions of human dimensions clarified by the fieldwork since 1990 and by analyzing statistical data published. The study area is given in Fig. 1. The wind and rain conditions were discussed elsewhere (Yoshino 1992).

2. Method of study

For the field work, we did interview with farmers in the Hotan and Qira oasis in the southern part of the Taklimakan desert and Korla, Aksu and Kasi in the northern and western parts. Items of interview question were: family construction, house plan, cultivation area, crop calendar, harvest and production, income, irrigation, ground water, living water demand, side work, wind damage, counter measure for desertification, fuel collection etc. The results were printed in publications by the Institute of Geography, Aichi University in Japanese. The analyzed results were published elsewhere (Yoshino, et al., 1994, 1995).

Statistical values were obtained from the officially published tables in Annual Report for 1985-1991.

3. Present status of Humam Activities

Main results obtained are as follows: (a) Annual gross production is 87-108 US dollar per head in the oasis in the Hotan and Cela regions, the southern part of the Taklimakan desert, which is 60-80% of the northern part. (b) Farmers are living in

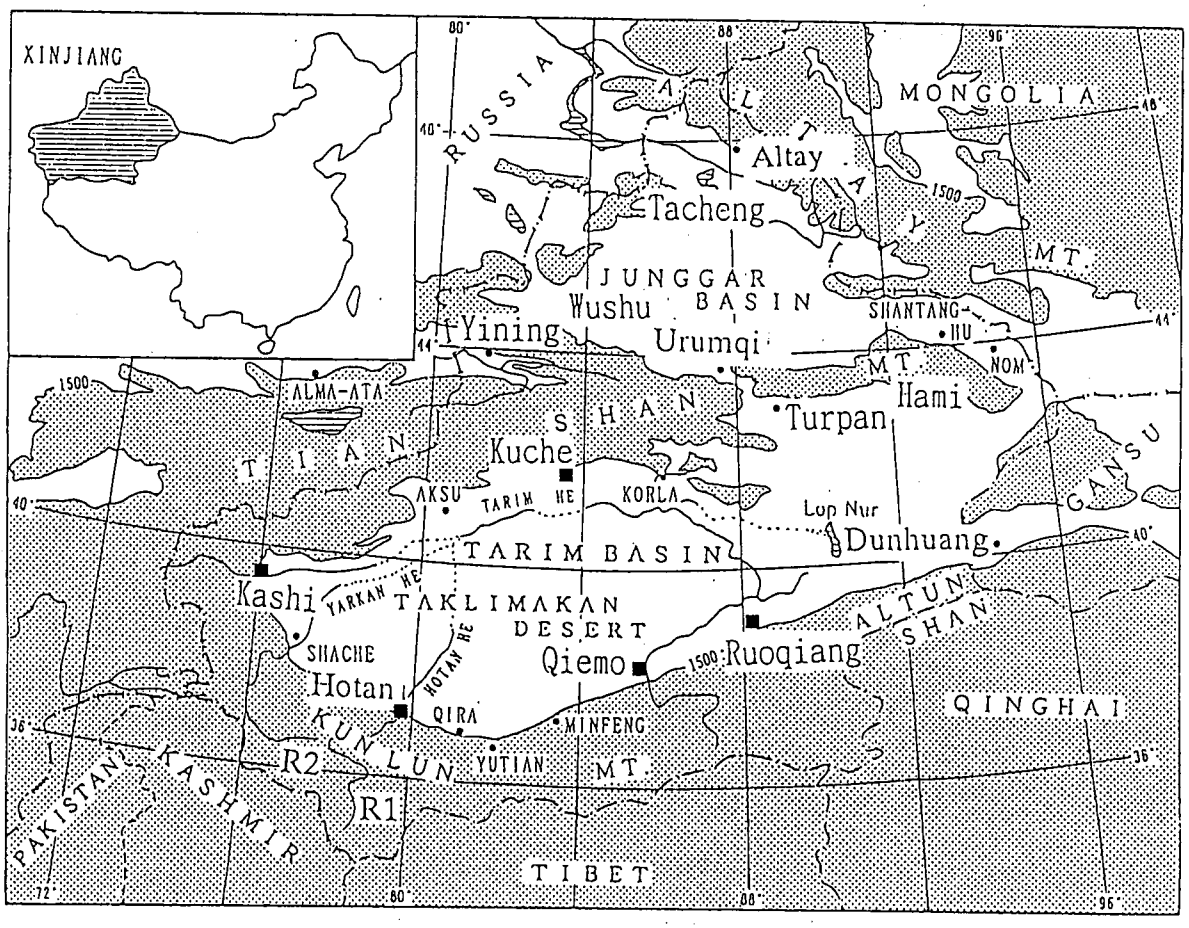

Fig. 1 Sketch map of study region and names of observation stations and oases.

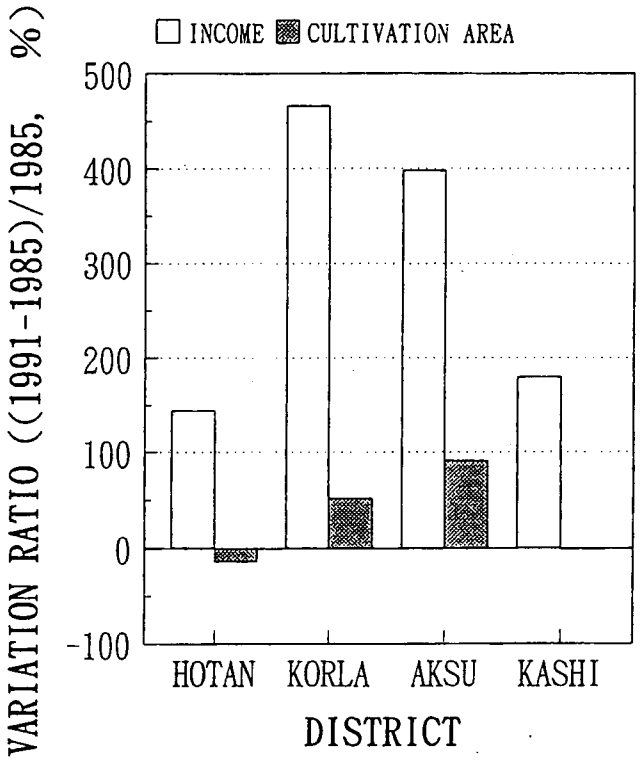

Fig. 2 Variation of farmers' income and the area of cultivation per person from 1985 to 1991 (expressed as (value of 1991 - value of 1985) / (value of 1985) × 100%).

most cases with old parents and several childrens. (c) The area of cultivated fields, houses and gardens is 9.6a per head. In the case of the interview farmers, the average is 58.0a per family. (d) The income and cultivation area in the northern and the southern parts of oases are given in Fig. 2. There are striking differences. (e) Corn, wheat, and cotton are main crops. Fruits such as grapes, apricots, peaches, jujubes, figs, and pomegranate are dominating. (f) Irrigation water is going to shortage particularly in spring. In such case, ground water is used. (g) Increase of population results in increasing demand of food and further expansion of cultivated area. But, the water amount needed has mostly reached the upper boundary. (h) Fuel consumption types are; i: materials of fire woods collected from desert for all season, ii: woods in summer, but coal in winter, and iii: coal for all season. Farmers with good income by side works can buy coal and use coal for all season. (i) Farmers go into the desert, for collecting fire woods by donkey-coaches. In the maximum case, they travel — from the oases to the places apart 125-135km. (j) Wind damage on wheat is serious in spring. Sand storms cause eye disease and lungs disease. (k) Carpet production is good side work. Annual production is 1,200-4,000 yuan per one worker. (l) In the northern part of the desert, there found no serious desertification. (m) Salinization is serious in the northern part, because they utilize enough water for irrigation.

4. Climatic Conditions

The climate in the arid regions in China has been changing. Surface air temperature has increased by 2℃ or more in winter during the last 40 years. On the other hand, it has decreased by about 1℃ in summer. Therefore, annual range decreased significantly. Precipitation has increased by 5-100% in summer, although the annual amount does not show any systematic trend as a whole. Figure 3 shows the tendencies as given for the Taklimakan desert, which is an average value obtained at five stations at Kuqa, Kashi, Hotan, Qiemo and Ruoqiang(Du et al., 1996).

The increase of air temperature at the ground surface level in winter is probably due to the effect of global change. It is suggested, however, that the causes for the increase in precipitation and the decrease in air temperature in summer are to be both the global change effect and the local environmental change, due to expansion of areas of oases, increase and grown-up of windbreak forests. That is: local environmental change is probably the main cause.

The effect of oases in Turpan (Du et al., 1994) on the diurnal change of air temperature is striking as shown in Fig. 4. In July, daily maximum and minimum air temperatures are higher and occur earlier in the desert than in the oasis. But in December, daily maximum and minimum air temperatures are lower and earlier in the desert than in the oasis. This means "oasis effect" is very clear: (i) cool in

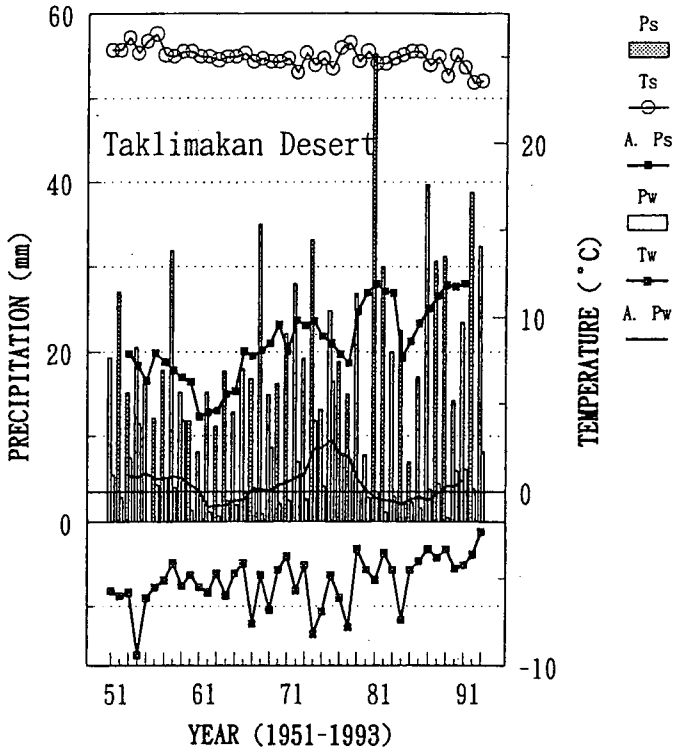

Fig. 3 Comparison of 5 years means of annual variation of temperature and precipitation in the Taklimakan desert (mean of 5 stations) between 1975-1979 and 1989-1993.

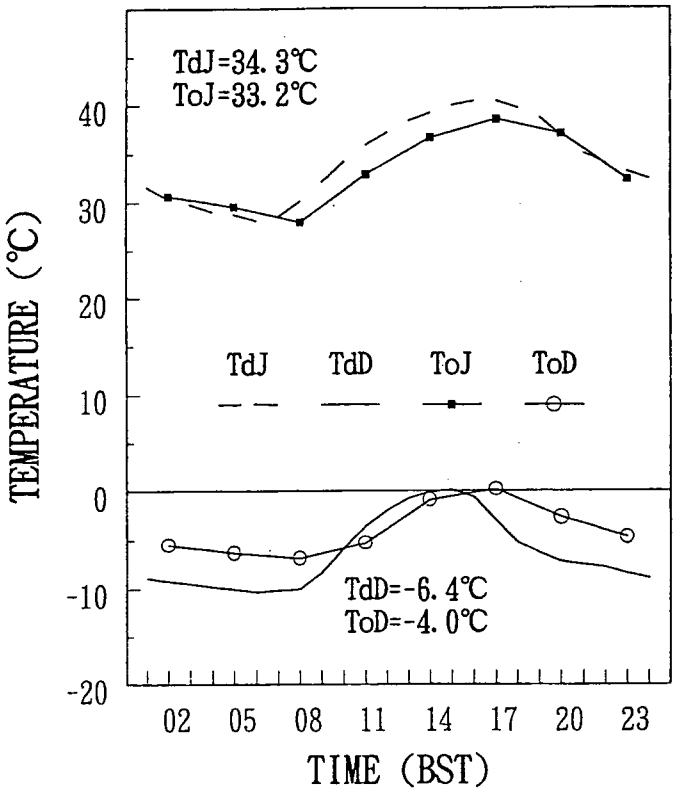

Fig. 4 Comparison of monthly mean diurnal variations of air temperature between an oasis (o) and desert (d) in Turpan, China, for July and December.

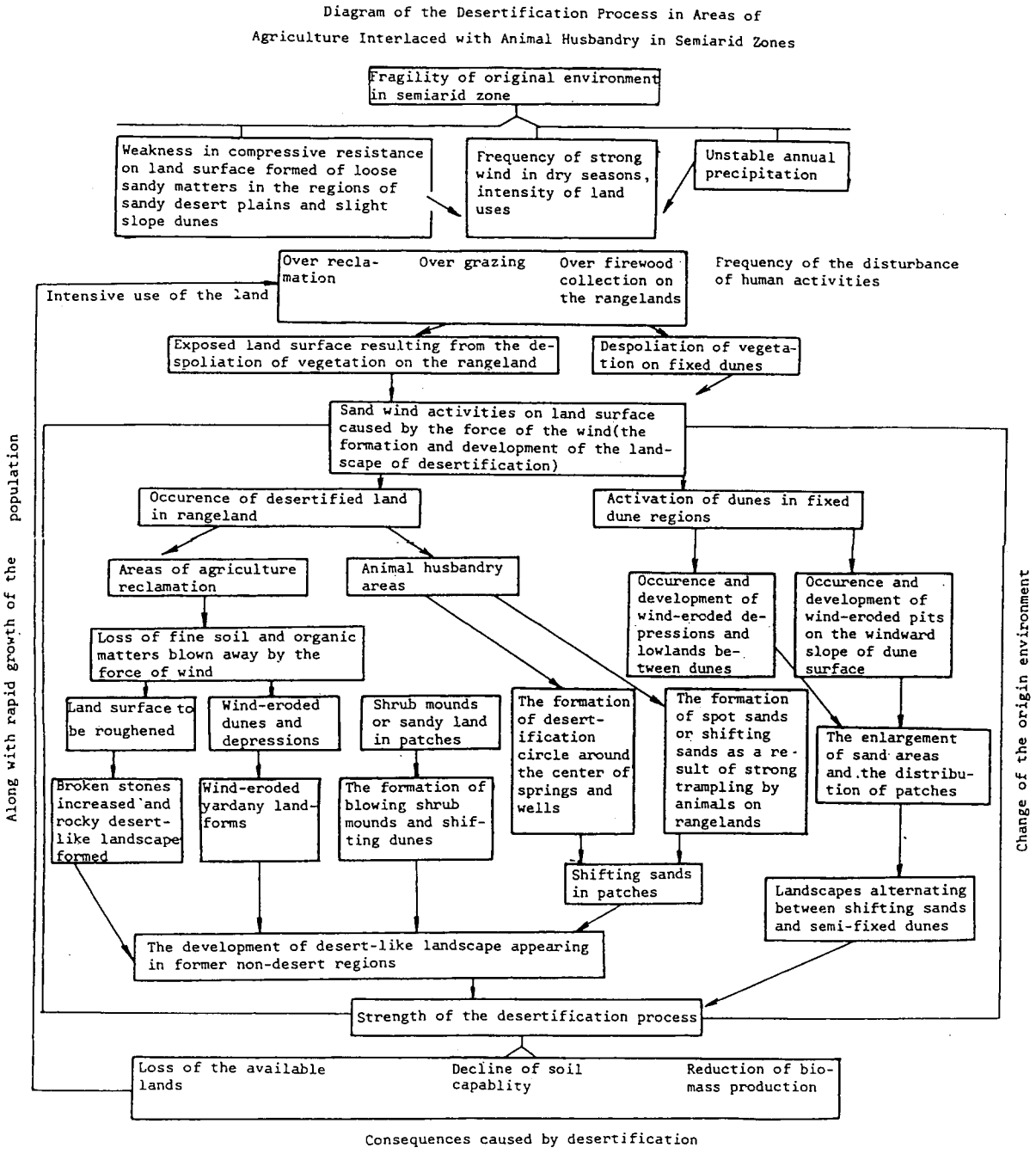

Fig. 5 Diagram of desertification processes in agricultural areas interplaced with animal husbandry in semiarid zone in China (Zhu, et al., 1994).

summer and warm in winter and (ii) the delayed occurrence of maximum and minimum in the oasis.

5. Desertification Processes

Desertification Processes are very complicate and are different place to piace and region to region in accordance with the related causes. For example, Zhu et al.(1994) has presented a diagram, as given in Fig. 5, on the desertification processes in agricultural areas interplaced with animal husbandry in the remiarid segions in China. It is stressed that the rapid growth of population in the region plays an important srole as written on the left side of the diagram.

In conclusion, the whole regional plan is needed to development, considering food demand caused by populetion increase, which results in the increase of cultivation fields and water demand in the oases. Also, economically, income of farmers should be increased.

References

Du, M.-y. et al.(1994): Climatic differences between an oasis and its peripheral area in Turpan Basin, Xinjiang, China. JIRCAS Jour., (1), 47-55.

Du, M.-y. et al.(1996): Climate change and agricultural activities in the Taklimakan Desert, China, in recent years. Jour. Arid Land Studies, 5, 173-183.

Yoshino, M. (1992): Wind and rain in the desert region of Xinjiang, Northwest China. Erdkunde(Bonn), 46, 203-216.

Yoshino, M. et al.(1994): Agricultural activities of Uygur farmers in Hotan and Qira on the southern part of Taklimakan Desert. Jour. Arid Land Studies, 3, 125-135 (in Japanese with Engl. Abstr.).

Yoshino, M. et al.(1995): Impact of agricultural landuse on desertification in the Taklimakan Desert. Jour. Arid Land Studies, 5, 107-115 (in Japanese with Engl. Abstr.).

Zhu, Z.-d. et al.(1994): Sandy desertification in China. Science Press, Beijing, 250p. (in Chinese)

ASSESSING DESERTIFICATION IN ARID AUSTRALIA USING SATELLITE DATA

Gary Bastin and Vanessa Chewings, CSIRO Division of Wildlife and Ecology,
PO Box 2111, Alice Springs, NT 0871, Australia

ABSTRACT

Large paddock size, complex vegetation patterns and variable rainfall combine to make assessment of grazing impact difficult in Australia's arid and semi-arid lands. Satellite data are useful in separating adverse grazing effects on vegetation cover from that caused by spatial and seasonal variability. Grazing is focussed on watering points and cover varies systematically with distance from water to produce a "grazing gradient". After good rains, vegetation cover is fully restored close to watering points if landscapes are not degraded while the persistence of a gradient indicates land degradation or desertification. Two operational methods for objectively determining desertification over large areas are illustrated. We also show how the results of analysing satellite data can be effectively verified with airborne video data.

INTRODUCTION

Australia's arid and semi-arid lands (the rangelands) occupy 75% of the mainland, some six million sq. kms. Of this area 58% (3.48 million sq. kms) is grazed by sheep and cattle as commercial livestock enterprises. Individual landholdings (sheep and cattle ranches) range in size from hundreds to thousands of sq. kms.

Ranches are fenced into a few, to many, paddocks; the paddock being the individual management entity. Paddocks may contain several sources of drinking water for livestock (i.e. watering points) and because animals must return regularly to these water sources to drink, grazing activity tends to be concentrated around water. Areas further from watering points are grazed less intensively and less often. However, livestock do not exhibit a simple radial pattern of decreasing grazing usage with increasing distance from watering points because their grazing activity is also influenced by the palatability of available forage (Low *et al.*, 1981). Large paddocks generally contain several different vegetation communities, each community having a different preference for livestock because of the suite of species present. The hierarchy of grazing use amongst vegetation communities may change as rainfall alters the relative attractiveness of the different plant species present.

The arid rangelands of central Australia have a highly variable rainfall and droughts are frequent. Vegetation growth responds to infrequent rainfall events as a pulse where, depending on the timing and size of the event, growth peaks and then declines as moisture again becomes limiting (e.g. Noy-Meir, 1973). The growth pulse following each rainfall event is of considerable importance because it determines the amount of forage available for grazing by livestock, often for some months. It also presents major opportunities for plant reproduction, growth and recruitment. Land managers (pastoralists) thus face a difficult task in matching animal numbers to forage availability resulting from erratic rainfall. They must also ensure that favoured grazing areas in the large and spatially complex paddocks are not damaged by over-utilisation.

DESERTIFICATION

Desertification is essentially a human rather than a physical problem and occurs when land use exceeds land capability. Methods that seek to assess the extent of desertification must therefore be specific to land use. In the rangelands, desertification caused by excessive levels of grazing can involve adverse changes in the species composition of pasture, loss of vegetation cover in some areas leading to accelerated erosion, and replacement of herbage species by unpalatable trees and woody shrubs in other areas. All processes result in a decline in grazing productivity.

Ground-based assessment of desertification usually involves a trade-off between approximate methods, which give broad spatial coverage but are subjective and non-repeatable, and precise methods which only apply to very small areas and are not representative of diverse landscapes. Satellite data, which are available for whole regions and have frequent coverage, offer the opportunity of objective and repeatable information. However traditional definitions of desertification, such as extent of rill and gully erosion or adverse changes in the species composition of vegetation, cannot easily be used to assess the extent and severity of desertification using remotely-sensed data. New criteria must therefore be developed based on surrogate indicators (Pickup *et al.*, 1994).

Spectral indicators of desertification

The low spatial resolution of satellite data means that it is generally not possible to detect and measure small features in the landscape such as rills and gullies. Nor is it possible to detect the mix of plant species present at a site, or change in species composition over time. However, the spectral contrast between bare soil and vegetation or different levels of vegetation cover at the scale of whole landscapes can be used to develop surrogate measures of desertification. Examples of the distribution of bare soil and vegetation in spectral space as measured by a truck-mounted radiometer are shown in Figure 1. This figure shows a clear separation between bare soil and vegetated targets in the parallelogram which makes up the visible-green / visible-red data space. There is also no obvious separation between dry and green vegetation when measured in terms of perpendicular distance from the soil line represented by bare targets at the top of the data space. This means that at the scale of both Landsat MSS and TM pixels, perpendicular distance from the soil line provides an index of both dry and green vegetation cover. The PD54 index (Pickup *et al.*, 1993) uses this principle and provides estimates of vegetation cover which correlate well with ground measures of cover (in the range r=0.8-0.9). The procedure for calculating the PD54 index is shown schematically in Figure 2.

Combining spectral indicators with spatial and temporal information

In the large paddocks of Australia's arid rangelands, free-ranging cattle return to sources of drinking water every one to three days. This spatially predictable aspect of grazing behaviour can be used as a partial solution to the problem of separating natural change in the vegetation from that caused by desertification. Vegetation cover typically decreases towards watering points to produce a "grazing gradient" (Pickup 1989). This concept is depicted as the lower solid line in Figure 3. Cover increases after significant rainfall and, where cover in the vicinity of watering points is fully restored to those levels present at some distance from water (upper line in Figure 3), grazing effects are temporary and no long term damage has occurred. However, where the gradient persists (dashed line - Figure 3), then some form of damage has

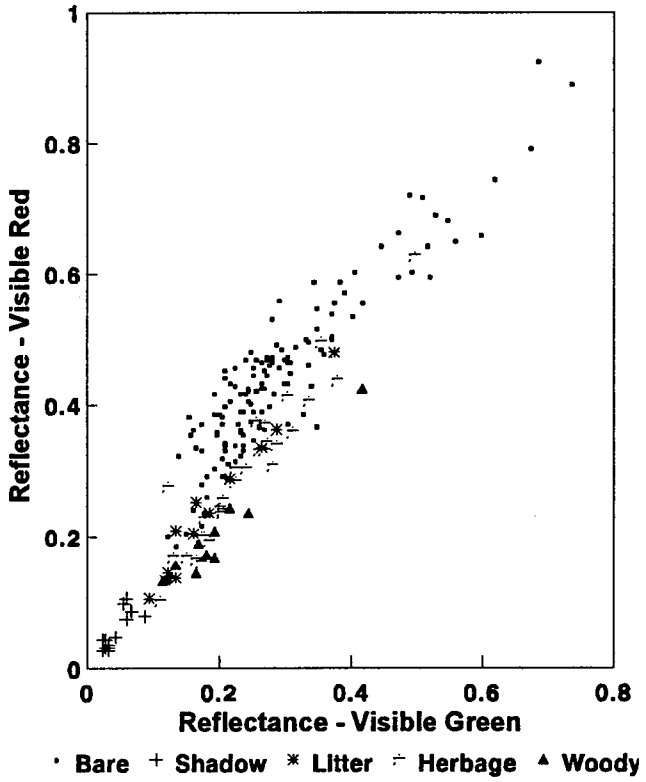

Figure 1. Truck-mounted Exatech radiometer data in the visible-green and visible-red spectral bands showing the structure of the bare soil-vegetation data space. (Figure adapted from Pickup *et al.*, 1993.)

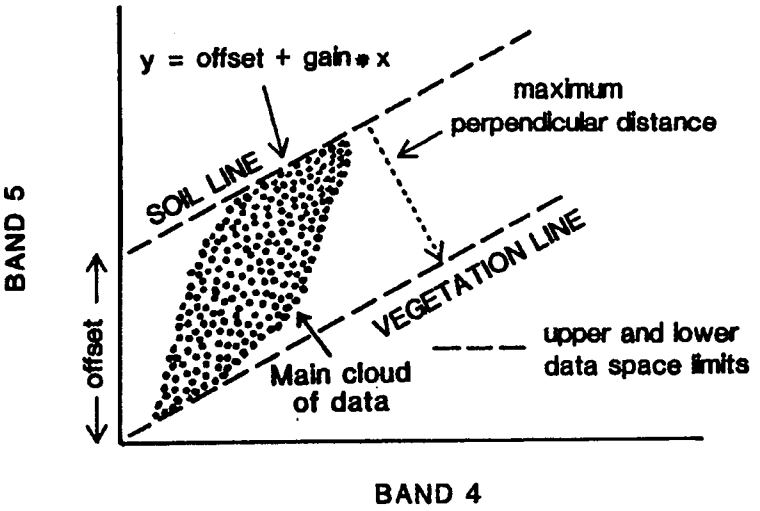

Figure 2. Parameters used to describe the Landsat MSS Band 4-Band 5 data space and to derive the PD54 index. (Figure adapted from Pickup *et al.*, 1993.)

occurred. We thus define desertification in the arid rangelands as *a grazing-induced reduction in the amount of vegetation cover likely to be present after the best growth conditions experienced in a reasonable time* (Bastin *et al.*, 1993).

GRAZING GRADIENT ANALYSIS

Grazing gradients are detected at the paddock scale by calculating average cover levels at increasing distance from watering points. This can be done by radiometrically standardising dry and wet period satellite data, calculating the PD54 index of vegetation cover from the

visible-green and visible-red spectral bands and incorporating spatial information which controls grazing behaviour. Such information includes the locations of fences and natural barriers (e.g. mountains) which form paddocks, distance from watering points and the boundaries of vegetation communities which influence grazing preference. We call this form of grazing gradient analysis the **wet period average cover** (WPAC) method. A variant of this approach, the **resilience method** (RM), is used to produce an image showing where vegetation response to rainfall is above or below that which might be expected given little or no grazing impact (Bastin *et al.*, 1996). Below-expected response often results from desertification and can be indicative of low productivity in the long term. Above-expected response indicates a resilient landscape which may be in good condition, recovers well from defoliation by grazing and is likely to be productive.

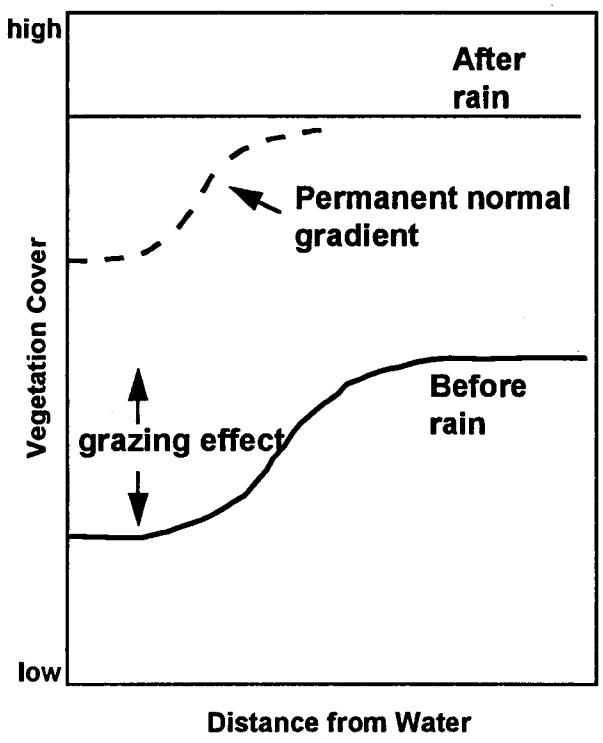

Figure 3. A normal grazing gradient. Vegetation cover increases with distance from water in the dry-period (solid line). Cover is either fully restored close to water after rain (horizontal line) or a permanent gradient (dashed line) is maintained.

Wet period average cover method

The wet period average cover method has been used to determine the extent of desertification attributable to grazing across 38,000 sq. km. of central Australia (Bastin *et al.*, 1993). Three characteristic patterns emerge where gradients are present: the normal gradient, the composite gradient and the inverse gradient. Typical examples of these patterns are shown in Figure 4. Normal gradients involve a progressive increase in average cover with distance from watering points. In some instances the gradient disappears after substantial rainfall indicating that the grazing effect is temporary. In the most degraded situations, the gradient often persists for between four and ten km from water. These persistent gradients are generally associated with the most preferred vegetation communities that have had an extended period of heavy grazing. These areas are often intensively grazed to the point where all edible forage is removed at times. Reduced cover results in increased runoff and erosion producing a less favourable soil environment and less moisture for pasture re-establishment following rain. Landscapes with

less erodible sandy soils tend to be less permanently affected by grazing. Soil disturbance by trampling adjacent to watering points may enhance rainfall infiltration while the accumulation of livestock excreta marginally increases soil nutrient availability. This produces increased growth of unpalatable ephemeral herbaceous species and the composite wet-period response depicted in Figure 4. Inverse gradients are generally associated with dams in areas of predominantly woody vegetation. These areas receive additional runon water following good rains, are prone to shrub increase and have a greatly reduced supply of palatable forage (Friedel *et al.*, 1990). Grazing animals are forced to forage further from water producing the inverse dry-period gradient of Figure 4. Vegetation may fully recover across the entire area of the vegetation community following rain or it may always remain higher in the vicinity of watering points. Landscapes with very little palatable forage are relatively unaffected by grazing and often have no discernible gradient in vegetation cover with distance from water.

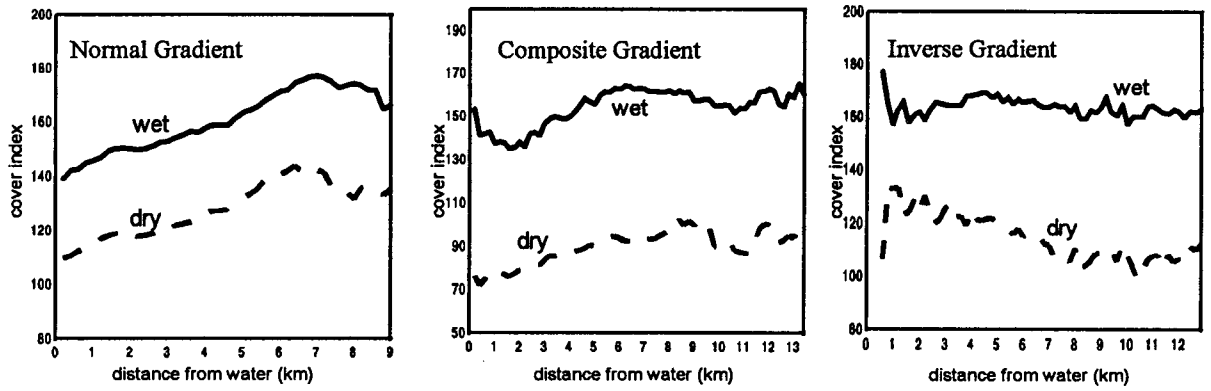

Figure 4. Examples of typical dry- and wet-period grazing-gradient types obtained from the analysis of Landsat MSS data across 38,000 sq km of arid rangeland grazed by cattle in central Australia. The cover index is the PD54 index of Pickup *et al.* (1993).

Resilience method

While WPAC is suitable for describing the state of a whole vegetation community, it provides no information on the location of areas with above- or below-average vegetation growth, apart from their distance from watering points. The resilience method can handle this problem of location-specific data. In keeping with local variability caused by moisture redistribution, soil differences, past grazing, etc., each location should have an expected response to rainfall (Pickup *et al.*, 1994) which represents behaviour in an ungrazed or sustainably-grazed situation. Observed response can be compared with expected response and areas which are below acceptable limits identified and mapped. The difference between observed and expected response then provides a measure of the resilience of the vegetation community.

Expected cover response is calculated as a linear regression between initial (dry-period) cover class and cover response following a major rainfall. Because cover response is partly dependent on the initial cover level (i.e. cover can increase only marginally where initial cover is high), residuals from the regression are scaled by the variance of cover response stratified with respect to initial cover.

The resilience image for the vegetation present on calcareous soils in a paddock following approximately 300 mm of rainfall in March 1989 is shown in Figure 5. Areas showing good vegetation response (i.e. darker appearance) are in better condition. Country surrounding a new water supply added midway along the northern fence in 1982 had some of the best response seven years later; evidence that until 1989 at least, this part of the paddock had been sustainably grazed. Conversely, some of the poorest response is concentrated in the south west portion of this 217 sq. km paddock - around a large dam which, for many years, was the main water supply in the paddock. Correspondingly, the "island" of calcareous country east of this dam is relatively remote from water and shows no adverse effects of grazing. Below-average response of vegetation south west of this main water supply may have occurred for a number of reasons. The most likely explanation is that this area is badly infested with rabbits and they have severely degraded the pasture.

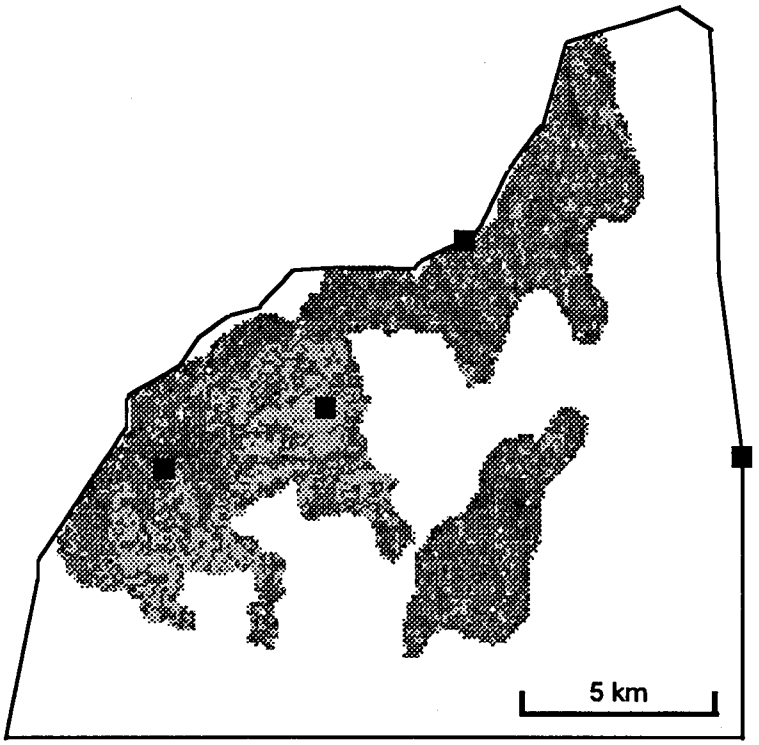

Figure 5. Resilience image of a calcareous landscape using February 1988 (dry period) and May 1989 (wet period) PD54 data. Cover response varies from bright, indicating poor response, through grey to dark which indicates the best response. The locations of watering points are indicated by solid squares. White areas represent less preferred grazing areas within the paddock. The resilience values of these areas are not shown so as to improve the clarity of the figure.

The resilience image can be compared with aerial photographs and verified in the field. The information portrayed is useful for paddock management because it suggests where further development (e.g. fencing or water reticulation) and reclamation activity are best directed. In this example (Figure 5), increased livestock production could result from shifting grazing pressure onto lightly grazed country to the east of the main watering point. This adjustment could be achieved by reticulating water through a pipeline. Reducing stock numbers in specific areas combined with rabbit control and suitable land reclamation techniques should assist the degraded country to improve in productivity. In the longer term, images can be produced following future good rains in an entirely repeatable manner and the output used to assist in determining the extent of desertification under continued, or changed, grazing management practices.

VERIFYING ANALYSES OF SATELLITE DATA USING VIDEOGRAPHY

Ground truthing of satellite data using conventional ground-based vegetation survey techniques is very difficult given the spatial complexity of the large areas commonly assessed. To reduce this problem, we have developed an airborne videography capability. This consists of four cameras, each fitted with a different filter in bands similar to the visible and near-infrared channels of the main remote-sensing satellites. The cameras are mounted in a frame in a small aircraft and frames are grabbed directly to the hard disk of a computer. Images are corrected to remove the effects of spatial distortion and differential illumination (Pickup *et al.*, 1995) and are then analysed using standard image processing techniques to produce estimates of vegetation cover.

Using image classification, we have found good agreement between the video data and estimates of vegetation and soil components made on the ground (Figure 6). Agreement is highest when categories of interest are spectrally distinct in each video image. In video data at coarser pixel resolutions, obtained by flying higher, we have used the PD54 index to estimate vegetation cover. We have then been able to compare this measure of vegetation cover with that derived from contemporaneous Landsat TM data processed to produce the same (PD54) index of cover. Figure 7 illustrates an example of good agreement in vegetation cover obtained from the two data sources for a highly patterned area of floodplain in central Australia.

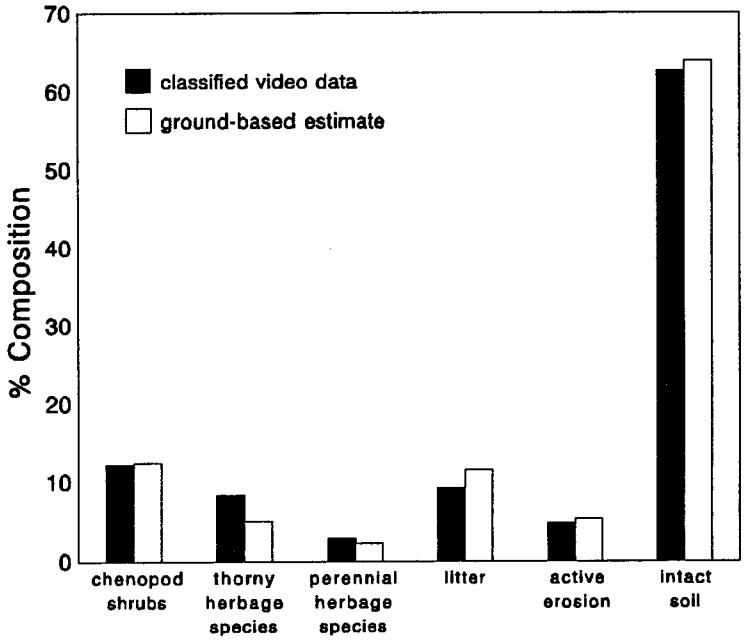

Figure 6. Comparison of percentage cover categories obtained from classified video data with ground-based measurement for a floodplain site in central Australia.

Based on these results we are confident that aerial videography can largely replace conventional ground-survey techniques in verifying satellite data. We are now routinely using the video system to acquire imagery at a range of pixel resolutions. These data are either classified or processed to the PD54 index to produce estimates of vegetation cover on what is often spatially complex landscapes. In this way, we are progressively verifying the results of our grazing gradient analyses made over extensive areas in central Australia.

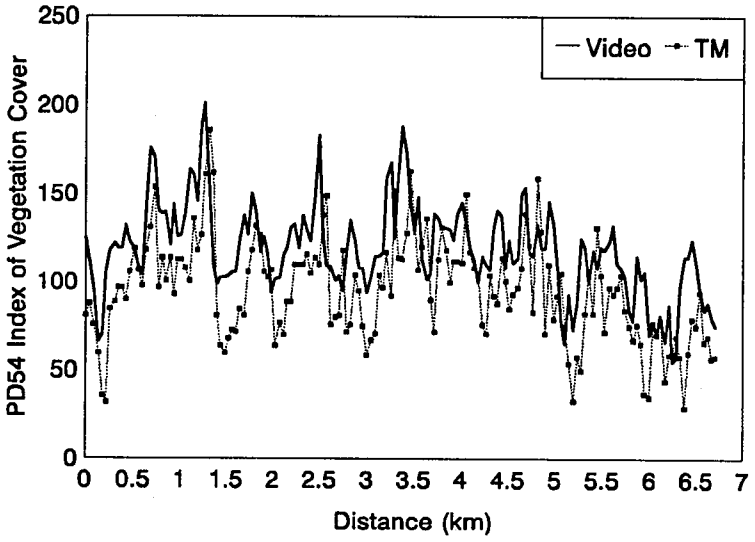

Figure 7. Comparison of PD54 cover index values derived from contemporaneous and co-registered Landsat TM and video data for a floodplain vegetation community. The video data were acquired at 1 m pixel resolution and resampled to 30 m. Higher PD54 values indicate higher cover up to a maximum of 254 (note that the two data types have not been calibrated to each other).

REFERENCES

Bastin, G.N., Pickup, G., Chewings, V.H. and Pearce, G. (1993). Land degradation assessment in central Australia using a grazing gradient method. *The Rangeland Journal*, **15**: 190-216.

Bastin, G.N., Pickup, G. Stanes, J. and Stanes, A. (1996). Estimating landscape resilience from satellite data and its application to pastoral land management. *The Rangeland Journal*, **18**: 118-135.

Friedel, M.H., Foran, B.D. and Stafford Smith, D.M. (1990). Where the creeks run dry and ten feet high: pastoral management in arid Australia. *Proceedings of the Ecological Society of Australia*, **16**: 185-191.

Low, W.A., Dudzinski, M.L. and Müller, W.J. (1981). The influence of forage and climatic conditions on range community preference of Shorthorn cattle in central Australia. *Journal of Applied Ecology*, **18**: 11-26.

Noy-Meir, I. (1973). Desert ecosystems: environment and producers. *Annual Review of Ecology and Systems*, **4**: 25-51.

Pickup, G. (1989). New land degradation survey techniques for arid Australia - problems and prospects. *Australian Rangeland Journal*, **11**: 74-82.

Pickup, G., Bastin, G.N. and Chewings, V.H. (1994). Remote sensing-based condition assessment for non-equilibrium rangelands under large-scale commercial grazing. *Ecological Applications*, **4**: 497-517.

Pickup, G., Chewings, V.H. and Nelson, D.J. (1993). Estimating changes in vegetation cover over time in arid rangelands using Landsat MSS data. *Remote Sensing of Environment*, **43**: 243-263.

Pickup, G., Bastin, G.N., Chewings, V.H. and Pearce, G. 1995. Correction and classification procedures for assessing rangeland vegetation cover with airborne video data. *Proceedings 15th Biennial Workshop on Videography and Colour Photography in Resource Assessment* (Terre Haute, Indiana, May 1-3, 1995). American Society for Photogrammetry and Remote Sensing, Bethesda, MD. pp. 305-314.

Dynamic Monitoring To Changes Of Land Utilization And Land Covering In Xinjiang

Han Delin

Xinjiang Institute of Geography, Urumqi, China 830011
Fax: 86—991—3835459
Email: XJGI@MS.XJB.AC.CN

Abstract

Xinjiang is a typical arid region with a large area of land. Because of the complexity and diversity of natural conditions, land utilization and land covering situations change diversely. There are three main land utilization types as mountain, desert and oasis utilization. Grassland utilization is the main part and agricultural utilization of oasis land is the most important type. Under poor management, the benifits of land utilization are also poor and land degradation, such as desertification, secondary salinization and swampiness, is serious. The changes of land covering are affected by population, human activities, regulation and distribution of water resources, selection and adjustment of land utilization trends, social and economic factors, etc. The remote—sensing technique could be used in the investigation, analysis and monitoring of grassland and forests in mountains, of oasis scale and its evolution, of environmental changes of plain water, of vegetation changes on the transition belt between oases and deserts, and of development of soil salinization and swampiness in oases.

Locating in the hinterland of Asia— Europe Continent, Xinjiang is a typical arid region with the annual precipitation of 154 mm and the annual evaporation of 2000 mm to 3000 mm. Because of complexity and diversity of natural conditions in the large area, the land utilization types are also abundant and diverse. The study of land utilization and land covering in Xinjiang concerns with the environmental study very much. The remote—sensing technique is an effective means in the study of current situations and changes of land utilization and land covering.

1. The Current Characteristics of Land Utilization in Xinjiang

1.1 There are three, as mountain, desert and oasis, utilization systems

The geographical system in the arid area of Xinjiang consists of three sub—systems as mountains, deserts and oases. Under the influence of people's long—term exploitation and management to such a system, three main types of land utilization have been established. Mountains, including hills, take up about 39% of total land area and are the forming area of glaciers, snows and other water resources. They are mainly used for grassland herbing and forest cutting. Plain deserts, including both deserts and gobis, take up 57% of total land area and are mainly used for herbing and mineral resource exploitation. Surrounded by deserts, oases take up only 4% of the total land area but are not only densely—populated and resource—consuming areas, but also bases for production and human living. The land in oases is mainly used for agriculture, towns, country resedential areas and special purposes.

1.2 Grassland utilization is the main part while agricultural uses of oasis land are the most important type

Calculated according to utilized area, the grassland utilization for herbing is the main land utilization type in Xinjiang. Among the 0.57×10^8 ha grassland resource, there are 0.48×10^8 ha grassland which could be used for herbing and grass cutting, taking up 84.2% of total grassland area and 72.7% of the land being used. But considered according to values and benifits, land utilization in oases, especially land used for agricultural purposes, which takes up about 60% of oasis land, is the most important type. While utilized land in oases only takes up 10% of total used land, it produces more than 90% of total economic benifits.

1.3 With irrational exploitation and utilization, total outputs and benifits are low

Four—season nomadic herbing, which has been lasting for thousands of years, is a typical backward land— utilization manner with poor livestock —producing capacity. Averagely, 1 head of livestock needs as much as 1.3 ha to 1.7 ha nat-

ural grassland to survive. With almost no artificial input, 1 ha grassland could only produce an annual output valued 100 to 150 Chinese Yuan. The intensity of land utilization is relatively high in oases. But the input to farmland is insufficient and land management is rather poor. So the average density of output value, which is the ratio of total output value to the area of land that is being used, is still rather low. In 1995, it is only 160 Chinese Yuan per hectre. Averagely, the net economic benifit of farmlands is only 3, 000 Chinese Yuan.

1. 4 **Land degradation, such as desertification and secondary salinization , is very serious**

Due to people's irrational exploitation and utilization and the fragility of ecological environment, there are some serious land degradation problems, such as desertification, secondary salinization, swampiness, soil sterilization, grassland degradation, lake shrinkage and lake water salinization. For example, 30% of farmland is with varying degrees of salinization in oases. Since 1950s, the farmland abandoned because of desertification has reached up to 60×10^4 ha in oases.

2. The Trends of Land Utilization Changes

The factors which result in the changes of land utilization include population growth, human activities and their intensity, spatial and departmental distribution of water resources, adjustment of economic structure, administrative systems and policies, scientific and technological progresses, and economic development. The coming trends of land utilization changes in Xinjiang are as follows: (1) The scale of land reclamation will extend periodically. So farmlands and oases will expand continually and grasslands will decrease. Meanwhile, the intensity of water utilization will increase . As a result, the ecological quality and lake environment in the lower reaches of rivers will continue to change unfavorablly. (2) the changes of precipitation in mountains, which will occur as the response to global climatic changes, and the increase of herbing intensity will result in the further degradation of mountain grassland. But if the construction of artificial forage bases in plains is strengthed and the producing potentiality of livestock husbandry in oases is brought into full play, the degradation of mountain and desert grasslands could be delayed. Furthermore, if the herbing activity is scientific, the quality of natural grasslands even could be improved. (3) With

the acceleration of urbanization, the land used by cities and towns will continually expand and more farmlands will be occupied. (4) With the development of industries and mining industries, the land share of industries will increase. (5) To strengthen the construction of oases, the land used for ecological purposes will remarkably expand.

3. The Investigation and monitoring of land utilization and land covering with remote sensing techniques

As a reaction to global changes, the changes of land utilization and land covering are a dynamic process. The changes of grasslands, oases and plain waters are an important symbol of land covering changes. Xinjiang is very large and has diverse land utilization and land covering types . To find out and understand the changing situations of land utilization, remote sensing methods must be used. And the investigation and monitoring of land covering changes with the remote sensing methods should be pursued in some typical areas. The main contents should include:

. Investigation of grasslands and forests in mountains with remote sensing techniques.

. Dynamic monitoring of the formation, scale and evolution of oases with remote sensing techniques.

. Analysis of remote sensing data for plain water environment.

. Analysis of remote sensing data for desert vegetation and desertifying situations in oasis—desert transition belts.

. Investigation of soil salinization and swampiness in oases with remote sensing techniques.

REMOTE SENSING OF COASTLINES IN SEMI-ARID ENVIRONMENT IN SOUTHERN ARABIAN GULF

A.S.Alsharhan
Faculty of Science, United Arab Emirates University
P.O.Box:17551, Al Ain, U.A.E.

Different remote sensing technologies are presently used to map and assess coastlines in semi-arid environments in southern Arabian Gulf along the United Arab Emirates(UAE) coast. The lagoonal and coastal system has been classified and mapped for its bathymetric and geologic features using digital image processing technique. Dune ridges, alluvial fans, sbkha flats, algal mat beds, and mangroves associated with the tidal flats were identified and differentiated on a Landsat Thematic Mapper(TM) scene of the region.

The shallow subtidal to supratidal environments of the UAE coastal system have been extensively studied and is characterized by numerous sub-environments within the shallow subtidal, intertidal and supratidal zones. This semi-arid carbonate coastline and immediate offshore area of UAE are an important modern example of a complex interplay between carbonates, siliciclastics and evaporites and characterized by complex sedimentation along the Abu Dhabi coast is strongly influenced by an offshore barrier system oriented obliquely to the coastline into which it is progressively incorporated to the east. While the coastline extended from Dubai to Ras al Khamiah lacks an offshore barrier and, as a result, faces directly into the intense winds and maximum fetch of the Arabian Gulf which is marked by storm beaches, coastal dunes, and only local alongshore spit accretion. Sand dunes of the Arabian desert extend inland to the alluvial fans of the Oman Mountains.

In this study several pilot areas are selected in Abu Dhabi region and it is characterized by the following features. In eastern Abu Dhabi the Holocene coast trends northeast-southwest and the barrier/lagoon complex narrows. To the west, the protecting barrier islands are more widely spaced than those to the east. They occur on extensive sandy shoals and coral banks cut by tidal channels. The lagoon south of the barrier, the Khor al Bazam is a continuous open body of water. It has less restricted circulation than the lagoons to the northeast and at its western end it is connected to the Arabian Gulf. The distribution of the sediments reflects the above physiographic differences. to the east, oolites form on the inter-island tidal deltas and coral reefs are restricted to small patches. To the west, coral reefs grow along most of the

offshore banks to the north of the Khor al Bazam. Eastward of Dhabaiya, in the protected lagoons, carbonate muds and pellets are accumulating, whereas to the west of Dhabaiya, carbonate muds accumulate only in a narrow belt south of the offshore bank. Carbonate sands and skeletal debris are the dominant components. The entire province is undergoing constant change. The offshore bank is accreting seaward through the agency of coral growth and tidal delta formation. South of this bank, supratidal flats are encroaching on the lagoons with the development of beach ridges and algal flats. This interpretation of the different facies along the Abu Dhabi coast is not possible without a combination of field work and laboratory analysis accompanied by areal photographs and remote sensing maps.

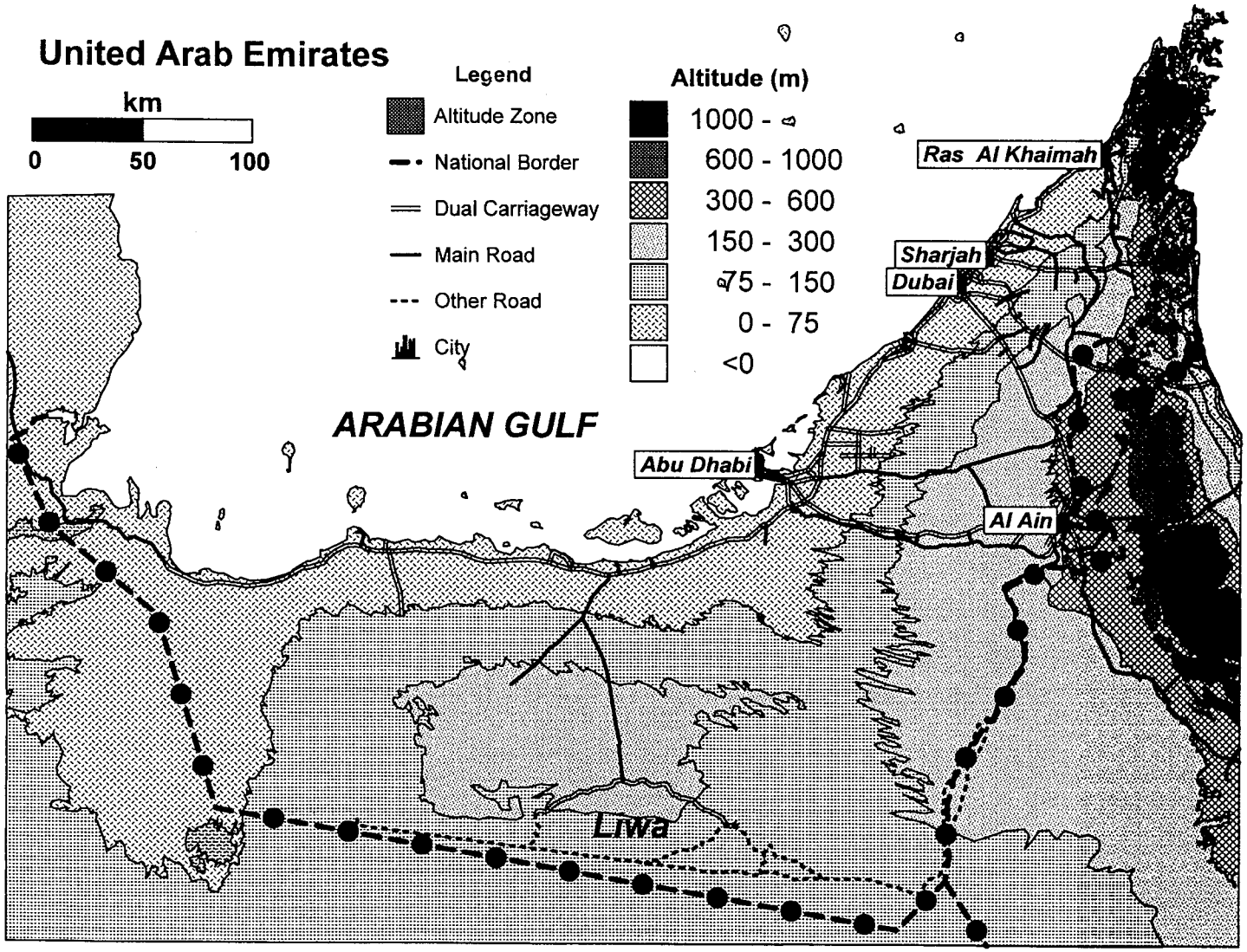
United Arab Emirates
km
0
50
100
Legend
Altitude Zone
National Border
Dual Carriageway
Main Road
Other Road
City
Altitude (m)
1000 -
600 - 1000
300 - 600
150 - 300
75 - 150
0 - 75
<0
ARABIAN GULF
Ras Al Khaimah
Sharjah
Dubai
Abu Dhabi
Al Ain
Liwa

Landscape Structure and Dynamics of the Mu-Us Sands, China

Tatsuaki Kobayashi (*)

* Department of Environmental Science and Landscape Architecture, Chiba University
643 Matsudo Matsudo 271 Japan
Fax:+81-473-63-1497
Email:tatsu@veg-boss.h.chiba-u.ac.jp

Abstract

Natural landscape unit of the Mu-Us Sands are classified into four types as hill, active sand dune, fixed sand dune and meadow. Pastoral use is concentrated on meadow. Sand-dune-fixation planting and windbreak tree-planting are applied on active sand dune and on meadow, respectively. The development of crop field and the results of intensive tree planting were clearly recognized in satellite remote-sensing images. The biomass in the basin of the reservoir was much suppressed in 1993 due to the decline of groundwater level. There is a possiblity that it was caused by the increase of irrigational use.

1. Introduction

Desertification has been one of the most serious environmental problems in China. The Mu-Us Sands is well known as a representative area which has long histories of desertification and efforts of revegetation. To evaluate the effects of desertification and revegetation, effective way of landscape monitoring is required.

This year, this area is noticed as a cause of the discontinuity of the Huan-He River. Newspaper reported that the Huan-He River could not have reached the sea for a long period in these years because of the lack of water-flow. There is an opinion that revegetation and agricultural development of semi-arid region including the Mu-Us Sands affect the over-consumption of water resources of the Huan-He River.

For sustainable use of this region, eco-functional studies with large spatial scales are requested. In this paper, landscape structure and function of the Mu-Us Sands are shown at first. In the later half part, actual dynamics of landscape is analyzed with the comparison of two satellite images in 1978 and 1993.

2. Landscape structure of the Mu-Us Sands

Figure 1 Landscape structure and geological base of the Mu-Us Sands.

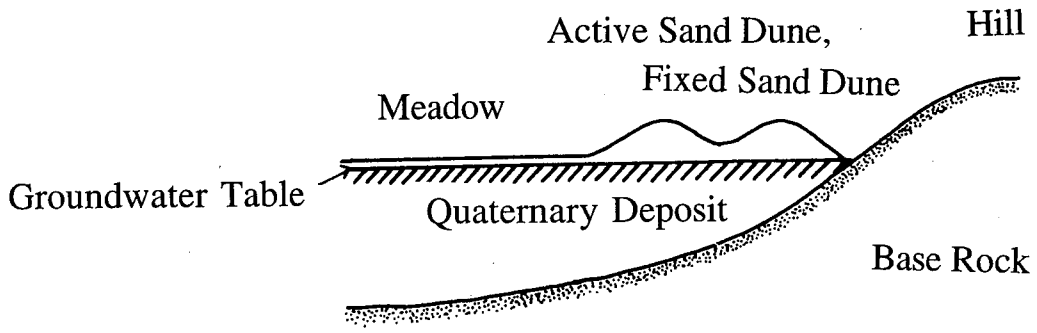

Table 1 Ecological properties of the landscape elements of the Mu-Us Sands.

Landscape element	Area (km^2)	Vegetation	Dominant plants	Soil
Hill	2408	Sparse grasses with half-shrubs	*Stipa* spp. *Lespedeza davurica* *Artemisia frigida*	Thin layer of chestnut soil or brown soil
Active sand dune	14408	Bare ground with few psammophytes	*Agriophyllum arenarium*	Sand
Fixed sand dune	14586	Shrubs and half-shrubs with grasses	*Artemisia ordosica* *Caragana korshinskii* *Sabina vulgaris*	Chestnut soil (topsoil) and sand (subsoil)
Meadow	5447	Perennial grasses	*Carex stenophylla* *Puccinallia tenuifolia* *Calamagrostis pseudophragmites* *Aneurolepidium dasystachys* *Achnatherum splendens*	Meadow soil partly with peat layer, or saline soil

Landscape element	Soil moisture	Land stability	Risk of desertification	Land use
Hill	Dry	Stable	Medium erosibility	Pasture with low productivity
Active sand dune	Medium with quite dry surface layer	Unstable	-	Sand dune fixation planting
Fixed sand dune	Dry	Stable	High erosibility	Conservation
Meadow	Wet	Stable	Low erosibility, high risk of salinization	Pasture, hayfield, crop field, windbreak planting

The Mu-Us Sands develops on the Ordos Plateau which extends flat for 40,000km^2 at the altitude of 1000 to 1500m. It is situated in the ecotone between the temperate arid and humid regions. Though the average of annual precipitation is 362 mm, not so low for steppe, the ecosystem is not stable because of the large year-to-year variance of climate.

The direct origin of sand accumulation is considered to be Quaternary deposits in dry and humid periods which were supplied from weathered sand stone originated in the Mesozoic era. Such sandy deposits cover the wide and flat basin formed on stable geological basis.

Human impact is recognized as the major factor of desertification. Though this area belongs to pastoral region, settlement of farmers has been sometimes promoted in modern history. Inappropriate cultivation had destroyed vegetation and thin soil-layer, which invited the extensive wind-erosion of land surface.

From the ecological point of view, the total landscape of the current Mu-Us Sands mainly consists of the following four landscape elements; hill, meadow, active sand dune and fixed sand dune (Fig.-1). Each landscape element is characterized by its physical attributes as follows;

1) Condition of geomorphologic force. Hill is eroded by the hydrodynamic force. Sand dune is formed under the aeolian force. In particular, mobility of active sand dune is wholly controlled by wind condition.

2) Water supply to soil. Since the groundwater level is high at meadow, soil moisture is not only supplied by precipitation but also by groundwater. At hill and sand dune, as the groundwater level is low, water supply to psammophytes and xerophytes is almost due to precipitation.

3) Soil composition. Active sand dune is constructed by sands with regular particles. Soil of hill, fixed sand dune and meadow contains more or less fine particles as loess deposits and organic products.

The ecological properties of each element are summarized in Table 1. Primary factor of habitat is soil moisture condition. As the soil moisture condition is dry in hill and sand dune, such habitats are occupied by xerophytes and psammophytes. In meadow, soil moisture is so wet that the land is covered by mesic and hydric grasses. A part of meadow with saline soil is dominated by halophytes.

Soil fertility is high in meadow, therefore plant productivity is large. Meadow is the major field of pastoral life and most highly utilized. The productivity of grassland is affected by the changes of groundwater level and its salinity.

Fixed sand dune has two layers of soil with contrary properties. Topsoil is fertile and has high water-holding capacity. However, its layer is thin and the subsoil is so sterile. Since the fertility of topsoil is high, fixed sand dune has been sometimes developed as farmland. But such farmland has been abandoned because its productivity quickly decreased. Abandoned field on fixed sand dune is apt to be eroded by strong wind without covers. Consequently, fixed sand dune easily changes to active sand dune through such desertification processes.

Active sand dune is subjected to aeolian force. Plant establishment is very hard due to high erosibility except some specific psammophytes. Even in active sand dune, if the wind force was

reduced under some conditions, sand dune fixating plants such as *Artemisia ordosica* could invade. Development of pioneer plants promotes the process of sand dune fixation and vegetative succession. Through these processes, active sand dune changes to fixed sand dune.

3. Method of landscape change monitoring with satellite data

Two NDVI images of the south-eastern part of the Mu-Us Sands were produced from the data of LANDSAT/MSS (1978/8/19) and MOS/MESSR (1993/7/17). Geometric relationship of two images was adjusted by the nearest neighbor resampling method. Radiance was transformed from the digital value of each satellite using each inherent equations. NDVI (normalized differential vegetation index) was calculated with the following equation;

$$NDVI = (NIR - R) / (NIR + R),$$

where, NIR and R show radiance in the region of near-infrared wave and red wave. NDVI is considered to represent the abundance of vegetation.

The changes of NDVI image were compared with the land use, which was identified with the map of "Natural Condition and Improvement of the Mu-Us Sandy District" published in 1983.

4. Interpretation of the changes of landscape

Fig.-2 shows NDVI images of the south-eastern part of the Mu-Us Sands in the summer of 1978 and 1993. From the north and west part to the center of each image, the Mu-Us Sands is located on the Ordos Plateau. Here, I call it "plateau area" in a simple word. The south-eastern corner of the figure belongs to the loessial district which presents deep relief, namely the Huan-Tu (Yellow Soil) Hills. I call it "loess area". In the boundary of them, some rivers carve valleys and flow towards the south-eastern direction. The word, "boundary area" is used for it. Yu-Lin City, the place of local government and the economic center of this area, is located along the Yu-Xi-He River.

In this figure, dark tone shows the place with high NDVI. The plateau area consists of various tones of mosaics. Compared with the land use map, dark tone part, dark gray part and light gray part almost correspond to the following landscape units; meadow, fixed sand dune and active sand dune, respectively. The white part shows the surface of water. The boundary area is dominated by light gray parts, that is, active sand dune. Riverside plain shows the dark tone with the striking contrast to active sand dune. It shows crop field and riparian vegetation. The loess area is colored with gray.

Fig.-3 shows the image of the changes of NDVI from 1978 to 1993. The dark tone shows the increase of biomass, while the light tone shows the decrease of it. In this figure, some characteristic site with sharp changes can be pointed out.

NDVI-increased place is observed along the rivers. It illustrates that crop field has expanded in this location. There are other NDVI-increased places as Site A and B in Fig.-3. The landscape type of Site A belongs to meadow and the land use of it is described as crop field in the map. This site also

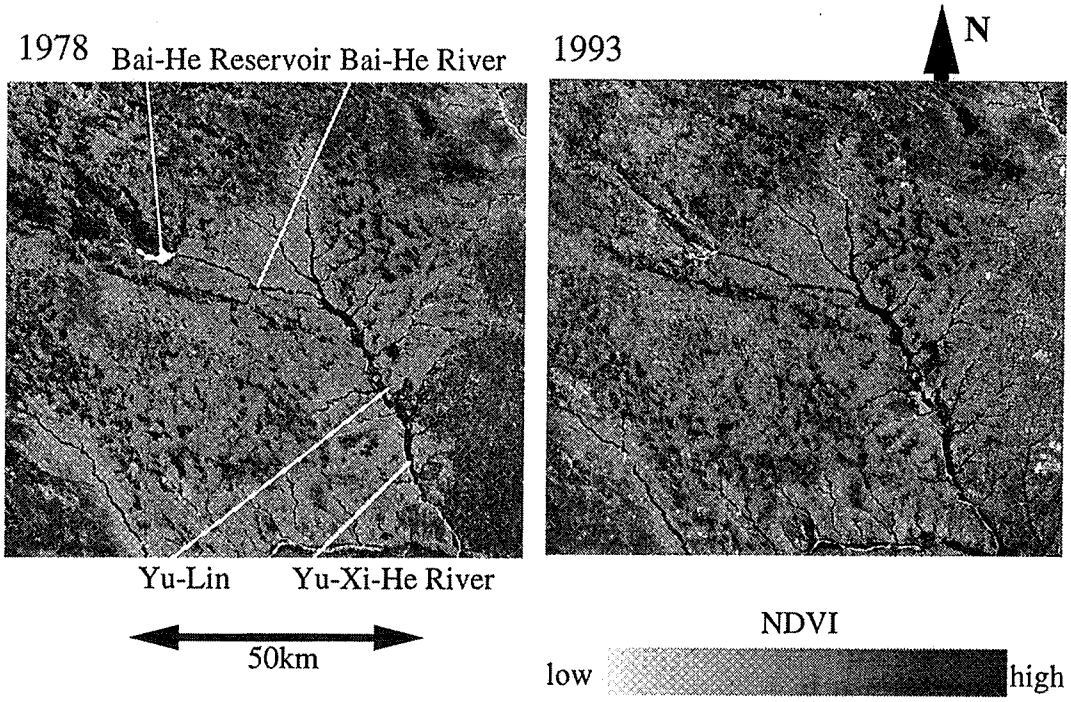

Figure 2 NDVI images of the south-eastern part of the Mu-Us Sands in the summer of 1978 and 1993.

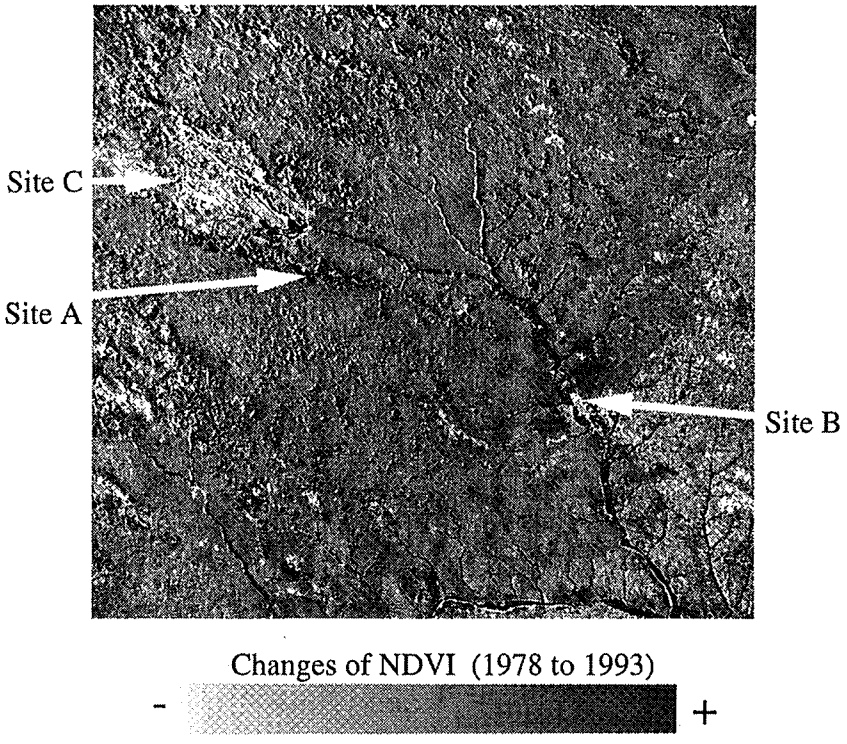

Figure 3 Image of NDVI-changes of the south-eastern part of the Mu-Us Sands from 1978 to 1993.

overlaps with the places where tree-planting project was intensively promoted.

Site B corresponds to Yu-Lin City and its surroundings. As the NDVI of the center of it decreased, it is considered that urbanization has proceeded in the city area. The increase of NDVI in its surroundings shows that farmland and windbreak planting have been developed near the city area.

On the other hand, prominent NDVI-decreased place was recognized in the basin of the Bai-He Reservoir (Site C). The most part of degenerated vegetation around the Bai-He Reservoir is subjected to natural meadow. Since plants is naturally irrigated by groundwater in meadow, primary factor of this phenomenon should be attributed to the decline of groundwater level. The meteorological data of Tai-Yuan, 280km apart eastward from Yu-Lin, shows that the precipitation from June to July in 1978 was 163mm , while in 1993, that was 62mm. That of Lan-Zhou, 550km apart westward from Yu-Lin, was 194mm in 1978 and 99mm in 1993. Consequently, it is easily speculated that the precipitation in the early summer of 1993 was much less than 1978 here. It is considered that the groundwater level is apt to change because the catchment of groundwater is enclosed in the Ordos Plateau without the effective recharged area. The changes of precipitation are supposed to affect the groundwater level here.

However, the decline of it is partly due to an anthropogenic factor, because the decrease of NDVI was eminent, compared with other meadows. As mentioned above, agricultural development and tree planting have been promoted down-stream along the Bai-He River. Such development should increase the consumption of water resource of the Bai-He Reservoir; as a result, the groundwater table of the basin might particularly fall down.

5. Conclusion

The increase of NDVI was most obvious at the places where human activity dominates. It should be appreciated that human efforts have operated well as a promoting force of revegetation in this region. Nevertheless, there is a possibility that such development also promoted the decline of water resources as shown in the Bai-He Reservoir. Agricultural development and man-made revegetation often have both sides of effect in semi-arid area. To secure sustainable development, further quantitative researches are required in the style of inter-disciplinary study among ecology, hydrology, meteorology and related fields.

6. References

Department of Geography, Peking University *et al.* (1983) *The Natural Condition and the Improvement of the Mu-Us Sandy District.* Science Press, Peking (in Chinese).

Kobayashi, T. (1990) "Origin and land classification of the Mu-Us Sands, China", *Jap.J.Reveget.Tech.*, Vol.15, pp.43-57 (in Japanese).

Geology, Topography and Soils in Naiman, Inner Mongolia, China

Yasuhito Shirato, Ichiro Taniyama(*), Zhang Tonghui and Zhao Halin(**)

*National Institute of Agro-Environmental Sciences
3-1-1 Kannondai Tsukuba 305 Japan
fax:+81-298-38-8278
Email:yshirato@niaes.affrc.go.jp
**Institute of Desert Research
174 Donggang West Road Lanzhou 730000 China
fax:+86-931-8847514

Abstract

The characteristics and distribution of soils in Naiman, Inner Mongolia were studied. Soils were classified into 3 types, which were distributed corresponding to geology and topography; loess-derived soils in the southern loess plateau, aeolian sandy soils in Horqin sandy land and alluvial soils along rivers or in inter-dune areas. It was pointed out that each type has a different type of land degradation.

Introduction

Desertification or land degradation is an important environmental problem in the world today. In Jirem prefecture, eastern Inner Mongolia, desertification-prone land has enlarged from 20% in 1950's to 54% in 1970's (Zhu,1988). This area is situated in the semi-arid zone, where the moisture and vegetation conditions are much better than that in arid zone. The main cause of land degradation in this area seems to be human activities such as overgrazing and over-cultivation. When the excessive human pressures ere dispelled, desertification-prone land can be rehabilitated. It is important to establish adequate land use systems to prevent land desertification. And it is necessary to evaluate productivity and environmental capacity of soils for such purpose.

The objective of this study was to obtain informations about the caracteristics and distribution of soils in relation to geology and topography in Naiman, eastern Inner Mongolia.

Materials and methods

1. Study area

Naiman is located in eastern Inner Mongolia, about 500 km northeast of Beijing, as shown in Fig.1. The mean annual air temperature in this area is about 6 to 7 ℃ and the mean annual precipitation is about 370 mm; 70% of it is concentrated in summer season, June to August. The natural vegetation of this area was temperate sparse woodland rangeland (Zhu, 1988).

Geologically this area can be divided into 2 parts as shown in Fig.2; the north part is the open plain of the Xiliao River and the south is a loess plateau. The surface sediment of the north part is sandy alluvial deposit of the Xiliao river (Zhu, 1988) and this region is called "Horqin Sandy Land". Elevation is high in the south (about 500 to 700 m above sea level) and low in the north (about 200 to 300 m).

2. Soil profile survey, soil sampling and analytical methods

Totally 14 soil profiles were surveied in August and September, 1995 (Fig.3). Land use of survey sites was grassland or woodland. Soil samples were collected from each horizon after examining morphological features of soil profiles.

Soil analysis for physico-chemical properties was carried out using the methods described by Hamazaki and Paningbatan Jr.(1988).

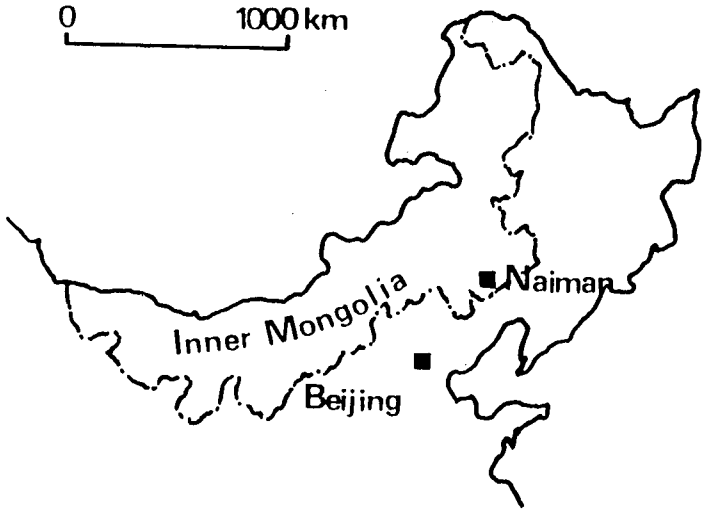

Fig.1. Location of study area

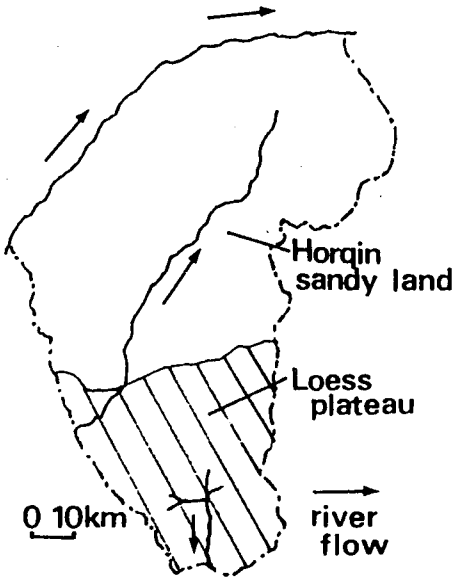

Fig.2. Geology and topography of Naiman

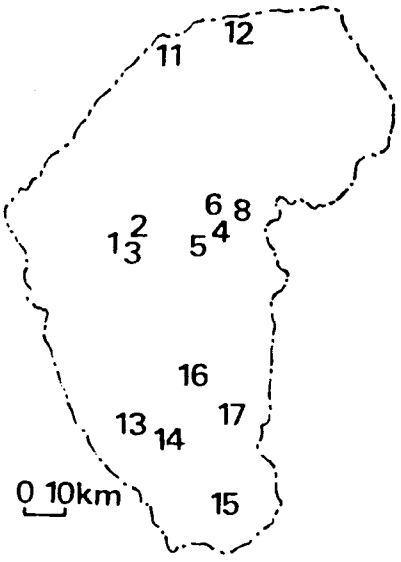

Fig.3. Map of soil survey site

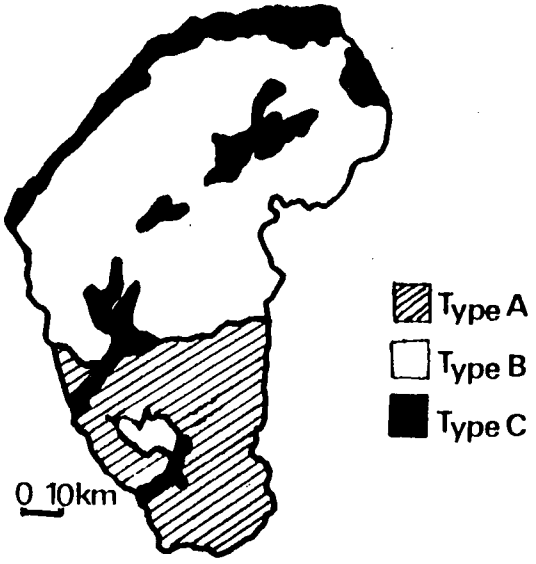

Fig.4. Distribution of major soil types

Results and discussion

1. Major soil types: The soil of Naiman can be classified roughly into 3 types according to their morphology and physico-chemical properties. The distribution of soils corresponds to geology and topography as shown in Fig.4.

TypeA: Soils derived from loess in the southern area of Naiman.

TypeB: Aeolian sandy soils in the Horqin sandy land. This type can be divided into 2 subtypes; one is moving aeorian sandy soil and the other is fixed or half-fixed aeolian sandy soil.

TypeC: Alluvial soils distributed along the river and in inter-dune areas. This type can be divided into 2 subtypes; saline soil and non-saline soil.

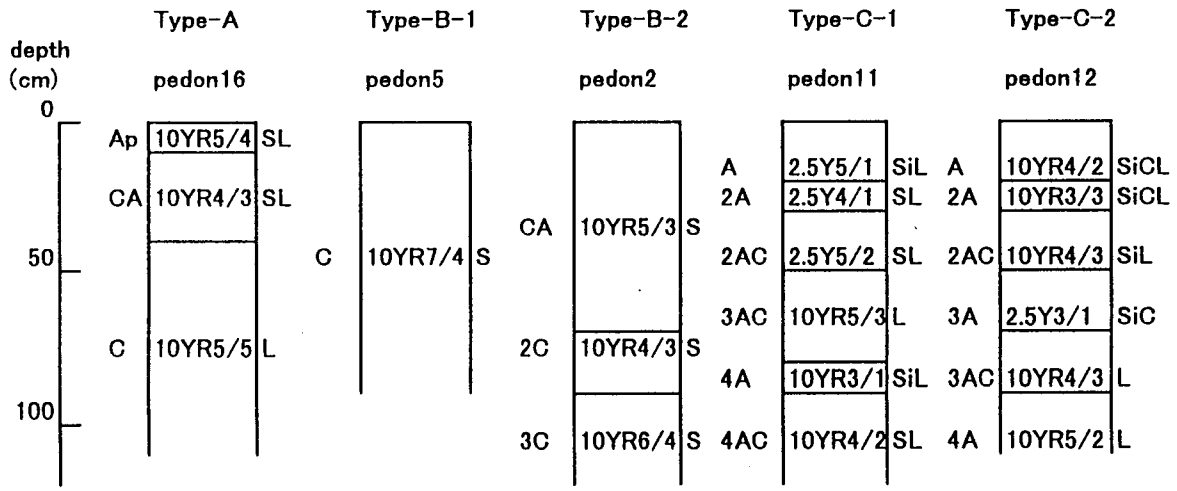

Fig.5. Soil profiles of major soil types in Naiman

2. Morphology:

Fig.5 shows the morphology of major soil types. Type A has a thin A horizon and a C horizon of loessial deposit. Type B-1 does not have a differentiation of horizons and type B-2 has a weakly developed soil profile. Type C has many stratas, which are typical in alluvial soils.

3. Physico-chemical properties

Table 1 shows the physico-chemical properties of major soil types.

Particle size analysis: Type A has about 10% of clay and almost 0% of coarse sand fraction. Silts and fine sands are main particles in this type of soil. Type B-1 has only 1 or 2 % of clay and major particles are coarse sands. Type B-2 also is sandy but finer than B-1. Type C has variant texture in each horizon, but type C-1 has coarser texture than type C-2.

Availabl moisture: Almost all soils have moderate values except for B-1 which has low available moisture because of its coarser texture.

Saturated hydraulic conductivity: Almost all soils have moderate values, but type C-2 has very low value because of its clayey texture and alkalization.

pH: About 8.0 to 9.0 in type A and B. Type C has higher pH and specially in C-2 it is about 10.0, which indicates the alkalization.

EC: Only type C-2 has a very high value and it indicates the salinization. Other soils have normal values.

T-C: Low in all soils but it varies from 0.04 to 1.2 %. It is very low in type B and relatively high in type C.

CEC: Type A has moderate, type B has very low and type C has high values, corresponding to clay and organic matter content.

Exchangeable cations: Ca is very rich in almost all soils because of the semi-arid climate and characteristics of parent materials of soils. Type C-2 has much Na, which indicates the alkalization.

Available phosphorus: All types of soils have low values except for type C-2.

Table 1. Physico-chemical properties of Naiman soils

soil type	pedon	horizon	depth (cm)	particle size distribution(%) clay <0.002 mm	silt 0.002-0.05mm	fine sand 0.05-0.2mm	coarse sand 0.2-2mm	textural class	available moisture pF1.8-4.2 (vol.%)	saturated hydraulic conductivity (cm/s)	pH (H2O)	EC (mS/cm) 1:5 extract	T-C (%)	CEC	exchangeable cations (cmol(+)kg-1) Ca	Mg	K	Na	available phosphorus (mgP2O5 /100g soil)
	16	Ap	0-7	7.0	17.8	75.1	0.1	SL	31.6	1.34E-03	8.2	0.08	0.27	7.5	7.7	1.5	0.3	0.02	0.65
A		CA	7-25	9.2	28.6	62.1	0.1	SL	30.1	1.30E-03	8.3	0.08	0.23	9.5	11.6	1.4	0.2	0.04	0.17
		C	25-110+	9.6	39.6	50.7	0.1	L	28.7	1.29E-03	8.2	0.03	0.12	10.6	10.4	2.2	0.2	0.03	0.20
B-1	5	C	0-85+	1.1	1.2	14.8	82.8	S	8.8	4.59E-03	8.0	0.02	0.04	1.8	1.2	0.2	0.1	0.00	0.69
	2	CA	0-72	4.8	31.6	47.0	16.6	SL	28.2	1.00E-03	8.7	0.07	0.24	6.8	16.3	0.8	0.3	0.03	0.14
B-2		2C	72-88	5.0	25.5	59.2	10.2	SL	30.6	1.24E-03	8.7	0.07	0.26	7.0	17.0	0.8	0.3	0.03	0.55
		3C	88-155+	0.9	0.8	17.9	80.4	S	9.6	5.89E-03	8.6	0.04	0.07	2.4	2.4	0.2	0.1	0.01	0.55
	11	A	0-18	5.6	74.2	20.1	0.1	SiL	35.2	1.16E-04	8.8	0.18	0.56	8.7	22.2	3.7	0.3	0.74	1.21
		2A	18-30	8.4	39.0	48.2	4.5	SL	17.8	2.48E-07	9.7	0.39	0.41	8.1	18.7	3.2	0.2	4.47	0.27
C-1		2AC	30-52	4.4	34.9	49.3	11.4	SL	27.0	2.37E-04	9.3	0.19	0.30	7.2	17.5	6.2	0.2	1.17	0.19
		3AC	52-75	7.5	48.7	42.8	1.0	L	29.6	5.72E-04	8.9	0.22	0.50	8.5	18.2	7.2	0.1	0.78	0.30
		4A	75-93	17.4	64.7	17.2	0.7	SiL	26.4	3.67E-04	8.5	0.17	0.95	16.5	41.4	7.7	0.4	0.18	0.74
		4AC	93-120+	4.3	23.7	32.9	39.1	SL	18.6	7.20E-04	8.5	0.13	0.48	5.5	17.3	2.8	0.4	0.09	1.17
	12	A	0-21	39.1	56.4	4.2	0.3	SiCL	37.0	4.87E-07	10.3	3.05	1.01	22.4	34.7	6.5	1.6	38.52	18.45
		2A	21-25	40.4	56.6	2.8	0.1	SiC	30.4	7.02E-07	10.3	2.01	0.93	27.2	32.3	5.4	0.9	37.11	10.32
C-2		2AC	25-52	11.7	77.5	10.7	0.1	SiL	31.4	1.80E-07	10.5	1.46	0.29	9.3	15.7	3.0	0.3	16.47	4.69
		3A	52-64	43.0	55.8	1.1	0.1	SiC	33.4	2.39E-08	9.8	1.44	1.24	31.3	33.8	6.8	0.9	33.23	4.34
		3AC	64-89	7.2	42.0	50.2	0.5	L	32.0	2.06E-06	10.2	0.54	0.14	6.2	15.9	2.3	0.2	5.97	2.60
		4A	89-110+	19.9	45.3	21.5	13.3	L	20.0	1.65E-08	9.9	0.68	0.46	12.5	35.6	8.0	0.8	9.95	4.97

4. Present state of land degradation

Each type of soil has another type of land degradation, which corresponds to geology, topography and characteristics of soil.

In type A, water erosion is the main problem caused by silty texture and hilly topography. Surface soils were removed by water erosion and it causes the decline of soil productivity. There are many deep gully erosions, which are difficult to be recovered.

In type B, wind erosion is a serious problem caused by its sandy texture and low water retention. If vegetation cover is destroyed, surface sand starts moving by wind, specially in the windy season in spring. Soils become coarse sandy and poor in nutrients, productivity is very low in this type.

In type C, the productivity of soils is higher than other types. But salinization is a problem in type C-2 caused by a high water table and clayey texture.

Adequate measures and rational utilization of land based on soil characteristics will be needed to prevent land desertification and facilitate rehabilitation of already degraded land.

References

Hamazaki, T. and Paningbatan Jr., E.P. (1988) "Procedures for soil analysis", 94pp., College of Agriculture, University of the Philippines at Los Baños and Tropical Agriculture Research Center.

Zhu, Z., Liu, S. and Di, X. (1988) "Desertification and Rehabilitation in China", 222pp., The International Center for Education and Research on Desertification Control.

Vegetation distribution in Naiman, Inner Mongolia, China

Toshiya Ohkuro*, Masayuki Nemoto*, Shenggong Li** and Halin Zhao**

*National Institute of Agro-Environmental Sciences
3-1-1 Kannondai Tsukuba-shi Ibaraki-ken 305 Japan
Fax:+81-298-38-8327
Email:ohkuro@niaes.affrc.go.jp

**Institute of Desert Research, Chinese Academy of Sciences
174 Donggang West Road, Lanzhou 730000 China
Fax:+86-931-8889950
Email:cibidr@ns.lzb.ac.cn

Abstract

The pattern of the vegetation distribution in Naiman, Inner Mongolia, was studied. The 163 quadrats (1 m x 1 m) in 13 sites differing in landform and land use were situated and vegetation surveys were carried out. The samples were divided into five vegetation types corresponding to soil water condition, landform and land use by TWINSPAN classification. DCA ordination also showed a similar trend. On the basis of those results, the possibility of detecting vegetation types by remote sensing techniques in relation to the evaluation of carrying capacity was discussed.

1. Introduction

Recently the degradation of grassland vegetation has been increasing due to destructive land use such as over grazing and over cultivation in semi-arid regions of eastern Inner Mongolia. Sand dune remobilization, which is one of the most significant phenomena of "desertification", has occurred particularly on sandy lands (Zhu *et al.* 1988, Liu *et al.* 1990). Therefore, ecological evaluation of carrying capacity and appropriate land use planning based on detailed investigations of natural conditions including vegetation and soil property, should be needed to maintain sustainable agricultural activities in such regions. This paper focuses on grassland vegetation in Horqin sandy land which is one of the largest rangeland areas, and documents the pattern of vegetation distribution. On the basis of the results, the possibility of detecting vegetation types by remote sensing techniques in relation to the evaluation of carrying capacity was also assessed.

2. Study site and Method

Naiman county which we selected as a field for the study, is located in the southern part of Horqin sandy land and is the most serious county where desertification has spread widely (Zhu *et al.*

1988). The geomorphic frame in Naiman mainly consists of loess hills in southern part and sandy plain of Xiliao river in other part. The latter can be divided into several landform units according to the degree of soil moisture and sand accumulation.

Vegetation surveys were conducted in early September of 1993, 1994 and 1995. The 163 quadrats (1 m x 1 m) in 13 sites differing in landform (loess hill, dune, interdune depression, lowland and flat sandy land) and land use (grazed and mown) were situated and plant height (H) and percent cover (C) of each species were recorded.

Two-way indicator species analysis (TWINSPAN; Hill 1979a) was performed for all samples to classify the floristic data on the basis of species cover values transformed as follows: <2(%); 1, 2-5; 2, 5-10; 3, 10-20; 4, 20<; 5. Detrended correspondence analysis (DCA; Hill 1979b) was also applied using cover values to ordinate those samples. Species which appeared in more than 5 quadrats were used in those analysis.

3. Results and discussion

A total of 125 species were recorded in 163 quadrats and 71 species appeared in more than 5 quadrats. These samples were classified into two types based on the soil water conditions by the first division of TWINSPAN. Those stand groups were divided into 5 stand groups by the second and third division of TWINSPAN corresponding to landform types and land use types (Table 1).

The 5 types of the stand groups are described as follows:

Type 1 (2N) : This type of vegetation occurs in loess hills and is characterized by *Stipa bungeana* and *Thymus mongolicus*. *Stipa* sp. is one of the dominant species that form zonal vegetation in Inner Mongolian grassland.

Type 2 (5N) : This vegetation type occurs in flat sandy lands and is characterized by the dominance of annual grass species such as *Chloris virgata*, *Aristida adscensionis Setaria viridis* and *Digitaria cilliaris*.

Type 3 (5P) : This type occurs in dune areas. Mean vegetation cover is about 40 %, ranging from more than 70 % on the sites dominated by *Artemisia halodendron* to less than 10 % on shifting dunes where only pioneer annuals such as *Agriophyllum squarrosum* occur. 5N and 5P belong to the same stand group (2P) at the second division level of TWINSPAN.

Type 4 (3N) : This type of vegetation mainly occurs in mown lowlands and is dominated by hygrophytes such as *Phragmites australis*, *Puccinellia macranthera* and *Pycreus korshinskyi*.

Type 5 (3P) : This type occurs in grazed lowlands. Species composition is similar to 3N although vegetation height and cover is lower because of grazing effects. In some sites halophilous plants such as *Iris lactea* var. *chinensis*, *Suaeda corniculata* and *Kochia scoparia* occur.

Figure 1 shows the DCA ordination diagram of all samples. Stand groups of wet sites (3N and 3P) were separated from other groups along axis 1, and that of loess hills (2N) were separated along axis 2. These results suggested that axis 1 and 2 represent the gradient of soil moisture and the difference in bedrock, respectively.

Table 1 Species composition, percentage of the number of quadrats included in six types of landform and land use, mean vegetation cover and height in each stand group classified by the TWINSPAN. Numerals in the body of the table indicate mean transformed cover values (see text).

Species	2N	5N	5P	3N	3P
Agriophyllum squarrosum	-	1	3	-	-
Artemisia halodendron	-	1	4	1	-
Cynanchum thesioides	-	1	1	-	-
Ferula bungeana	-	1	1	-	-
Inula salsoloides	-	-	3	-	-
Melissitus ruthenicus	1	1	1	-	-
Corispermum macrocarpum	-	1	1	-	-
Chloris virgata	-	4	-	-	-
Euphorbia esula	-	1	1	-	-
Gueldenstaedtia stenophylla	-	1	1	-	-
Kummerowia stipulacea	1	1	1	1	-
Aristida adscensionis	-	3	1	-	-
Salsola collina	-	1	1	-	-
Bassia dasyphylla	-	1	1	-	-
Convolvulus arvensis	-	1	-	-	-
Digitaria cilliaris	1	5	1	1	-
Tragus mongolorum	-	1	-	-	-
Tribulus terrestris	-	1	-	-	-
Echinops gmelini	-	1	-	-	-
Eragrostis pilosa	1	1	1	-	-
Pennisetum centrasiaticum	-	1	-	-	-
Artemisia scoparia	1	1	-	1	-
Euphorbia humifusa	1	1	1	-	-
Setaria viridis	2	3	2	2	1
Lespedeza davurica	2	2	1	-	-
Cleistogenes squarrosa	2	1	-	-	-
Asparagus dauricus	1	-	-	-	-
Astragalus sp.	1	-	-	-	-
Glycyrrhiza uralensis	1	1	-	-	-
Gnaphalium sp.	1	-	-	-	-
Heteropappus altaicus	1	-	-	-	1
Oxytropis sp.	1	-	-	-	-
Polygala tenuifolia	1	-	-	-	-
Polygonum divaricatum	2	-	-	-	-
Potentilla tanacetifolia	1	-	-	-	-
Stipa bungeana	4	-	-	-	-
Thymus mongolicus	5	-	-	-	-
Artemisia frigida	2	1	-	-	-
Ixeris chinensis	1	1	1	1	-
Xanthium sibiricum	1	1	-	1	1
Aneurolepidium dasystachys	1	1	-	-	1
Saussurea amara	1	1	-	1	1
Chenopodium glaucum	-	-	-	1	1
Echinochloa crusgalli	1	-	-	1	1
Lactuca tatarica	-	-	-	1	1
Polygonum hydropiper	-	-	-	1	1
Artemisia gmelinii	-	-	-	1	-
Calamagrostis epigeios	-	-	2	4	1
Equisetum ramosissimum	-	-	1	1	1
Populus simonii	-	1	1	1	-
Salix gordejevii	-	-	1	1	-
Salix matsudana	-	-	1	2	1
Inula salicina	-	-	1	3	-
Melilotus suaveolens	-	-	-	1	-
Plantago depressa	1	-	-	1	1
Puccinellia macranthera	-	-	-	4	1
Pycreus korshinskyi	-	-	-	2	1
Typha minima	-	-	-	4	1
Potentilla anserina	-	-	-	1	1
Potentilla chinensis	-	-	-	1	1
Agropyron cristatum	1	-	-	2	2
Phragmites australis	-	1	1	4	3
Suaeda corniculata	-	-	-	1	1
Iris lactea var. chinensis	-	-	-	-	2
Kochia scoparia	-	-	-	1	1
Polygonum sibiricum	-	-	-	-	1
Carex duriuscula	-	-	-	2	5
Crypsis aculeata	-	-	-	1	1
Halerpestes ruthenica	-	-	-	1	1
Triglochin palustre	-	-	-	1	1
Taraxacum sp.	-	-	-	1	1
Number of quadrats	20	48	42	24	29
Percentage of the number of quadrats included in					
Loess hill*	12.3	0	0	0	0
Flat sandy land*	0	27.0	0	0	0
Sand dune*	0	2.5	22.7	0	0
Inter dune depression*	0	0	3.1	3.7	0
Lowland **	0	0	0	11.0	2.5
Lowland*	0	0	0	0	15.3
Total cover (%)	76.3	65.7	41.9	87.7	49.9
±	±	±	±	±	±
standard deviation	14.8	17.4	27.5	12.9	29.4
Community height (cm)	46.5	31.8	55.3	105.2	42.9
±	±	±	±	±	±
standard deviation	11.0	16.1	18.7	29.4	23.7

*grazed, **mown

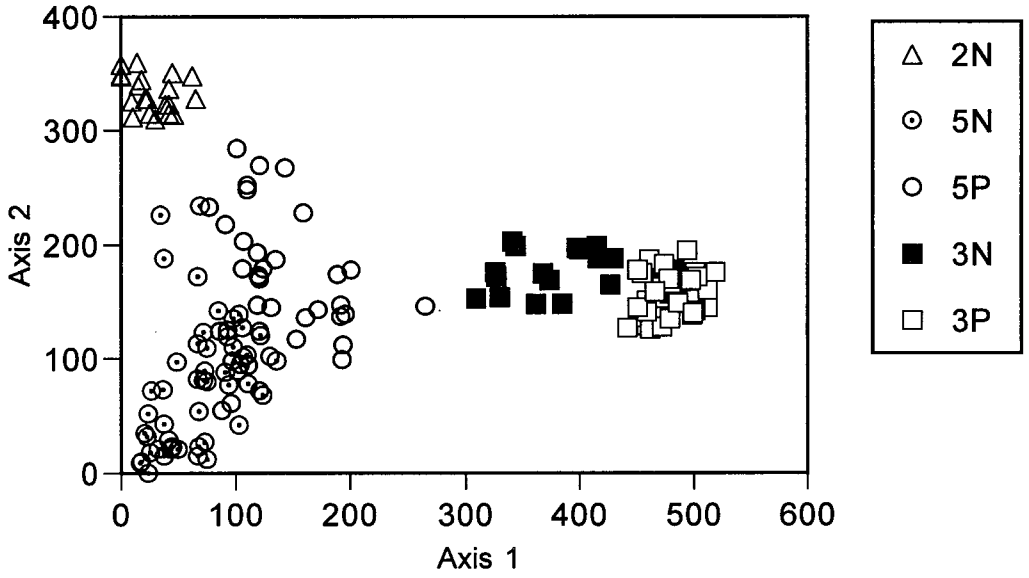

Fig.1 DCA ordination diagram of samples. Symbols indicate stand groups classified by TWINSPAN.

The results of the field surveys revealed that vegetation types in Naiman clearly correspond to physical conditions such as soil moisture and geomorphic frame. Sand dune remobilization has occurred mainly on dune areas and flat sandy lands (Zhu *et al.* 1988), which correspond to 5P and 5N, respectively. However, vegetation dynamics and carrying capacity would be different between the two types even if these sites show the same biomass, because of the differences in the dominant species and the effect of grazing (Ohkuro *et al.*, unpublished). Therefore, it would be important to detect the micro landform patterns which correspond to the above-mentioned vegetation types to develop detailed land evaluation and land use planning using remote sensing techniques in the surveyed regions.

4. References

Hill, H.O.(1979a) *TWINSPAN- A FORTRAN program for arranging multivariate data in an ordered two-way table by classification of the individuals and attributes.* Cornell University Press, Ithaca, New York, .

Hill, H.O.(1979b) *DECORANA- A FORTRAN program for detrended correspondence analysis and reciprocal averaging.* Cornell University Press, Ithaca, New York.

Liu, X., Zhao, H. and Xu, B.(1990) Mechanism of destruction and restoration of the grassland ecosystem in the Korqin Steppe region. *Proc. the Third International Conference on Desert Development, Beijing*, 1-32.

Zhu, Z., Zou, B., Di, X., Wang, K., Chen, G. and Zhang, J.(1988) *Desertification and rehabilitation - case study in Horqin sandy land.* Institute of Desert Research, Academia Sinica, Lanzhou, 113pp.

A Monitoring Method of Desertification in Naiman, Inner Mongolia, China

Toshiaki Imagawa*, Michikazu Fukuhara**, Wang Tao*** and Zhu Zhenda****

*National Institute of Agro-Environmental Sciences, MAFF
3-1-1 Kan-nondai, Tsukuba, Ibaraki, 305 Japan
Fax:+81-298-38-8277
Email:imagawa@niaes.affrc.go.jp
**National Institute of Agro-Environmental Sciences, MAFF
3-1-1 Kan-nondai, Tsukuba, Ibaraki, 305 Japan
Fax:+81-298-38-8203
Email:fukuhr@niaes.affrc.go.jp
***Institute of Desert Research, Chinese Academy of Sciences
174 Donggang West Road, Lanzhou 730000, China
Fax:+86-931-8889950
****Institute of Geography, Chinese Academy of Sciences
Building 917, Tatun Road, Beijing, 100101, China
Fax:+86-10-64911844

Abstract

Naiman Qi is located in the east edge of Horqin desert and recently affected by desertification. The desertification has progressed by overgrazing and overcutting and fixed sand dunes began to move again in this area. In this study, we intended to develop a monitoring method of desertification using Landsat data in order to understand how the desertification has progressed. We could define the desertified area using land use classification and following three indexes; vegetation [(TM4-TM3) / (TM4+TM3)] , structure [(TM5-TM1) / (TM5+TM1)] , and redness [(TM3-TM1) / (TM3+TM1)] . And we obtained yearly changes by superimposing desertified areas identified from data of different year.

1. Introduction

The term "desertification" in its technical sense has a broader meaning than simply describing the phenomenon occurring in peripheral areas of deserts. Therefore, "desertification" has been redefined in Agenda 21 as "land degradation in arid, semi-arid and dry subhumid areas resulting from various factors, including climatic variations and human activities". The term "desertification" is clearly used now to refer not only surrounding deserts, but also major food producing areas into semi-arid and subhumid areas.

Even in East Asia, where there is little arid area, we can see that the new definition brings this problem closer to home. In particular, in Eastern China, which contains 50% of the land and over 90% of the population of that country, climatic conditions are changing from the semi-arid regions in the north to the subtropical, subhumid areas in the south. Zhu et al[1] estimated that

desertification in China was induced by water and wind erosion, affecting 1.483 million km^2, about 15% of the land area of China.
The purpose of this study is to develop a monitoring method of desertification using Landsat data in order to understand how desertification has progressed.

2. Some characteristics of desertification in Naiman

Naiman is located about 400km NE of Beijing (Fig.1). This semi-arid region has an annual average rainfall of 372mm and annual average temperature of 6.4℃. Lacustrine sediments in the Quaternary are the main surface layer deposits in this region, and widely distributed sand dunes, formed in an earlier dry period, have fixed and become covered by soil and vegetation with humidifying of climate. On fixed sand dunes and in the lowlands between dunes, field crops are grown, especially corn and sorghum. In addition, the grasslands in northeastern Naiman have been extensively developed.

Fig.1 The study area

Desertification has been caused by the destruction of natural vegetation and about 1-2 m of topsoil, and begins with the movement of unconsolidated sand. In this region, a strong wind of 5m/s (18km/h) often blows the sand in the spring. Landsat images have shown wave-like patterns on the ground surface facing the dominant wind direction, with widely-distributed sand dunes extending from west to east. The movement of sand is inversely related to particle size, i.e., the smaller the sand particle the greater the movement, and annual dune movement of 5 m/yr has been observed. Furthermore, in the grassland we can confirm points where the sand has been expanding in elliptical patterns around ponds. At present, measures have been put into effect to stop the movement of sand, and there are places in peripheral areas where vegetation has invaded.

3. Extracting methods by land use classification

When we extract desertified areas using Landsat Data, the most precise method is to define the desertified areas and land use types based on existing maps and field survey.
So, we examined land use classification in a test area of Naiman using land use units of the desertification map of Naiman Qi. Those units contain active dune, grassland, cropland, forest, wetland, village and water body.
First, in the test area we established about five typical points of each unit where have not changed since the map published. Second, we checked reflectances of the every points using Landsat data observed on different five times from May to September in 1992. Figure 2 shows a example of the result. Some characteristics are summarized as follows. Active dune has the highest reflectance as compared with other units through bands and times. In contrast, water body has the lowest one on both 4th and 5th bands, which belong to near infrared region, through bands and times. And so, active dune and water body are easily distinguished from other units using only one datum by above reasons. In the case of other units we could divide those units using two data of late May and late July. Because cropland and grassland have poor vegetation and forest area is already covered with green leaves in late May. And cropland has higher density of vegetation than

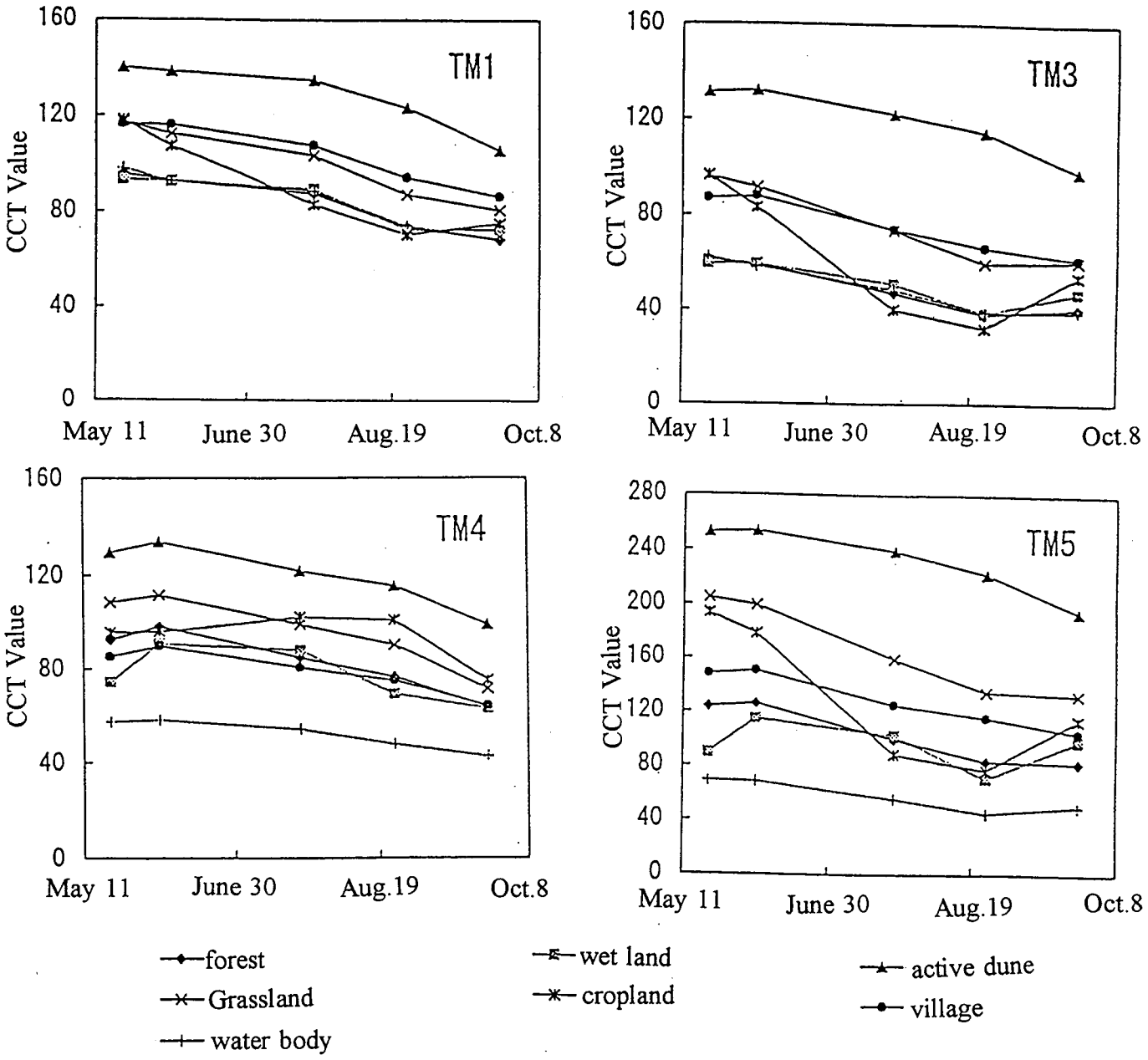

Fig.2 Seasonal changes in spectral reflectance of each land cover/land use type

grassland in late July. These phenomena show difficulty to divide into cropland, forest and grass land by only one image. However we could solve this problem by using different two images which observed on spring and summer. Because in late May cropland and grass land are almost bare before seeding and trees are covered in fresh green, in late July and August cropland and grass land are covered in green and cropland has a higher density than grass land. This changes reflect a value of red band which is 3rd band in TM and has high reflectance against the phytosyntic pigment chlorophyll.

In this study, we used five bands data of Landsat TM for classifying land use as shown below; 3rd band of May 20th and 1st, 3rd, 4th and 5th bands of July 23rd. We took the places where we checked the reflection of each land use type for training ares and classified those types with supervised classification. And we had a high probability in the classification(Table1). Each units

was discriminated from the other units with more than 80 % of probability. Especially, cropland and grassland were discriminated with 95% of probability. As mentioned above, we confirmed this method was useful for land use classification. If we can annually classify the land use in the same area and compare the results, we will be able to get desertification trends as well as reclamation and abundant of cropland and clearing and plantation of trees.

Table 1 Verification of land cover/land use classification with maximum likelihood method

	active dune	grassland	cropland	forest	Wetland	village	Water body
active dune	96.87	1.25	0.00	0.00	0.00	0.00	0.00
grassland	0.29	94.71	0.29	1.14	0.86	1.29	0.00
cropland	0.00	2.82	94.86	0.91	0.00	0.00	0.00
forest	0.00	4.51	0.00	80.56	12.85	1.04	0.00
wetland	0.00	2.50	0.00	6.75	81.25	2.50	5.75
village	0.00	0.54	0.18	2.06	8.04	86.03	0.00
water body	0.00	0.00	0.00	0.61	2.74	0.00	95.43

4. An extracting method by land cover changes

The classification method of land use is effective in monitoring desertification, but there is no guarantee that Landsat data are provided for it every year. So, we examined a method to define the desertified area by only one image and proposed following three indexes.

First, a vegetation index was used to identify unvegetated regions.

For LANDSAT TM data (TM4-TM3) / (TM4+TM3)

For LANDSAT MSS data (MSS7-MSS5) / (MSS7+MSS5)

Low values of this index represented unvegetated areas. Comparisons were made with composite images to derive the threshold, then unvegetated areas were identified. And, to consider seasonal fluctuations in vegetation, we used autumn and spring data and common areas were identified.

Second, water bodies and man-made structures such as settlements, which were included in the unvegetated regions, had to be removed. For that purpose, the ratio (TM5-TM1) / (TM5+TM1) was obtained. Since bare land in this band ratio was higher than water bodies and man-made structures, it was possible to separate the two. Therefore, the index derived from this ratio was named the structure index. Since there was no MSS sensor corresponding to TM 5, old data were masked by water bodies and man-made structures derived from the new images. Third, using the redness index (TM3-TM1) / (TM3+TM1) which reflects the amount of oxidized iron contained in the ground, desert areas were identified by the ground color in each region. Finally, desertified areas identified from data of different year were superimposed to obtain yearly changes.

Next, we verified a application of this method in a test area, a 30 km square area was selected as the test area, and was analyzed for desertification patterns in the last 10 years. Desertifying regions have low vegetation indexes. White colored areas showing the soil colors of this areas were identified, the results from analysis of old and new images were superimposed to clarify the changes(Fig.3).

The spatial proportions of the test area undergoing desertification were roughly 40%. And the area of reclaimed land and the area of newly desertifying land were roughly 12% in the districts. This fact indicated that the spatial extent of desertification is almost constant in the last 10 years.

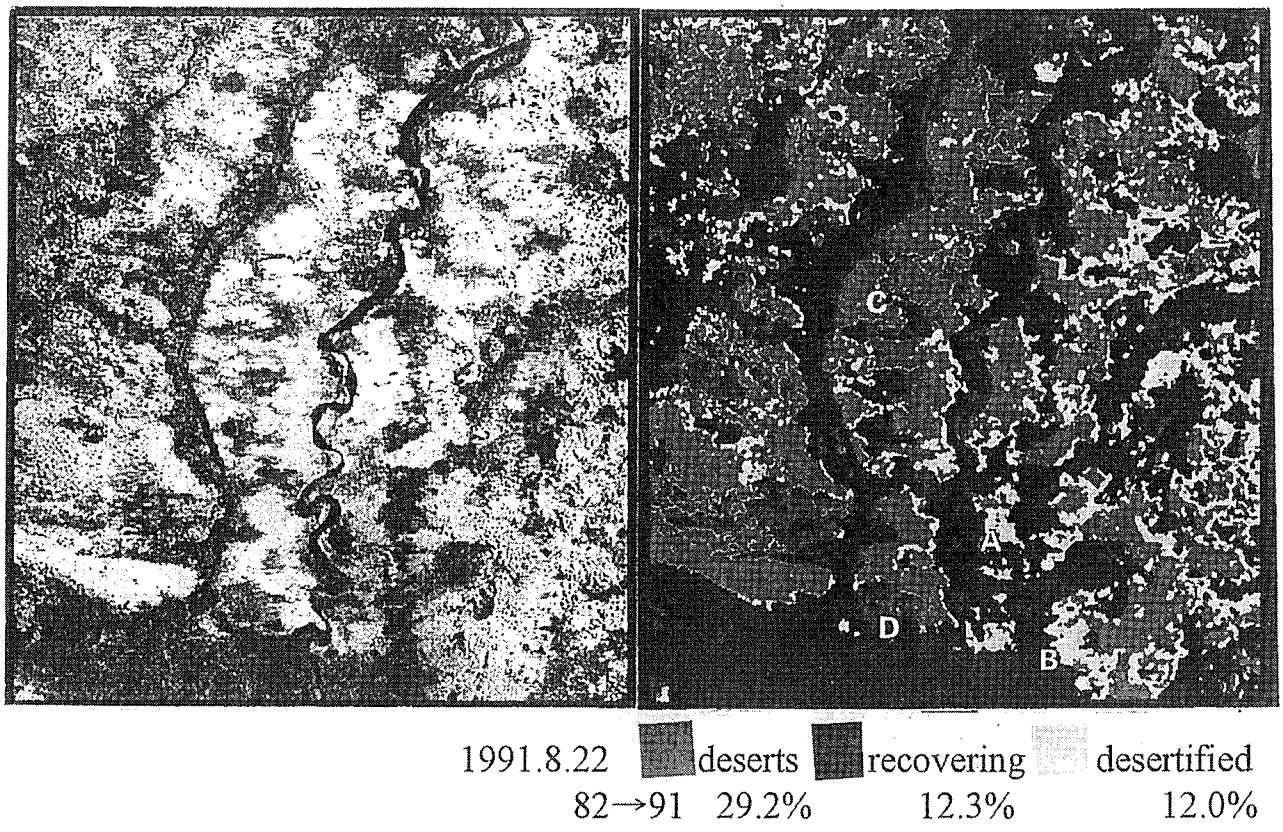

Fig.3 Composite photo of Landsat TM(left) and recent trend of desertification in Naiman, Inner Mongolian Autonomous Region

Especially the areas around the settlements and around the N-S running road and railway in the eastern part of the town showed some recovery from 1982-91, in contrast to outlying areas, where desertification continued. These facts show that desertification does not proceed unilaterally regardless of the state of degradation; rather, thanks to some sort of measures implemented when relatively easy to do so, the progress of desertification could be restrained.

Furthermore, we verified the results of the analysis by ground truth. Here, we introduce following three sites.

"A" point (42° 49' 56"N, 120° 45' 15"E), situated on about 10km of fixed sand dunes in eastern Naiman (A in Fig.3), is an area which Landsat data analysis showed to be desertifying from 1982-1991. According to a desertification map compiled by the Chinese Academy of Science, cropland that had been cultivated by the dry farming method was classified as abandoned farmland in 1958 and as shrubland in 1974, and shrublands of willow were seen in the area. There was no trace of cultivation on the forest floor, just a scant covering of grass, and sand dunes had begun to encroach on some parts of the area. This condition corresponded well with the results of the image processing.

"B" point(42° 49' 8"N, 120° 47' 33"E) located about 8km SSE of "A" point(Fig.3), was also judged to have been desertifying from 1982-91. According to the desertification map, this area was classified as grassland in both 1958 and 1974, but a comparison of the two years shows a vast reduction in spatial extent and a transformation into semi-solid sand dunes. A field study revealed scant traces of cultivation in depressions, but the ground was nearly covered by sand, and the sand dunes had begun to move again.

"C" Point(42° 51' 2"N, 120° 42' 11"E) differs from the two previous sites in that it was determined to be land that was reclaimed from the desert in 1982-91. This is an area of sand dunes about 5km east of Naiman (Fig.3). The desertification map showed the surrounding area to be one of moving and semi-moving sand in 1958; by 1974, the central area had become a moving sand area, with the surrounding area consisting of solidified sand dunes. In the composite Landsat images from 1991, this area clearly differs from the white color of the moving sand dunes, leading us to assume that vegetation in the area has recovered. Moreover, the topography of the area consists of small patches of undulating moving dunes (maximum size 7-8m), but most of the ground surface has vegetation cover such as grasses of the Artemesia family and young willows and other scrub. The sand dunes have also been observed to be solidifying. This is the result of a prohibition on grazing enacted about 5 years previous. In addition to naturally recovering grasses, poplar groves have also been planted in part of the area.

5. Concluding remarks

Desertification in Naiman was characterized by reactivating of fixed sand dunes. In this study, we proposed a monitoring method of desertification using Landsat data in order to understand how desertification has progressed.

At first, we developed a monitoring method of land use change by supervised classification. This method needs data of two different times in the same year, but shows how land use changed in each pixel. We did no more than show the high possibility of application in this study. In near future, we want to show a result using this methods, if we will be able to get the data of different years in this area. Second, we investigated a monitoring method of land cover changes by following three indexes; natural vegetation, structures, and soil redness. These indexes were very effective to understand the conditions and trends of desertification. We confirmed that no significant changes in spatial extent of desertification were seen in the test district. Land management around major settlements, roads, railway lines, etc., was relatively meticulous and desert land was being reclaimed. Conversely, in outlying regions new desert land was appearing.

As described above, we could understand the conditions and trends of desertification through this method.

6. Acknowlegement

The authors express many thanks to Prof. Liu Xin Min and Prof. Zao Halin, Institute of Desert Research, Chinese Academy of Sciences, for many helpful suggestions and their help in our field works. The authors also express many thanks to Mr. Takeshi Watanabe, Japan International Research Center for Agricultural Sciences, for his assistance in image processing. Landsat data were owned by the United States Government and supplied by EOSAT/NASDA.

7.References

Zhu, Zhenda et al (1992): China: Desertification Mapping and Desert Reclamation. Form "World Atlas of Desertification," UNEP. pp.46- 49.

Formation of the Dry Surface Layer and Its Effect on Bare Soil Evaporation : Field Observation and Numerical Experiments

Tsutomu Yamanaka(*), Atsushi Takeda(**) and Jun Shimada(***)

*Doctoral Program in Geoscience, University of Tsukuba
Tsukuba, Ibaraki 305, Japan
Fax: +81-298-51-6451
Email: yamanaka@ess.bosai.go.jp

**National Research Institute for Earth Science and Disaster Prevention
Tsukuba, Ibaraki 305, Japan
Fax: +81-298-51-1622

***Institute of Geoscience, University of Tsukuba
Tsukuba, Ibaraki 305, Japan
Fax: +81-298-53-2568
Email: shimada@atm.geo.tsukuba.ac.jp

Abstract

Field measurements of soil water content, temperature, and relative humidity were made at several depths within a lysimeter where the dry surface layer (DSL) formed. The observed water content was almost constant in the DSL, while it increased toward deeper depth below the DSL. In addition, the peak of vapor density was observed at the bottom boundary of the DSL. Similar features to those observed was shown by numerical computations using a one-dimensional model of water and heat with high vertical-resolution. Furthermore, the result of numerical computations also demonstrated that the evaporating zone was located at the bottom boundary of the DSL, and that the thickness of the evaporating zone was extremely small, except for highly retentive soils. These results of both the field observation and numerical experiments indicate that information of the thickness of the DSL is required rather than that of water content of surface soil, to evaluate evaporation from bare soil surfaces.

1. Introduction

Soil moisture conditions of land area can have major effect on global climate through evapotranspiration. Many of the previous studies have empirically parameterized the availability of surface moisture for evaporation from bare soil, by using water content of surface soil layer. On the other hand, it is well known that so-called 'dry surface layer' (DSL) forms during soil drying.

According to several previous works, evaporation of soil water occurs mainly at the bottom boundary of the DSL instead of at the soil surface. In such case, the direct determining factor of the surface-moisture availability is considered to be the thickness of the DSL rather than the surface water content. In order to clarify the formation mechanism of the DSL and the effect of the DSL on evaporation from bare soil surfaces, field observation and numerical experiments were carried out.

2. Field observation

A field observation was conducted by using a lysimeter in which uniform fine sand was packed and groundwater level was maintained at a depth of 0.8 m, under the framework of the TSUKUBA 92 field campaign (Sugita *et al.*, 1993) held in Tsukuba, Japan, in the summer of 1992. Soil water content, soil temperature, and relative humidity in soil pores were measured at several depths below the soil surface by means of heat probe type soil moisture sensors, platinum resistance thermometers, and capacitance humidity sensors, respectively. The soil moisture conditions were fairly dry due to low precipitation during the field campaign, and the DSL which had a few to 10 cm thickness was observed. The observed soil water content showed clear difference between in and below the DSL (Fig. 1), that is, it was almost constant in the DSL, while it increased toward deeper depth below the DSL. The relative humidity of pore air was almost unity below the DSL. On the other hand, the relative humidity in the DSL was less than unity, and shows the tendency to decrease toward the soil surface. As a result of this humidity gradient and opposite temperature gradient, the peak of the vapor density was found out around the bottom boundary of the DSL. These observed results indicate that the divergence zone of vapor flux, namely 'evaporating zone', was located at the bottom boundary of the DSL.

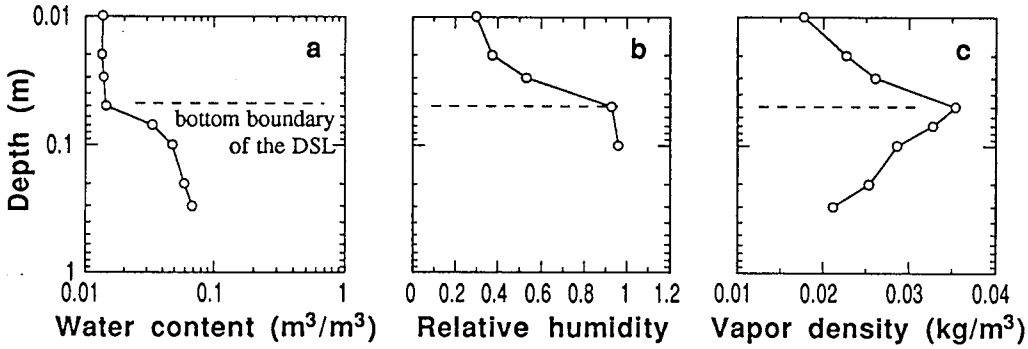

Fig.1 Vertical profiles of (a) water content, (b) relative humidity and (c) vapor density observed at 15:00 (JST) on Aug.10, 1992. The thickness of the DSL was determined by the difference in color of soil profile.

3. Numerical experiments

In order to clarify the microscopic structure of evaporating zone, numerical experiments was conducted using a one-dimensional model of water and heat flow with high vertical-resolution. The model used was fundamentally based on the modified Philip and de Vries theory (Philip and de Vries, 1957; Milly, 1982). In the model, the water flux consisted of liquid and vapor water flux driven by

matric-head gradient and temperature gradient. The liquid water flux driven by the temperature gradient, however, was not considered in the present study, since it is less important in dry soils. The heat flux consisted of conduction and latent heat transfer due to vapor movement.

At the upper boundary, evaporation into the atmosphere (E_s) was given as the sink of water, and R_n-H-lE_s was given as the source of heat, where R_n is the net radiation, H the sensible heat flux into the atmosphere, and l the latent heat for vaporization. The E_s can be expressed as

$$E_s = \rho_a C_E u (h_s q_{sat}(T_s) - q_a) \quad (1)$$

where ρ_a is the density of air, C_E the bulk transfer coefficient, u the wind speed, $q_{sat}(T_s)$ the saturated specific humidity at the soil surface, h_s the relative humidity at the soil surface, and q_a the specific humidity of atmosphere. The hs can be given by following equation, as

$$h_s = exp(\psi_s g / R T_s) \quad (2)$$

where ψ_s and T_s are the matric head and temperature at the soil surface, g is the gravitational acceleration, and R the gas constant of water vapor. Diurnal variation of atmospheric conditions was not considered, and constant values of atmospheric conditions were given in the present study. The lower boundary conditions were constant temperature and no water flux at a depth of 0.6 m. This model consisted of 144 layers, and had very fine resolution (min., 0.5 mm) near the soil surface.

Table 1 Soil hydraulic parameters for the three example soils

Soil name	θ_{sat} (m^3/m^3)	θ_r (m^3/m^3)	α (m^{-1})	n (-)	K_{sat} (m/s)
Toyoura Sand	0.412	0.0239	3.14	7.0	1.25×10^{-5}
Silt Loam G.E.3 †	0.396	0.131	0.423	2.06	5.73×10^{-7}
Beit Netofa Clay†	0.446	0.0	0.152	1.17	9.49×10^{-9}

† data from van Genuchten (1980)

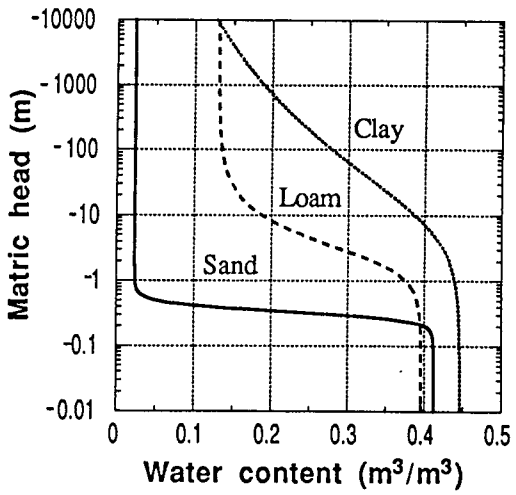

Fig.2 Soil moisture characteristic curves for the three soils used in the numerical experiments.

Hydraulic properties of soils were given by van Genuchten (1980)'s model. The parameters for three example soils used in the present study are listed in Table 1, and soil moisture characteristic curves for those soils are shown in Figure 2.

As an example, computational results for sand are shown in Figure 3. Very good similarities were recognized between observed and computed profiles of water content, relative humidity, and vapor density, respectively. These similarities demonstrate the validity of the model used. From comparison between the observed and computed results, the position of a inflection point in water content profile was considered to be corresponded to that of the bottom boundary of the DSL. It is remarkable that the evaporating zone was located at the inflection point in water content profile and that the evaporating zone was extremely thin.

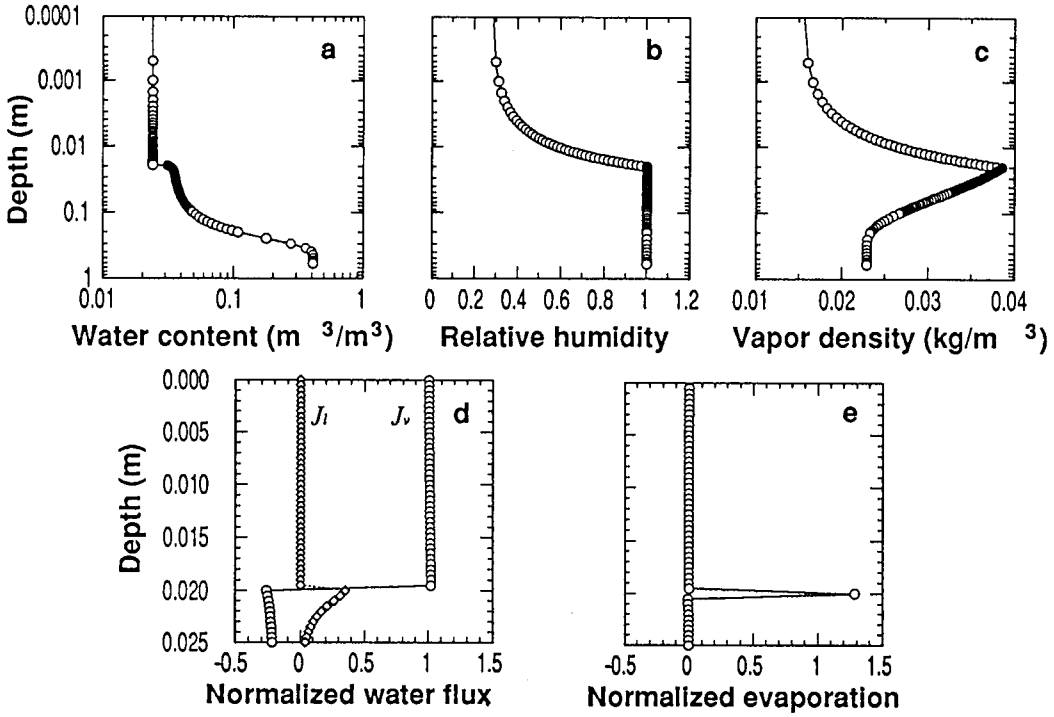

Fig.3 Computed vertical profiles for sand of (a) water content, (b) relative humidity, (c) vapor density, (d) liquid (J_l) and vapor (J_v) water fluxes, and (e) evaporation from each calculation node. The water fluxes and evaporation are normalized by evaporation into the atmosphere E_s.

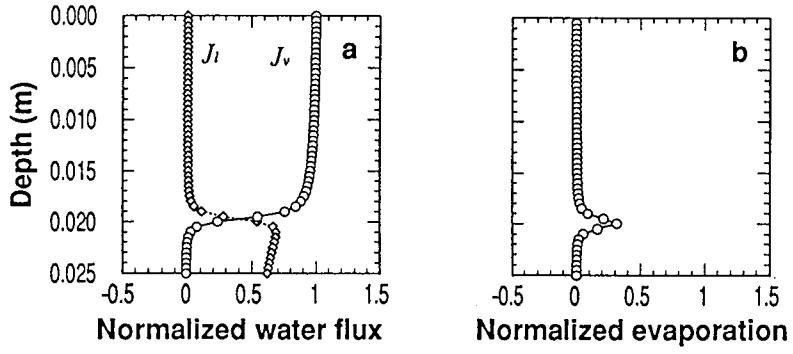

Fig.4 Computed vertical profiles for clay of (a) liquid (J_l) and vapor (J_v) water fluxes, and (b) evaporation from each calculation node. The water fluxes and evaporation are normalized by E_s.

The features like the above were also found out in the computed result for loam. On the other hand, for clay, two major points of difference can be found out (see Fig. 4). The first is that the decrease of liquid water flux toward soil surface around the bottom boundary of the DSL was relatively gentle, and thus, the thickness of the evaporating zone was relatively large. The second is that the vapor flux slightly increased toward soil surface at the upper region of the DSL, where no liquid water transport from deeper soil layer existed. The first point of difference is thought to be due to the difference of the properties of the unsaturated hydraulic conductivity and vapor conductivity between clay and other types of soil (see Fig. 5). For sand and loam, the unsaturated hydraulic conductivity rapidly decreased against the decrease of matric head, while it did not for clay. Therefore, the gentle shifting of water flux components for clay is thought to be owing to the gentle decrease of its hydraulic conductivity against matric head.

The second point of difference is related to the retention properties of soils. From the soil moisture characteristic curves (Fig. 2), the water contents of sand and loam demonstrate to have almost constant values at low matric-head level, where water transport in liquid phase is difficult to be made. On the other hand, it is shown that clay can retain abundant water at same level of matric head. Thus, it can be concluded that the soil water can evaporate from dry layer, where no liquid water supply from underlying soil, for highly retentive soils.

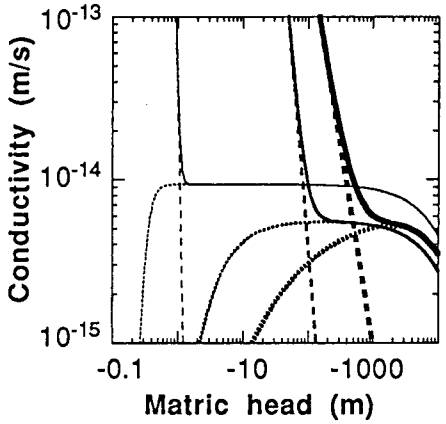

Fig.5 Relationships between conductivity and matric head for sand (thin line), loam (medium line) and clay (thick line). Broken and dotted line represent unsaturated hydraulic conductivity and vapor conductivity, respectively, and solid line represents the total of those.

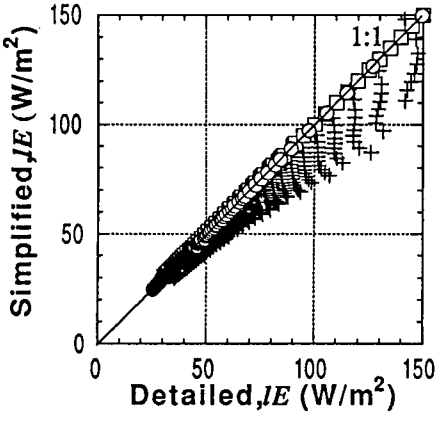

Fig.6 Comparison between evaporation estimated by the simplified method with eq. (3) and that obtained by the detailed model for sand (circle), loam (square) and clay (plus). Evaporation rate is presented as latent heat flux, where l is the latent heat for vaporization.

Assuming that the evaporating zone can be regarded as a horizontal plane, and that relative humidity at the evaporating zone is equal to unity, the evaporation rate can be represented by following equation, as

$$E_s' = \frac{\rho_a (q_{sat}(T_e) - q_a)}{1/C_E u + z_e/D_{ve}} \qquad (3)$$

where T_e is the temperature at the evaporating surface, z_e the depth of evaporating surface, which is corresponded to the thickness of the DSL, and D_{ve} the effective diffusivity of water vapor in the DSL. Figure 6 shows comparison of the evaporation estimated by the simplified method with equation (3) and that obtained by the detailed model mentioned the above. The values estimated by simplified method agree very well those obtained by the detailed model for sand an loam, although the simplified method tends to be lower than the detailed model due to the contribution of the evaporation occurred within the DSL. This indicates that equation (3) is effective to estimate the evaporation into the atmosphere, except for highly retentive soils.

Although it is not easy to directly measure the depth and temperature of the evaporating zone, the method to estimate the above two parameters from the conventional micro-meteorological measurement has been proposed by Yamanaka (1995).

4. Concluding remarks

It was clarified that the evaporating zone was located at the bottom boundary of the DSL, and was extremely thin for sand and loam. It was also shown that the parameterization, which regards the evaporating zone as a plane, is effective for those soils. These results indicate that information of the thickness of the DSL is required rather than that of water content of surface soil, to evaluate evaporation from bare soil surfaces. However, It should be noted that the above conclusions are obtained by assuming somewhat ideal conditions. The effects of the spatial variability in soil properties, the variation of atmospheric conditions, and the other factors, on the formation of the DSL and the structure of evaporating zone need to be investigated further.

Acknowledgements We thank Tokuo Kishii and Yasuhisa Kuzuha of National Research Institute for Earth Science and Disaster Prevention, and Fumi Sugita of Chiba University of Commerce, for their support and advice in conducting numerical computation. This research has been supported and financed, in part, by the Special Research Project on Global Environmental Change of the University of Tsukuba.

References

Milly, P.C.D., 1982. Moisture and heat transport in hysteretic, inhomogeneous porous media: A matric head-based formulation and a numerical model. *Water Resour. Res.*, 18: 489-498.

Philip, J.R. and de Vries, D.A., 1957. Moisture movement in porous materials under temperature gradients. *Trans. Am. Geophys. Union*, 38: 222-232.

Sugita, M., Ueda, S., Endo, N., Ohte, N., Oki, T., Kai, K., Kayane, I., Koike, T., Kondo, A., Shimada, J., Tanaka, T., Tsujimura, M., Tian, S-F., Nirasawa, H., Harazono, Y., Hiyama, T., Fukami, K., and Yasunari, T., 1993. Tsukuba 92 : an intensive field campaign to address scale issues in hydrology and boundary layer meteorology, (1) fluxes from land surface into the atmosphere. *J. Jap. Assoc. Hydrol. Sci.*, 23: 127-137.

van Genuchten, M.T., 1980. A closed-form equation for predicting the hydraulic conductivity of unsaturated soils. *Soil Sci. Soc. Am. J.*, 44: 892-898.

Yamanaka, T., 1995. Effect of Atmospheric Forcing on the Relation between Soil Moisture and Bare Soil Evaporation. M.S. Thesis, University of Tsukuba, 123 pp.

A Rational Parameterization of the Soil-Surface Evaporation for Estimating the Rate in Arid Regions by Remote Sensing

Wenjun He and Tetsuo Kobayashi
Faculty of Agriculture, Kyushu University
Fukuoka 812-81 Japan
Fax: +81-92-642-2804
e-mail: hewenjun@agr.kyushu-u.ac.jp
kobayasi@agr.kyushu-u.ac.jp

Abstract

The evaporation from bare soil changes in mechanism as well as in magnitude and proceeds in three stages as the surface dries. Therefore, only the parameterization schemes for soil-surface evaporation which take account of this stage switching should be considered as rational. A rational parameterization of soil-surface evaporation is proposed, in which the switching from one stage to another is determined by the difference in temperature between soil surface and surface air in the midafternoon. The evaporation rate under dry condition, or during the third stage is parameterized by the DSL bulk formulation which demands only remotely sensed data on temperature and soil moisture.

1. Introduction

The mechanism of evaporation from bare soil changes as the soil surface dries. Most conventional parameterization schemes for soil-surface evaporation are based on the assumptions that the whole evaporation process can be described by a single model without regard to the surface dryness and the change in rate can be predicted by using a few parameters, such as "water availability" or "resistance of water transport". However, these assumptions are divorced from reality, especially, under dry conditions.

In the last century, a lot of soil physicists and engineering chemists have studied on the mechanism of evaporation from, or for drying of, soil and concluded that the soil-surface evaporation proceeds in three stages as the surface dries (Lemon, 1956; Hillel, 1980). Thus, for the parameterization to be rational, this stage switching must be taken account of.

This paper describes a clear, objective definition of the three stages and a rational parameterization of the evaporation from bare soil. The evaporation rate from soil with a dry surface, or during the third stage is formulated by the parameters which can be evaluated by remote sensing techniques. The means of determining the stage switching is also discussed.

2. Three stages of soil-surface evaporation

The site of vaporization, or of phase transformation of water constitutes a zone (Phase Transformation Zone, PTZ), the location and thickness of which can be used to define the three stages of evaporation from bare soil.

1st stage : PTZ is located at the surface and its thickness is practically zero;
that is, complete vaporization occurs at the soil surface.

2nd stage: PTZ is located at the surface, but its thickness is not zero;
that is, vaporization occurs also within the soil.
3rd stage : PTZ is located within the soil and its thickness is not zero;
that is, complete vaporization occurs within the soil.

3. Structure of PTZ

In PTZ, water vapor density in soil pores decreases upward in linear fashion. During the third stage, a dry surface layer of soil (DSL), in which water moves exclusively in the vapor phase, is formed between the surface and PTZ. The gradient of water vapor density in the lower part of DSL is the same as that in PTZ, although the gradient in the upper part of DSL is not necessarily equal to it because the mechanism for water vapor transfer near the surface may differ from molecular diffusion. Thus, the thickness of PTZ increases with a increase in the thickness of DSL.

Soil moisture moves upward in both liquid and vapor phases in PTZ. If the ratio of the upward water flux in the liquid phase Q_L to the total one Q is denoted by γ, i.e.

$$\gamma \equiv Q_L / Q \qquad (1)$$

$0 < \gamma < 1$ in PTZ, $\gamma = 0$ in DSL, and $\gamma = 1$ below PTZ.

4. Models

4.1 First stage

The process of soil-surface evaporation during the first stage may be treated similarly to that of water-surface evaporation. Thus, the evaporation rate E_1 is nearly equal to the potential evaporation E_P, i.e.

$$E_1 = E_P \qquad (2)$$

4.2 Second stage

The second stage is a transition stage being on the way from atmosphere-controlled to soil-controlled evaporation, when the fraction of wet soil surface to the whole surface by geometric area may be approximately equal to γ (see (1)). Thus, the evaporation rate E_2 can be written in the form

$$E_2 = \gamma E_P + (1-\gamma) E_3 \qquad (3)$$

where E_3 is the rate during the third stage, which will be given later (see 4.3). Since $E_3 \ll E_P$, (3) becomes

$$E_2 \fallingdotseq \gamma E_P \qquad (3')$$

4.3 Third stage

During the third stage, water vapor produced within PTZ moves upward through DSL and comes out of the surface. Since the constant-flux layer of water vapor is not expected to develop in the surface air layer under these conditions (Tamagawa, 1996; Kobayashi et al., 1996), we shall focus attention on the water vapor flux in DSL.

Using the temperature T_o (K) and the water-constant (on a volume basis) θ_o ($cm^3 cm^{-3}$, %) in the uppermost about 2mm of bare soil, the average water content over a 5-cm slab of soil just below the surface θ_s, and the water content at the boundary between DSL and PTZ

(hygroscopic coefficient, pF=4.5) θ_δ, the evaporation rate from soil with a dry surface can be formulated as

$$E_3 = D'\{\theta_o - \theta_\delta\} / \delta \qquad (4)$$

where D' is a kind of diffusion coefficient (cm^3s^{-1}) and is expressed as $D' = C_T D(T_o)$, C_T being a factor for nonisothermal effects (<1) and $D(T_o)$ a function of T_o determined on the basis of molecular diffusion. δ is the thickness of DSL(cm) and is assumed to be expressed by a function of θ_s, i.e. $\delta = \delta(\theta_s)$. θ_o is also assumed to be a function of T_o and θ_s.

Consequently, the rate of soil-surface evaporation in the third stage can be estimated from T_o and θ_s which may be evaluated by remote sensing techniques. This formulation will be called the "DSL bulk method".

5. An example application

An experiment was conducted in a sand field at Kyushu University to get the relations which is needed to apply the DSL bulk method to a soil. The Tottori Dune sand was used, and all measurements were made at about 1500 (JST) when the soil-surface evaporation can be considered as a near steady state process. The actual evaporation rate was measured by the DSL method (Kobayashi and Nagai, 1995).

The results obtained from the experiment are

$$D(T_o) = 7.53 \exp(0.0649\, T_o - 34.88) \qquad (5)$$

$$\delta(\theta_s) = 6.30 \exp(-0.41\, \theta_s) \quad \text{(Fig. 1)} \qquad (6)$$

$$\theta_o(T_o, \theta_s) = 2.75 + 0.0267\, \theta_s - 0.00795\, T_o \quad \text{(Fig. 2)} \qquad (7)$$

$$\theta_\delta = 1.53$$

$$C_T = 0.89$$

6. Estimation of daily evaporation by the DSL bulk method

The evaporation rate E_3 estimated using, for example, the relations obtained above is the rate at 1500 (JST). Since the rate of evaporation from soil exhibits a diurnal variation, it is necessary to clarify the pattern of diurnal change in evaporation rate and to integrate it in order to get the daily amount of evaporation.

Fig.3 shows the time changes of the daily mean evaporation rate E_{dm} (open circles), which is estimated based on four measurements made at 0600, 1000, 1500 and 1900 by the DSL method, and of the rate at 1500 E_{1500} (closed circles). On 25 July, the sand field was irrigated with approximately 5cm of water and then allowed to dry, the weather being fine during the period of study 25 to 31 July, 1995.

Dotted lines show 0.3 (open squares), 0.4 (closed squares) and 0.5 (open diamonds) the rate at 1500, respectively. In a few days after the irrigation, the ratio of E_{dm} to E_{1500}, denoted by R_{dm}, decreased and approached the value of 0.39. This value of R_{dm} is consistent with the result obtained at the HEIFE desert station in the northwest of China (Kobayashi and Nagai, 1995).

Although R_{dm} changes with time elapsed since the irrigation or rainfall, the daily evaporation from dry soil may be estimated from a measurement of evaporation rate made in the midafternoon by the DSL method or by the DSL bulk method along with R_{dm}.

7. Determination of the stage switching

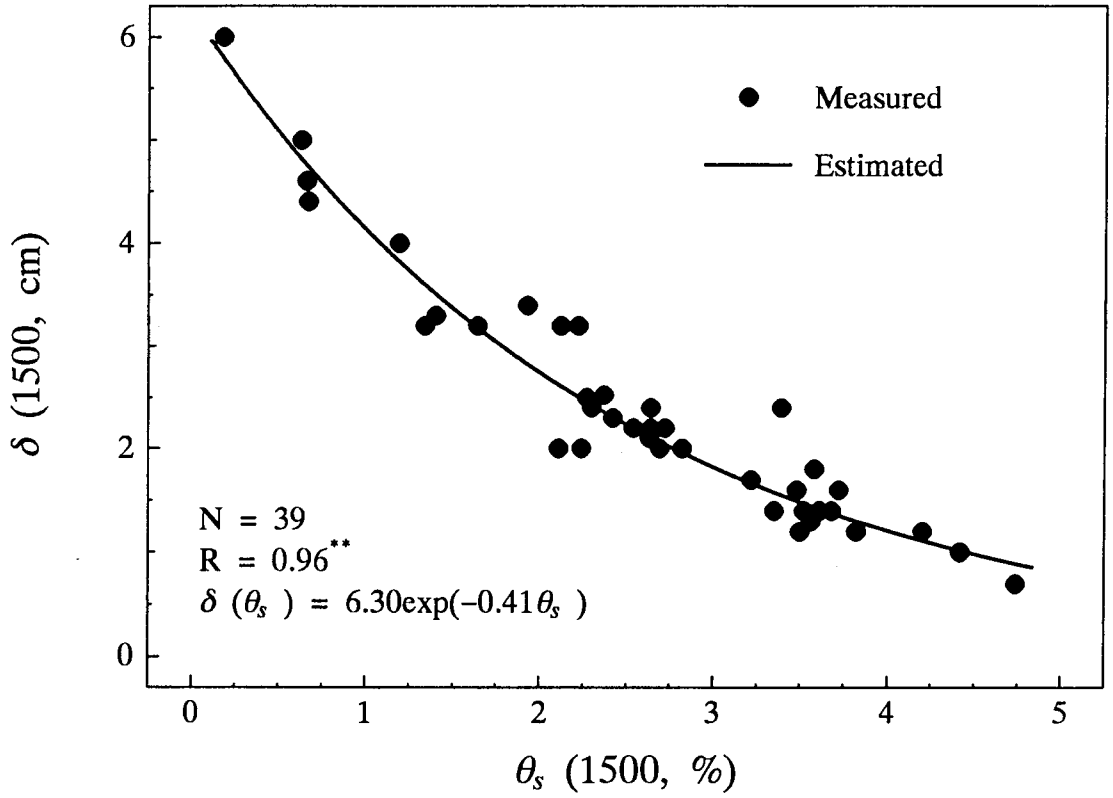

Fig.1 Relation between δ and θ_s at 1500 on clear days

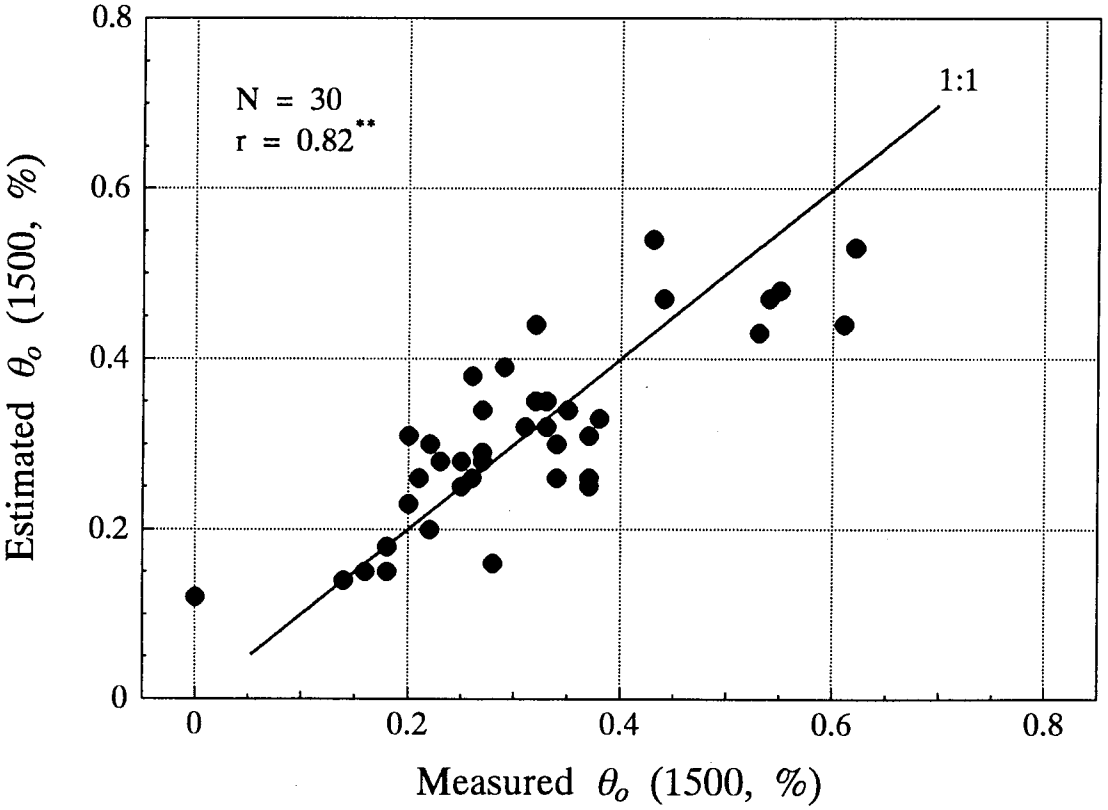

Fig.2 Relation between θ_o and its estimate made with a regression equation on θ_s and T_o (see (1))

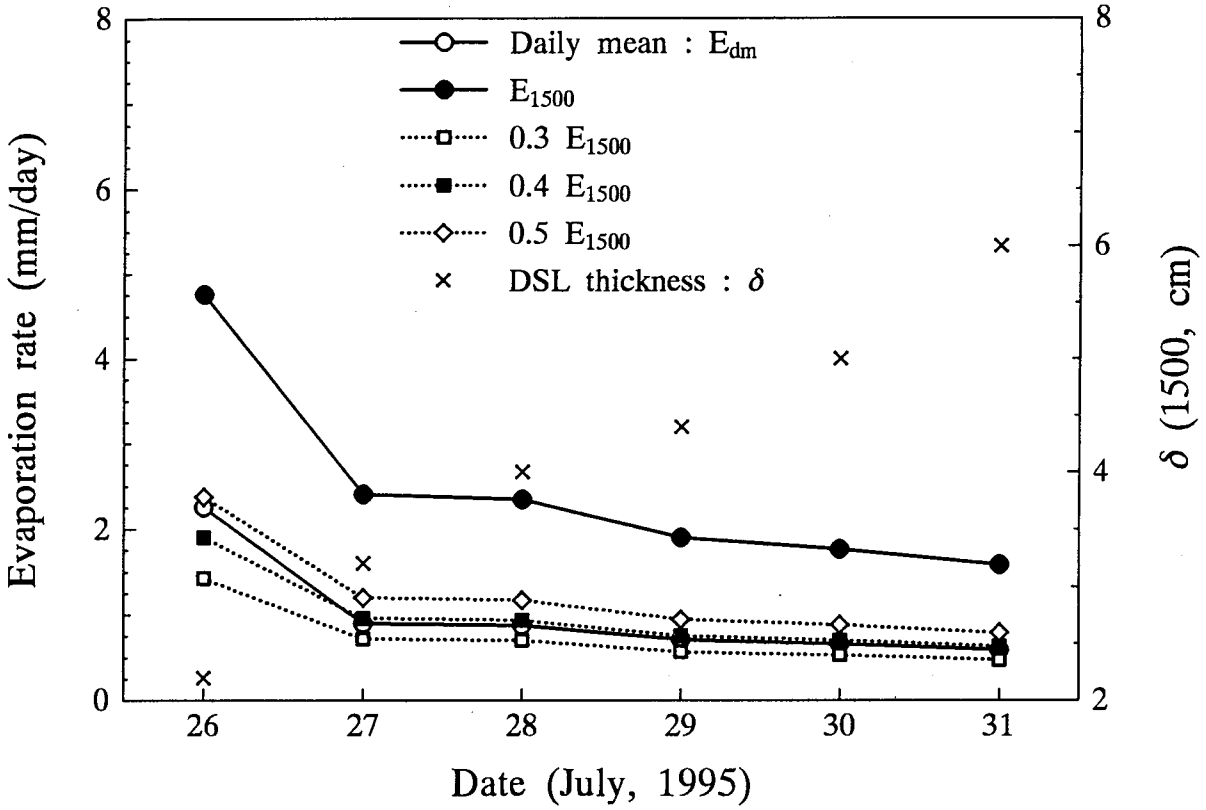

Fig.3 The variations of the daily mean evaporation rate obtained by the DSL method, E_{dm} and the rate at 1500, E_{1500} The cross showes the thickness of DSL at 1500.

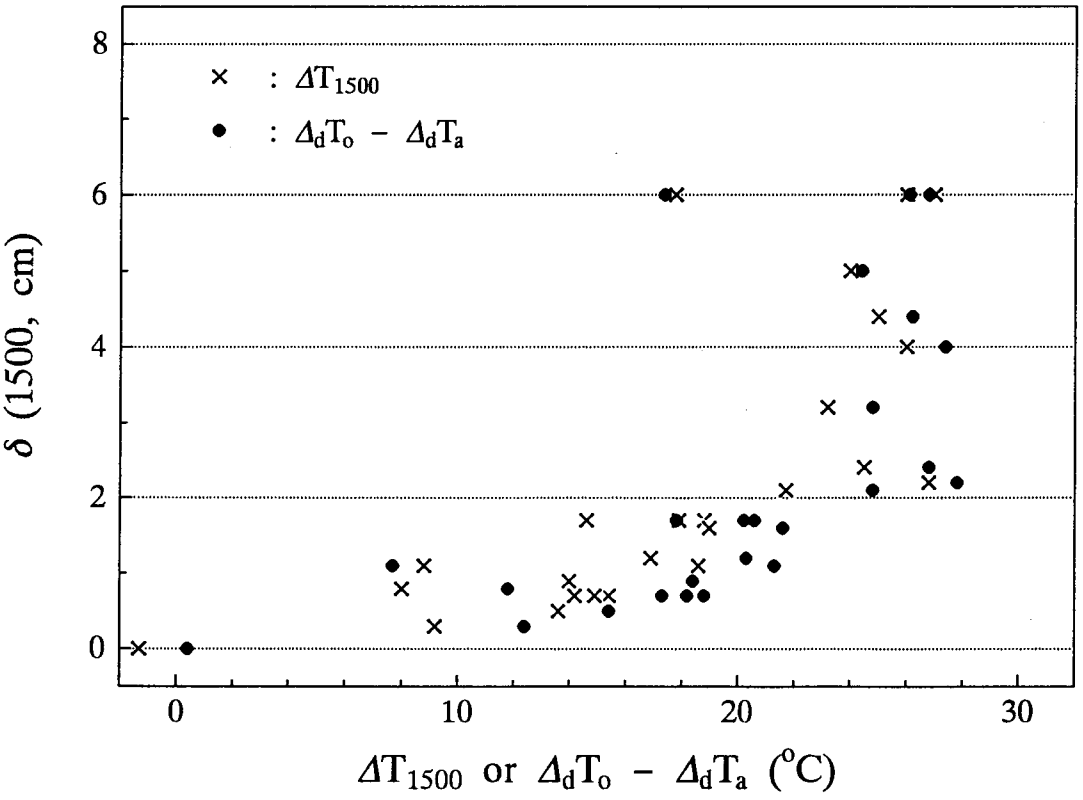

Fig.4 Relation between δ and ΔT_{1500} or $\Delta_d T_o - \Delta_d T_a$ at 1500 on clear days.

The transition points between the different stages have been investigated by a few scientists (Idso et al., 1974; van Bavel and Hillel, 1976). They pointed out that albedo measurements or diurnal surface temperature amplitudes might be effective to depict transitions from one stage to another. In the present study, the difference in diurnal range between surface temperature and air temperature at 1.2m height, $\Delta_d T_o - \Delta_d T_a$, and the difference between surface temperature and air temperature at 1.2m height in the midafternoon (1500 JST), ΔT_{1500} are utilized.

Fig.4 shows the relation between the thickness of DSL and ΔT_{1500}(crosses) or $\Delta_d T_o - \Delta_d T_a$ (closed circles), which were obtained in the sand field at Kyushu University on clear days. When DSL is visible, the third stage evaporation is occurring. From these results it might be concluded that if the temperature difference ΔT_{1500} is larger than about 10℃ on clear days, the third stage of soil-surface evaporation is already reached. During the first and second stages DSL is not formed yet, and so ΔT_{1500} should be smaller than several degree C, although few data were taken because DSL was formed in the clear, midafernoon except immediately after irrigation or rainfall in the sand field.

8. Concluding remarks

Most parameterization schemes for soil-surface evaporation heretofore in use are based on the concept that vaporization of liquid water occurs at the surface and the effects of the drying of soil surface can be represented by such parameters as "water availability" or "resistance of water transport". However, in the present scheme, the change in mechanism as the stage progresses was accepted as an essential idea.

A new parameterization of soil-surface evaporation during the third stage (DSL bulk method) was proposed, which demands the data on temperature and soil moisture that can be evaluated by remote sensing.

References

Hillel, D., 1980 : *Applications of Soil Physics.* Academic Press, 109-146.

Idso, S. B., R. J. Reginato, R. D. Jackson, B. A. Kimball and F. S. Nakayama, 1974 : The three stages of drying of a field soil, *Soil Sci. Soc. Amer. Proc.*, **38**, 831-837.

Kobayashi, T., W. He, H. Nagai and K. Adachi, 1996 : Discontinuity in the vertical profile of water vapor density at hot, dry soil surface, *J. Japan Soc. Hydrol. & Water Resour.*, **9**, 438-443 (in Japanese with English summary).

Kobayashi, T. and H. Nagai, 1995 : Measuring the evaporation from a sand surface at the HEIFE desert station by the dry surface layer (DSL) method, *J. Meteor. Soc. Japan*, **73**, 937-945.

Lemon, E. R., 1956 : The potentialities for decreasing soil moisture evaporation loss. *Soil Sci. Soc. Amer. Proc.*, **20**, 120-125.

Tamagawa, I., 1996 : Turbulent characteristics and bulk transfer coeffients over the desert in the HEIFE Area, *Boundary-Layer Meteor.*, 77, 1-20.

van Bavel, C. H. M. and D. I. Hillel, 1976 : Calculating potential and actual evaporation from a bare soil surface by simulation of concurrent flow of water and heat, *Agr. Meteor.*, **17**, 453-476.

Surface Flux Measurements at Desert and Oasis in HEIFE Project

Osamu Tsukamoto(*), Ken Sahashi(**), Jiemin Wang(#) and Yasushi Mitsuta(&)

* Faculty of Science, Okayama University
3-1-1 Tsushima-naka Okayama 700 Japan
Fax:+81-86-251-8506
e-mail: tsuka@cc.okayama-u.ac.jp

** Okayama University

\# Lanzhou Institute of Plateau Atmospheric Physics,CAS
Lanzhou,Gansu,730000,P.R.China
Fax:+86-931-8821158

& Disaster Prevention Research Institute, Kyoto University
Gokasho, Uji, 711 Japan
Fax: +81-774-33-0026

Abstract

In the field campaign of air-surface interaction in north-west China(HEIFE), surface flux measurements were carried out over complex land use area in arid region. The contrast between desert and vegetated oasis are remarkable in the surface radiation balance and surface heat balance. A large amount of radiative energy is released from desert surface and lead to less net radiation than the plant canopy surface. Most of the radiative energy absorbed by the oasis surface are released as the latent heat flux due to evapotranspiration. Another interesting finding is the diurnal variations of air temprerature and humidity. Air temperature over oasis surface are lower than over desert throughout a day and have larger amplitude of diurnal variation. The significant evening peak of vapor pressure is a characteristic over oasis in calm fine days.

1.Introduction

For the understanding of land-surface processes in semi-arid region of north-west China, the HEIFE project was planned as a Sino-Japanese cooperative program as a sub-program of HAPEX. The experimental area is situated in the Hexi corrodor in Gansu province extending 37°15'-42°42'N, 92°21'-104°05'E as illustrated in Fig.1. The north of the area is a part of extending Gobi and/or desert. While, Qilian mountains are extending in the south of the HEIFE region as a important water source. The Heihe river originates in the glaciers of Qilian mountains and irrigates the river basin. HEIFE area consists of complex land usees, such as desert, Gobi, irrigated field and so on. HEIhe river Field Experiment(HEIFE) was planned for the study of land-surface processes over complex land use area in this arid region.

The project was carried out in 1989-1993, and Intensive Observation Periods(IOP) were set in 1991 and 1992 as field experiment. Various kinds of filed measurements were carried out including upper air soundings and surface observations at several basic stations representing the land use of the local area.

In the present paper, the results of surface flux measurements at desert and oasis are summarized.

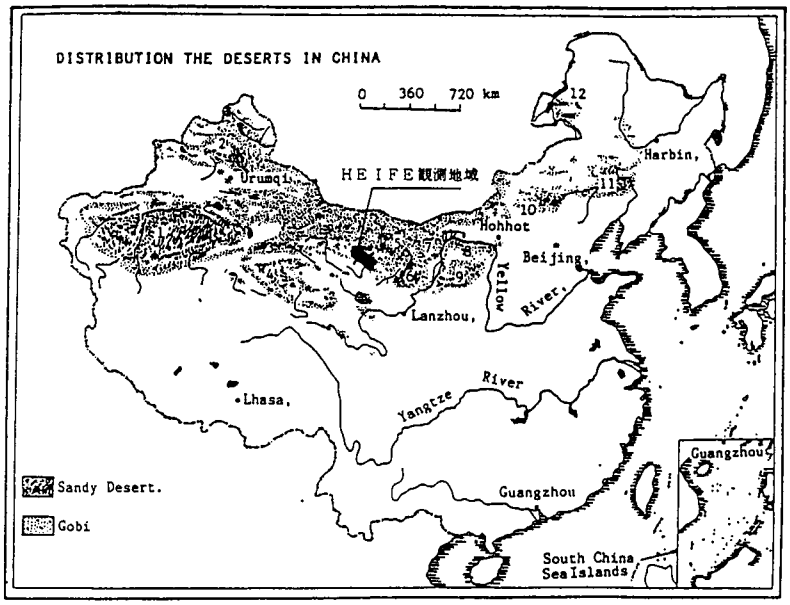

Fig.1 Map of HEIFE area

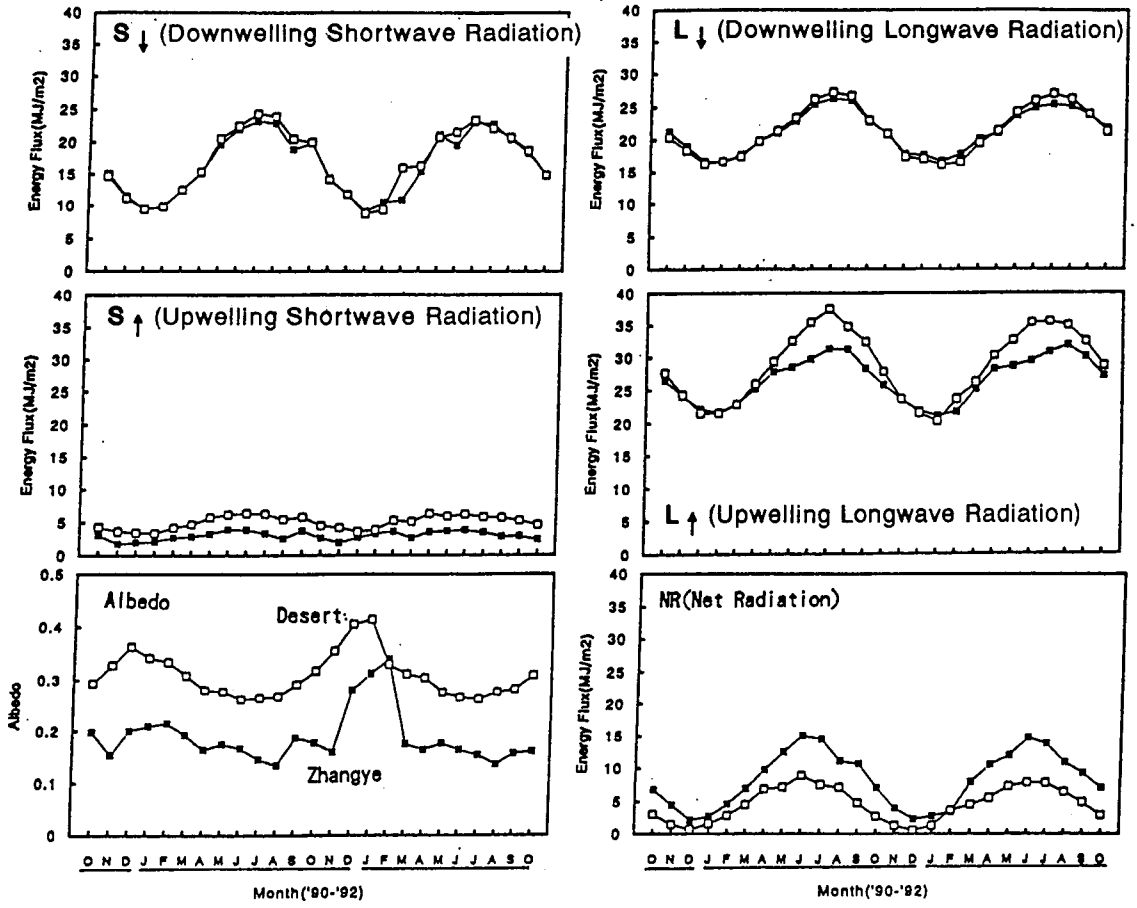

Fig.2 Comparisons of radiation components between oasis and desert for 2 years of FOP

2.Radiation fluxes

4-components of radiation fluxes were measured separately at basic stations. Downwelling and upwelling shortwave/longwave radiation data were obtained from 2 sets of pyranometers(EKO, MS-801) and pyrgeometers(EKO, MS-200). Net radiation was calculated as a sum of 4-components. The data were obtained continuously during the period of Fundamental Observation Period(FOP;Oct 1990-Sept 1992) as a 30 minutes mean values.

Fig.2 shows the comparison of radiation components between Zhangye oasis and desert as a daily integrated values. It is clearly observed that downwelling shortwave/longwave radiations($S\downarrow$, $L\downarrow$) are almost identical between the two sites, which is separared by about 80km. While upwelling radiations are remarkably different. From the upwelling shortwave radiation($S\uparrow$), it is found that surface albedo is about 0.2 over oasis and about

0.3 over desert, except in winter. In winter, relatively large values of albedo were observed due to snow fall and low solar angles. Upwelling longwave radiation($L\uparrow$) also reflects the difference of surface condition. However, the values are almost equivalent in winter because of little vegetation over oasis surface. As a result, remarkable difference of net radiation flux(NR) are observed especially in summer season. Desert surface can only absorbe about two-third of oasis surface due to large amount of upwelling radiative fluxes.

Diurnal variations of radiative components are compared in Fig.3 as a clear day data in summer. Downwelling components are almost identical. It should be commented that downwelling longwave radiation measurement include the effects of dome heating and shortwave contamination and a kind of correction was applied in the present study. When those errors are removed, the diurnal variation is almost neglected. While the upwelling shortwave/longwave radiation data reflect the effect of surface vegetation over oasis surface.

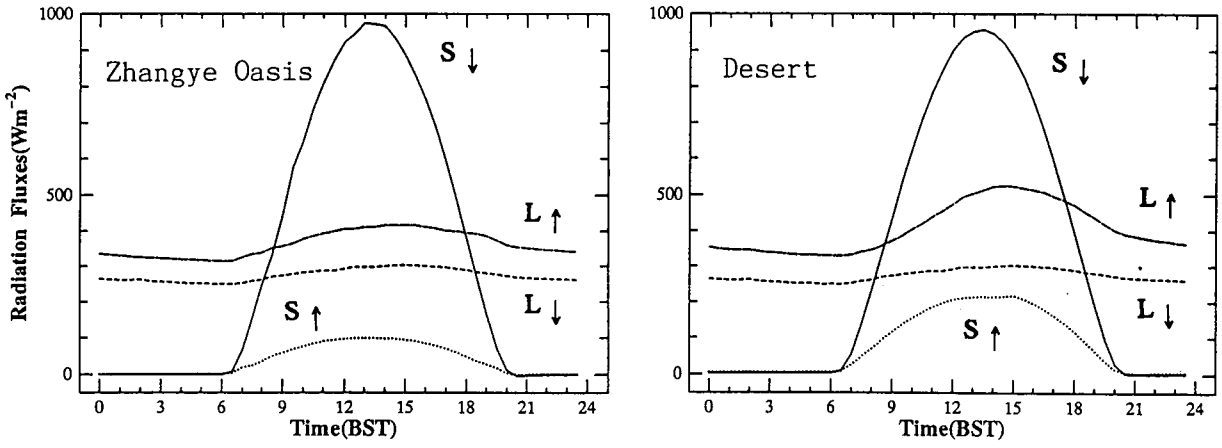

Fig.3 Comparisons of diurnal variations of radiation components between oasis(left) and desert(right) on a summer fine day

3.Turbulent heat and water vapor fluxes

Turbulent fluxes of heat and water vapor(latent heat) were obtained with eddy correlation method during the Intensive Observation Period(IOP). The turbulence measurement system consists of a three dimensional sonic anemometer-thermometer(Kaijo, DAT-300) and an infrared hygrometer(Kaijo, AH-300). The system also includes 2 sets of clinometers to measure the level of the anemometer probe. The anemometer probe was

faced against the mean wind direction with a rotation system. The turbulence data acquisition system was operated every 2hours throghout the IOP to get 30 minutes statistics.

The eddy correlation method was applied only the IOP and it it not enough to understand the seasonal variation of turbulent fluxes. Continuous measurements of surface layer profiles were carried out with a VAISALA MILOS system during FOP. The profile system includes the measurements of air temperature/humidity and wind speed at 5 levels(20m, 8m, 4m, 2m, 1m) and wind direction at 3 levels(20m, 4m, 1m). Continuous data of surface fluxes can be obtained from profile method with the use of eddy correlation flux data as a standard.

In addition to the surface layer profile measurement, soil temperature/moisture data were also obtained at 5 depths(-5cm, -10cm, -20cm, -40cm, -80cm). Soil heat fluxes were calculated as a integration of soil temperature changes.

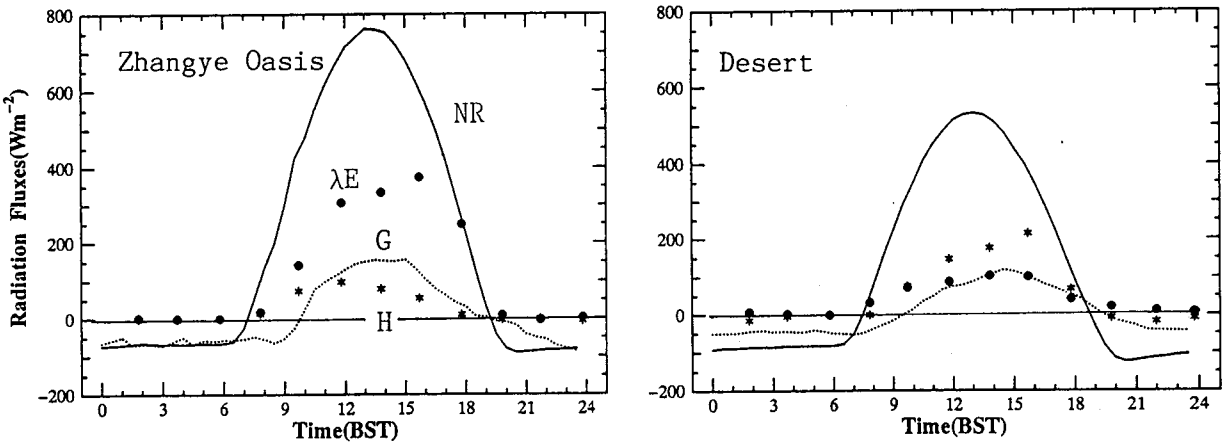

Fig.4 Comparison of diurnal variations of surface fluxes between oasis(left) and desert(right) on a summer fine day. NR: Net Radiation(solid line), G: Soil Heat Flux(dashed line), H: Sensible Heat Flux(asterisk), λE: Latent Heat Flux(closed circle)

4.Surface heat balance

Fig.4 compares the surface heat balance components on a fine day in summer. It is shown that net radiation is smaller in desert and large values of sensible heat flux were observed. While in oasis station, most of the energy is released as latent heat caused by evapotranspiration from vegetated surface.

Fig.5 indicates the daily integrated surface heat balance component in various seasons. The height of each column corresponds to net radiation and turbulent fluxes of sensible

and latent heat are marked in the column. The representative value of the Bowen ratio (H/λ E) is about 0.2 over oasis and 3-10 over desert. The latent heat flux correspond to surface evapotranspitations of 3.4/0.61mm(Aug), 1.7/0.11mm(Oct), 0.2/0.03mm(Dec), 2.8/(none)mm(May) and 3.9/0.31mm(Jun) as daily integrated values at oasis/desert. During BIOP-2, remarkable downward sensible heat flux was observed during daytime accompanied by large amount of latent heat release. Wang et al.(1993) has pointed out that this might be due to warm air advection from the surrounding desert and this is considered to be a kind of "oasis effect". Considering that daily integrated soil heat fluxes are almost negligible, a large amount of energy is missing especially in vegetated surface.

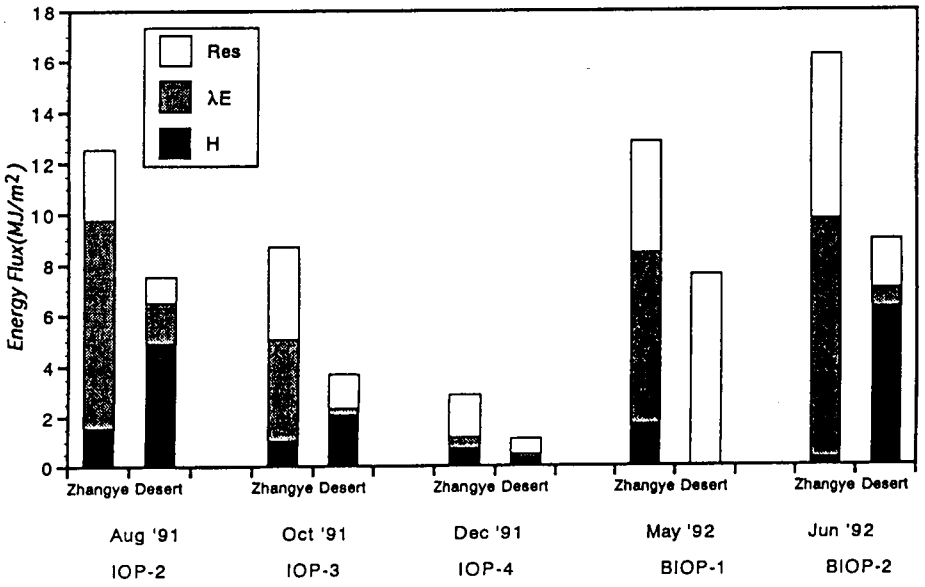

Fig.5 Seasonal variation of surface heat budget components at Zhangye oasis and desert. The height of the column represent the net radiation over a day and heat fluxes of sensible(H) and latent(λE) heat are hatched in the column. The residuals(Res) are left open. No turbulent heat fluxes were obtained in BIOP-1 at desert.

5.Conclusive remarks

Fig.6 compares the diurnal variations of air temperature, relative humidity and vapor pressure over oasis and desert. It is found that air temperature of oasis is always lower than that of desert even in nighttime. And it is also interesting that oasis air temperature rises/falls more quickly than over desert and lead to a larger amplitude of diurnal variation. However larger amplitude of soil temperature is observed at desert. This can be attributed to the difference of heat capacity of the dry sand and wet soil in the field. Another interesting observation is the significant evening peak of vapor pressure over oasis as

shown in the top figure. This is observed in calm fine days especially in summer. Fig.7 shows the time series of air temperature and vapor pressure for several days in Zhangye oasis. It is clearly observed in the evenings of 15th,16th and 17th accompanied by temperature changes. These interesting phenomena should be related to surface processes of heat and water balance as well as desert-oasis interaction including horizontal advection.

In the HEIFE project, a lot of surface measurements were carried out over various surface condition. However spatial study with remote sensing is very limited(Masuda,1993; Zhong and Wu,1993). Wang et al.(1995) reported a preliminary study of scaling up of surface measurements with LANDSAT data and further detailed study should be required to the understanding of desert-oasis interaction over heterogeneous surface.

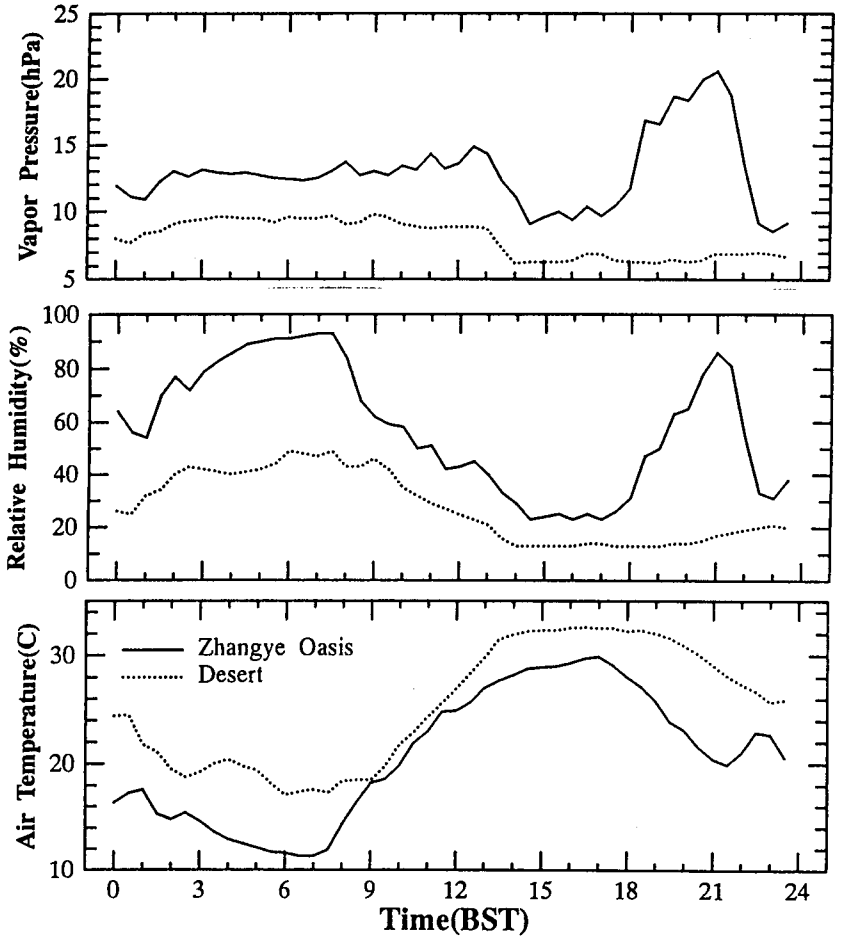

Fig.6 Diurnal variations of air temperature, relative humidity and vapor pressure at oasis(solid) and desert(dashed) on a summer fine day

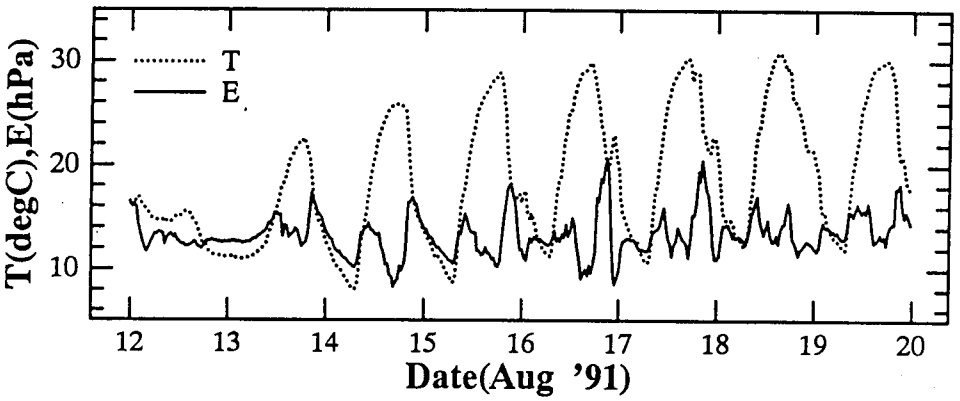

Fig.7 Time series of air temperature and vapor pressure at Zhangye oasis for several days in summer. Significant evening peaks are observed in 15,16,17th.

6.References

Masuda,K.(1993), "Processing NOAA satellite data for HEIFE", Proc. International Symposium of HEIFE, 575-579.

Mitsuta,Y.(1993),"Proceedings of International Symposium on HEIFE", Disaster Prevention Research Institute, Kyoto University,722p.

Sahashi,K.,Tsukamoto,O.,Mitsuta,Y. and Wang,J.,"Peculiar daily cource of the specific humidity and the air temperature over Zhangye filed",Proc. International Symposium of HEIFE,430-436.

Tsukamoto,O.,Sahashi,K. and Wang,J.(1995), "Heat budget and evapotranspiration at an oasis surface surrounded by desert", J.Meteorol.Soc.Japan,73,925-935.

Tsukamoto,O., Wang, J. and Mitsuta Y.(1992),"Significant evening peak of vapor pressure at an oasis in the semi-arid region", J.Meteorol.Soc.Japan,70,1155- 1159.

Wang,J.,Y.Ma,M.Menenti,W.Bastiaanssen and Y.Mitsuta(1995):The scaling-up of processes in the heterogeneous landscape of HEIFE with the aid of Satellite remote sensing", J.Meteorol.Soc.Japan,70,1235-1244.

Wang,J., Y.Ma, J.Li, K.Sahashi, E.Ohtaki, O.Tsukamoto, T.Maitani and Y.Mitsuta (1993): Downward sensible heat flux during daytime observed in the oasis station, Proc. International Symposium of HEIFE, 449-457.

Zhong,Q. and Wu,A.(1993), "Determination of surface albedo over HEIFE experimental area by combining satellite and surface measurement data",Proc. International Symposium of HEIFE, 580-587.

Use of Satellite Data for Studying the Land Surface-Atmosphere Interaction over the African Sahel

Masato Shinoda(*), Hirokazu Iwashita(*), Akiyo Yatagai(**), and Minoru Gamo (***)

*Department of Geography, Tokyo Metropolitan University, Hachioji, Tokyo, Japan 192-03
Fax: +81-426-77-2589 E-mail: shinoda@geog.metro-u.ac.jp
**EORC, National Space Development Agency of Japan, Minato-ku, Tokyo, Japan 106
***National Institute for Resources and Environment, Tsukuba, Japan 305

Abstract

A time-series analysis on the seasonal and interannual time scales has been applied to ground-observed rainfall data, NOAA-derived normalized difference vegetation index, and mixing layer temperature data of objective analysis for the western Sahel region. The results suggested that rainfall anomalies that are produced over western Sahel during a short rainy season are maintained in the land surface (soil moisture/vegetation) anomalies persisting over the following dry season. The land surface anomalies may function as transmitter of the rainfall anomalies to the next rainy season.

1. Introduction

The semi-arid region of the world is characterized by the dry savanna or steppe vegetation and a small amount of annual precipitation concentrated on a short rainy season along with a large amplitude of its interannual variability. For example, the Sahel, defined climatologically as the region located south of the Sahara desert receiving an annual precipitation of 200-800mm (Fig.1), experienced recurring droughts in this century, especially a long-term persistent drought during the late 1960s to 1980s (Fig.2) (Shinoda, 1995a).

Since the 1970s, a large number of observational and numerical simulation studies have long been made on the causes of such a long-term drought; global sea surface temperatures (*e.g.*, Folland *et al.*, 1986) and regional land surface conditions (*e.g.*, Charney, 1975). The recent statistical analysis showed that more than half of the variance in Sahel rainfall is explained by the top three modes of global SST anomalies derived from a rotated empirical orthogonal function analysis (Shinoda, 1995a), confirming the previous study of Parker *et al.* (1988). These results indicate that the land surface processes, whose importance has been pointed out by Charney (1975) and among others, play only a secondary role in the interannual variation in Sahel rainfall.

No attempts have, however, been made to estimate the quantitative effect of anomalous land surface conditions on atmospheric and rainfall anomalies over the semi-arid region. NOAA satellite data, that have been accumulated over nearly two decades, yield a valuable basis for studying the year-to-year variations of the large-scale land surface and atmospheric conditions. In the present study, a comprehensive analysis of ground-observed and NOAA satellite-derived

land surface/atmospheric data and objective analysis atmospheric data has been conducted in order to reveal the mechanism how the anomalous land surface conditions affect the overlying atmosphere on the seasonal and interannual time scales.

2. Seasonal changes in rainfall, soil moisture, and vegetation: their interactions

A seasonal phase lag in the response of vegetation to rainfall and its dependence on the type of vegetation in tropical Africa have been investigated, using weekly-basis data of the NOAA/AVHRR-derived normalized difference vegetation index (NDVI) and outgoing longwave radiation (OLR) (Shinoda, 1995b). The lag-correlation analysis of the NDVI and OLR data demonstrated that over the dry savanna regions (including the Sahel), the NDVI responds most markedly to the OLR by 6-9 weeks (Figs.3 and 4). This relatively long time-lag, compared with that for the equatorial forest region, may be explained by the time required for accumulating soil moisture available for the vegetation growth and/or the time for the physiological start of growth to the establishment of green biomass (Fig.5).

The ground-based observation in the Sahel of southern Niger revealed detailed seasonal changes in rainfall, soil moisture, and leaf area index (LAI) of millet (Fig.6), indicating a time-lag similar to that found in the response of the NDVI to the OLR. That is, the rainy season of 1995 begins in early June, resulting in the increase in soil moisture and finally the growth of rain-fed millet at the end of the rainy season.

3. Interannual variations of rainfall, NDVI, and mixing layer temperature: their interactions

The time series of monthly rainfall (a), biweekly NDVI (b), and monthly thickness between 850-700 hPa (c), spatially averaged over western Sahel (see Fig.1) are presented in Fig.7. The NDVI data set used here is developed by Kevin P. Gallo of National Oceanic and Atmospheric Administration (NOAA)/National Environmental Satellite, Data, and Information Service (NESDIS). The biases observed in the NDVI time series, derived from the changes in the NOAA-series satellites and the delays of the equator-crossing time of each NOAA satellite, are calibrated by removing, from the western Sahel time series, the time series for the adjacent Sahara desert which exhibits only small vegetation activity all year round.

The thickness in the above layer represents the overall temperature of the mixing layer which generally develops up to the 700hPa level with the exception of the northern winter season. The thickness values are calculated from objective analysis grid-point data of geopotential height produced at the National Centers for Environmental Prediction (NCEP).

As for the annual cycle (solid curve), the rainfall reaches its maximum during August or September, leading that of the rainfall by 0-1 month. Rainfall anomalies (dotted curve) from the seasonal change averaged over 1986-1990 (broken curve) also appear to precede anomalies of the NDVI by 0-1 month. It should be noted that the anomalies in the NDVI which are created during a rainy season tend to persist over the following dry season such as 1987/88 and 1988/89 until the next rainy season. This implies that the land surface anomalies persisting over the dry season may act as transmitter of rainfall anomalies that occur during the preceding rainy season.

Interestingly, the lower tropospheric temperature between 850-700 hPa increased during the 1987/88 dry season when less vegetation was observed from the NOAA satellite, while it reduced during the 1988/89 dry season when more vegetation was found. The timing of change

in the sign of the thickness anomaly generally coincides with that of the NDVI anomaly. These results suggest that the land surface conditions affect the lower tropospheric temperature through sensible heat transfer.

The analyses of the NDVI and mixing layer temperature for the Sahel will be extended to the period 1982-1994. In relation to the NDVI (that is, vegetation activity), an examination will be made of the monthly evapotranspiration over the region that is derived from precipitation minus atmospheric moisture flux convergence.

4. Concluding remarks

The time-series analysis of the rainfall, NDVI, and mixing layer temperature suggested a possibility that rainfall anomalies produced over the semi-arid region during a short rainy season are maintained in land surface (soil moisture/vegetation) anomalies persisting over the following season. The anomalous land surface conditions appear to affect the mixing layer temperature through sensible heat transfer. If the long-term decline in Sahel rainfall is due, in part, to the land surface processes, a rainfall anomaly may lead to the anomaly of the same sign during the following rainy season, through the anomalous land surface conditions persisting over the long dry season. This mechanism may operate as positive feedback.

The future investigation should focus attention on the detection of such persistent land surface anomalies and their impacts on the overlying atmosphere by using the satellite date sets having long-term homogeneous quality.

5. References

Charney, J.G. (1975): Dynamics of deserts and drought in the Sahel. *Quart.J.R.Met.Soc.*, 101, 193-202.

Folland, C.K., Palmer, T.N., and Parker, D.E. (1986): Sahel rainfall and worldwide sea temperatures, 1901-85. *Nature*, 320, 602-607.

Parker, D.E. , Folland, C.K., and Ward, M.N. (1988): Sea-surface temperature anomaly patternsand prediction of seasonal rainfall in the Sahel region of Africa. In Gregory, S. ed.: *Recent climatic change.* Belhaven Press, London, 166-178.

Shinoda, M. (1995a): Roles of sea surface temperatures and land cover on the Sahelian drought. *J.Geogr.*, 104, 592-598.

Shinoda, M. (1995b): Seasonal phase lag between rainfall and vegetation activity in tropical Africa as revealed by NOAA satellite data. *Int.J.Climatol.*, 15, 639-656.

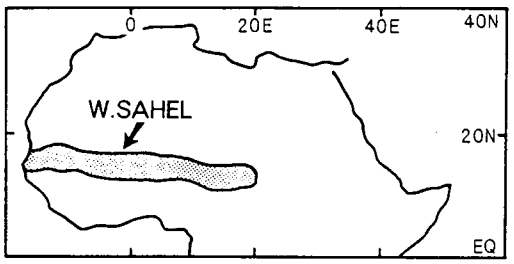

Fig.1 Location of western Sahel (Shinoda, 1995a).

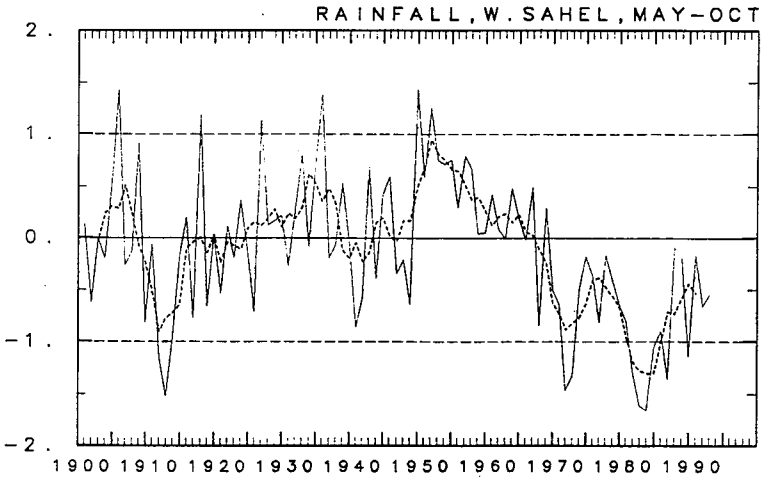

Fig.2 Interannual variation of May-October rainfall for western Sahel. The broken curve indicates the five-year running mean (Shinoda, 1995a).

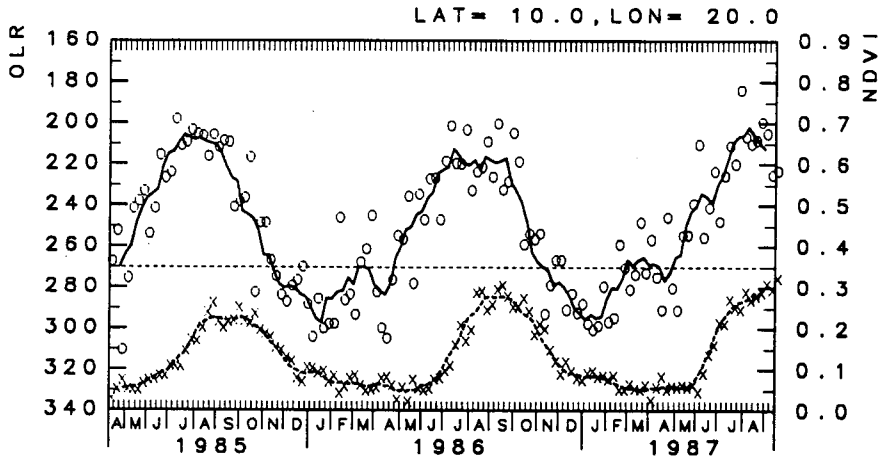

Fig.3 Seasonal changes in weekly data of the NDVI (cross) and OLR (circle) at 10°N, 20°E during April 1985-September 1987 (Shinoda, 1995b). The broken and solid curves indicate the respective 5-week running means. The OLR threshold of 270 Wm^{-2} below which seasonal rainfall is expected to occur is denoted by the horizontal broken line. Note that the y-axis of OLR is inverted.

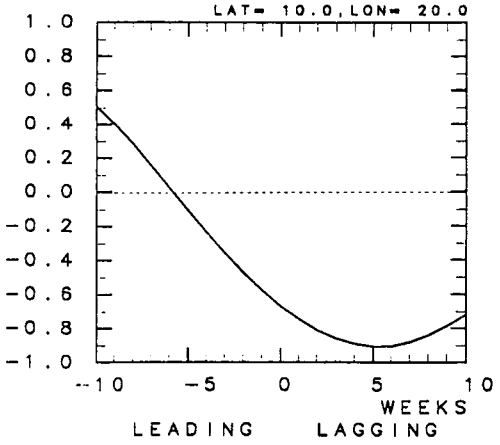

Fig.4 Lag correlation between the NDVI and OLR at 10°N, 20°E (Shinoda, 1995b). The leading (lagging) indicates that the NDVI is leading (lagging) the OLR. The lag-correlation coefficients are calculated by using the 5-week running means of the NDVI and OLR.

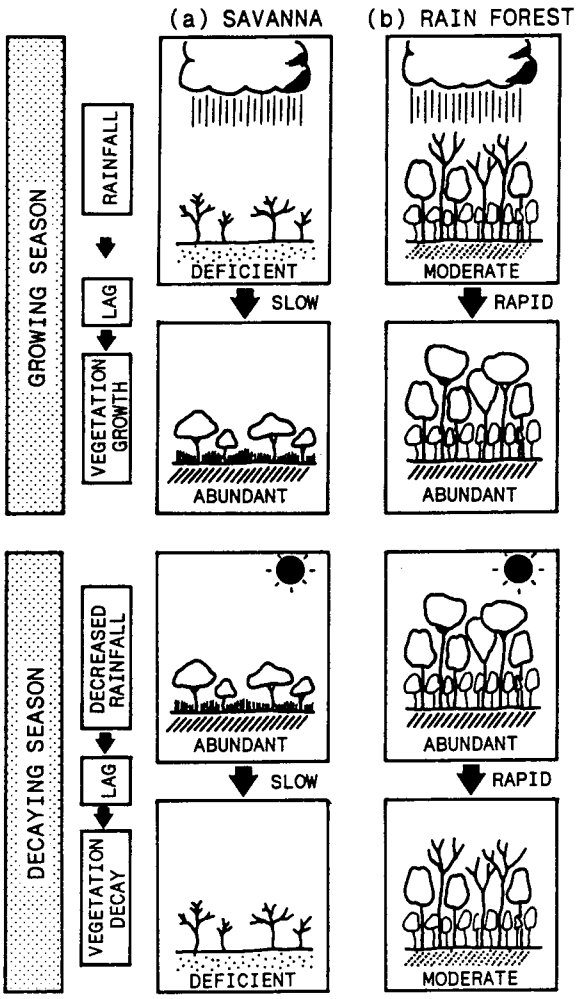

Fig.5 Schematic diagram showing the response of the NDVI to rainfall over the (a) tropical savanna and (b) equatorial rain forest (Shinoda, 1995b).

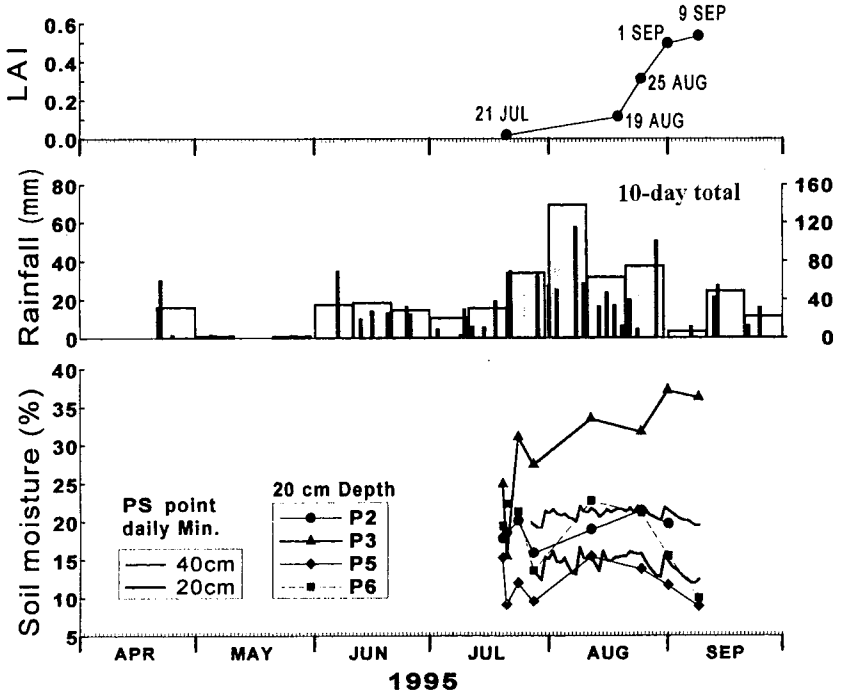

Fig.6 Seasonal changes in rainfall, volumetric water content (%), and leaf area index at a site located in southern Niger. Points PS, P2, and P3 are located in the lowlands, while Points P5 and P6 are located on the plateau

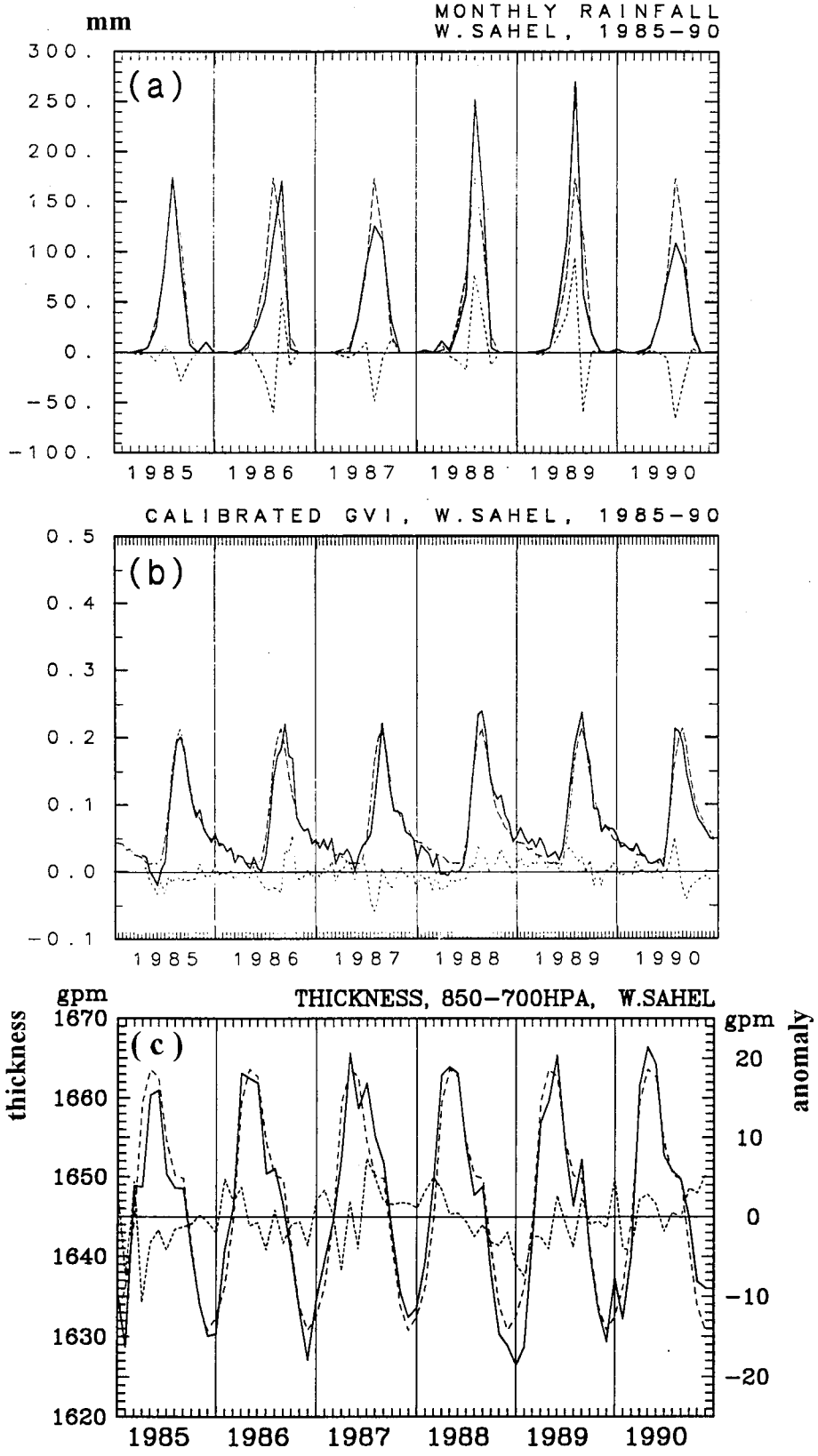

Fig.7 Time series of (a) monthly rainfall, (b) biweekly NDVI (Shinoda, 1995a), and (c) thickness between 850-700 hPa for western Sahel during 1985-1990 (solid curve). The broken and dotted curves denote the seasonal changes averaged over 1986-1990 and anomalies from the averaged seasonal changes, respectively.

Monitoring the Drying Process Using Multi-Temporal AVHRR Data in 1990, Huaihe River Basin, China

Atsushi Higuchi[1] , Akihiko Kondoh[2], Shinkichi Kishi[3], Teruki Fukuzono[3], and Jiren Li[4]

ABSTRACT

Recent researches have shown that the combination of spectral vegetation indices (VIs) with thermal infrared observations may provide an effective method for parameterizing surface processes at large spatial scales. In this study, we tested a hypothesis that seasonal changes in the slope of VIs and surface temperature T_s derived from the satellite remote sensing are sensitive to drying processes of surface moisture status.

Huaihe River Basin, which is the study area, is characterized by steep climatological gradient from southeast to northwest. Annual precipitation in the study area decreases from southeast to northwest.

NOAA/AVHRR (Advanced Very High Resolution Radiometer) GAC (Global Area Coverage) data over the study area for the continuous 80 days after *Meiyu* (the name of rainy season from June to July, in China) of 1990 were used to derive VIs as well as T_s values, while meteorological data provided by NOAA GDS (Global Daily Summery) CD-ROM was used for analysis.

After applying radiometric and geometric correction, we evaluated the slope and intercept, i. e. T_s versus VIs relationships (T_s/VIs). Results of this study are summarized as follows

Seasonal changes in slope and intercept derived from T_s and VIs relations for agricultural fields correlate well to these of antecedent precipitation index (API). Moreover, It was clear that seasonal changes in T_s versus VIs relations were not only affected by seasonal changes of land surfaces moisture status, but also sensible to the effect of irrigation practice.

INTRODUCTION

Interactions between the land surface and the atmosphere, and the resulting exchanges of energy and water have a large effect on climate. The partitioning of energy at earth's surface, between sensible and latent heat fluxes, is strongly controlled by surface moisture status.

Recent researches have indicated that the combination of spectral vegetation indices (VIs) with thermal infrared observations is an effective method for parameterizing surface processes at large spatial scales. Fig. 1 shows an example of these studies (Nemani and Running, 1989). Concept of these studies is based on Goward *et al.* (1985) suggestion. Goward *et al.* (1985) suggested the possibility of using the rate of change in surface temperature with amount of vegetation to describe surface characteristics.

In this study, we tested a hypothesis that seasonal changes in the slope of VIs and surface temperature T_s derived from the satellite remote sensing are sensitive to drying process of surface moisture status.

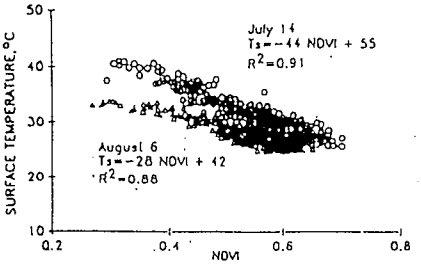

Fig. 1 Relation between surface temperature and normalized differenced vegetation index, a measure of leaf area index, from NOAA AVHRR on 6 August (Wet) and 14 July (Dry) (Nemani and Running, 1989).

[1]Doctoral Program in Geoscience, University of Tsukuba, Environmental Research Center (ERC), University of Tsukuba, 1-1-1 Tennodai, Tsukuba-shi, Ibaraki 305, JAPAN, higu@erc2.suiri.tsukuba.ac.jp

[2]Center for Environmental Remote Sensing*(CEReS)*, Chiba University, 1-33 Yayoi-cho, Inage-ku, Chiba 263, JAPAN

[3]National Research for Earth Science and Disaster Prevention, 3-1 Tennodai, Tsukuba-shi, Ibaraki 305, JAPAN

[4]Water Resources Development and Utilization Laboratory, Hohei University, CHINA

DESCRIPTION OF THE STUDY AREA

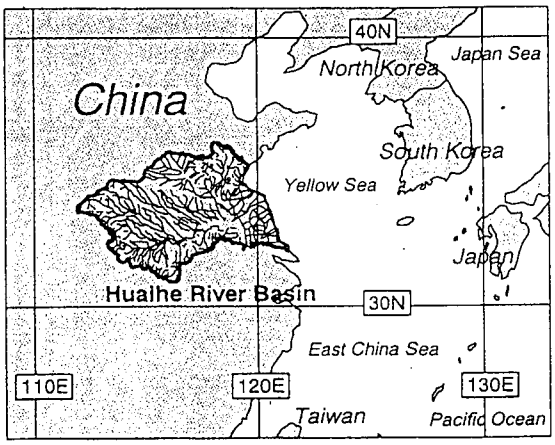

Fig. 2 Location of the Huaihe River Basin.

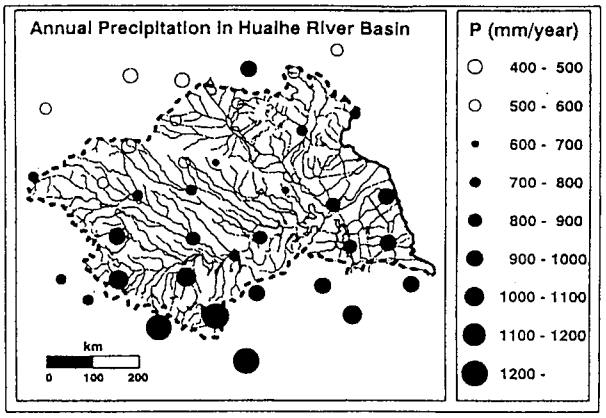

Fig. 3 Distribution of annual average precipitation in Huaihe River Basin.

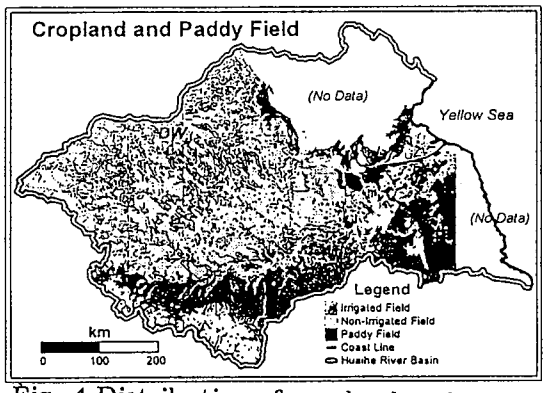

Fig. 4 Distribution of cropland and paddy field.

Huaihe River Basin (HRB) lay the south of Yellow River and the north of Yangzi River, China (Fig. 2). Catchment area of HRB is 260 $\times$ 10^3 km^2, and two third of HRB is occupied by a vast stretch of a flat plain.

Climates of the study area drastically change within catchment. Southeast of HRB is in subtropical climate, and annual precipitation of this area is over 1000 mm. In contrast northwest of HRB is in semi-arid climate, and annual precipitation of this area is less than 500 mm (Fig. 3).

Vegetation and land use of the study area are generally classified into two areas (Fig. 4). Main land cover in the study area is cropland (irrigated field or non-irrigated field) in northwest, and paddy field in the southeast, although forests are present in mountainous area. Main vegetation is wheat or beans in northwest , and rice in southeast.

METHODOLOGY

Data source

In this study, NOAA 11 AVHRR GAC (Global Area Coverage) data over HRB for continuous 80 days (from 198 DOY (Day Of the Year) to 277 DOY) after *Meiyu* of 1990 were used.

Precipitation records were used from NOAA GDS (Global Daily Summery) CD-ROM (NOAA, 1994). Among 10000 stations, sixty stations are located within HRB.

Radiometric correction

The raw NOAA AVHRR data are 10-bit data (from 0 to 1023 counT$_s$). In order to convert AVHRR data into radiance (channel 1 and channel 2) or brightness temperature (channel 3, channel 4, and channel 5), it is necessary to apply the radiometric correction.

Method of the radiometric correction was followed as Kidwell (1991). Moreover, we applied calibration considering the sensor degradation (Kaufman and Holben, 1993) and solar zenith angle correction for channel 1 and channel 2.

Geometric correction

Geometric correction for registering the images on a base image employed distributed GCPs (Ground Control Points). As the base image, RESTEC (Remote Sensing Technology Center of Japan) NOAA AVHRR MOSAIC IMAGE over China which included HRB was used. We used nearest-neighbor method as interpolation method, which interpolates nearest observation point to interpolation point.

Evaluation of Vegetation Indices (VIs), surface temperature (T_s), Antecedent Precipitation Index (API), and T_s/VIs relationships

After applying radiometric correction and geometric correction, vegetation indices (VIs) were evaluated.

$$NDVI\ (Normalized\ Difference\ Vegetation\ Index) = \frac{\rho_{ch.2} - \rho_{ch.1}}{\rho_{ch.2} + \rho_{ch.1}} \quad (1)$$

$$SAVI\ (Soil - Adjusted\ Vegetation\ Index) = \frac{\rho_{ch.2} - \rho_{ch.1}}{\rho_{ch.2} + \rho_{ch.1} + L_s}(1 + L_s) \quad (Huete,\ 1988) \quad (2)$$

$$MSAVI\ (A\ Modified\ Soil - Adjusted\ Vegetation\ Index) = \frac{\rho_{ch.2} - \rho_{ch.1}}{\rho_{ch.2} + \rho_{ch.1} + L_m}(1 + L_m) \quad (3)$$

(Qi et al., 1994)

L_s ;soil adjustment factor ($L_s = 0.5$)
L_m ;soil adjustment factor ($L_m = 1 - 2\gamma NDVI \times WDVI$)

γ ;primary soil line parameter ($\gamma = 1.06$)
WDVI ;Weighted Difference Vegetation Index ($WDVI = \rho_{ch.2} - \gamma\rho_{ch.1}$)

Surface temperature T_s for each pixel was estimated using split-window techniques. Split-window technique was originally developed to estimate sea surface temperature (SST) by McMillin and Crosby (1984) as follows;

$$SST = 3.175 + 0.429T_3 + 2.698T_4 - 2.139T_5 \quad (McMillin\ and\ Crosby,\ 1984) \quad (4)$$

Antecedent precipitation index (API) as an index of surface moisture status by the algorithm of Choudhury *et al.*,(1987) was estimated from precipitation and temperature data within NOAA GDS, as follows;

$$API_{j+1} = K_j(API_j + P_j) \quad (5)$$

P_j ;total rainfall on day j
API_j ;the soil wetness (mm of water available for evaporation) on day j
K_j ;soil water recession coefficient on day j

$$K_{j+1} = exp(-E_j/W_m) \quad (6)$$

E_j ;potential evaporation (mm) on day j
W_m ;maximum depth of soil water available for evaporation (15mm)

According to the algorithm by Nemani *et al.*,(1993), scatterplots of T_s and VIs are created in 10 × 10 pixels window region (about 40 × 40 km^2), and the slope and intercept of upper envelope are extracted automatically.

RESULTS AND DISCUSSION

Response of different VIs

Fig. 5 shows a comparison between different VIs (NDVI, SAVI and MSAVI) values. According to Qi *et al.* (1994), MSAVI show the density of vegetation. When MSAVI values are close to SAVI, density of vegetation is intermediate. MSAVI values in HRB are similar to SAVI (MSAVI = 0.875123 SAVI - 0.00300534)(see Fig. 5 (c)).Vegetation over HRB indicates intermediate vegetation in the growing season. NDVI values are higher than ether SAVI or MSAVI (see Fig. 5 (a) and (b), respectively). It indicates that NDVI is affected by soil reflectance noise.

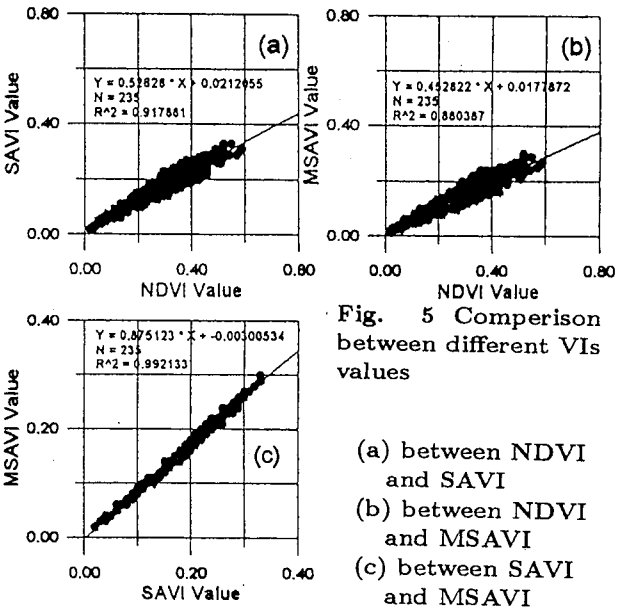

Fig. 5 Comperison between different VIs values

(a) between NDVI and SAVI
(b) between NDVI and MSAVI
(c) between SAVI and MSAVI

Relationship between T_s and VIs relations and Antecedent Precipitation Index (API) for different land uses

If the land surfaces are wetted by rainfall, much of the absorbed short radiation energy is consumed in evaporation (latent heat flux) and T_s values would show no difference between soils and leaves, resulting weak or no relationships between T_s and VIs. Inversely, if the land surfaces are being dry, steep relation in T_s/VIs because of changes in the partitioning of energy between sensible and latent heat fluxes. Are these assumptions confirmed in this study area?

Fig. 6 shows the time series of slope value and API in selected GDS stations. Climate condition in these GDS stations changes from semi-arid to subtropical, from Fig. 6 (a) to (d). During the *Meiyu* period, the slope values are relatively small in each station. In the rainless period after *Meiyu* between DOY 230 and DOY 250, the slope gradually becomes steep (large minus value). This change can be regarded as the drying process of ground surface. Because insolation is strong at the period just after the *Meiyu*, several no rainy days are enough to suppress soil evaporation. Dominated transpiration and suppressed soil evaporation make the slope in T_s/VI relationship steep.

Fig. 7 shows the spatial and temporal changes of the slope values in selected DOYs. Light color shows the dry condition, and the black (zero intensity) means the sea, cloudy condition, or out of image. In the rain period on DOY 212 (30 Jul.), slope distribution shows that middle of the basin is in wet condition. In the western and southern part of the basin, slope indicates the relatively dry condition. On DOY 240 (29 Aug.), there is a westward trend from wet to dry condition in the slope distribution. This slope distribution shows that the northern edge of the basin is in wet condition. It may be attributed to the irrigation practice, because rainfall do not occur this region from 10 days before. The general trend is from wet condition in eastern region to dry condition in western region, which is compatible annual precipitation distribution referred in Fig. 3. It offers the evidence that spatial and temporal slope values in T_s/VIs relationships can apply to the "useful indicator" monitoring drying process of surface moisture status .

CONCLUSION

This study tested a hypothesis that seasonal changes in the slope of VIs and T_s derived from the satellite remote sensing are sensible to drying process of surface moisture status. The time series of the slope values in T_s/VIs relationships were well corresponded to the API as an indicator of surface dryness. It indicated the usefulness of T_s/VIs relationships to estimate surface moisture status or to monitor drying process.

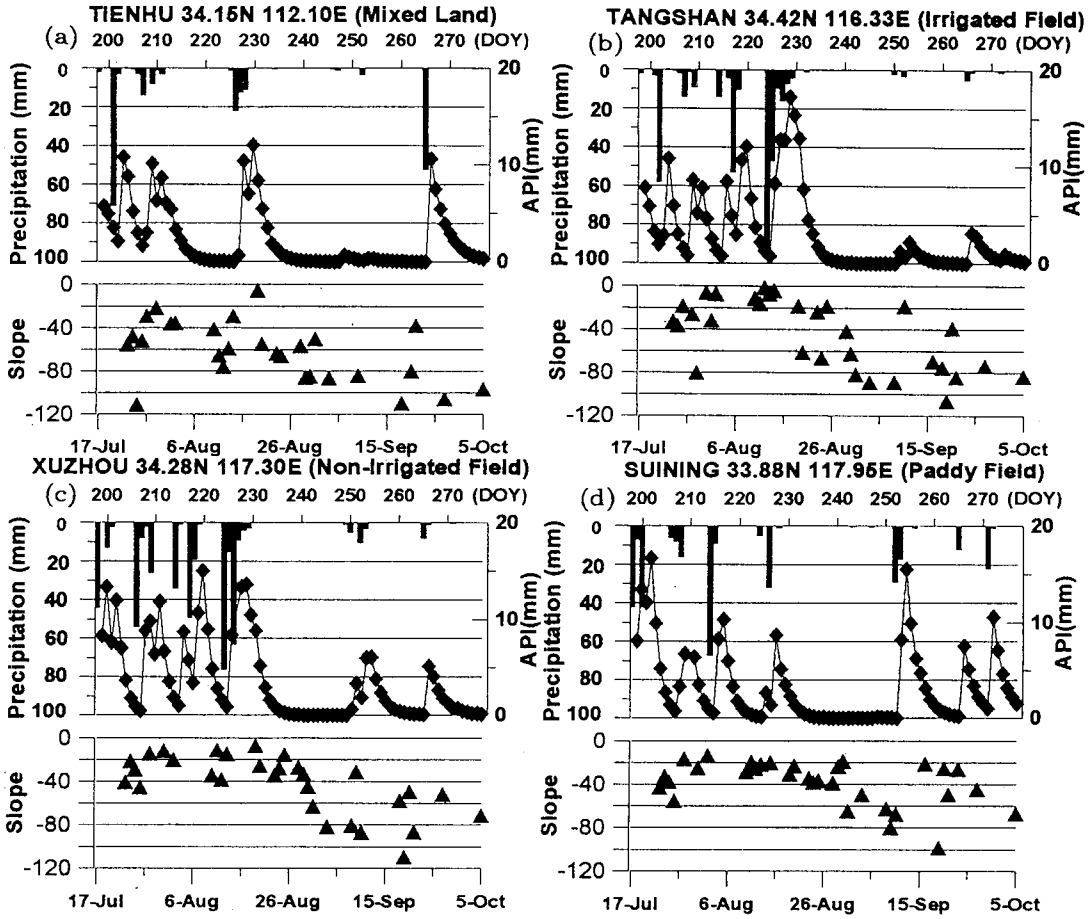

Fig. 6 The changes in dayly precipitation, antecedent precipitation index (API) and the slope of T_s/VI relationship in (a) mixed land, (b) irrigated field, (c) non-irrigated field, and (d) paddy field.

REFERENCE

Choudhury, B. J., Owe, J., Goward, S. N., Golus, R. E., Ormsby, J. P.,Chang, A. T. C., and Wang, J. R. (1987): Quantifying spatial and temporal variabilities of microwave brightness temperature over the U. S. Southern Great Plains, *Int. J. Remote Sensing*, **8**: 177-191

Goward, S. N., Cruickshanks G. D., and Hope A. S. (1985): Observed relation between thermal emission and reflected spectral radiance of a complex vegetated landscape, *Remote Sens. Environ.*, **18**: 137-146.

Huete, A. R. (1988): A soil-adjusted vegetation index, *Remote Sens. Environ.*, **25**: 295-309.

Kaufman, Y. J. and Holben B. N. (1993): Calibration of the AVHRR visible and near-IR bands by atmospheric scattering, ocean glint and desert reflection, *Int. J. Remote Sensing*, **14**: 21-52.

Kidwell, K. B. Ed. (1991): NOAA POLAR ORBITER DATA USERS GUIDE (TIROS-N, NOAA-6, NOAA-7, NOAA-8, NOAA-9, NOAA-10, NOAA-11, AND NOAA-12),NATIONAL OCEANIC AND ATMOSPHERIC ADMINISTRATION NATIONAL ENVIRONMENTAL SATELLITE, DATA, AND INFORMATION SERVICE NATIONAL CLIMATRIC DATA CENTER SATELLITE DATA SERVICE DIVISION.

McMillin, L. M. and Crosby D. S. (1984): Theory and validation of the multiple window sea surface temperature,*J. Geophys. Res.*,**89,C3**: 3655-3661.

Nemani, R. R., and Running S. (1989): Estimation of surface resistance to evapotranspiration from NDVI and thermal-IR AVHRR data,*J. Appl. Meteor.*,**28**: 276-284.

Nemani, R, R., Pierce, L., Running, S., and Goward, S. (1993): Developing satellite-derived estimates of surface moisture status, *J. Appl. Meteor.*, **32**: 548-557.

Qi, J., Chehbouni A., Huete A. R., Kerr Y. H., and Sorooshian S. (1994): A modified soil vegetation index,*Remote Sens. Environ.*,**48**:119-126.

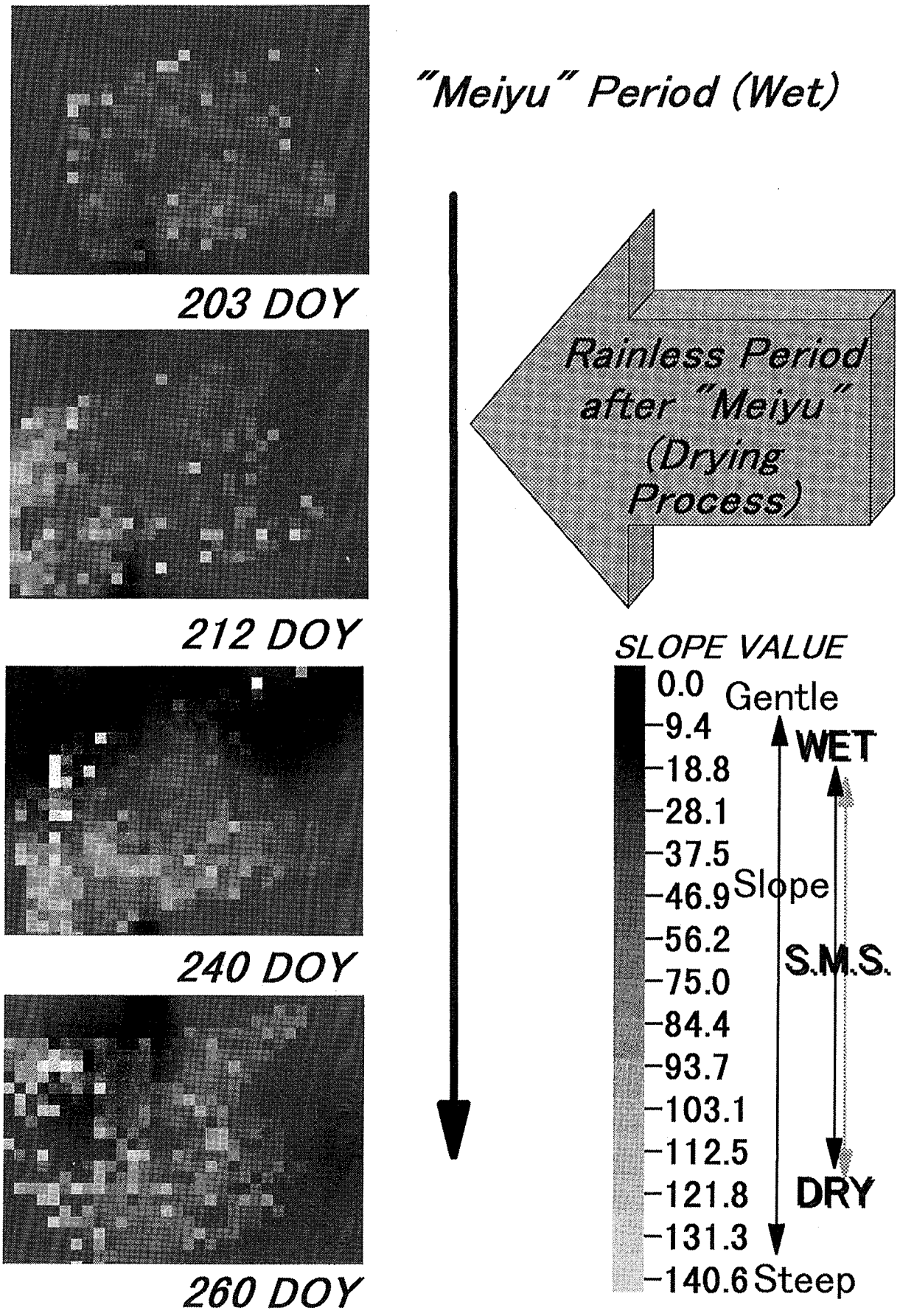

Fig. 7 Time series of spatial slope values which represent the drying process. (S.M.S. means Surface Moisture Status.)

Estimation of Groundwater Recharge on Various Sites in a Tropical Semiarid Basin using a Water Balance Model in Dry Surface Soil.

Shinichi Onodera

Environmental Science, University of Tsukuba
1-1-1 Tennodai Tsukuba 305 Japan
Fax:+81-298-53-6709
Email:onodera@kankyo.envr.tsukuba.ac.jp

Abstract

In this study, a simple water balance model linking with Green-Ampt model was improved on basis of measured results in a semiarid upland, Tanzania, and it was applied to local areas under different soil or rainfall conditions in a same basin. In spite of only three parameters with regard to the part under the ground in this model, the calculated value simulated well the measured value. In this model, the critical rainfall which groundwater recharge occurs was determined by the soil physical properties, and field observations also indicated this tendency. Furthermore, the effects of the soil and rainfall condition on the groundwater recharge were confirmed.

1. Introduction

Evaluation of groundwater recharge in a regional basin is a basic information for efficient groundwater resource management as well as for forecasting hydrologic process with the change in climate or land use (Allison et al.,1994). It is particularly important in regions where groundwater is a water source for municipal use. In recent years, many studies on groundwater recharge in various semiarid zones have estimated the natural groundwater recharge rate using physical (Gee et al., 1994) and chemical methods (Sukhija et al., 1988; Gee and Hillel,1988; Sharma, 1989 etc.). On the other hand, spatial and temporal informations of plant cover or soil condition can be obtained using remote sensing data. In spite of the accumulation of many case studies, it has been difficult to predict recharge rate in a regional basin where local areas under the various conditions might exist. Because the large errors were included in estimating the actual evapotranspiration and water flux in the vadose zone (Gee and Hillel,1988) , there were few applicable physical models to predict recharge rates in various local areas.

For developing the applicable physical model to groundwater recharge in semiarid zones, it is necessary to confirm the hydrological process in surface soil using direct physical methods, and to improve the classic physical model on the basis of measured processes. In this study, a simple water balance model linking with Green-Ampt model was improved on basis of measured results in a semiarid upland, Tanzania, and it was applied to local areas under different soil or rainfall conditions in a same basin.

2. Water balance model in surface soil

The case considered here is the water balance in surface soil without the absorption by the plant roots in the deep soil under the tropical semiarid. If the transpiration is negligible in deep soil, the evaporation front locates near ground surface. Therefore, the water balance in surface soil is described as:

$$R = P - E - Q + \Delta V \qquad (1)$$

where R, P, E, Q, ΔV are the groundwater recharge, precipitation, evaporation, overland flow, and change in soil water content, respectively. In tropical semiarid regions, the annual potential evapotranspiration exceeds 2000mm, and daily potential evapotranspiration exceed 5mm even during a rainy season. On the other hand, the daily actual evapotranspiration (AE) rapidly decreases with the soil water content after the rainfall event, and it always is extremely lower than the potential evapotranspiration (PE) during the dry season (Hayashi, 1990). In this model, the runoff was used measured values and evaporation rate was calculated by the estimated PE (Onodera et al., 1996) and the measured linear relationship between the PE and AE.

During a rainfall event, the rain water usually fills with pores in surface soil and flows over the ground surface (Onodera, 1996). In addition, it penetrates concentratedly and partially in dry sand (Grass et al., 1989; Onodera, 1993) or through the preferred pathway (Stephens, 1994) . The infiltration process in the dry soil with the overland flow is similar to Green-Ampt Model. Based on the assumption of the model, the infiltration rate (q) is written using Darcy's equation as,

$$q = Ks\,(1 - (\psi b - \psi t) / Ls) \qquad (2)$$

where, Ks is the permeability and it equals the saturated hydraulic conductivity, ψb shows the pressure head at the wetting front and equals the water entry value (ψw), ψt shows the pressure head at the ground surface, and Ls shows the length of the wettiig zone. ψt is the positive value under the ponded infiltration and equals the ponded depth or overland flow depth. Then ψt becomes the air entry value (ψa) under the redistribution process. Based on the equation (2), it is deduced that the hydraulic gradient is negative and the water flux will be upward when Ls is smaller than the difference between ψw and ψa. Therefore, the depth of the surface soil layer (Le) where little soil water contribute to groundwater is determined as the difference between ψw and ψa. Because ψt becomes ψa at the end of the rainfall, the wetting zone is approximately the saturated condition (θs), and the critical rainfall amount (Pc) is defined as,

$$Pc = Le\,(\theta s - \theta i) \qquad (3)$$

where, θi is the soil water content before a rainfall event. According to the equation (1), it is determined that groundwater recharge occurs when the difference between P and Q exceed Pc. The excess water rapidly moves downward as partial and concentrated flow without evapotranspiration (Onodera, 1993).

Parameters (ψa and θs) of the model used the physical properties measured by the laboratory experiments (Table 1). In other hand, because the experimental method of ψw in the laboratory have not been established, the observed value by Onodera (1996) was applied to ψw. Onodera (1996) observed that the pressure head at the depth of 20cm increased rapidly from the dry condition to -3cm ($\pm$3cm) with the arrival of the wetting front. Therefore, it was assumed that ψw was -3cm in this model.

Table 1 Soil physical properties.

soil type	ψa	θs	Ks	color
sand	-10	35	$5x10^{-3}$	grayish brown
silt	-16	50	$5x10^{-4}$	reddish brown

* ψa: pressure head at the air entry,
Ks : saturated permeability
θs: water content at the saturated condition

3. Study area and method

The study area is located in Makutapora Basin, 25km north of Dodoma, the Capital city of Tanzania

(Fig.1). The main hills, Chenene Hills, lie in the northeastern margin of the basin, and Makutapora Swamp is surrounded by pediplain uplands in the center of the basin. The elevations of the hills, swamp and pediplain upland are around 1200 to 2000, 1060, and 1090 to 1150 a.m.s.l., respectively. The basement consists mainly of Precambrian granitic rocks and small block of metasediments. The basement is complexly faulted. A thin sandy soil of the high permeability and reddish silty soil of the low permeability (Table 1) covers the granitic and sedimentary rock on the slope and upland, respectively. On the other hand, a thick silty or clayey soil covers on the swamps and lowlands. The deep groundwater exists in the weathered or fissured rocks under the Swamp. The area has a tropical semiarid climate. Most of the annual rainfall, about 600mm, occurs from December to April. Shindo (1994) measured the distribution of rainfall in the basin, and indicates that the amount at Chenene on the foot of the hills was 1.9 times of that at Makutapora, and that the frequency of rainfall events exceeding 50mm at Chenene was twice that at Makutapora.

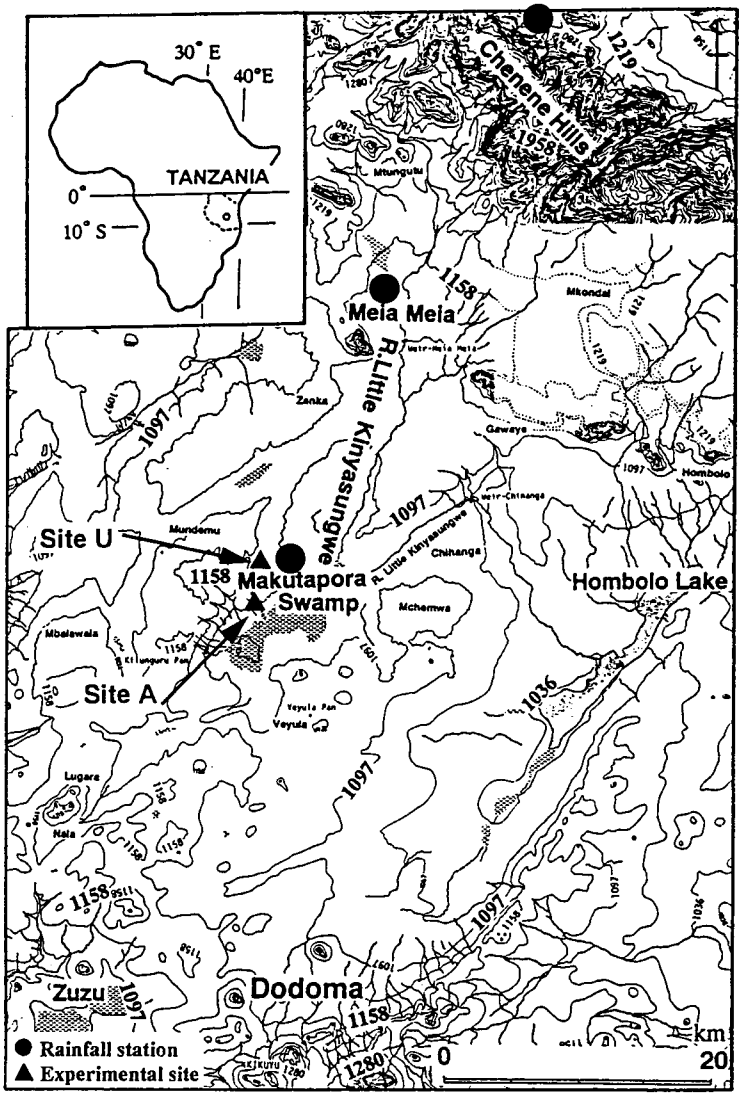

Fig.1 Location of study area.

To evaluate the effects of the rainfall and soil conditions on the groundwater recharge and calibrate the model with observed values, the observations of hydrological processes were carried out at two experimental sites of the western side of Makutapora Swamp, from December in 1989 to March in 1991. One is on the pediplain upland with sandy soil (Site U) and the other is on the gentle slope with reddish soil (Site A). At Site U, the tensiometer observation, soil water sampling and estimation of evaporation were conducted, respectively. The evaporation rate was estimated using the direct physical method. An undisturbed 100cc soil sample was collected on the ground surface every morning using a steel cylinder of the length of 5cm and weighed to measure the water content. The collected sample cylinder was installed on the ground surface every day and weighed after one day to measure the daily actual evaporation rate. As the bottom of the cylinder was sealed by a cover, the evaporation rate was estimated by considering rainfall and overflow amount. However, this method may underestimate the evaporation rate when the evaporation front locates below the 5cm deep such as during the dry season. Therefore, the values observed during the rainy season was used for calibrating the model. On the other hand, the tensiometer observation and measurements of every event runoffs at Site A were conducted, respectively. The runoff was measured at four field plots of 3.2m x 3.2m ($10m^2$) in size.

4. Results and discussions

4.1 Water balance in the sandy soil on the upland

Figure 2 shows the seasonal variation in the water contents and recharge rates estimated using the direct method and calculated using the water balance model from November 1990 to April 1991, respectively. Based on the water balance in the surface soil, the recharge rate was estimated by the difference between the rainfall at one event and the evaporation rate accumulated during the period from that rainfall event to the next one. The recharge rate was obviously high after a rainfall event of more than 40 mm/day, and water content in the surface soil increased. In contrast, the recharge rate was negative after a rainfall of less than 10mm/day except for the wet period. From these results, the recharge rate was related linearly to the rainfall amount (Onodera,1996) . The relationship indicates that the recharge rate is negative at events of less than 15mm and the loss rates with evaporation is relatively constant and around 15mm for the rainfall at events of more than 15mm. On the other hand, the Pc on the upland was calculated to be 21mm under the dry condition and 11mm under the wet condition using the parameters in Table 1, respectively. The observed tendency agreed with the calculated results in the basis of the concept of the model.

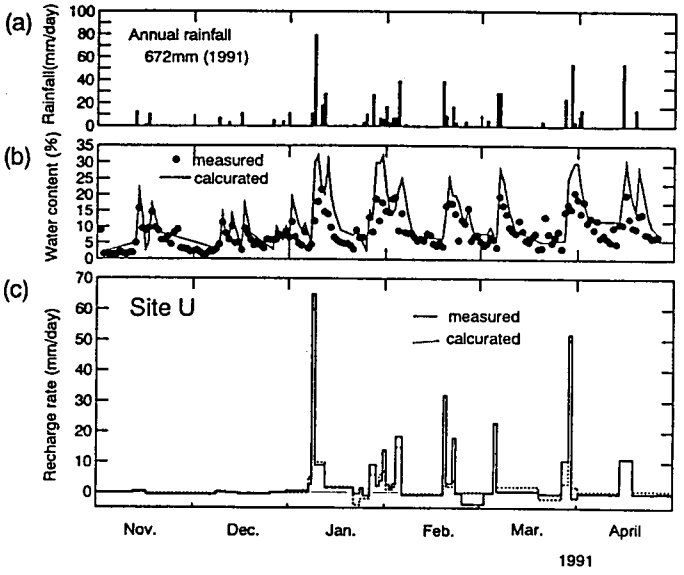

Fig.2 Seasonal variations in the (b)water content and (c)recharge rate at Site U.

Furthermore, the variation in the recharge rate calculated using the model approximately agreed with the observed variation, whereas the variation in the calculated water content was larger than the observed one because the calculated range in the model was narrower than the observed one. The cumulative recharge rate during this rainy season was estimated to be 341mm from the observed data and 328mm from the calculated data, respectively. The recharge rate of shallow groundwater on the same site was also estimated to be 330mm/year by Onodera (1993) using the tracer method. It estimated using the direct method was similar to one using the tracer method. These results support the validity of this model.

4.2 Effects of the soil condition on groundwater recharge

Based on the validity of the model described above, the applications of it to the estimations of recharge rates under the various soil and rainfall conditions were attempted. To evaluate the effect of the soil condition, the groundwater recharge rates were estimated in the adjacent hydrogeomorphological units with the reddish silty soil and sandy soil around Makutapora and Meia Meia, respectively. The Pc in the reddish silty soil was calculated to be 59mm under the dry condition and 20mm under the wet condition, respectively, based on the model parameters. In the gentle slope (Site A) around Makutapora, the annual recharge rate was estimated to be 1mm. The observed variation in pressure heads at Site A supported the results calculated using the model. The pressure head at the depth of 20cm rose up to 0cm H_2O after a rainfall event, whereas it at the depth of 100cm kept very low throughout the rainy season.

The results indicate that the wetting front stops at the surface soil layer.

In addition, the groundwater recharge was evaluated on the pediment slope with the reddish silty and sandy soil in Meia Meia, where the annual rainfall was 1.2 times of that at Makutapora. Figure 3 shows the variation in calculated recharge rates on the pediment slopes with the reddish soil and sandy soil around Meia Meia. The effect of the soil condition on the groundwater recharge is clear. The annual recharge rates were estimated to be 65mm in the reddish soil and 427mm in the sandy soil, respectively. The recharge rate in the reddish soil was less than that in the sandy soil. The grain size of soil affects the ψ a as well as the permeability. The smaller the grain size is, the lower the ψ a is and the larger the Le and Pc are, respectively.

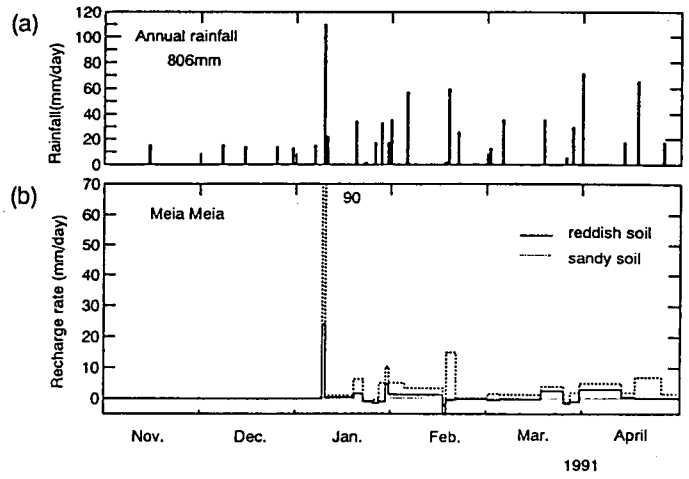

Fig.3 Seasonal variations in recharge rates in the reddish silty soil and sandy soil.

4.3 Effects of the rainfall condition on groundwater recharge

To evaluate the effect of the rainfall condition, the groundwater recharge rates were estimated on the three areas, Makutapora, Meia Meia, and Chenene, where the annual rainfalls in 1991 are 672mm, 806mm, and 1414mm, respectively. The calculated annual recharge rates on the sandy soil were 328mm in Makutapora, 427mm in Meia Meia, and 893mm in Chenene, respectively. The rates were 48.8% of the annual rainfall in Makutapora, 53.0% in Meia Meia, 63.2% in Chenene, respectively. These results indicated that the recharge rate increased with rainfall amount. Particularly, it increased with the frequency of the rainfall event of more than 50mm as well as the event rainfall amount. On the other hand, the calculated recharge rates on the reddish soil were 1mm in Makutapora, and 65mm in Meia Meia, respectively. The rates were 0.1% of the annual rainfall in Makutapora and 8.1% in Meia Meia, respectively. Because the Pc is the distinct value for the soil type, the effect of the rainfall condition was different according to the soil condition.

5. Concluding remarks

In this study, the simple water balance model linking with Green-Ampt Model was applied to the semiarid basin in Tanzania, to evaluate the groundwater recharge in a regional basin using the less parameters under the ground. Thought the parameters under the ground in this model were only three, the calculated value simulated well the measured value. Furthermore, the effects of the soil and rainfall conditions on the groundwater recharge were confirmed. In the future study, the determination of spatial distribution of soil and the estimation of the variation in rainfall and evapotranspiration will be possible using the remote sensing technique. Therefore, it is still more necessary to establish the experimental method of the soil parameters and to evaluate the water absorption by the deep plant root in this model.

6. Acknowledgements

This research is a part of the Japan-Tanzania Joint Research. The author appreciates the members of this project, particularly Prof. Shindo, Prof. Sato and Prof. Kondoh and Mr. Kongola (Ministry of

Water, Tanzania) for their support and advice. Special thanks are given to Mr. Sadiki, Mr. Nahozya and Mr. Katanga for the help in field researches.

7. References

Allison, G. B., Gee, G. W., and Tyler, S. W. (1994) "Vadose-zone techniques for estimating groundwater recharge in arid and semiarid regions", *Soil Sci. Soc. Am. J.*, 58, pp.6-14.

Gee, G. W. and Hillel, D. (1988) "Groundwater recharge in arid regions: review and critique of estimation methods", *Hydrol. Process.*, 2, pp.255-266.

Gee, G. W., Wierenga, P. J., Andraski, B. J., Young, M. H., Fayer, M. J., and Rockhold, M. L. (1994) "Variation in water balance and recharge potential at three western desert sites", *Soil Sci. Soc. Am. J.*, 58, pp.63-72.

Grass, R. J., Steenhuis, T. S. and Parlange, J-Y. (1989) "Mechanism for finger persistence in homogeneous, unsaturated, porous media : theory and verification", *Soil Sci.*, 148, pp.60-70.

Hayashi, M .(1990) "Study on groundwater recharge mechanism in inland Tanzania", MS Thesis, Chiba University (unpublished).

Onodera, S. (1993) "Estimation of rapid recharge mechanism in the semi-arid upland, Tanzania, using soil water ^{18}O and Cl^-", *IAHS Publication*, 215, pp.151-160.

Onodera, S. (1996) "The mechanism of concentrated groundwater recharge in a tropical semiarid region", *J. Jap. Assoc. Hydrol. Sci.*, 26, pp.87-98. (in Japanese with English abstract)

Onodera, S., Kondoh, A., Sato, Y., Hayashi, M., Shindo, S., Matsumoto, E. and Ikeda, H. (1996) "Subsurface water cycle in semiarid Tanzania, East Africa", *J. Jap. Assoc. Hydrol. Sci.*, 26, pp.75-86. (in Japanese with English abstract)

Sharma, M. L. (1989) "*Groundwater recharge*", Balkema, Rotterdam, 323p.

Shindo, S. (1994) "Study on the recharge mechanism and development of groundwater in the inland area of Tanzania", Progress report of Japan-Tanzania joint research (4), Chiba.

Stephens, D. B. (1994) "A perspective on diffuse natural recharge mechanisms in area of low precipitation", *Soil Sci. Soc. Am. J.*, 58, pp.40-48.

Sukhija, B. S., Reddy, D. V., Nagabhushanam, P., and Chand, R. (1988) "Validity of the environmental chloride method for recharge evolution of coastal aquifers, India", *J. Hydrol.*, 99, pp.349-366.

The present status, potential and limits of simulation models of desertification in the world

Kaoru TACHIIRI(*), Kazuhiko TAKEUCHI(**) and Atsushi TSUNEKAWA(*)

*Graduate School of Agricultural and Life Sciences, The University of Tokyo

1-1-1 Yayoi Bunkyo-ku Tokyo 113 Japan

FAX +81-3-3815-5851

email(Tachiiri): aa67004@hongo.ecc.u-tokyo.ac.jp

email(Tsunekawa): atsushi@hongo.ecc.u-tokyo.ac.jp

**Asian Natural Environmental Center, The University of Tokyo

1-1-1 Yayoi Bunkyo-ku Tokyo 113 Japan

FAX +81-3-3815-5851

email: take@uf.a.u-tokyo.ac.jp

Abstract

A simulation model is one of means representing and explaining complex systems. Recent progress in the field of environmental sciences has seen the development of many types of simulation models. Desertification is, however, a very complex system involving social factors such as economics as well as physical, chemical and biological processes. Therefore simulation models have rarely been applied to desertification phenomena. However, recent developments in computer engineering have made it possible to apply simulation models to a wider range of scientific fields. In this paper, we present an overview of past simulation models dealing with desertification phenomena, and discuss the possibilities and limits of their models. In addition, the present status of their models and the development of a simulation model of actual desertification in the semi-arid Kerqin Sandy Land of Inner Mongolia are presented.

Introduction

Desertification is defined by the United Nations (1994) as "land degradation in arid, semi-arid and dry sub-humid areas resulting from various factors, including climatic variations and human activities". Currently, of the world's drylands used for agriculture, 70% are affected to some degree by various forms of land degradation, and one sixth of the world's population is threatened by the effects of desertification (United Nations Environment Programme, 1992). Desertification is closely related to important global issues including population growth, the economic gap or so-called North-South

Problem and global warming. For example, global warming is thought to be cause of recent climatic fluctuation. In the international community, a positive campaign started following the since United Nations Conference on Desertification held in 1977, and the "United Nations Convention to Combat Desertification in Those Countries Experiencing Serious Drought and/or Desertification, Particularly in Africa" was signed in June 1994.

Meanwhile, what progress has been made in the research field? Our understanding of specific processes involved in desertification has progressed, but studies that take a general view of desertification are usually qualitative or superficial and quantitative studies combining elements of received relatively little attention. Countermeasures to desertification have been developed separately and inconsistently in each area, and fundamental desertification control methods such as suitable landuse planning have been rarely discussed. In this paper, a quantitative method for making an integrated simulation model was considered, and the application of such a model to desertification was discussed.

1. Present status of simulation models of desertification

Vinogradov (1995) described changes in landuse by a mathematical simulation model. He explained the expansion of sandy land around the Black Sea by exponential function, and the change of land cover of the Amudarya Delta as a sum of power functions. Moreover, the future land cover was predicted by using Markovian model as to the latter. In his examinations of the processes of desertification, only 2 or 3 sets of data obtained every 5 or 8 years were used.

Grunblatt *et al.* (1992) examined the internal processes of desertification. Potential water and wind erosion were estimated using data on precipitation, land inclination and land cover. Moreover, the population density data was overlaid on the results to judge the hazards of desertification.

Hanan (1991) studied the state of vegetation regression around the wells by analyzing NDVI, in which a spatial model, excluding temporal aspects, was applied. Proctor (1990) predicted future landuse up to the year 2000, by extrapolating from trends between 1961 and 1984. Field survey, analysis of aerial photos and statistics of fuelwood usage and cattle number were considered in this model. The relationship between population growth and resource limits was also discussed. Ive *et al.* (1992), divided the study area into 1/8 degree square grids, and developed a simulation model explaining the expansion of salinized areas. Since this model showed latent hazard, it could not be well correlated to the present status.

The results of these studies have been summarized in Table 1.

Table 1 Characteristics of previous models of desertification

	field	temporality	spatiality	soil type	erosion	vegetation	climate	human impact
Vinogradov (1995)	Amudarya	○	○	×	×	×	×	×
	Black Sea	○	×	×	×	×	×	×
Grunblatt *et al.* (1992)	Kenya	×	○	×	○	○	○	○
Hanan (1991)	Sahel	×	○	×	×	○	○	○
Proctor (1990)	Swaziland	○	×	×	○	○	(○)	○
Ive *et al.* (1992)	Victoria, Aus.	×	○	○	×	×	×	×

In this table, ○ indicates that the factor was considered with temporal changes and × indicates that the factor was not considered. (○) means that the factor was considered without temporal change.

Among these papers, Vinogradov's model succeeds in examining whole desertification. However, it has some shortcomings. No internal processes were taken into consideration and only a small amount of data was used. On the other hand, the aim of the studies by Grunblatt *et al.* (1992) and Hanan (1991) were to estimate the hazards of desertification, but their methods can be applied to simulation models. Proctor (1990) used various kinds of data, but the spatial data was not effectively incorporated. Ive *et al.* (1992) excluded spatial change, but their approach is very interesting because of the use of a lattice model.

2. Potential and limits of simulation models

2.1 Potential and significance of simulation models

In the previous section, a general overview of simulation models was taken. The potential of simulation models in the near future is now examined.

One potential approach is a spatial-temporal model, established using data on vegetation, soils, climate, satellite images and statistical data (e.g. human and livestock population). This model should include mathematical formulae expressing each process, and combine social and economic processes with physical, chemical and biological ones. Detailed spatial and temporal data need to be included in making this type of model. We could not find any studies using this type of model. If successfully established, desertifications in different areas could be recognized as a change of parameters. A clearer understanding of the mechanism of desertification could identify basic solutions to the problem.

2.2 Limits of simulation models

There are some limits to the simulation model approach. Even if all available data are used. This may be insufficient to understand all phenomena that occurred in the study area. There is no guarantee that factors excluded from the model do not play an important role, and this may affect the accuracy of the model. Another problem is regional differences in desertification phenomena. Desertification is occurring in a

variety of regions in the world which have both common and unique aspects. Applying a model developed in one region to another region is often difficult. In the early stages of making models, applying a model to regions with different processes may be difficult.

There is also the fundamental problem that desertification includes very complex systems, causal relationships become vague understanding of the whole picture becomes difficult. Progress in handling high density data and trial-and-error in model making are necessary to solve this problem.

3 Towards application of a simulation model to Naiman-qi, Inner Mongolia

3.1 Characteristics of Naiman-qi

We selected Naiman-qi ('qi' means prefecture or county in Chinese) in Inner Mongolia, China as a study area to produce a desertification simulation model. The reasons for this choice are 1) typical causes of desertification in the world such as overgrazing, over farming and deforestation are represented here; 2) typical effects such as sand dune remobilization, salinization and soil erosion are seen; 3) social factors such as population growth and accompanying rapid change of landuse are seen.

3.2 Desertification in Naiman-qi

3.2.1 General view

Naiman-qi is located in the central part of the Kerqin Sandy Lands occupying 42°20′~44°20′N, 118°30′~123°30′E. Mean annual rainfall at Naiman is 377 mm and mean annual temperature is 6.6°C (1949~1994). In the Kerqin Sandy Lands, the eastern part is more humid than the west. Hence Naiman-qi is, at the same latitude, more humid than Wulan-Aodu, 80km west of Naiman that was studied by Takeuchi *et al.* (1995).

Soil profiles indicate that this region had historically experienced the cyclic processes of desertification and restoration three times (Liu *et al.*, 1993). However recent rapid population growth and development of civilization accelerated co-incident desertification in this region that was obviously different to the historical one.

Naiman-qi is, however, recently undergoing a recovery process. Windbreaks and sandbreaks planted by local government occupy large areas and the climatic condition is in a humid stage (see below). Imagawa (1995) reported that the areas around roads, railways and settlements are being restored, although the outer area is becoming desertified.

Annual precipitation and its residual mass graph are shown in Figs.1 and 2. Residual mass curve method is used to easily describe long term changes in

precipitation (Iwasaki, 1983,1984).
This is calculated as follows.

$$Xi=1000\times \sum_{n=1}^{i} \left(\frac{r_n - \bar{r}}{\bar{r}}\right) \quad (1)$$

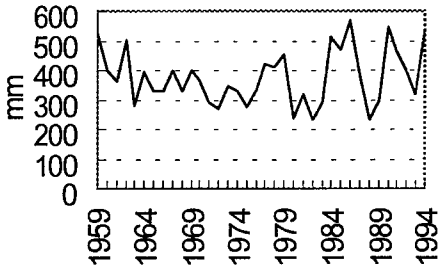

Fig. 1. Precipitation at Naiman

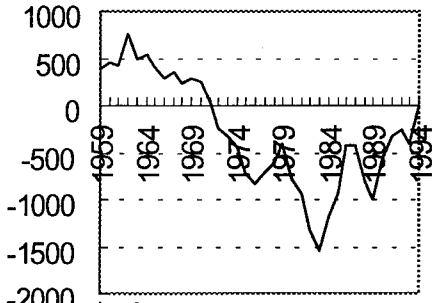

Fig. 2. Residual mass graph of precipitation

Where, Xi is the value of residual mass in "i"th year, $\bar{r}$ is average precipitation and r_n is precipitation of "n"th year. Figure 2 shows that Naiman-qi has been in a relatively wetter period after a dry period that lasted from the 1960's to the early 1980's. Landsat TM images also shows almost no expansion of desertified area between 1982 and 1991 (Imagawa, 1995).

3.2.2 Development of dunes and vegetation

Field vegetation surveys were carried out at the beginning of September 1996 to clarify vegetation regression caused by sand dune remobilization. Ten tansects were placed on sand dunes in various parts of Naiman-qi (including fixed dunes, semi-fixed dunes and active dunes). Each transect was set from a sand dune ridge to the interdune depression. The length of each transect ranged from 24 to 129 m. Along each transect, quadrats (1 m × 1 m) were set every 3 m.

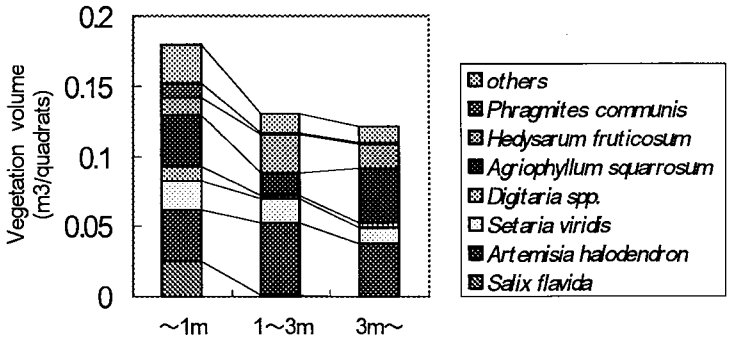

Fig. 3. Result of vegetation research

Figure 3 shows the vegetation volume index calculated as coverage (m^2) x plant height (m) for each species. 79, 55, 171 quadrats were located on the sand dune less than 1m, 1~3m, more than 3m from the bottom of the depression.

As a result, the estimated vegetation volume index above ground and the number of species presented (a total number of species presented per quadrat) are 0.179m^3 and 3.8 species at less than 1 m, 0.130 m^3 and 1.9 species for 1~3 m and 0.121 m^3 and 2.1 species for more than 3 m from the bottom of the depression (Fig.3). This shows that the quadrats at less than 1m from the lowest depression is remarkably rich in vegetation volume and species diversity.

3.3 Towards developing a simulation model of desertification

3.3.1 Estimating net primary productivity (NPP)

Estimating of the potential of particular land is very important in establishing suitable landuse guidelines based on a balance between land conditions and human activities. Net primary productivity (NPP) is an indicator of land potential. NPP is estimated by using climatic data, soil maps and erosion maps. The Chikugo model is a representative model used for estimating NPP from climatic data. In this model, NPP is calculated as follows.

$$NPP=R\{0.29\exp(-0.216RDI^2)\} \quad (2)$$

Where R is the annual net radiation (kcal/cm^2), RDI (=R/lr) is radiative dryness index, latent heat value of water evaporation (kcal/gH_2O) is l, and r is annual precipitation (cm).

In semi-arid zones, the main factors are related with water such as evapotranspiration, soil moisture and precipitation (Raich *et al.* 1991). The Chikugo model, however, evaluated to be applicable from humid regions to arid regions (Seino and Uchizima, 1988).

Land productivity for each soil type should be evaluated quantitatively using obtainable data. For estimating actual productivity, additional factors such as salinization (in the northern part of Naiman-qi), water erosion (south part) and steepness (south east mountainous region) should be included. The vegetation index obtained from satellite images, and the results of field survey will make accurate estimation possible.

3.3.2 Process of simulation model

NPP should be used in the simulation model. In addition, the data on human population, livestock population (for each kind of animal) and farm area should be included. Fig.4 shows the outline of our model. For evaluating natural processes,

satellite images taken between in the 1970's and 1980's will be used, because during this period, less action was taken to combat desertification.

Conclusion

As discussed in Chapter 1, no current models explain the whole phenomena of desertification in both a spatial and temporal manner. A simulation model in Chapter 2 will describe the recent desertification in Naiman-qi. It will include the population and economic growth and climatic change as described in Section 3.2.

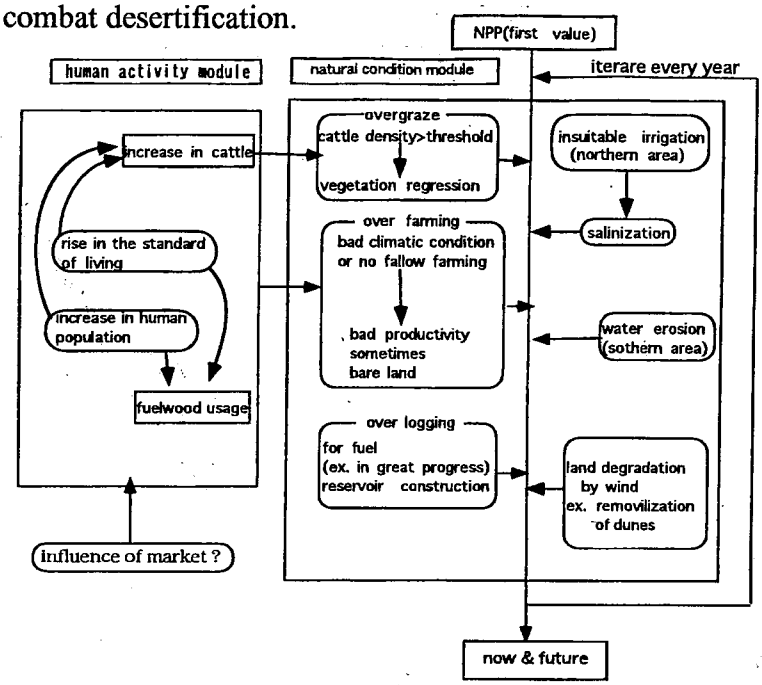

Fig.4 Framework of simulation model of desertification in Naiman-qi

Acknowledgments

This research is supported by Global Environment Research Program Budget, set aside by the Japan Environment Agency for the promotion of comprehensive research on the global environment.

The authors wish to express their thanks to Mr. H. Zhao, Chief of the Naiman Station of Desertification Research, Institute of Desert Research, for giving us the opportunity for field investigation. The authors also thank Mr. X. Chang, Mr. S. Li and Mr. T. Zhang, Naiman Station of Desertification Research, for their kind co-operation throughout the field survey. We also thank Mr. T. Imagawa, Mr. T. Ohkuro and Mr. Y. Shirato, researchers in National Institute of Agro-Environmental Sciences, for their kindness.

References

Granblatt,J., Ottichilo,W.K. and Sinange,R.K.(1992): A GIS approach to desertification assessment and mapping, Journal of Arid Environments, 23, 81-102.

Hanan,N.P., Prevost,Y., Diouf,A., and Diallo,O.(1991): Assessment of desertification around deep wells in the Sahel using satellite imagery: Journal of applied ecology 28(1), 173-186.

Imagawa,T. (1995): 衛星データを利用した中国東部の土地荒廃域の抽出方法と荒廃域の特徴 (The method

of extract the land degraded regions in the east part of China using satellite data, and the characters of these regions):Proceedings of International Workshop on Land Use System for Combating Land Degradation in East Asia; 1995 Feb. 22-24; Tsukuba, Japan: Science and Technology Agency ,and National Institute of Agro-Environmental Sciences 113-122.(in Japanese)

Ive,J.R., Walker,P.A. and Cocks,K.D.(1992): Spatial modeling of dryland salinization potential in Victoria, Australia: Land degradation & rehabilitation, 3, 27-36.

Iwasaki,K.(1983): オーストラリアの気候 -降水量から見た気候地域-(the climate in Australia -climatic regions considered by rainfall-: *Chiri* (Geography),28(12),66-73 (in Japanese)

Iwasaki,K.(1984): オーストラリアにおける降水量の長期傾向と地域差 (Regional difference of long term tendency of rainfall fluctuation Australia.: *Chigaku-zasshi*(J. Geography) ,93,15-29 (in Japanese)

Proctor,I.D.(1990): The limits to growth debate and future crisis in Africa: A case-study from Swaziland: Land degradation & rehabilitation , 2, 135-155.

Raich,J.W., Rastetter,E.B., Melillo,J.M., Kicklighter,D.W., Steudler,P.A. and Peterson,B.J.(1991): Potential net primary productivity in South America-Application of a global model: Ecological Applications 1,399-429.

Liu,X., Zhao,H. and Xu,B. (1993): Mechanism of destruction and restoration of Kerqin Steppe ecosystem： 科尔沁沙地草原生態環境総合整治研究(Integrated environmental rehabilitation research of Kerqin Steppe ecosystem)：12-26 (in Chinese with English summary).

Seino,H. and Uchizima,Z. (1988): Mesh maps of net primary productivity of natural vegetation of Japan.: National Institute of Agro-Environmental Sciences of Japan, Tsukuba, pp131 (in Japanese).

Takeuchi,K., Katoh,K., Nan,Y. and Kou,Z.(1995):Vegetation cover change in desertified Kerqin Sandy Lands ,Inner Mongolia :Geographical Reports of Tokyo Metropolitan University 30.

United Nations (1994): United Nations Convention to Combat Desertification in Those Countries Experiencing Serious Drought and/or Desertification, Particularly in Africa.

United Nations Environment Programme(1992): World atlas of desertification: Edward Arnold ,London pp69.

Vinogradov,B.V.(1995): Aerospace monitoring of desertification dynamics, Desertification Control Bulletin 27 35-44.

Characteristics of Streams in South Part of Xinjiang, China

Changyuan Tang*, Shizuo Shindo*, Xing Li** and Changming Liu***
* Center for Environmental Remote Sensing, Chiba University, Japan
** Institute of Xinjiang Geography, CAS, China
*** United Research Center for Water Problems, CAS, China

Abstract

As well known, water is an active driver to control the environment in arid and semiarid region. In this paper, the attention has been paid on the water balance and water quality in the south part of Xinjiang, one of typical arid regions of China. The increases of agriculture activities in past forty years have made great changes distributions of water both in quantity and quality. Based on the field surveying results, the relations among the water use, desertification and salinity were discussed.

I. Introduction

The geomorphic construction of Xinjiang is "two basins between three mountains". Three mountains mean Altay Mountain in the north, Tianshan Mountains in the middle. and Kunlun-Karakorum Mountain in the south. As usual, Xinjiang is divided in to two parts, the south and the north by Tianshan Mountains. Xinjiang is a typical arid region with the annual evaporation ranging from 2000 mm to 2500 mm, and the annual precipitation of 154 mm. Table 1 shows annual temperature, precipitation and potential evaporation in some typical cities. Comparing with the annual precipitation in Urumqi, the annual precipitations in cities of south part of Xinjiang, such as Korla, Aksu, Atushi and Kashi, were less than 100 mm. Just as other arid region, these geographical and geology characteristics determine the "field" for the water movement in Xinjiang. In turn, water ,as a "dynamic driver", controls the whole ecological system there. In past 40 years, water use in Xinjiang has caused many changes in natural environment. Unsuitable use of water resource was a neck problem. For example, increase of farmland changed the vegetation distribution. As a result, salinity occurs near farmland since water table rising, and desertification occurs along the river banks since trees died with

Table 1 Climate Conditions in South Part of Xinjiang

Cities	Urumqi	Turpan	Korla	Aksu	Atushi	Kashi
Altitude (m)	918	35	932	1104	1298	1289
Annual Temp. (℃)	5.7	13.9	11.4	9.8	12.9	11.7
Annual Precipitation (mm)	277.6	16.6	50.0	62.1	76.2	62.7
Potential Evaporation. (mm)	1196.2	1366.3	1549.7	981.0	1340.5	1205.1

water table lowing. Without protection barrier by trees, farmland was attacked by desert invasion. In other words, the changes of natural ecology environment respond very sensitively to water utilization

in arid region. Therefore, ecology in arid environment is always in the processes to keep balance with water distribution. In many cases, these processes are irreversible.

II. Water Balance

Surface water is one of important water resources in Xinjiang, and almost all rivers are inland water systems and end in lakes or deserts. There are 89 rivers flow down from south slope of Tianshan Mountain with annual runoff of $1.985X10^{11}$ cubic meters. Except for large rivers which flow into the lakes of deserts, most rivers disappear and infiltrate into groundwater soon after leaving from mountain area.

With the development of agriculture in past forty years, many canals have been built to transfer almost all stream waters for irrigation and salt-washed. After then, waters flow back to the stream channel with much less volume and high salt contents. During the flood period, flood water flows along stream channels rather than irrigation canals because of its high concentration of sediments. In viewpoint of water balance, the more water is used in upstream, the less water is available in downstream. In fact, some lakes in desert have been disappeared because stream water become less and less, which causes expansion of the desertification. At the same time, many farmland in downstream were wasted. For example, irrigation land has increased more than $4.0x10^5$ ha at upstream of Akus River and the Tarim River in past forty years, which use almost 40% of stream water. According to the flow statistics of Tarim River in past forty years, the stream flow in upstream (Aral hydrological station) ranged from $44.0x10^8$ to $51.3x10^8$ cubic meters. However, the stream flows in middle stream (Daba hydrological station) and downstream (Kala hydrolgical station) were decreased 50% and 85%, respectively. As a result, water in downstream of the Tarim River decreased sharply and Noburu Lake disappeared from the desert. Area of farmland in downstream of the Tarim River is only $1.47x10^4$ ha, it means near half of farmlands have been wasted.

III. Water Quality

Mineralization of rivers ranged from 0.5 to 4.46g/L which were almost 5 times larger than that in early 1960s. Figure 1 shows the statistics of hydrochemical types of stream waters. According to 52 sampling points of streams that come from the south slope of Tanshan Mountain, it was found that about 37% of water quality is Ca^{2+}-HCO_3^- type. There was more than 40% of water with either Na^+-Cl^- type or Na^+-SO_4^{2-}. In general, the water in former type is the water of streams that flow down into The Tarim River, which shows the natural hydrology conditions. On the other hand, the water in later type is the water of stream that passes the irrigation farmland or that of middle-stream and down-stream of the Tarim River, which shows the effects of agriculture activities on the stream water quality. For example, the Cl^- ion concentration of waters disposed from farmland was 10 times higher than that before entering the farmland in Aksu region.

Electrical conductivity (EC) is less than 230 μ m/cm in upstream, and increases with downstream. The high EC value is found in the stream discharged by the irrigation channels and the lakes at the end of stream. Despite of the water quality differences among streams, pH value of stream waters were all

above 7.5, which means the water in research region is controlled by the geological conditions.

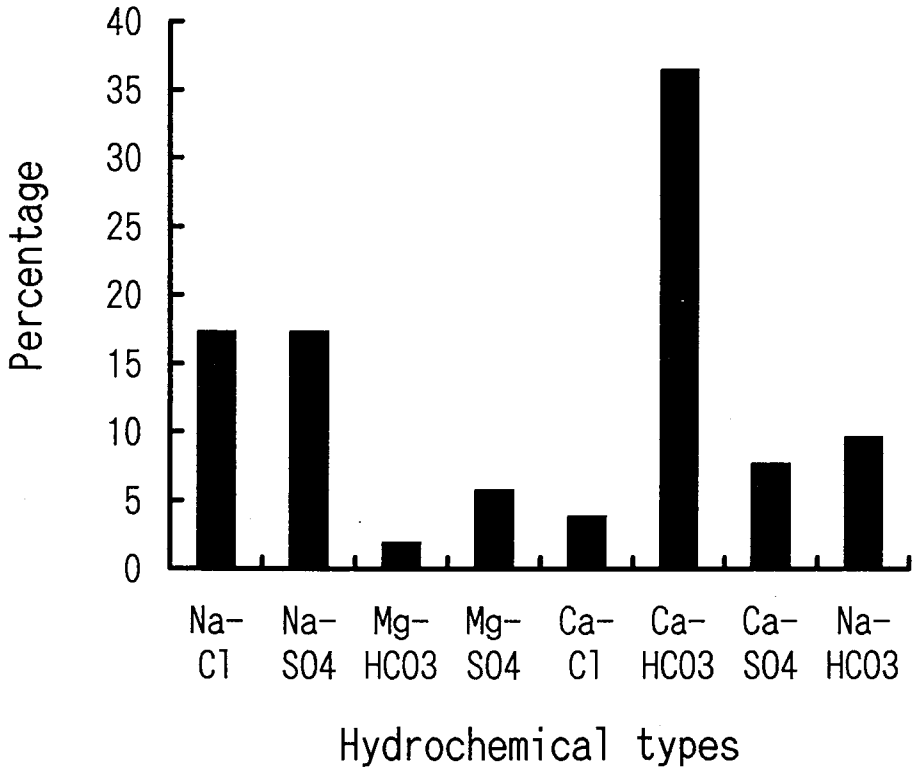

Figure 1 The statistics of water quality types in streams

IV. Discussions

From the viewpoint of water use in arid and semi-arid region, desertification and salinity are twin problems. In fact, the agriculture activities cause the spatial and time redistribution of water, then change the ecology environment. Therefore, there are two big ecological problems occurring. First, some lakes in desert have been disappeared because stream water become less and less, which causes desertification and the ruin of farmlands in downstream. Secondly, the area downstream of irrigation farmlands, salinity become more serious, because the water table is very shallow.

Hydrological states in saturated and unsaturated zone pay a great role in salinization processes. Since much river water was used for irrigation, water table in farmland rose up, then salinity became very serious. In fact, the basic characteristics of salinity dynamics are in close relation to water. The saline soils are mostly found depression near downstream of oases area, where water table is very shallow. In the research region, irrigation water is also used to wash salt out from farmland. As a result, high salt content water discharged from farmland flow downstream and infiltrated into groundwater. Finally, the shallow groundwater contains higher concentration of salts as saline water and brackish water. With the water table rose up, evaporation and capillary bring salts up to the topsoil.

Opposing to the oases where agriculture activities use much river water. water table decreased in sediment fan outside oases. Comparing with 1958, tresses and grasslands in areas of the middle stream and downstream along the Tarim River has decreased about 16% and 77%, respectively. With decrease of trees and bushes, desert area expanded and some oases have been attacked by mobile sand dunes. The environmental changes caused by dersertification are mainly manifested by the occurrence and growth of landscape similar to desert-like environment on the aboriginal non-deseert regions or steppe. In the aboriginal vegetated dune areas, desertification is characterized by the acceleration and encroachment of mobile sands. As results of the spreed of desertification and wind effect, fine materials and organic matters in surface composition were eroded and arable land became infertility. The Windy days were 20 to 40 days in the north part and more than 100 days in the south part of the Tarim River, respectively. Table 2 shows statistics sand storm occurring in some cities in the south part of Tianshan Mountain. With the decrease of flow in streams or water table, vergetative converage became lower. The degradation of plant reduced the fodder production and influenced rangeland quality. The densely distributed sand dunes caused the degradation of the function of ecosystem and decreased availbe land reource as well as biomass production.

Table 2 Statistics of Sand Storm Days in South Part of Xinjiang

Cities	Urumqi	Turpan	Korla	Kuche	Aksu	Atushi	Kashi
Annual Sand Storm (days)	4.7	5.1	7.5	15.8	19.1	14.5	13.3
Annual Strong Wind (days)	26.9	25.0	22.1	20.8	21.7	26.2	25.2
Average Wind Direction	SWS	E	NE	N	SW	NW	NW

V. Conclusions

Ecology environment in arid and semiarid region is very sensitive to hydrological conditions. The results shown here hinds that effects of human activities on the environment usually are resulted from unsuitable water use. In other words, redistribution of water in spatial and time means to change the hydrological states and action style of water on the environment. It is needed to deal with salinity problem and desertification problem at the same time. In order to keep ecology balance in a good way, how to rationally utilize water resources is the key to solve the problems in arid and semiarid region.

References

[1] Dong, Y., Y. Liu and Y. Liu, 1995, Research on Some Problems of Desertification, Xi'an Map Press, 271p. (in Chinese)

[2] Institute of Xinjiang Geography, 1995, Research on Resources, Environment and Oasis in Arid Land, Scientific Press, 273p. (in Chinese)

[3] Zhu, Z., 1989, Desertification and rehabilitation in China, Scientific Press, 126p. (in Chinese)

REGIONAL SALINITY MANAGEMENT BASED ON SHALLOW GROUNDWATER CONTROLLING: A CASE STUDY IN THE NORTH CHINA PLAIN

Changming Liu*, Changyuang Tang** and Shizuo Shindo**
* United Research Center for Water Problems, Chinese Academy of Sciences, China;
** Center for Environmental Remote Sensing, Chiba University, Japan.

Abstract
This paper deals with regional salinity management of the North China Plain. The authors of present paper paid careful attention to the fact that the basic characteristics of salinity dynamics are in close relation to water. Particularly in semiarid and semihumid flat areas, the water is not only a driving force for salts, but also the most important state variable having a decisive influence on soil salinity. On basis of such principle, the authors studied the approaches to control the salinization in the North China Plain.

I. Introduction

In China the saline soils can be found in wide areas of its northern and northwestern parts [1]. The total area of saline soils with different types amounts to about 20 - 25 million ha, of which nearly 10 million ha of cultivated lands under secondary salinization. The salinization process is dynamic one found in the North China Plain (NCP).

The NCP locates in north but it's politically, economically and culturally central place for the country. Beijing City, the country's capital, just lies in the northern edge of the NCP. Specially, it's important region of agriculture. For instance, the NCP's annual grain and cotton yields make up 18% and 50% of the nation's total yields, respectively. However, the problems in the development and environment are still remained to be solved in terms of sustainability in the future. For example, lower yield areas occupies millions of hectares of farmlands. The land degradation has benn formed by influences of following issues:

1. Flooding and droughts occurring across with a high frequency;
2. Salinization and alkalization spreading several ten counties;
3. Waterlogging problem in many depressions;
4. Seawater intrusion along several reaches of coastal regions because overdraft of groundwater;
5. Sedimentation and water shortage problems.

Obviously, above listed issues are all subject to water-related constrains, which have seriously influenced the further development , consequently will be a chief threat on sustainability in the NCP.

II. Saline Soils and Regional Salinity Balance

The NCP is located in a deposition area of salt and sediment, which results from its surroundings of west mountainous regions including the Loess Plateau, Taihung and Yanshan Mountains and of eastern sea water introsions. So the area can be generalized by slow processes of salt accumulation in regional soils. Apparently, the soils are under potential change into salinization even alkalization in accordance of hydrological states and the environment.

There are different types of saline soils mainly found in Heilonggang low-lying plain and coastal plains. The former covers more than 40 counties as inland saline soil area with bad drainage conditions. The latter locates along sea shores and salt accumulation has been affected by the Bohai and Huanghai seas for long time periods.

The regional salinity balance is of importance in better understanding of regional salinity management in terms of larger scaled engineering designing to effectively control salinization. A principal model can be written as follows:

$$\mathbf{RSB = C_1P + C_2Ri - C_3Ro - Si + Sr + Sf} \qquad (1)$$

where RSB = regional salinity balance in tons;

C1 = salinity content of precipitation (P);

C2 = salt content of surface runoff (Ri) inflowing into salinity balance region (given region);

C3 = salt content of surface runoff (Ro) outflowing from the given region;

Si = salts used by crops / plants;

Sr = salts remained by crops / plants;

Sf = salts brought by fertilizing.

According to the data observed in the NCP, the salts are accumulating annually amounting to about 300 kg[2]. They are mainly came from inflowing runoff and diverting water for farmland irrigation. It is dominant part of salt's accumulation in the NCP. Because large quantity water comes from precipitation, it also brings certain amount of salts into the plain, through its salt content is much lower than surface flows.

As for other terms in equation (1), Ro also plays important role in balancing the salinity in the given region. Due to increasingly human activities since 1970's, the Ro has been decreased sharply with intercepting more and more water from Ri and P for water supply to irrigation and urban-industrial sectors. Therefore, the problem in present salinity accumulation of the NCP mainly results from reduction of Ro (Table 1). This table also means that the NCP is now suffering from serious water shortage.

Table 1. A decrease in runoff outflowing into the sea from NCP for last 4 decades.
(in 100 million cu. m)

Decades	1950's	1960's	1970's	1980's
Runoff of NCP	291	295	293	330*
Outflow Runoff	224	165	120	100
Ratio in %	77	55	41	33

* plus diverted water from the Yellow River

III. Water and Salinity Relations

As above-mentioned, water plays important role in terms of its duality as a driving force for salt movement and a state variable of salinity dynamics. The fugure 1 shows how the water fluxes drive the salts.

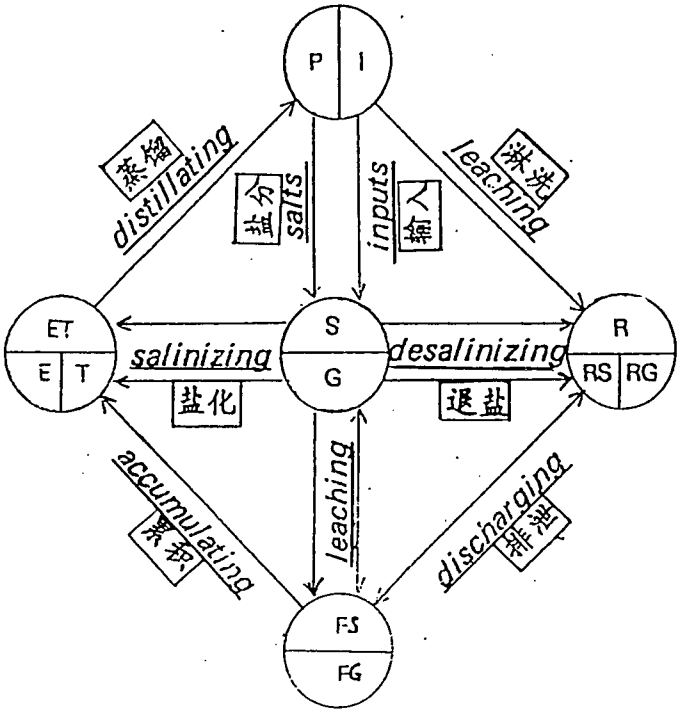

P: Precipitation

I: Irrigation

ET: Evapotranspiration (E and T)

R: Runoff (surface: R_S and Subsurface R_G)

FS, FG: Groundwater recharge and discharge

S, G: Soil and Ground

Figure 1 Water Cycle Driving Salt Movement

From Figure 1 we can see that the action of hydrological cycle brings salts to move building up the basic processes of salinity formation: aggregation and scatter.

In addition to above-mentioned driving force of water, hydrological states also have important role in salinization processes. In the NCP the saline soils are mostly scatter in depressions with shallow buried groundwater table. So the salts in soil vary greatly coinciding with changes in groundwater table. In general, the higher the level of groundwater table is, the more the salt will be in top soils. Particularly, in the NCP, the shallow groundwater found in many places contains higher concentration of salts as saline water and brackish water. Table 2 shows a common feature of relationship between the salt contents in soil and buried groundwater tables.

Table 2.Relations between soil salinity and buried depth of groundwater table in NCP

water table buried	0.3-1.5	0.5-1.5	0.7-2.0	1.2-2.1	> 2.1
concentration (g / l)	> 4	3-8	2-6	1-3	< 1.0
soil salt contents (%)	> 0.6	0.42-0.6	0.22-0.4	0.12-0.4	< 0.1

From Table 2 we can see that the mineral concentration also is in close relation to groundwater table. Therefore buried depth of groundwater table can be considered as a critical indicator to evaluate and to control the salinity.

Considering above-mentioned two aspects, the authors defined that in the NCP an optimal buried depth of groundwater table below the land surface is greater than 2.1 meters or so. In addition, there were other buried depths of groundwater table defined, which can be employed to regulating water and salinity relations for land use management (see figure 2)

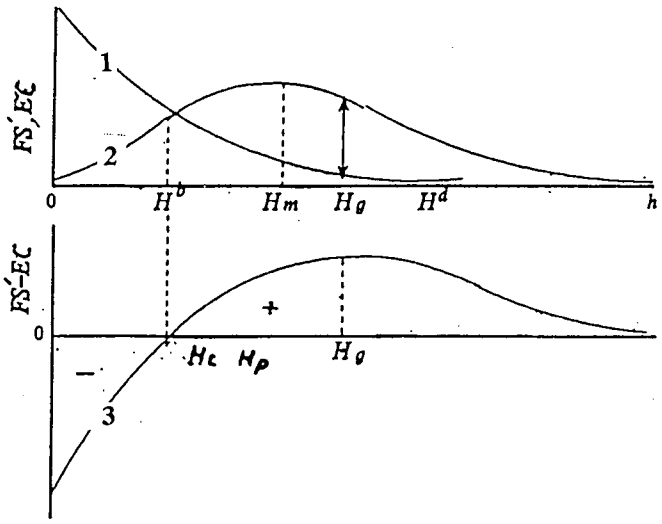

Figure 2 Schematic diagram of the significance in water table states.

In figure2 the symbols are "1" and "2" present groundwater discharge (EC) and recharge (FS) vs their buried depths of water table, respectively; "3" is balance curve: "3"=FS-EC; h is buried depths of groundwater table; Hb is balanced depth of FS and Ec; Hm is maximum recharge depth; Hg is net maximum value of FS-EC; Hd is a depth at which EC=0; Hc is the critical depth of salinization, below which the salts can not be upwards to topsoil; Hp is the depth desirable for high yield of crops.

IV. Regional salinization controlling

Although water and its movement are critical for salinization formation, there are many other waters related factors[3], which can involve in controlling the salinity. They are mainly structural and adaptive measures or nonstructual measures:

1. Principal structural measures

- To improve regional drainage systems in terms of reconstruct enlarged drainage canals, referring to balance Ri and Ro i.e., Ro= Ri as in the equation (1);
- To reduce surplus water in the waterlogged depressions by setting up underground pipe and well pumping networks, referring to keeping the field water table below the Hc as in figure 2;
- To pump groundwater for irrigation in order to low down groundwater table associated with washing and diluting salinity of top soils. This measure has been developed in the NCP since 1970's with fairly good result;

2. Major adaptive measures

These measures are nonstructural ones including various agricultural methods:

- To level land surface in order to prevent accumulated salt spots associated with planting salt-tolerant crops in line with local conditions;
- To develop paddy fields with rice production in the waterlogged depressions, where are hard to discharge water by structural methods;
- To improve saline soils by modifying soil property in terms of employing green manure / organic manure, for example, planting sesbania;
- To plant windbreak forest belts for reducing wind speed and evaporation;

3. Salinity control modeling

This model was developed for rational irrigation in order to prevent secondary salinization in the NCP. The basic consideration was the controlling groundwater table depth to avoiding salts going up to top soils and to save water. Figure 3 shows the structure of the model.

EP: effective precipitation for soil water storage

HA: initial buried depth of groundwater table

WS, WF and WK: soil water constances

WA: initial water content in soil

P: precipitaion

u: specific yield

E: evapotranspiration

PE: potential evaporation

FS: infiltration

RS: surface runoff

FA: groundwater discharge.

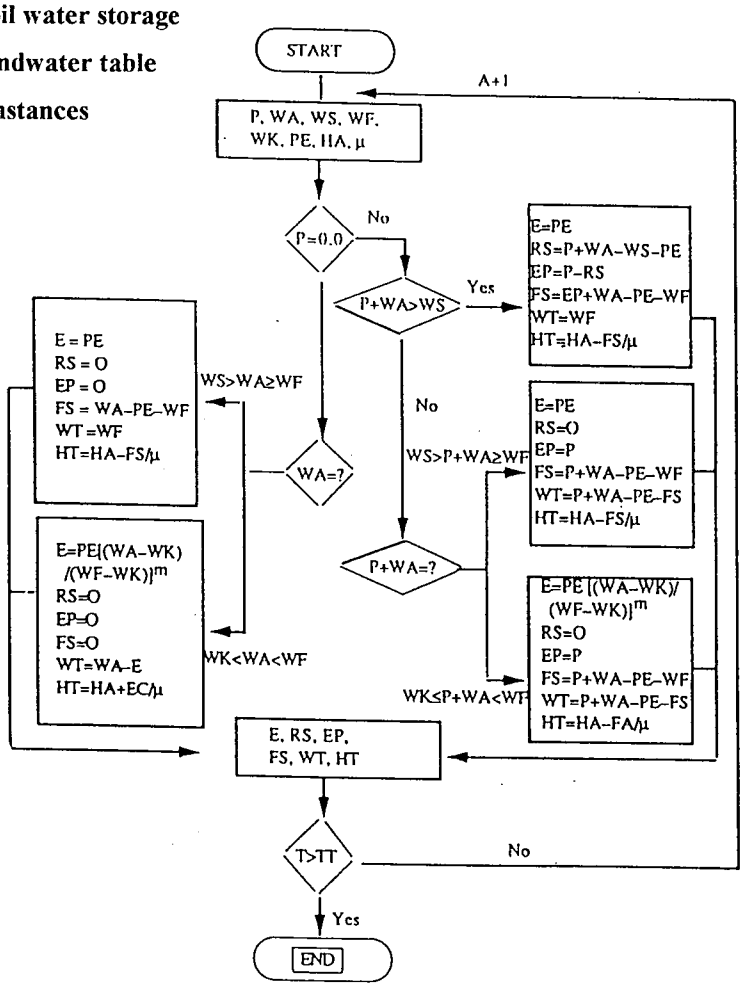

Figure 3 Diagram of water interaction modeling.

V. Brief conclusions

An experience of the farmers in the NCP said that "the salt comes with water and leaves with water". It's really scientific truth. The regional salinity control will be a great challenge for water conservation work . It requires us to rationally utilize water resources with special reference to prevention of our limited land resources against land degradation. Finally, we can be towards the sustainability.

References

[1] Wang Zunqin et al (ed.), 1994, Saline Soils in China, Science Press , Beijing.(in Chinese).

[2] Changming Liu , Zhongyi Wei, 1989, Agricultural Hydrology and Water Resources of the North China Plain, Science Press, Beijing. (in Chinese)

[3] Changming Liu, 1996 .Soil Salinity Control Regarding Subsurface Water Regulation in North China Plain, **Journal of Chinese Geography,** Vol. 6 , No. 4, Beijing.

Development and Implementation of Spectral Crust Index over Dune Sands

Arnon Karnieli
The Remote Sensing Laboratory, J. Blaustein Inst. for Desert Reserach
Ben Gurion Univ. of the Negev, Sede Boker Campus 84990 ISRAEL
Tel: 972-7-565874 Fax: 972-7-555058 E-mail: karnieli@bguvms.bgu.ac.il

Abstract

Advantage is taken of a unique spectral feature of soil biogenic crust containing cyanobacteria. It has been shown that the special phycobilin pigment in cyanobacteria contributes in producing a relatively higher reflectance in the blue spectral region than the same type of substrate without the biogenic crust. A spectral crust index (CI) has been developed, based on the normalized difference between the RED and the BLUE spectral values:
$CI = 1 - (RED - BLUE)/(RED + BLUE)$.

Applying the index to a sand dune environment, it has been shown that the CI can be used to detect and to map, from remote sensing imagery, different lithologic/morphologic units such as active sands, crusted interdune areas and playas, which are expressed in the topography. As a mapping tool the CI image is much more sensitive to the ground features than the original image. The absence, existence, and distribution of soil crust are an important information for desertification and climate change studies. They are also highly valuable information for developing agricultural regions and/or infrastructures in arid environments since soil crusts contribute to soil stability, soil build-up, soil fertility, and to the soil water regime.

1. Introduction

Soil crust formation is a common and widespread phenomenon in arid and semi-arid soils. Distinction should be made between "physical" and "biogenical" crust formations. Physical crust is defined either as one formed by a combination of raindrop impact on the soil surface along with physiochemical dispersion of soil clay, or as one formed by the sedimentation of fine material as turbid water infiltrates following overland flow (Singer, 1991).

The biogenical soil can be formed by different combinations of microphytic communities including mosses, lichens, liverworts, algae, fungi, cyanobacteria, as well as bacteria (West, 1990). The microphytes can grow on different rocky materials such as limestone, chalk, dolomite, flint, sandstones, granite, as well as on different soil types such as loess and dune sand (West, 1990). They are well adapted for primary colonization of arid environments due to their extraordinary ability to survive desiccation and extreme temperatures (up to 70°), high pH and salinity. Consequently, well developed microphytic soil crust communities are found on soils in arid and semi-arid areas throughout the world.

Data about the soil crusts in arid lands contents considerable information with respect to the desert ecosystems since the soil crusts contribute to soil stability, soil build up, soil fertility, and to the soil water regime. Therefore, absence, existence and distribution of soil crust is an important information with conjunction to desertification and climate change studies. It is also a high value information for developing agricultural regions and/or infrastructures in arid environment.

However, despite the importance of the soil crust and its vast distribution over arid and semi–arid soils, little is known about the ability to detect and map desert crusts by remote sensing methods. Spectral reflectance curves of different desert microphytic communities are presented by Ager and Milton (1987), O'Neill (1994), Tromp and Steenis, (1995), Karnieli and Tsoar (1995), Karnieli *et al.* (1995) and Karnieli and Sarafis (1995). Some efforts to map biogenic crusts microphytes based on Landsat–MSS images have been made by Wessels and van Vuuren (1986) and Tsoar and Karnieli (1995). These works show the capacity to visually differentiate and classify several types of crusts. The aim of the present work is to map various types of crusts by relating new knowledge about their spectral features to aerial photographs and satellite images.

2. Data analyses and results

Field measurements were carried out *in–situ* by using the Li–Cor LI–1800 portable spectrometer. All measurements were obtained almost simultaneously in the sand dune area at Sede Halamish site.

Five spectra are presented in Fig. 1: interdune playa crust, bare active dune sand, and three cyanobacteria crusts sampled at the north and south facing of the basal dune as well as from the interdune crusty surface. These spectra differ from each other by the fines content. These spectra have a typical soil shape, namely, relatively low in the blue region and increases gradually towards the near infrared region, however, one can notice the slight dip of the crust spectra from 600 to 700 nm on account of the organic material of the cyanobacteria. The playa spectrum has the highest reflectance values in all bands. Lower is the active dune sand spectrum which is relatively high in the red and NIR spectral bands while all the others biogenic crust spectra cross it at different points along the visible range.

The spectral feature described above, i.e., higher reflectance values of the crusted samples when cyanobacteria exists relative to the bare dune sand has been observed in several other examples which recently published by Jacobberger (1989) Tromp and Steenis (1995) and Karnieli *et al.* (1996) (Fig. 2). Note that in all the spectra where cyanobacteria is involved, either as a free algae or in conjunction with lichens, the reference spectrum (bare substrate consists of either soil or rock without crust) and the crust spectrum cross each other at about 500 nm. The reference curves have higher reflectance in the red and NIR regions and the crust curves have a higher reflectance in the blue region. In other cases, when no curve crossing is observed, the slope of the microphytic spectrum is gentler than that of its substrate. Several examples of this phenomenon are presented in Ager and Milton (1987).

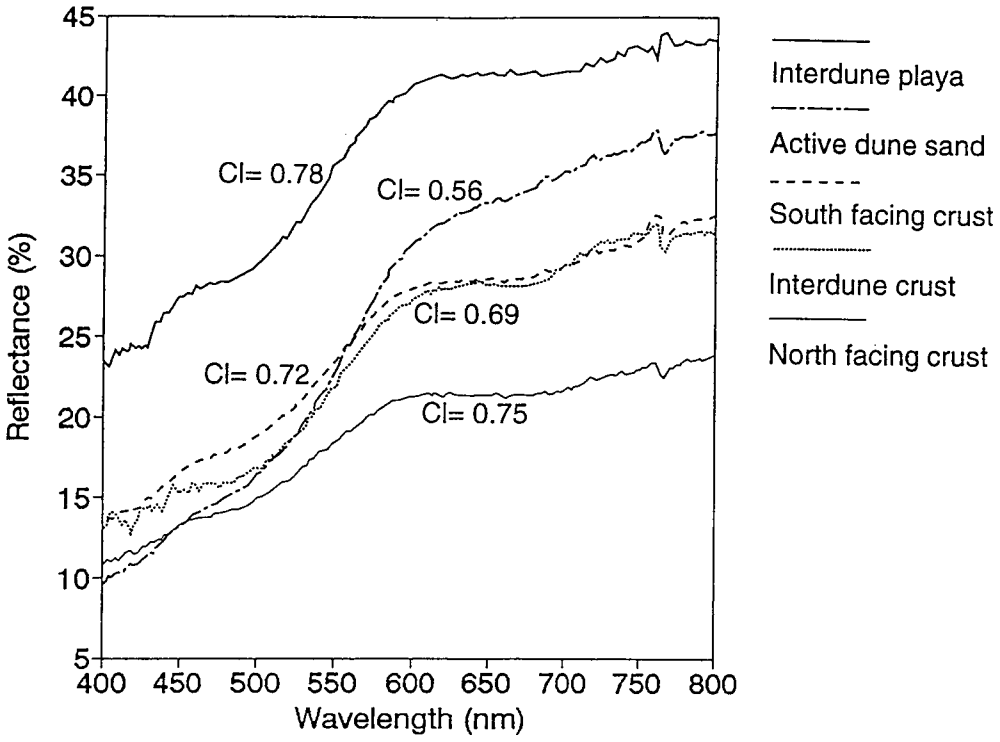

Figure 1: Spectral reflectance field measurements of different geomorphological-sedimentological units in the study area with the respective values of the calculated crust index (CI).

Karnieli and Sarafis (1996) showed that relative higher reflectivity of crust in the blue region is caused due to the spectral characteristics of the phycobilin pigments. Phycobilins are protein pigments containing a linear tetrapyrrol as the chromophore. This type of pigment is unique for cyanobacteria and generally not detectable in higher plants.

The unique spectral feature of the biogenic crust discussed previously was used for deriving a crust index (CI). This index is aimed to differentiate between crusted and uncrusted areas as well as among areas with different fines and organic matter contents. The proposed crust index has the form of:

$$CI = 1 - \frac{RED - BLUE}{RED + BLUE} \approx 1 - \frac{NIR - BLUE}{NIR + BLUE} \tag{1}$$

where $BLUE$, RED and NIR are the $400 - 500$, $600 - 700$, and $700 - 800$ nm spectral bands, respectively, in units of radiances, reflectance or at least 'apparent reflectance'. The CI values lie in the range of -1.0 to $+1.0$ but usually positives. The idea behind this equation is to calculate the normalized difference between the relative higher reflectance which occurs in the red region and the minimal reflectance in the blue region. The substcaction of the difference from 1 is suggested in order to create higher values for soil riched with fines and organic matter contents. The calculated CI values for the field spectral measurements are presented in Fig. 1.

The index has been implemented on the color photograph of Sede Halamish site (Fif. 3). The brightest tones, almost white, in this photographs reflect from the playa areas. Less

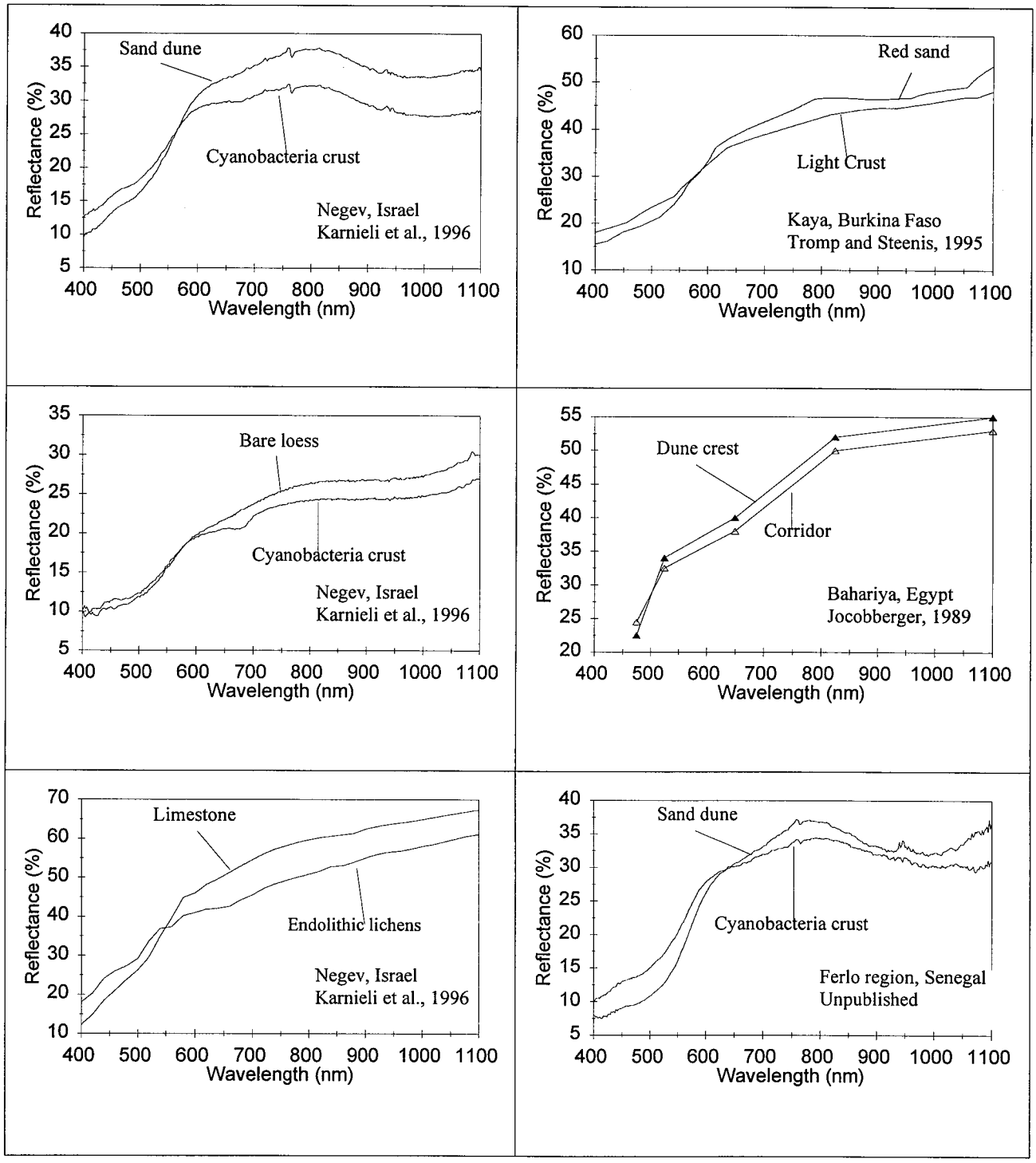

Figure 2: Spectral reflectance curves of cyanobacteria and different soil and rock substrates. Note the curve crossing points at the green region (500–600 nm). Adapted from Jacobberger (1989), Tromp and Steenis (1995) and Karnieli *et al.*, (1996).

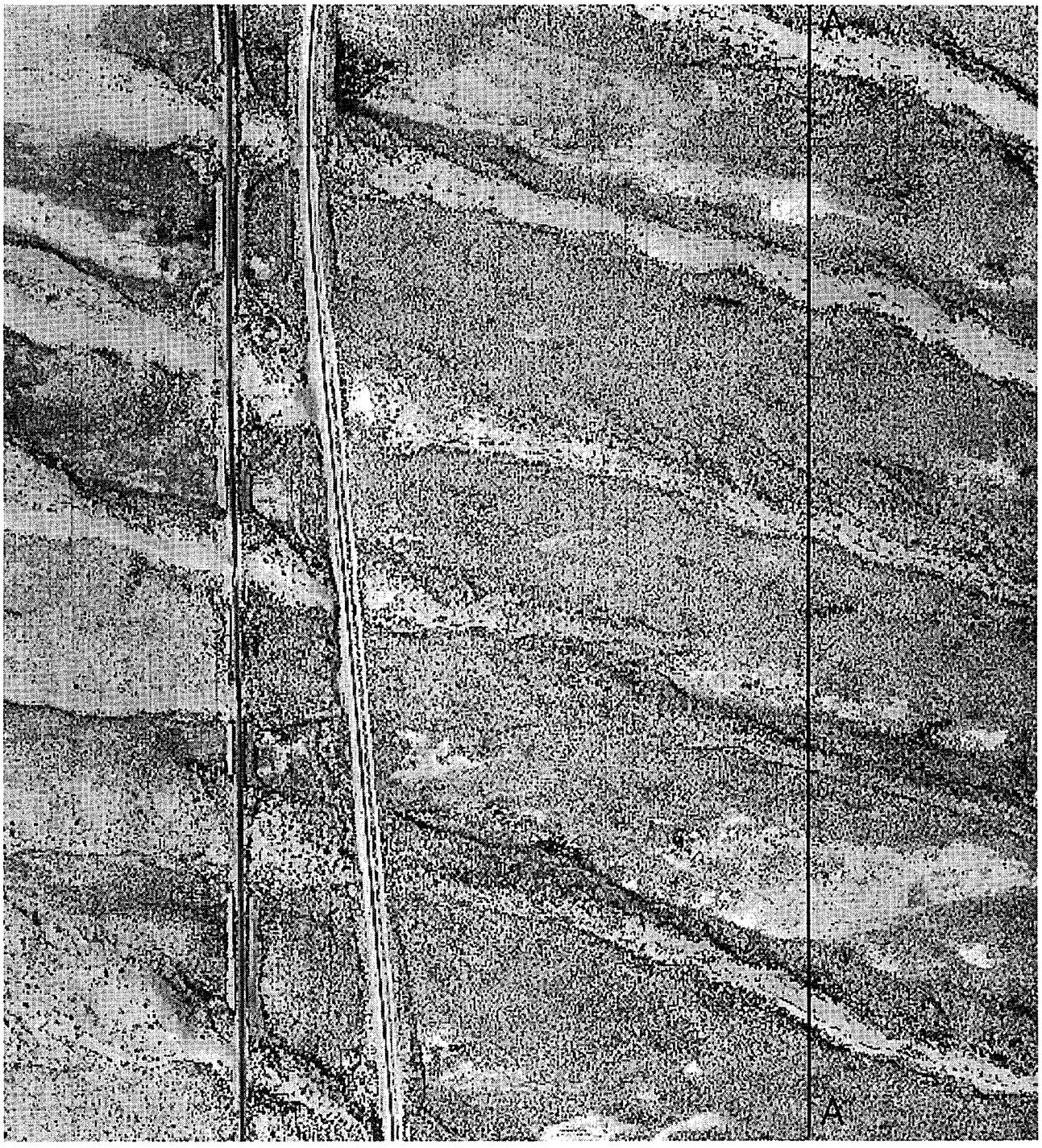

Figure 3: Color aerial photograph of the study area. Note the active dune sands in yellow, biogenic crusts in gray, and playa areas in white.

bright tones reflect from the dune sand areas while the darker tones reflect from the crusted areas. In the resulted image one might notice that the same playa areas appear in black, the sand dune in bright tones, almost white, and biogenic crusted areas in different gray levels between the previous two extremes. The results of the CI computation are presented in Figure 4. One would notice that the same playa areas which originally appear in bright tones, here appear in dark tones, the sand dunes remain in bright tones (almost white), and biogenic crusted areas in different gray levels in–between.

Two cross sections of gray levels are presented in Figure 5. One profile has been generated from the red color of the original aerial photograph (line A – A in Figure 3). The other similar profile has been generated from the resulting CI image (line B – B in Figure 4). From Figure 5 it can be seen that by applying the CI, the overall image contrast has been enhanced almost to the entire dynamic range of the display device (0 – 255). Therefore the CI profile is much more sensitive to the ground features than the original profile. The most interesting issue in this figure is that the playa areas turn from relatively bright tones in the original spectrum to almost a black color. Here the playa areas have the highest CI values (> 0.725) and the lowest gray levels (0 – 70). The interdune crusts appear in intermediate gray tones. Their CI values are confined within 0.625 – 0.725 and the corresponding gray levels are 70 – 150. Lastly, the active dune sands which appear in bright tones in Figure 4 have CI values of 0.55 – 0.625 and gray levels of 150 – 220.

References

Ager C. M. and Milton, N. M. 1987. Spectral reflectance of lichens and their effects on the reflectance of rock substrates. *Geophysics*, **52**, 898–906.

JACOBBERGER, P. A., 1989, Reflectance characteristics and surface processes in stabilized dune environments. *Remote Sensing of Environment*, **28**, 287–295.

Karnieli, A. and Sarafis, V. 1996. Reflectance spectrophotometry of cyanobacteria within soil crusts - a diagnostic tool. *International Journal of Remote Sensing*, **17**, 1609–1615.

Karnieli, A., and Tsoar, H. 1995. Spectral reflectance of biogenic crust developed on deseret dune sand along the Israel–Egypt border. *International Journal of Remote Sensing*, **16**, 236–374.

Karnieli, A., Shachack, M., Tsoar, H., Zaady, E., Kaufman, Y., and Porter, W. 1996. The effect of microphytes on the spectral reflectance of vegetation in semi–arid regions. *Remote Sensing of Environment*, **57**, 88–96.

O'Neill A. L. 1994. Reflectance spectra of microphytic soil crust in semi–arid Australia. *International Journal of Remote Sensing*, **15**, 675–681.

Singer, M. J. 1991. Physical properties of arid region soils. In J. Skujiņš (Ed.): *Semiarid Lands and Deserts: Soils Resource and Reclamation.* Marcel Dekker, New York. pp. 81–109.

Tromp, M. and Steenis, Z. 1995. Deriving sub–pixel soil characteristics in northern Burkina Faso with spectral unmixing. *Proceedings of the International Symposium Remote*

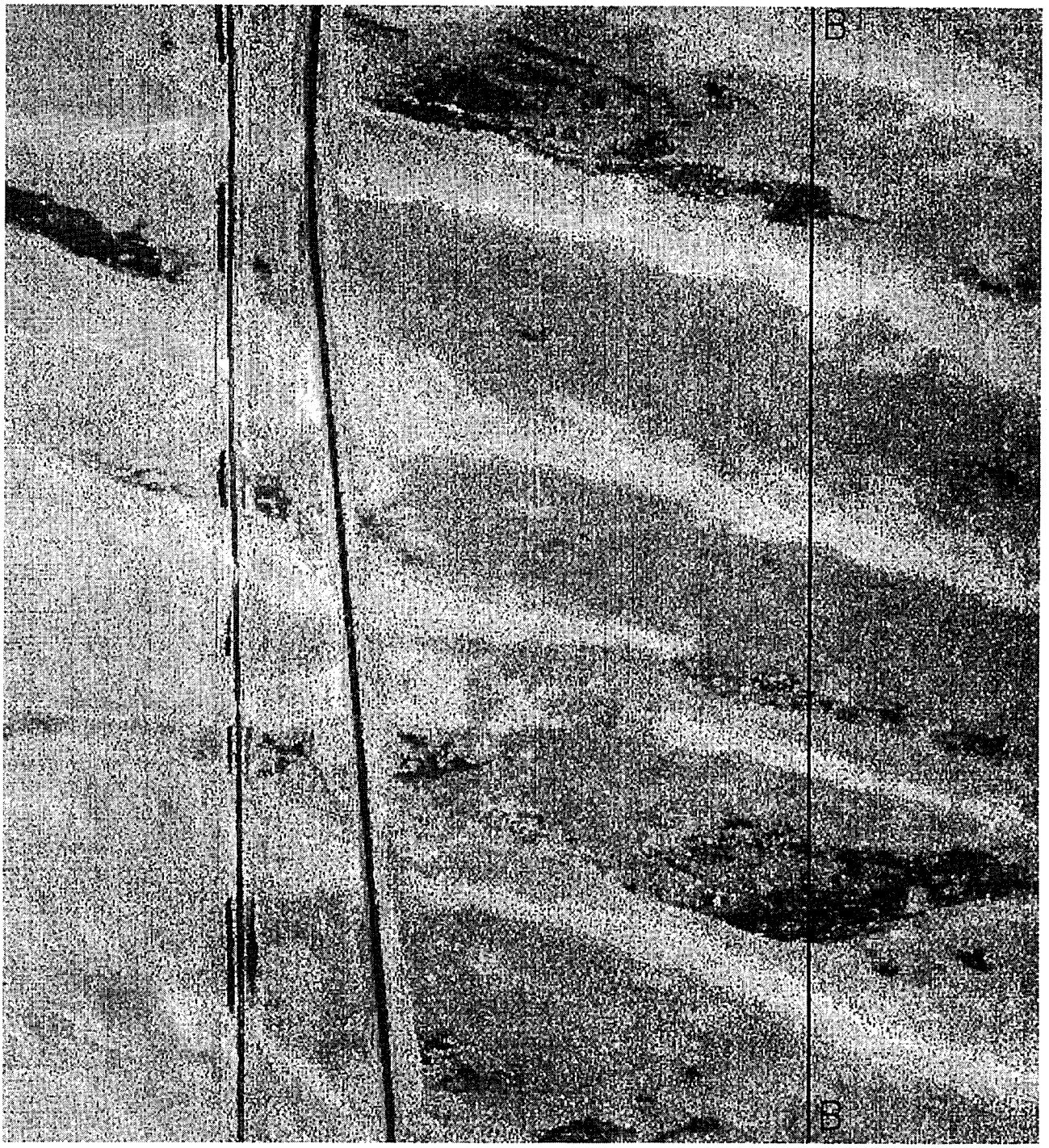

Figure 4: Crust index (CI) image generated from the color aerial photograph in Figure 3.

Sensing and GIS as tools for monitoring soils in the environment, held in Ouagadougou, Burkina Faso.

Tsoar, H. and Karnieli, A. 1995. What determines the spectral reflectance of the Negev–Sinai sand dunes. *International Journal of Remote Sensing*, (in press).

Wessels, D. C. J. van Vuuren. 1986. Landsat imagery - its possible use im mapping the distribution of major lichen communities in the Nanib Desert, South West Africa. *Madoqua*, **14**, 369–373.

West, N. E. 1990. Structure and function of microphytic soil crusts in wildland ecosystems of arid to semi-arid regions. *Advances in Ecological Research* **20**, 179–223.

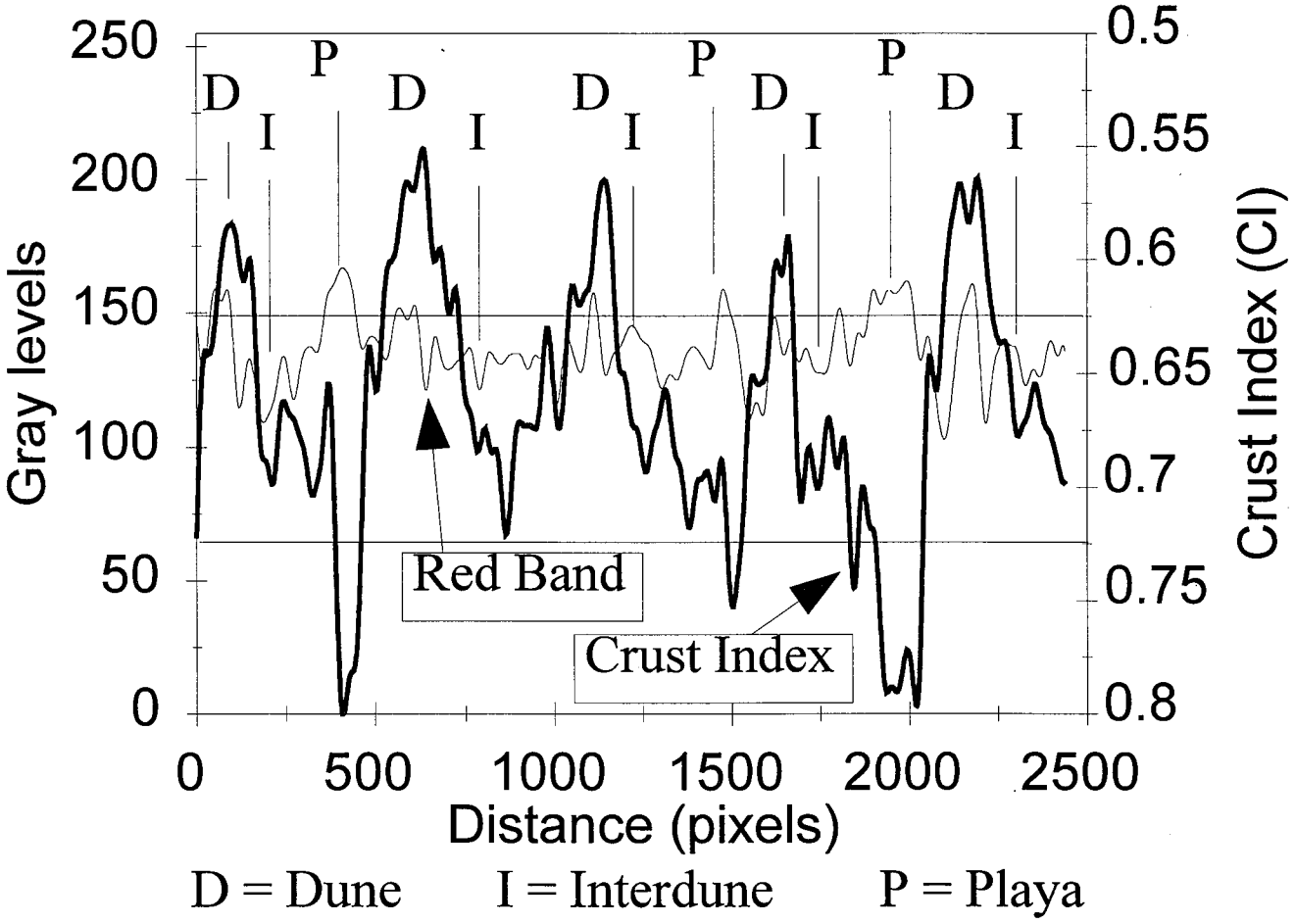

Figure 5: Gray levels profiles of the red band of the original color aerial photograph along the dune study area and after performing the crust index. Cross section locations are presented in Figure 3 and Figure 4, respectively.

The Effect of Biogenic Crusts on the Spectral Reflectance of the Semi–arid Regions

Arnon Karnieli
The Remote Sensing Laboratory, J. Blaustein Inst. for Desert Reserach
Ben Gurion Univ. of the Negev, Sede Boker Campus 84990 ISRAEL
Tel: 972-7-565874 Fax: 972-7-555058 E-mail: karnieli@bguvms.bgu.ac.il

Abstract

The Normalized Difference Vegetation Index (NDVI) which is derived from satellite sensor images is widely used as a measure of vegetation and ecosystem dynamics, change in land use, desertification and climatic change processes on a regional or global scale. Surprisingly, in semi–arid regions, relatively high values of NDVI were measured in landscapes where little, if any, photosynthetic activity of higher plants exists. We tested the hypothesis that the high NDVI values may be caused by the photosynthetic activity of microphytes (lower plants), consisting of mosses, lichens, algae, and cyanobacteria, which cover most of the rock and soil surfaces in semi–arid regions. We found that the spectral reflectance curves of lower plants can be similar to those of the higher ones and their derived NDVI values can be as high as 0.30 units. We conclude that in semi–arid environments, the reflectance of lower plant communities may lead to misinterpretation of the vegetation dynamics and overestimation of ecosystem productivity.

1. Introduction

In this study, we explore the hypothesis that the high NDVI values obtained in arid and semi–arid environments result from the reflectances of microphytes (lower plants) which cover most soil and rock surfaces in the absence of higher plants. These lower plants include mosses, lichens, and cyanobacteria (blue–green algae), which potentially can carry out photosynthetic activity. Our study has been conducted in the northern Israeli Negev desert. Different types of microphytic crusts are common in loess soils. It has been observed that cyanobacteria crust dominates in regions where the rainfall is less than 100 mm, soil lichens in regions of 100 to 200 mm of rain, and mosses in regions of 200 to 300 mm.

2. The loess environment

Microphytic crust representing the most common communities were collected by scraping to one centimeter depth in loess soil in an area with 200 mm mean annual rainfall. These samples were collected in 1993 during the month of January which is considered the wettest month of the rainy season. It was observed that at this period of the year the annuals had

not yet germinated while the perennials had hardly sprouted. Nevertheless, the microphytic communities were in full activity.

The reflectance spectra of the samples were measured in the laboratory using the Li–Cor LI–1800 spectrometer. Figure 1 shows the spectral reflectance curves of the different microphytic communities sampled. They include (a) a community dominated by cyanobacteria (mainly *Microcoleus vaginatus, Nostoc punctiforme* and *Chroococcus* sp.); (b) a community dominated by soil cyanophilous lichen (*Collema* sp.); (c) a community dominated by two species of moss (*Aloina bifrons* and *Crossidium crassinerve var. loevipilum* from a south–facing slope; and (d) a community dominated by the same two species of moss, but in different proportions, from a north–facing slope. It is pertinent to observe that in the northern hemisphere, within the same location, south–facing slopes generally are drier that north–facing slopes. Figure 1 also shows the spectral reflectance curve of the loess soil without crust. This has been included as a reference.

The curve representing the crust–free soil portrays a convex shape typical of soil curves. On the other hand, although the spectra representing the mycrophytic communities have a convex shape also, they show an appreciable dip in the 600 to 700 nm region, indicative of chlorophyll absorption. In particular, the moss community from the north–facing slope has almost a typical vegetation curve. NDVI values of 0.08, 0.10, 0.14, 0.19, and 0.30 were calculated for soil, cyanobacteria, lichens, south–facing slope mosses, and north–facing slope mosses, respectively.

The above results reflect the relationship between the soil moisture content and the microphytic community structure (i.e. species composition and abundance). The cyanobacteria occupies the drier end of the moisture gradient while the north–facing slope mosses are at the wetter end. The higher the soil moisture, the more prominent the chlorophyll absorbance features in the reflectance spectra and the higher the NDVI values. We suggest that the variation in the reflectance spectra and the NDVI values of the communities is due to: (1) differences in the microphytic community structure, i.e., species composition; and (2) the differences in the abundance of the various species. Community structure and species abundance reflect the spatial variability in soil moisture content. The variation in the soil moisture content is, on a local scale, mainly due to slope direction, while on a regional scale it is mainly due to differences in the amount of rainfall.

Special attempt should be given to the difference between the south and and the north sides of the hill (Figure 2). The first is facing the direct solar radiation while the other the principal rainfall direction. These two opposite conditions cause drastic difference between the dominant microphytic communities. On the average, 29.2 leafy stems per cm^2 of mosses were found on the south facing slope, 77% of them belong to the *A. bifrons* and the rest 23% to *C. crassinerve*. Equivalently, on the north facing slope 157.5 leafy stems per cm^2 of mosses were found on the south facing slope, 93% of them of *C. crassinerve* and 7% of *A. bifrons*. Note that although both species exist only in semi–arid region, the *A. bifrons* can persist under drier conditions and therefore more stems of this species are found on the south facing slope. On the south facing slope the mean crust thickness was found to be only 4 mm while on the north facing slope the mean crust thickness was found to be 12 mm.

3. Conclusion

It can be concluded from this study that the signal produced by microphytes, especially under wet conditions, is characteristic of that of higher vegetation. Their NDVI values can be as high as 0.30 units. In arid and semi-arid regions where higher vegetation is sparse, microphytes can cover most of the ground surface. As such, during remote sensing image acquisition, most of the signal reaching the satellite may come from the microphytes. Since this signal is similar to that of higher plants, the relatively high NDVI values computed may be misinterpreted for the presence of higher vegetation and may lead to overestimation of such quantities as green leaf biomass or productivity.

This type of influence from microphytes can occur in the rainy season as well as in the dry season. At the early part of the rainy season when higher plants are still very low in activity, microphytes make a quick response and reach their peak activity. This is due to their ability to respond rapidly to variation in moisture.

It can be farther concluded that the differences between the reflectance spectra resulting with respective different NDVI values are caused by (1) variation in microphytic species; (2) the spatial variation of the microphytic density; and (3) variation in crust thickness. These differences reflect changes in the microclimatic environment due to spatial distribution of water regime and radiated sunlight.

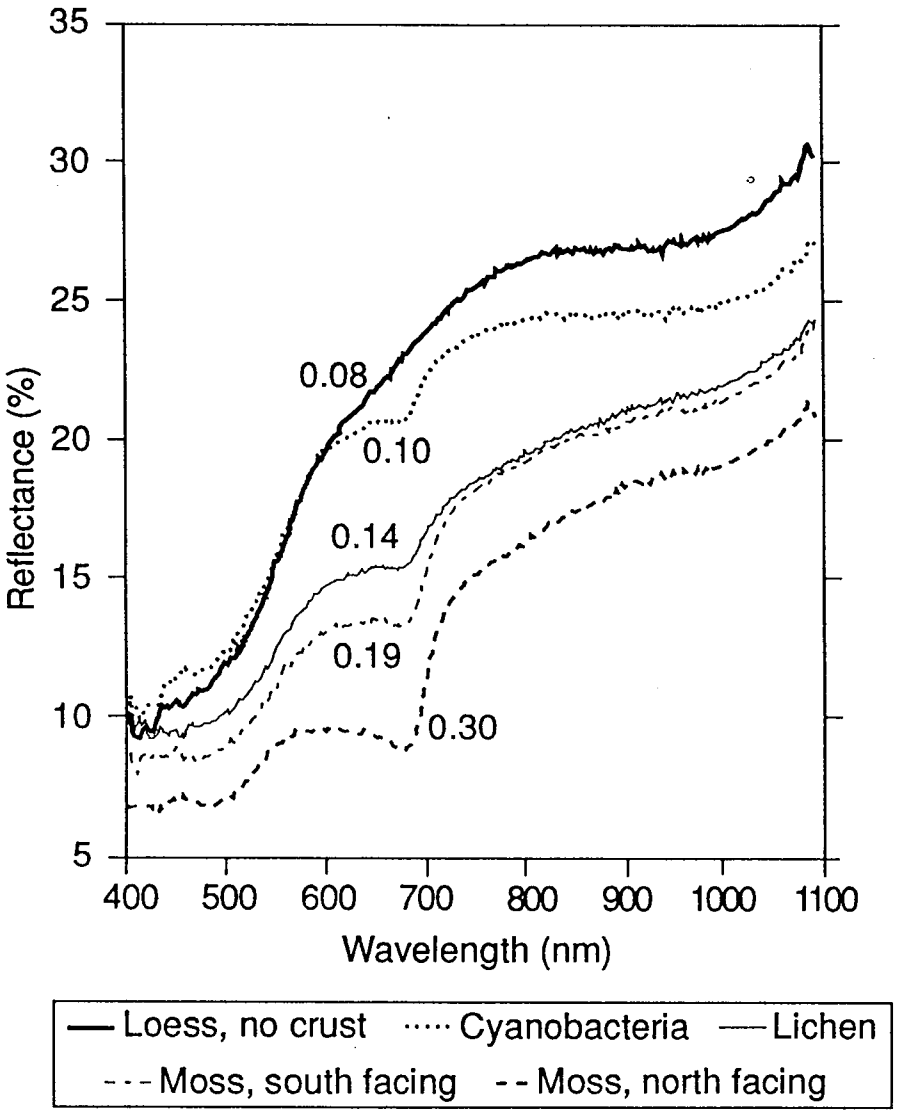

Figure 1: Spectral laboratory measurements of different microphytic communities on loess soil, sampled on 7 January, 1993, with their respective NDVI values.

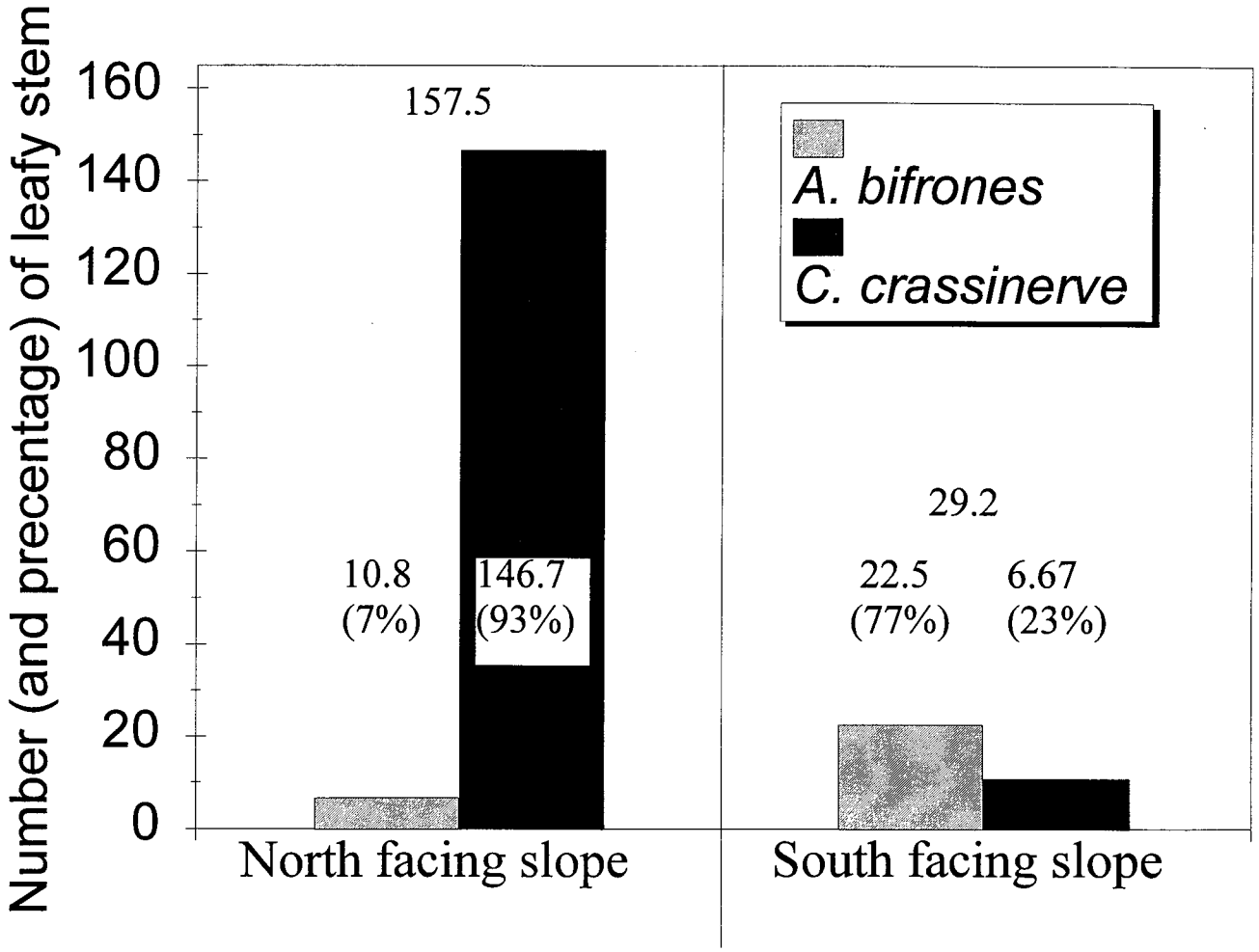

Figure 2: Number and precentage of average leafy stems of mosses communities found on south facing vs. north facing hillsides.

Comparison of JERS-1 SAR and SPOT-2 Panchromatic Data over a Semi-Arid Zone in Central Australia

Y.Oguro(*) and K.Tsuchiya(**)

* *Hiroshima University, Faculty of School Education, 1-1-1 Kagamiyama, Higashi-Hiroshima, 739, Japan*
FAX: +81-824-24-7108
E_mail: yoguro@sed.hiroshima-u.ac.jp

** *Hiroshima Earth Environmental Information Center, 2-1-1 Miyake, Saeki-ku, Hiroshima, 731-51, Japan*
Fax: +81-3-3617-4870
E_mail: MFN68086@pcvan.or.jp

ABSTRACT

Analyses of the data observed with JERS-1 SAR and SPOT-2 panchromatic mode over a semi-arid zone in central Australia under a similar environmental condition indicate that (1) the high resolution data are useful for detection of small gullies or a degraded area caused by rare floods, (2) the narrow woody space in a widely bare land can be recognized in SAR data while not in the panchromatic data and (3) land cover classification image can be made with SAR data and panchromatic data.

INTRODUCTION

In cooperative research projects on desertification with China and Australia, it has been found that desertification is taking place in comparatively narrow spatial scale, and the high resolution satellite data are very useful for desertification studies [1]-[5]. In general analyses, the desertification is detected as the change of vegetation in semi-arid and arid zone, and SPOT-2 multi-spectral and JERS-1 OPS (OPtical Sensor) data are available for vegetation analyses while the spatial resolutions are 20m*20m and 24m*18m respectively. SPOT-2 panchromatic data is also useful with 10m spatial resolution while the vegetation analysis is difficult. These above mentioned satellite data, however, have a disadvantage since the chance of getting cloud-free data is very small. On the other hand, JERS-1 SAR (Synthetic Aperture Radar) data is very useful with 12.5m spatial resolution while the speckle noise and geometric distortion are the disadvantage since the data getting whole weather conditions and also getting day and night. The analyses of the high resolution data observed by JERS-1 SAR and by SPOT-2 panchromatic over a semi-arid zone of central Australia will be reported in the following sections.

THE ANALYSES OF THE DATA

Figure 1(a) and (b) are satellite images of JERS-1 SAR (August 20 1992) and SPOT-2 panchromatic (July 22 1992) respectively. In 1992, it was no precipitation from June 13th through August 26th. Furthermore the observation time difference of both satellites is within 30 minutes thus it is considered that the surface condition of two images was almost same.

Registration of the Data

Following procedures are taken to register two images with different resolution.

(1) For speckle noise reduction, the median filtering (window size: 5*5) is performed for SAR data.
(2) Taking SPOT-2 panchromatic image (10m resolution) as reference, 50 GCP's (Ground Control Points) are selected in JERS-1 SAR (12.5m resolution) image.
(3) Twenty Affine coefficients in Eq.(1) are computed [6].

$$p = a_0 + a_1*P + a_2*L + a_3*P*L + a_4*P^2 + a_5*L^2 + a_6*P^2*L + a_7*P*L^2 + a_8*P^3 + a_9*L^3$$
$$l = b_0 + b_1*P + b_2*L + b_3*P*L + b_4*P^2 + b_5*L^2 + b_6*P^2*L + b_7*P*L^2 + b_8*P^3 + b_9*L^3 \quad (1)$$

where, P and L are pixel and line numbers of a GCP of JERS-1 SAR while p and l are those of SPOT-2 panchromatic in pixel-line coordinate system. Although the equation must be solved under the condition that the average error becomes 0, in reality the absolute error cannot become zero.
(4) Moving one GCP in 8 directions (up-down, right-left, diagonal) and selecting one which minimizes the absolute and root mean square (RMS) errors, the process is repeated until the errors become negligibly small.

Correlation of the Whole Data

Figure 2 indicates the relation between Normalized Radar Cross Section (NRCS) of JERS-1 SAR data and radiance of SPOT-2 panchromatic data. The values of NRCS and that of radiance are compute from Eq.(2) and Eq.(3) respectively [7],[8].

$$NRCS = 20 * Log_{10}(X) - 70.5 \quad [dB] \quad (2)$$

$$Radiance = (X/A + B) * \cos(Z) * C \quad [W/m^2/Sr] \quad (3)$$

where X, A, B,C and Z denote digital counts recorded on CCT's(Computer Compatible Tapes), gain for conversion from digital counts into radiance, offset, solar zenith angle and bandwidth respectively. The coefficient of correlation between NRCS and radiance is -0.29. Next, the NRCS for undulating area such as hill or mountain is distributed as higher signal and that for flat area is distributed as lower one. Here the forward slopes of mountains make the maximum NRCS. On the other hand, the radiance for bare land and woody space are distributed as higher and lower reflectance respectively.

Detail Analysis for a Line Data

Figure 3 indicates the detail analysis of NRCS of JERS-1 SAR and radiance of SPOT-2 panchromatic data. From Figure 3 it can be seen that the trees are recognizable well in SAR data while not in the panchromatic data, approximately 10 meter width road is recognizable while in case of panchromatic data due to similar reflectivity of the unpaved road and surrounding bare land it is not possible to

recognize. The very small gullies of 30 - 50cm order made by floods are detected in SAR data while not in the panchromatic data.

Land Cover Classification

Figure 4 indicates the land cover classification with JERS-1 SAR and SPOT-2 panchromatic data over the area shown in Figure 1 in four categories of woody space, dense grass land, sparse grass land (including small gullies or land degraded area caused by rare floods) and bare land. Following procedures are taken to make the image of land cover classification.

(1) For simplifying the threshold level selection, transform the JERS-1 SAR and SPOT-2 panchromatic data shown in Figure 1. into ten levels data with Ohtsu's threshold selection method since the method is automatically selected the minimum error thresholding levels [9],[10].
(2) Selecting the two threshold levels (PAN_H and PAN_L) for classifying the panchromatic data into three categories as bare land, grass land and woody space.
(3) Selecting the one threshold level (SAR_M) for classifying the SAR data into two categories as undulating area (such as woody space, hill or mountain) and flat area (such as grass land or bare land).
(4) Firstly, classifying into four categories of woody space, dense grass land, sparse grass land and bare land with two-dimensional multi-level slice method (pallarelpiped classification) while a little overlapping area cannot be classified. The classification are made as following roles:

IF	PAN≦PAN_H	&&	SAR>SAR_M	THEN	WOODY SPACE
IF	PAN≦PAN_L	&&	SAR≦SAR_M	THEN	DENSE GRASS LAND
IF	PAN_L≦PAN≦PAN_H	&&	SAR≦SAR_M	THEN	SPARSE GRASS LAND
IF	PAN>PAN_H	&&	SAR≦SAR_M	THEN	BARE LAND
IF	PAN>PAN_H	&&	SAR>SAR_M	THEN	ERROR (SPECKLE NOISE)

(5) Secondly, the classification for the overlapping area are made with Mahalanobis's minimum distance method.

From Figure 4 some small gullies and degraded area caused by rare floods are detected. Furthermore the narrow woody space in widely bare land and the sparse grass land can be recognized while not in the panchromatic data. These features are comforted in situ survey and aerial video data.

CONCLUDING REMARKS

From the analyses in this study following conclusions were obtained. The high resolution data such as JERS-1 SAR (12.5m resolution) and SPOT-2 panchromatic (10m resolution) data are very useful for the detailed analyses of ground surface condition. The land cover classification image was also made with synthesized those two data. The accurate classification method with SAR data will be considered as future works.

REFERENCES

[1] K.Tsuchiya, Y.Oguro and M.Yamanashi, The Surface Features of Taklamakan Desert, Final Report of JERS-1/ERS-1 System Verification Program, Vol.1, pp.539-559, MITY(Ministry of

International Trade and Industry) and NASDA (National Space Development Agency of Japan) (1995).
[2] K.Tsuchiya and Y.Oguro, Taklimakan Desert as Seen from Satellites - Application of Remote Sensing -, Journal of Arid Land Studies, Vol.5, No.2, pp.145-154, The Japanese Association for Arid Land Studies (1996)*.
[3] Y.Oguro and K.Tsuchiya, Studies on the Vegetation and the Land Surface Condition in Arid Zone with JERS-1 SAR Data, SANE95-79(Space, Aeronautical and Navigational Electronics), pp.41-48, IEICE (The Institute of Electronics, Information and Communication Engineers) (1995)**.
[4] Y.Oguro and K.Tsuchiya, An Assessment of Vegetation in Arid Zone using JERS-1 SAR Image, Proc. of the 20th Japanese Conf. On Remote Sensing, pp.5-8 (1996a)**.
[5] Y.Oguro and K.Tsuchiya, Extraction of the Desertified Areas in Oases in Taklimakan Desert through the Analysis of SPOT Image Data, Journal of Arid Land Studies, Vol.5, No.2, pp.155-162, The Japanese Association for Arid Land Studies (1996b)**.
[6] NASDA, Reference Manual of JERS-1 SAR/ERS-1 AMI IMAGE Data Format, Vol.1, NASDA (1992)*.
[7] M.Shimada, User's Guide to NASDA's SAR products, HE93014, pp.11-13, NASDA (1993).
[8] RESTEC, Reference Manual of SPOT data CCT Format, Vol.94-J, RESTEC (Remote Sens. Tech. Center of Japan) (1986)*.
[9] N.Otsu, An Automatic Threshold Selection Method Based on Discriminate and Least Squares Criteria, IECE Trans. of J63-D, No.4, 349-356 IECE(The Institute of Electronics and Communication Engineers) (1980)**.
[10]J.Kittler and J.Illingworth, Minimum Error Thresholding, Pattern Recognition, Vol.19, No.1, pp.41-47, Pattern Recognition Society (1986).

* Original text in Japanese.
**Original text in Japanese with summary, table and figure captions in English.

500m

(a)

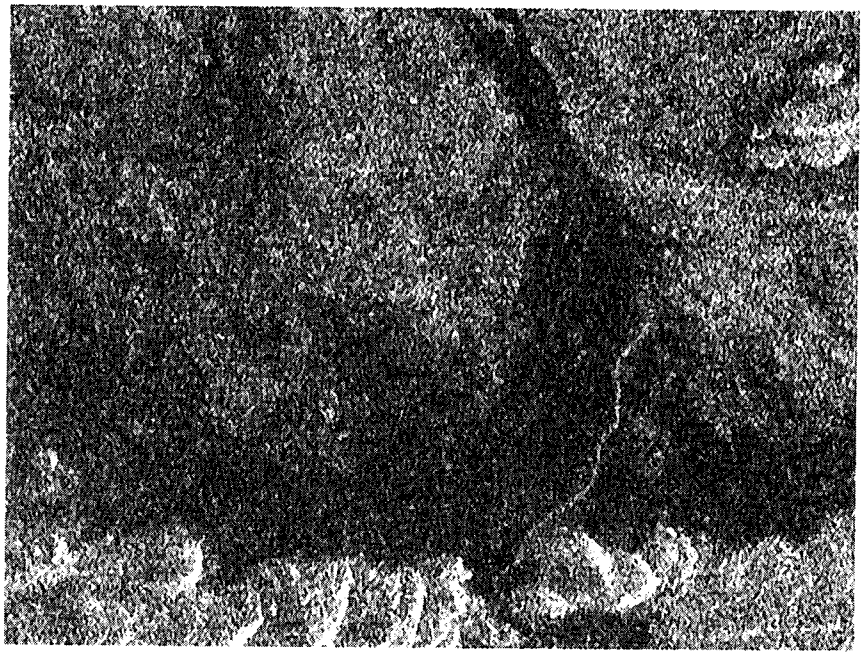

500m

(b)

Fig. 1. Satellite images of (a) JERS-1 SAR (August. 20 1992) and (b) SPOT-2 panchromatic (July 22 1992). The center at 23.34N/133.35E in central Australia.

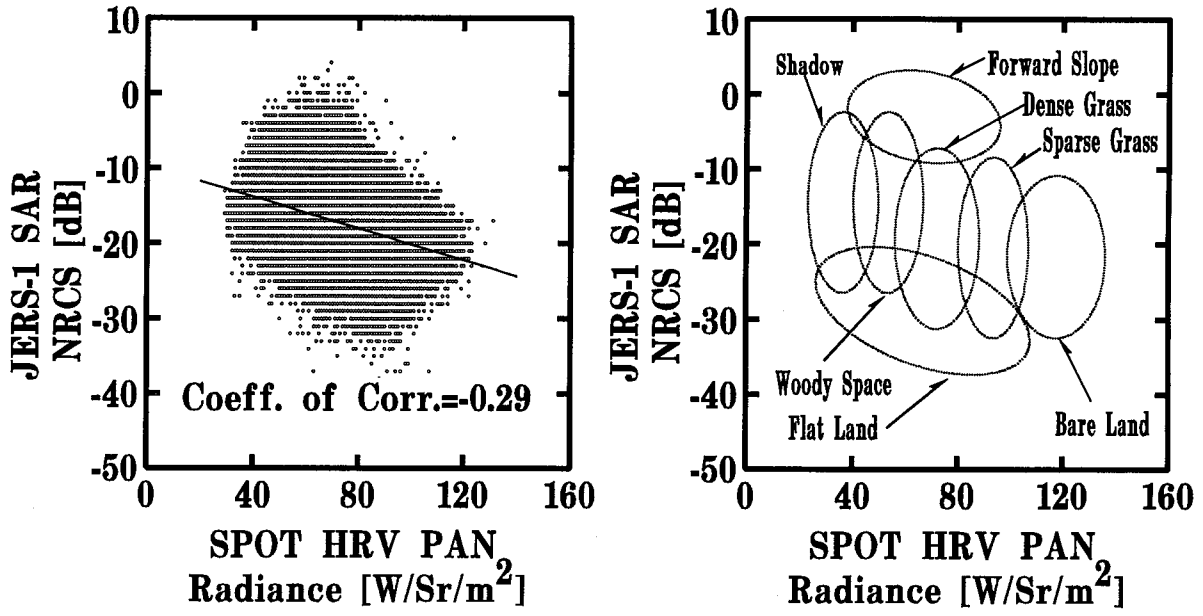

(a) Correlation

(b) Distribution

Fig. 2. Relation between Normalized Radar Cross Section (NRCS) of JERS-1 SAR data and radiance of SPOT-2 panchromatic data.

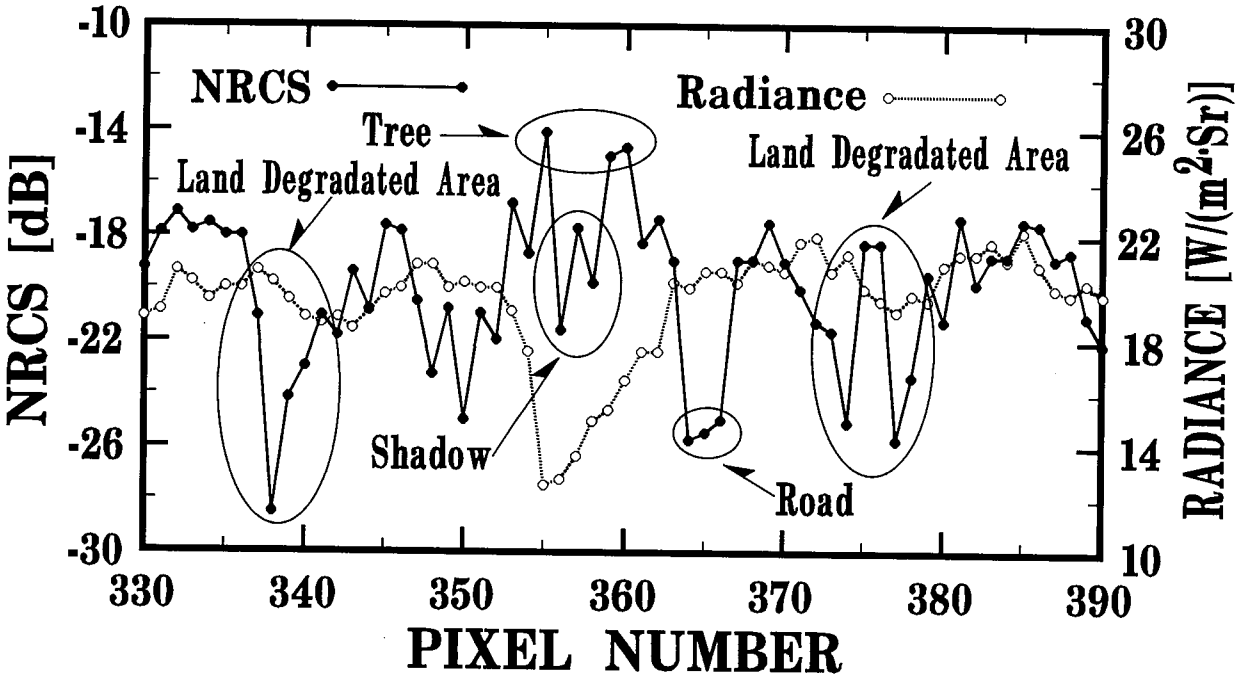

Fig. 3. Indicates the Normalized Radar Cross Section of JERS-1 SAR observation and radiance observation of SPOT-2 panchromatic for a line data.

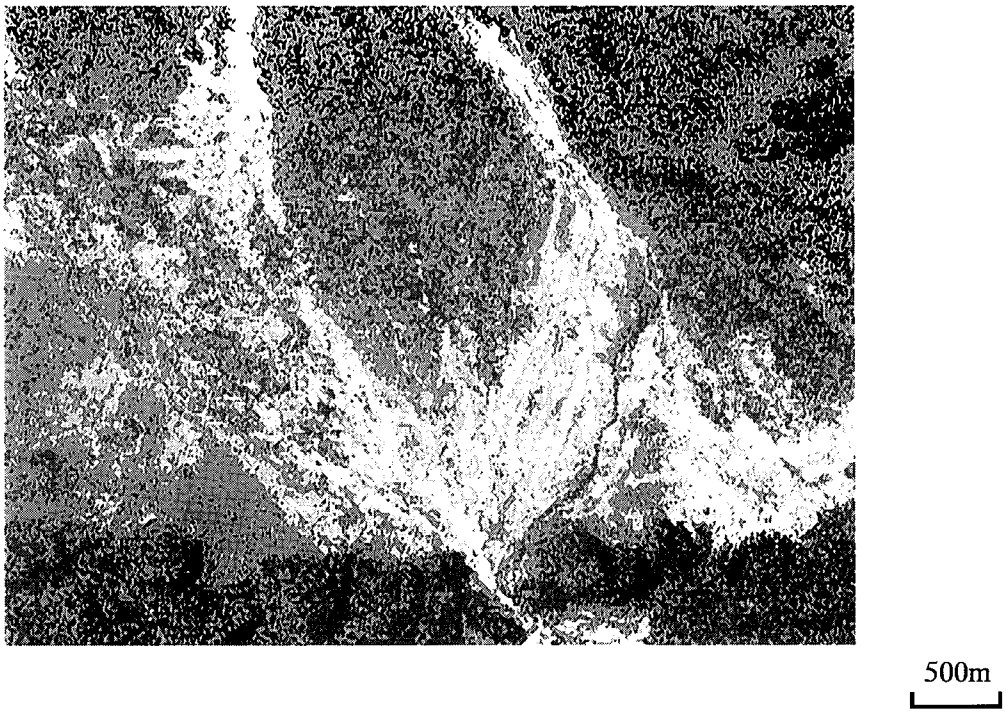

Fig. 4. Land cover classification over the area shown in Figure 1 in four categories of woody space, dense grass land, sparse grass land and bare land. The color schemes; (1) Black: woody, (2) Dark gray: dense grass land, (3) Bright gray: sparse grass land (including small gullies or land degraded area caused by rare floods) and (4) White: bare land.

Vegetation Indices of High and Low Vegetation Density Areas in Southern Part of Taklimakan Desert

T. Ishiyama[1], Y. Nakajima[2], Koji Kajiwara[1] and K. Tsuchiya[3]

1 Center for Environmental Remote Sensing, Chiba University, 1-33, Yayoicho, Inageku, Chiba-shi, 263 Japan (E-mail: ishiyama@rsirc.cr.chiba-u.ac.jp)

2 Remote Sensing Technology Center of Japan, 7-15-7 Roppongi, Minato-ku, 106, Japan

3 Hiroshima Earth Environmental Information Center, Miyake, Saeki-ku, Hiroshima, 731-51 Japan

Abstract

In estimating the vegetation coverage from NDVI (Normalized Vegetation Index, Rouse et. al., 1974) or SAVI (Soil Adjusted Vegetation Index, Huete, 1988) which are calculated from the satellite data, the vegetation density within a pixel affect the results. To eliminate this undesirable effect, an optimum vegetation index (OPVI) is presented in this paper. In this method, the vegetation coverage within each pixel is calculated from the reflectance ratio of radiance in TM 5 band to that in TM 7 band. Then, if the reflectance ratio is larger or smaller than a critical value, we select either NDVI or SAVI for calculating the vegetation index in each pixel. In this case, the critical value must be set in advance. For determining the critical value, the relationship between vegetation coverage and the reflectance ratio are studied from the spectral reflectance of plants and soils as a function of ratio of coverage area of plants to that of soils in the laboratory. Then, the critical value is determined by comparing the results obtained by NDVI and SAVI. Comparison of results obtained by OPVI method with those by both NDVI and SAVI are made by using the satellite data collected in and around oases in Taklimakan Desert in China since the vegetation is expected to vary over the wide range. The results show that OPVI gives a better indicator of actual vegetation cover in an arid area than single NDVI or SAVI alone.

1. Introduction

Many researchers have presented on methods for evaluating the vegetation biomass since the initial stage of remote sensing technology. From remote sensing data, however, the quantitative and efficient evaluation is not easy since interactions between vegetation and electromagnetic waves are complex. Plants strongly absorb the blue and red in the visible light through chlorophyll while exhibiting a high reflectance in the near infrared part out of the red edge (Horler et.al., 1983). These spectral reflectance characteristics are in contrast to that of soil, which shows gentle characteristics within the same spectral ranges.

Some vegetation indices utilizing these reflectance of plants have been presented up to now. Among them, NDVI is a representative index and many researchers have prepared regional or global vegetation maps using this method. However, one of the problems in NDVI is an increase of errors in those areas where vegetation is sparse such as those in arid land because of strong influences of the reflectance from the background soil. To overcome such the defects of NDVI, Huete proposed SAVI, which is described later in details. In addition to NDVI, PVI (Perpendicular Vegetation Index, Richardson and Wiegend, 1977) and TSAVI (Transformed Soil Adjusted Vegetation Index, Baret and Major, 1989) have been proposed by other researchers. These indices, however, have the difficulties in practical use since reflectance from

soil must be known. The above mentioned all vegetation indices use the radiance in the red band and near infrared band. The selection of the same bands is also found in other indices reported, and few algorithms use other bands for evaluation of the vegetation. One exception is found in an indices proposed by Pickup et al.(1993); they obtained the vegetation coverage based on the MSS bands 4 and 5 to extract the vegetation index on the red soil. Although this was practically a modified PVI, they reported that better results were obtained than that calculated from MSS bands 5 and 7 in the case of the red soil background. The present studies will examine several vegetation indices proposed up to now, and develop and discuss an algorithm to overcome the defects of such vegetation indices.

2. Evaluation of LAI using a Vegetation Index

2.1 Vegetation indices (NDVI, SAVI)

This section briefly describes the several algorithms proposed in the past for the evaluation of the biomass of vegetation. In earlier studies, the ratio between the red band radiance (R) and near infrared band radiance (NIR), i.e. RVI (Ratio Vegetation Index, Pearson and Miller, 1972), was proposed for evaluating vegetation after removing the influence of the reflection from soil. Since this method showed a very large error, NDVI, which uses the ratio between the difference and sum of radiance at two bands, was proposed. This method uses radiance at the red band in the visible part and near infrared band. NDVI is defined by,

$$NDVI=\frac{NIR-R}{NIR+R} \quad (1)$$

The accuracy of NDVI was estimated by the Baret and Guyot (1991) , and their results are shown in Fig. 1. In the figure, the variation of isoline for NDVI and LAI (Leaf area index is defined as the cumulative one-sided leaf area per unit ground area measured from the canopy top to a plane a given distance above the ground. The total LAI is the value determined at the plane of the soil, Allen, 1970) are plotted on R-NIR coordinate as a parameter of LAI and the reflectance of background soil. The reflectance used here was calculated by the SAIL model (Verhoef, 1984), which is a reflection simulation models for plant leaves. When LAI is large, NDVI is effective index for evaluating vegetation since the isolines of NDVI and LAI almost overlap each other as seen in Fig. 1. When LAI is small, however, error increase. This deviation is ascribed to the increase of the reflection from background soil when vegetation is sparse, particularly when soil is dark. In this case, the apparent vegetation index becomes large since the reflectance in the red band is low. In order to improve this situation, PVI was proposed by Richardson and Wiegand (1977) as an index for evaluating sparse vegetation. The reflectance of soil varies with the water content, etc. In the visible and near-infrared region of spectrum, however, the plot of reflectance in the near-infrared against that in visible light falls on near the line of direct proportion. The line is called the soil line (corresponding the line in case of LAI=0.0 in Fig. 1), and PVI is defined by the Euclidean distance from the soil line. In this case, it is necessary to know the soil line in advance to use this vegetation index.

On the other hand, Huete (1988) proposed SAVI which is applicable for sparse vegetation and practically modified NDVI. SAVI can be expressed as,

$$SAVI=\frac{NIR-R}{NIR+R+L}(1+L) . \qquad \text{when } L=\ell_1+\ell_2 \quad (2)$$

The constant L (Soil adjusted factor) is introduced in order to minimize soil radiance influences and to produce

vegetation isolines more independent of the soil background (Fig 1). It can vary from zero to infinity as a function of the canopy density. If L=0, SAVI is equivalent to NDVI. For vegetation with intermediate density the best adjustment is obtained for L=0.5. Fig. 2 shows that the light, and dark soils and various LAI influences on the variation of SAVI with L. As far as L is located near the point where the characteristics soil curves for a low and high reflectances intersect each other, it is clear from the figure that the index calculated is not affected by the reflectance of soil.

However, the optimum value of L becomes smaller as LAI increases. This indicates that the influence of soil decreases as the vegetation coverage increases. Further, when L=0.5, the isoline of SAVI comes nearer to the isoline of LAI on the visible near infrared coordinate than that of NDVI. On the basis of these results, Huete suggested the validity of SAVI. When the value of L is 0.5, it is clear from Fig. 1 (SAVI) that the isolines are apart from each other more than in the case of NDVI in the area where LAI is high but the isolines come closer to each other when LAI is small. From the above results, it is concluded that NDVI and SAVI (L=0.5) are appropriate vegetation indices when vegetation index is high and low, respectively.

2.2 A semi-empirical model of vegetation index and LAI

The relationships between VI and LAI obtained from the reflectance in the red band and near infrared band, were studied by many researchers in the past, and they showed that vegetation index is gradually saturated as LAI increases. In order to relate the vegetation index to LAI, Verhoef presented a semi-empirical model.

$$VI=VI_{\infty}+(VI_g-VI_{\infty})\cdot\exp(-k_{VI}\cdot LAI). \qquad (3)$$

where, VIg is the value of VI for bare soil (LAI=1), VI∞, the saturated value for VI (practically reaches this limit always for LAI greater than 8.0), and KVI, the coefficient which determine the slope of the relationship (equivalent to an extinction coefficient). These constants vary with the solar irradiance and the distribution of leaves. The coverage values of VIg and VI given by Baret and Guyot (1991), are VIg=0.19 and VI =0.93 for NDVI and are VIg=0.12 and VI =0.77 for SAVI. KVI largely depends on the slope of leaves from the zenith and ranges between 0.7 and 1.4 for NDVI and 0.5 and 1.0 for SAVI. It was shown that the KVI for NDVI is always approximately 1.4 times larger than the KVI in SAVI. They evaluated LAI on each index through the simulation using the SAIL model. When LAI>3, their results show that dispersion becomes large in any index because of the saturated vegetation index. When LAI<3, however, they concluded that SAVI is suitable index for the evaluation of vegetation coverage .

3. Experiments

3.1 Spectral reflectance characteristics of vegetation in relation to vegetation coverage

Based on the relationship between the vegetation coverage and spectral reflectance obtained in situ spectral measurements, an algorithm to estimate vegetation coverage from the Landsat TM data will be introduced. The vegetation coverage determined by photographs in various coverage. The location of spectral measurements selected in around Hotan oasis in southern part of Taklimakan Desert. The spectral reflectance of typical vegetations observed in various vegetation cover are shown together with spectral solar irradinace in Fig. 3. The spectral reflectance of *Tamarix*, *Salsola collina* and *Halostashys caspica*, distributed sparsely in a gobi desert (stony desert). The reflectance in TM 4, TM 5, and TM 7 wavelength bands are obtained from the measurement of spectral reflectance and then the correlations between those reflectance ratios and vegetation coverage are obtained. Although the vegetation coverage and reflectance

show a high correlation in any wavelength band, particularly the reflectance in TM 5 and TM 7 bands show the higher correlation with vegetation coverage (Fig. 4). The relationship between the reflectance ratio between TM 5 and TM 7 and the vegetation coverage (x: %) can be expressed as follows:

$$\frac{TM\,5}{TM\,7}=0.9+0.01x\,. \qquad (4)$$

As described above, OPVI (Optimum Vegetation Index) proposed in this paper calculates the vegetation index using either NDVI or SAVI depending on whether TM 5/TM 7 in each pixel is above or below the critical value. From the ratio of radiance of TM 5 and TM 7 of satellite data, vegetation coverage is estimated by equation (4). A critical value is obtained from the values of estimated coverage which is obtained from the radiance ratio between TM 5 and TM 7 bands on each pixel of Landsat data.

3.2 Algorithm of the OPVI

Fig. 5 shows the vegetation indices of NDVI and SAVI and the reflectance of vegetation as a parameter of LAI and vegetation coverage on the red band and near infrared band coordinate. Red and NIR reflectance as a function of each vegetation coverages which obtained in Fig. 5 are also plotted in the figure. The isolines of SAVI (0.4) and LAI (0.8) cross each other around 75 % of vegetation coverage. On the other hand, the isolines of NDVI (0.6) and LAI (1.6) are parallel each other around 100 % of vegetation coverage. The results suggest that the critical value for selecting either NDVI or SAVI lies around 87.5 % which is an intermediate point between 100 % and 75 % of vegetation coverage. From Fig. 5, 1.75 in terms of the radiance ratio of TM 5/TM 7 at 87.5% of vegetation coverage, is determined as the critical value for OPVI.

Vegetation index of OPVI is calculated as follows. First, the ratio in radiance between TM 5 and TM 7 is substituted in equation (4) to obtain vegetation coverage. When the ratio (TM 5/TM 7) of satellite data is larger than 1.75, NDVI (equation 1) is adopted as the index. On the other hand, the ratio is smaller than 1.75, SAVI (equation 2) is adopted. Constants for NDVI and SAVI in equation (3) which is used for evaluating for LAI are different. Substituting the constants in equation (3), NDVI and SAVI are expressed as follows:

$$NDVI=0.93-0.74\exp(-1.4k_{SAVI}\cdot LAI)\,. \qquad (5)$$

$$SAVI=0.77-0.65\exp(-k_{SAVI}\cdot LAI)\,. \qquad (6)$$

From equations 5 and 6, we obtain a following equation valid for both OPVI and SAVI:

$$OPVI=0.93-0.74\cdot\left(\frac{0.77-SAVI}{0.65}\right)^{1.4}\,. \qquad (7)$$

From equation (7), LAI is obtained as,

$$LAI=\frac{1}{1.4k_{SAVI}}\ln\left(\frac{0.74}{0.93-OPVI}\right). \qquad (8)$$

4. Analysis of satellite image

To examine the validity of OPVI proposed in this study, the vegetation is evaluated from the satellite data collected over the arid area around the Hotan oasis in the southern part of the Taklimakan desert in China. This area contains the inside of the oasis with a relatively high vegetation density, semi desert with a low vegetation density, and desert with almost in the absence of vegetation. Although the in situ survey was not performed on the same days as overpass for the Landsat, it was repeated five times during the period of the end of summer to autumn in every year from 1991 to 1995. The TM data of Landsat 5 (path: 146, row: 34) observed on July 27, 1988 was used for analysis.

5. Results

In this study, the vegetation coverage is estimated from the ratio of radiance in TM 5 to that in TM 7 through the vegetation index algorithm selecting either NDVI or SAVI. Judging from the resultant vegetation index map as shown in Fig. 6 (a, b, c), NDVI is selected for most of the pixels inside the oasis indicating a high vegetation density. A few pixels for which SAVI is selected correspond to the bare soil inside the oasis and small scale of desertified areas. These results are confirmed by the in situ survey. Thus, we concluded the conventional evaluation from NDVI alone may cause errors in a mixture of farmland and bare soil, and OPVI proposed in this study is effective for more accurate evaluation of vegetation index. As shown in Fig. 6 (b), the vegetation index of nearly 90 % pixels is evaluated from NDVI in the high vegetation density areas due to irrigated farmland in spite of the location of boundary between the oasis and desert (fringe). On the other hand, the vegetation index in most pixels in the semi desert area are evaluated by SAVI as shown in Fig. 6 (c), indicating a low vegetation index. Thus, since wide range of vegetation density is found, in evaluated vegetation index results in lower the accuracy if NDVI alone is used in the oases and their peripheral area. Accordingly, OPVI is effective indicator for monitoring the vegetation in a mixture a high and low vegetation coverages.

6. Discussion

For further studies, however, it is necessary to examine the changes in reflectance in those cases where the background is wet soil showing a low reflectance and typical soils in various parts of the world, e.g. laterite, which is a popular soil in the tropical region. Further, effects of natural canopy upon the vegetation index to be evaluated must be studied experimentally in comparison with the results for a single leaf which was used in this study for obtaining the spectral reflectance of vegetation. It is also necessary to perform experiments about actual canopy. In addition, to estimate the accuracy of the analysis results from the satellite data, it is necessary to compare OPVI results from the satellite data quantitatively with in situ concurrent surveys of the biomass such as LAI and coverage of the vegetation. Recently, large-size deforestation is becoming at issue in tropical forest in South America and South East Asia. These area may be a mixture of a high vegetation density and bare soil resulted from deforestation. If NDVI alone is applied to estimating the vegetation index those areas, we could not obtain the results. Further, OPVI becomes effective to investigate the desertification, which is becoming at issue in many arid and semi-arid areas in the world.

References

Allen, W. A., T. V. Gayle and A. J. Richardson (1970): Plant-canopy irradiance specified by the Duntley Equations, *J. of the Optical Soc. of America*, **60**, 3, 372-376.

Baret, F., G. Guyot, and D. J. Major (1989): TSAVI: A vegetation index which minimizes soil brightness effects on LAI and APAR estimation, in 12th Canadian Symp. on Remote Sensing and IGARSS'90, Vancouver, Canada, 10-14 July 1989, 4pp.

Baret, F., and G. Guyot (1991): Potentials and limits of vegetation indices for LAI and APAR assessment, *Remote Sensing of Environment*, **35**:161-173.

Horler, D. N. H., M. Dockray, and J. Barber (1983): The red edge of plant leaf reflectance, Int'l. *J. Remote Sensing*, **4**: 273-288.

Huete, A. R. (1988): A Soil-Adjusted Vegetation Index(SAVI), *Remote Sensing of Environment* , **25**: 295-309.

Pearson, R. L. and L. D. Miller (1972): Remote mapping of standing crop biomass for estimation of the productivity of the short-grass Prairie, Pawnee National Grasslands, Colorado, in Proc. 8the Int. Symp. on Remote Sens. of Environ., ERIM, Ann Arbor, MI pp. 1357-1381.

Pickup, G., V. H. Chewings and D. J. Nelson (1993): Estimating changes in vegetation cover over time in arid rangelands using Landsat MSS data, *Remote Sensing of Environment*, **43**: 243-263.

Richardson, A. J., and C. L. Wiegand (1977): Distinguishing vegetation from soil background information, *Photogramm. Eng. Remote Sensing*, **43**: 1541-1552.

Rouse, J. W., Haas, R. H., Scell, J. A., Deering D. W., and J. C. Harlan (1974): Monitoring the vernal advancement of retrogradiation of natural vegetation, NASA/GSFC, Type III, Final Report, Greenbelt, MD, 371.

Verhoef, W. (1984): Light scattering by leaf layers with application to canopy reflectance modeling: The SAIL Model, *Remote Sensing of Environment*, **16**:125-141.

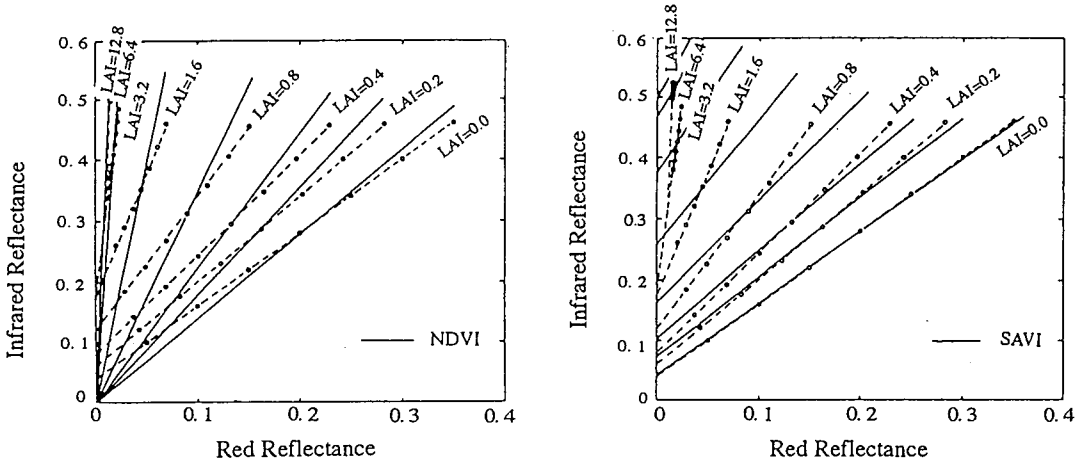

Fig. 1 Vegetation isolines plotted in NIR-red wavelength as a parameter of LAI and vegetation indices. The dashed lines correspond to canopies with different soil backgrounds the same LAI. The line, for which LAI=0, is the soil line. The open circles correspond to the canopy reflectance simulated SAIL model. The thin lines are the lines along which the different vegetation indices are constant. These indices are determined for each LAI and for the median value of soil reflectance (0.20 in red reflectance). (after Baret and Guyot, 1989).

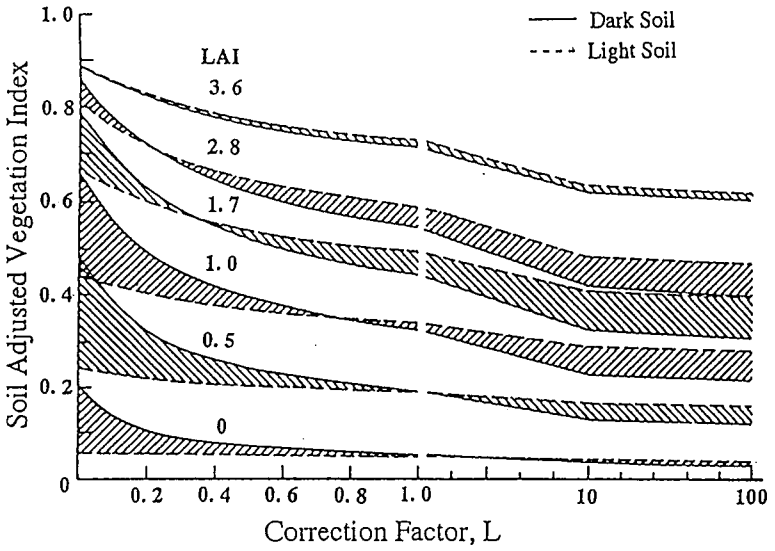

Fig. 2 Vegetation isolines in NIR-red coordinate as predicted by the ratio-, normalized difference-, and perpendicular-vegetation indices. The lines of constant vegetation amounts (isolines) as predicted by the ratio and orthogonal indices. The ratio indices are represented by vegetation isolines of increasing slopes diverging out from the origin while orthogonal index isolines remain parallel to the soil line. (after Huete, 1988).

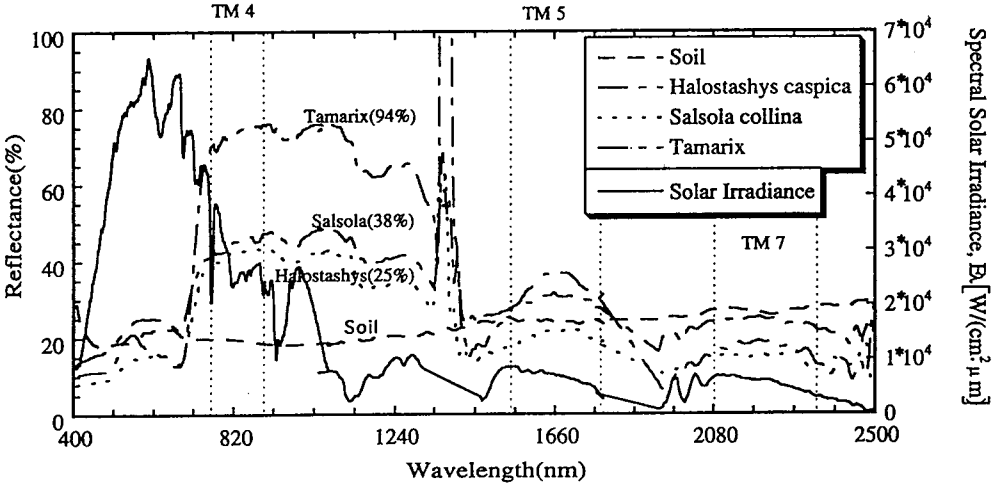

Fig. 3 Spectral reflectance of various vegetation cover of Sasola collina, Halastays caspica and Tamarix hispida together with incoming spectral solar irradiance measured at southern part of Taklimakan Desert.

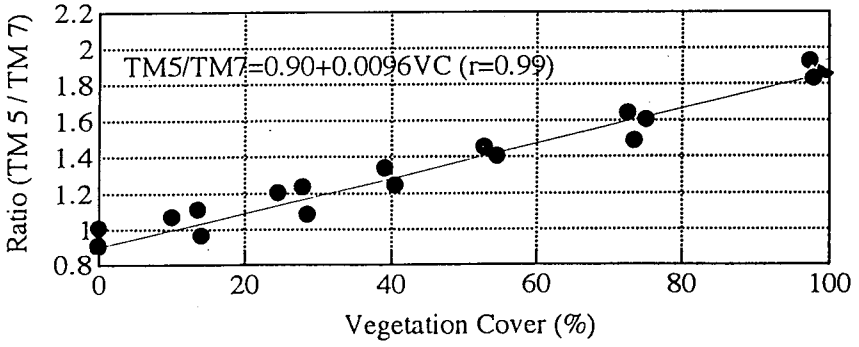

Fig. 4 Correlation between vegetation coverage and ratio of reflectance at TM band 5 to that at TM band 7.

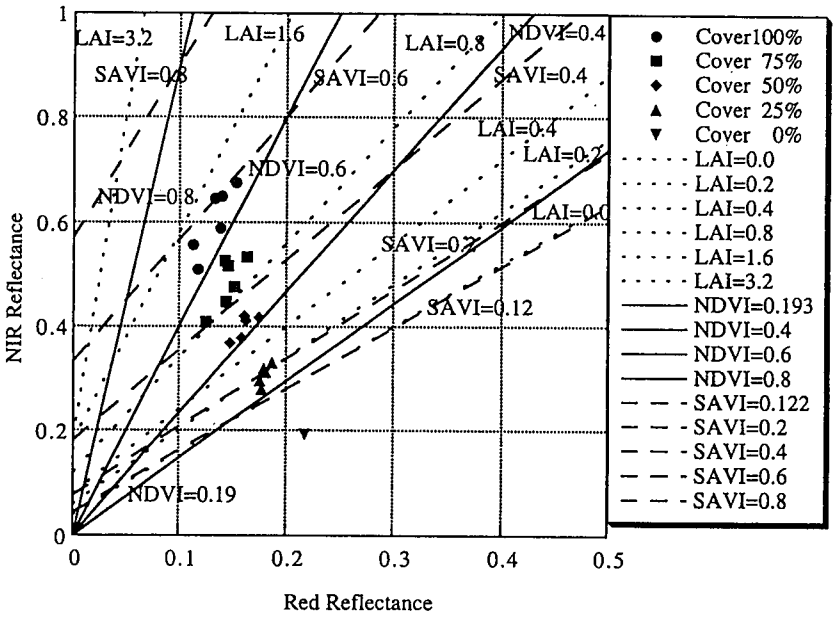

Fig. 5 Vegetation isolines plotted in NIR-red wavelength as a parameter of LAI, vegetation indices and various vegetation cover are shown in Fig. 4. The dashed lines correspond to canopies with different soil backgrounds the same LAI. The line, for which LAI=0, is the soil line. The thick and broken lines correspond to the different NDVI and SAVI.

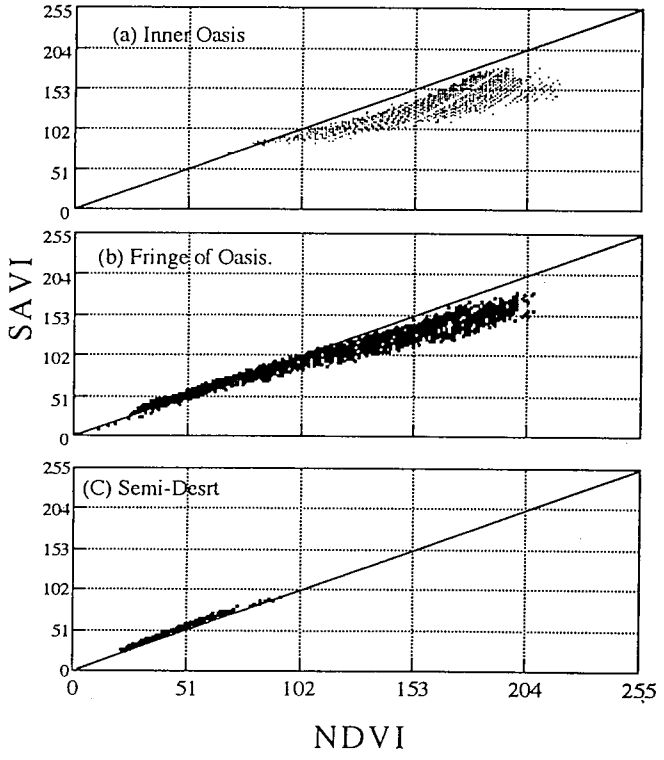

Fig. 6 Scatter diagrams of NDVI vs SAVI in the inner, fringe of oasis and semi-desert area.

Application of Remote Sensing for the Natural Resources-Management and Desertification Assessement in Arid and Semi-arid Regions

Hussein Harahesheh

Center for Environmental Remote Sensing, Chiba University
1-33 Yayoi-cho Inage-ku Chiba 263 Japan
Fax:+81-43-290-3857
Email:hussein@rsirc.cr.chiba-u.ac.jp

ABSTRACT Satellite remote sensing is an advanced technology for Earth observation where it provides synoptic views of large in real-time and in a repetitive mode useful in surveying large and inaccessible areas. Characteristically it permits the accessibility to some phenomena not visible by the conventional techniques, as those detected in the infrared and radar wavelengths. The use of satellite remote sensing to provide environmental information on the earth surface is becoming important in understanding the desert conditions, in monitoring desertification and assessing of natural resources and other environmental phenomena. The paper shows how far natural resources and desertification phenomena can be monitored and evaluated using the wealth of information on the earth surface conditions provided by remote sensing techniques and satellites imagery. However, the complexity of desertification process and its monitoring requires the simultaneous use and integration of data collected from the conventional sources and from satellites of various types through the a geographic information system, these data are presented in form of thematic maps showing the land use, geomorphology, drainage system, soil moisture...etc., of the study area. These maps were used to produce three important synthetic maps; land suitability, erosion susceptibility and desertification map.

1.0- INTRODUCTION

The use of satellite remote sensing to provide environmental information on the earth surface is becoming important in understanding the desert conditions, in monitoring desertification and assessing of natural resources and other environmental phenomena. The earth resources satellite data are considered a reliable source material from which various thematic maps of large areas can be produced efficiently and accurately. However, the complexity of desertification process and its monitoring requires the simultaneous use and integration of data collected from the conventional sources and from satellites of various types through the a geographic information system.

Natural resources in arid and semi-arid lands declining in productivity require special attention, if the determining ecological conditions persist, a further decline in resource may result in desertifcation which is more permanent. Therefor, we should look for the optimum solution regarding the land use plan in order to minimize the environmental degradation. The natural land resources can be divided into four major categories: Geology and geomorphology, soil, water and vegetation.

The large area perspectives of aerial and space-borne remote sensing lend themselves well to the type of regional analysis often undertaken by state agencies, the ability to reduce field work and decreasing travel costs are just a few of the many technical reasons for the increasing use of remote sensing by state resource manager. Remote sensing since the last decades averred as an important technique providing accurate, timely, complete and cost-effective information required by both executive and legislative decision-makers.

2.0- OBJECTIVES OF THE STUDY

The objective of ongoing study is to demonstrate the importance of remote sensing techniques in environmental resources mapping. So three synthetic maps were produced: The land suitability map for different kinds of culture (e.g.: annual crops, tree crops and afforestation), an erosion susceptibility map, to identify soil degradation features, solving problems of erosion and soil conservation and to define possible site of dams jointly with topographical, geological and hydrological data, and desertification map to be a basic element inforward to combat desertification. These maps and others such as land use could be a very good tool, in conjunction with the other traditional survey to address a range of policy issues for development planning.

3.0- STUDY AREA

The study area approximately 1300 km2 in extent, lies on the eastern plateau of Jordan some 40 km northeast of Amman. Geological formations occurring within the area consist of limestone, marls, chalky limestone, cherts and alluvial of Cretaceous buried below thick flows of basaltic lava.The study area can be divided geomorphologically into three sub-areas: the western limestone hilly area, the central alluvial area and the basaltic flat area in the eastern part of the study area. In altitude the study area range from 500m to 950m. The climate is classified as arid to semi-arid. However, the western hilly area have a Mediterranean climate, with average annual rainfall that varies from 350 mm to 100 mm decreasing from the western hilly area toward the eastern arid zone, and the climate present a wide range of temperatures and a high evaporation potential.

4.0- METHODOLOGY

The methodology has been consisted of the following steps:

STEP 1- Preparation of different Data (Previous studies, bibliography, topographic map, satellite images, thematic Data...)

STEP 2- Digital image processing(geometric correction, enhancement , classification. updating of geological map and soil map...)

STEP 3- Extraction of the study parameters(Land use map, vegetation cover , geomorphological map, soil salinity map, soil moisture map, irrigated areas, drainage system, vegetation density, drainage system density...)

STEP 4- Production of synthetic maps: Erosion map, desertification map and land suitability map.

STEP 5- Conclusions and Recommendations.

5.0- PARAMETERS OF THE STUDY AREA

5.1- Geology and Geomorphology

Geomorphology is considered as a resource because it controls the development of the renewable resources on the earth's surface. The land-use planning and the runoff of the surface waters. The site factor is in fact determining for the selection of the most suitable use for land. Geology is considered as a resource because it conditions the type of soil, the presence, distribution and flow of ground water, and the presence of mineral resource.

The study of geology and geomorphology by remote sensing techniques is undertaken by analyzing the two basic elements: drainage pattern and the land forms. The analysis of geomorphology includes two stages of investigation., the first stage aims to defining physiographic units, the second consists of the description of the analytical morphological features within and among the units: water-divide lines, slope breaks, scarps, terraces debris or alluvial, and drainage lines including their classification. We used the false color composite of bands 7, 5 and 3 of thematic mapper ,July 1989, the principal components bands, and other techniques such as ratio and filtering. The geological map scale 1-250.000 was used as reference data. The study area can be divided into five land units as follows:

1 -The sloping area: This unit is characterized by the existence of rill erosion, the overgrazing is the main problem in this unit.

2 -The gently sloping area: Their is rill and sheet erosion and formation of eroded rocky area, the overgrazing and plowing of rangeland increase the problem of erosion and decrease the livestock.

3 -The level-nearly level area: The colluvial material is the predominant formation in this unit. The sheet and wind erosion, marginal agriculture and soil salinity are the principal problems on the unit.

4 -Basaltic land: This unit occurs in the eastern part of the study area ,generally a flat area. The unit presents problems of salinity in the irrigated areas, and wind erosion.

5 -Infilled valley : This unit contains a deep homogeneous soil in general. Terraces of valley have been included in this unit which is very useful for the agriculture especially in west part of the study area.

5.2- Soil

Soil represent the meeting point between the physical and the biological worlds. Soil is a fundamental land resource because it allows and conditions the presence of vegetation and the utilization of land for agriculture. The study of soil concerns not only its location and classification but also the analysis of its potentiality, referred to the possible uses and the investigations related to its conservation. The soil surveys, especially at the reconnaissance and semi-detailed levels is based mainly upon the analysis of landforms with information coming from vegetation ,land use and geology. It must be kept in mind, however that no map made exclusively by remote sensing methods can be defined as a soil map. In fact the field description and classification of soils are indispensable. Texture, color or gray tone, land use and natural vegetation etc that may be recognized on satellite images and outline boundaries between soil units that differ for one or more of these factors. Soil characteristics that influence its reflectivity such as color mineral content, texture, surface roughness and moisture, may help for bare soils but are much hindered by vegetation. The study area contains two major soil associations (according to the soil taxonomy of the United States, Department of Agriculture-USDA):

1 -RHK-RHH/c: Gently undulating "Mafraq-Jisa soils". Located west and around of Mafraq, this unit appears as low undulating hills with round tops, scarp slopes and straight to concave valley bottoms. Annual rainfall average from 150mm in the east part to 350mm in the west. The indigenous vegetation consists mainly of winter grass, the land is used more extensively for grazing, winter cereals and orchards. About 60% of this unit contains dominant soils classified as Calciorthid soils, associated with Calciorthids are Camborthid soils covering 30% of the unit.

2 -RHK-RHH/a.b: "Umm al Jimal soils". This unit is located in the vicinity of Umm al Jimal village (20km east to Mafraq) on the basalt plateau. The relief is flat to gently undulating; the area is covered mainly by basaltic flows with a stony surface. Parent materials derived from weathering products of basalt and tuff consists of brown silty loams to clay loams with varying amount of basalt fragments and calcium carbonate concretions. The average annual rainfall is less than 150mm. The natural vegetation consists mainly of winter grasses. Vegetables and fruit trees are irrigated by ground water from wells in this unit. After a few years the salinity of soils reaches a degree to which crops are intolerated. Therefore farmers usually shift to another site repeating the same process. Artificial injection of surface water for ground water is practiced in the area. If this practice gives good results, the ground water will be fresh and suitable for agriculture. The dominant soils are classified as Calciorthids and they cover about 60% of this unit, the other soils associated with Calciorthids are Camborthids and Haploagrids, they cover less than 30% of this unit.

5.3 - Water

Water is indispensable for all human activities and is at the base of life on earth. It is, however, a vulnerable resource because it can be easily wasted or polluted. The rainfall map of our study area shows that the average rainfall varies from 350mm to 100mm decreasing from the western hilly area to the eastern semi-arid zone. The semi arid desert area lies on an isohyet of 200mm annual rainfall which passes from Mafraq to Dhuleil. Remote sensing techniques applied to the management of water resource can assist in considering:Ground water resources, Surface water resources and Water needs and distribution.

5.3.1 -Ground Water : The contribution of remote sensing refers, in this case, to the survey and interpretation of the geological and morphological conditions favorable to the presence of ground water, in order to plan and assist field geological and geophysical investigations.

5.3.2 -Surface Water: The assessment of surface-water resources using satellite images refers mainly to: Inventory location and area of natural and man-made standing water bodies, distribution of soil moisture content and mapping the drainage network.

5.3.3 -Water needs and distribution: The development and management of water resources, to be economically effective, must answer the needs of the user either as to quantity and quality or as to location of the supplies. Remote sensing can help in assessing these factors and planning a better exploitation of water resources through land use mapping, infrastructure planning and assessment of the environmental impact.

5.4 - Land use and Vegetation Cover

The vegetation cover is the most important renewable resource. Satellite Data are used for land use analysis because of their better spatial and spectral resolution. Digital classification becomes

interesting because of improved spatial resolution and increased the amount of data sets. In this study we used the maximum likelihood classification. Table 1 shows the result of classification

Table 1

classes	area(km2)	classes	area(km2)
Cropland	36	Dry land	775
Afforestation	33	Irrigated area	39
Rocky area	5	Rangeland	368
Orchards	10	Urban area	23
Reserved area	30	Total	1300

5.5 -Irrigated areas and Soil salinity.

Irrigated area have to be watched carefully to see if the soil properties have changed, especially drainage conditions, rising of ground water table and formation of saline and alkaline, but it depends very much on climatic conditions and nature of the soil. There is a good correlation between soil salinity development and the dryness of an area, the drier the area, the greater the risk of soil-salinity hazard. Salt accumulation takes place in low-lying areas in drier climatic regions where evaporation is higher than precipitation. Salinity may be also develpped if irrigation water itself contains a large amount of salts. Multitemporal satellite imagery are helpful in monitoring irrigated areas. In our study area we found that the surface of irrigated area increased from 1983 (6km2) to 1985 100% and from 1983 to 1989 150%, this means that the study area well have severe problem of salinity. (Laugeraar W.D 1987) suggest a digital image processing sequence (filtering) in order to identify the salinity extent in irrigated area. We found on the study area (60)km2 have problem of salinity.

5.6 - Soil Moisture

Information on the soil water budget in semi-arid or seasonally arid areas is vital for drawing the optimum agricultural strategy. Such information can be provided by combining satellite data and conventional data in theoretical and empirical models of the processes involved in the hydrological cycle. Water presents one of the highest thermal capacities in nature. And it is opaque to electromagnetic radiation in the region of infrared beyond 1 micon. The criteria to distinguish, by direct interpretation of satellite images different degrees of moisture content (on bare soil)are based on: opacity in the near-infrared, apparent thermal inertia and the spatial-temporal variation in temperature. The apparent thermal inertia is defined in remote sensing as the ratio between the energy absorbed by soil (in the visible and near-infrared range) in a given time interval divided by the corresponding variation in temperature. The TM data can be utilized to compute the thermal-inertia distribution and then to map the moisture of the soil. The formula used (Arnaldo, M. 1989):

$$A.T.I=M-(BAND1+B2-B3+B4)/B6-T$$

with, M: constant for computing the co-albedo. T: constant representing the minimum value of thermal emission on the scene expected at the end night , taken as uniform at the scene.

Four degrees of soil moisture were distinguished:

1 -low semi-arid area 2 -semi arid area 3 -arid area 4 -very arid area

In areas covered by vegetation, the approach is based on vegetation itself, which is seen as an environmental indicator. Several processing of the data can applied to monitor through the green canopy the amount of moisture in the soil, like this procuder propose by Arnold:

1 -density of vegetation"D". The density of green mass can be identified by applying the vegetation index formula, the new image will give a Seri of values increasing with the density of vegetation it self. The density of green mass is relative to the presence of moisture in the soil.

2 -Status of vegetation "S" is one of the best subject to be investigated in monitoring soil moisture. The status can be described with a formula in which a band with high rate of reflectivity is compared with bands of low reflectivity and with emission of heat. We can write the following expression

S=h+log near-infrared/green+red+thermal emission h=proper constant.

The values of S increase with the good status of vegetation.

3 -Normalization of vegetation status. The normalization of the status "S" to the density of green mass "D" helps to find out the soil moisture in area covered by vegetation. Thus we have to consider the ratio (NS=S/D) (Arnoldo M 1989) . The two out put data (for the bare soil and area colonized by vegetation) were integrated together, and they fit with out any discontinuity .

5.7- Erosion

Soil erosion is a dynamic problem and has to be continuously monitored as it not only results in loss of good soil for cultivation (fertile part of the soil)but also it is the primary factor for landslides. Soil erosion is caused by removal of vegetation, deforestation, overgrazing...etc. Which in turn results in to pollution of physical, biotic and socioeconomic environment. All sites are susceptible to erosion either by wind or water. An erosion susceptibility map was produced by integration of relief, parent material of soil, drainage system and the land use map. A cross-comparison system has been proposed to finally classify the erosion susceptibility map in four classes ranging from stable area to highly susceptibility to erosion area .

The amount of soil erosion can be reduced by a number of methods. Probably the simplest procedure is to keep the surface constantly covered by vegetation, however, this is not possible when arable cultivation is conducted but it should always be practiced on steep slopes, by having forest, orchards, or permanent grassland. A common form of erosion control is to construct terraces which restrict the speed of moisture on the flat terrace surface. In many situation it is possible to predict the erosion potential of the soil when most of the soil and environmental factors are known. As soil erosion is a dynamic problem, it is suggested that the erosion hazard map be regularly updated so that afforestation and other soil conservation methods could be planned will in time.

5.8 - Land Suitability

Land suitability evaluation is the process of assessing the suitability of land for specific use. These may be major kinds of land use such as rainfed agriculture, livestock production, afforestation,.....).

Our emphasis is on suitability for developmental purposes principally agriculture. The topographic characteristics of an area are of the most important determinants of the suitability land. For subdivision suitability, slope in 0° to 4° range are flat enough to provide for good surface drainage and interesting for annual crops, slope in the 4° to 8° range may more interesting for tree crops and more than 8° for afforestation purposes. The soil type and drainage condition also affect land use,

mediterranean soil hasn't limitations for cultivation purposes, yellow soil isn't a very developed soil so it presents some limitations for agriculture but may be acceptable for barley in addition to grassing. gray desert soil is a poor soil and not good for agriculture, it presents sever limitations on salinization and stones, it may be usable for seasonal grassing. The annual precipitation of 200mm is minimum for sustaining marginal agricultural activities. For annual and tree crops, the minimum level required of precipitation is 250mm.except for barley and razing crops 200mm may be sufficient.

Suitability assessment is made by comparison of land use with land. There are four steps to such comparison: mach, assessment of environmental impact, economic and social analysis and the field check Where it is found that the land is not well suited to the utilization types as originally defined, many modifications may be made in order to match the land use to the land more closely to the land utilization types, or to the land. Modification to the descriptions of land utilization types often involve changes in the defined input, examples are adding provision sprinkler irrigation, changing the level of fertilizer application, changing the numbers of livestock in a mixed farming system, or changing the farm size so as to improve the economic return. Following matching comes consideration of environmental impact, on theory this should already have been taken in to account, through suitability limit for soil erosion, vegetation degradation hazard, et. It is still necessary to give some consideration to both social and economic consequences of the various types of land uses. The field check, possibly carried out concurrently with economic and social analysis, is a further means confirming the soundness of the results, we should visit a selection of the sites in each suitability class, and discusses whether the results are in accord with common sense and experience , if the opinions of people already living there can be obtained, it would be better. If the results of the field check do not agree with experienced judgment, some of the criteria or limiting values will need to be changed.

5.9 -Desertification

Desertification is the process of degradation of agricultural productivity brought on by overgrazing, erosion, salinity and alkalinity, high water tables, cutting of woodland and other human pressure. Condition of grasslands is a good indicator of the status of the areas undergoing desertification.

The critical indicators of desertification can be summarize as follow: rainfall trends, high temperature, dust storms, receding water level, changes in sediment loads in rivers and lacks, extension of cultivation area into unsuitable dry land, occurrence of surface soil crust, destruction of vegetation for fuel and construction, changes in soil organic matters, changes in soil moisture, a consequent rise in the reflective capacity (albedo) of surface and process of salinization. Remote sensing can contribute on all of these indicators of desertification to some degree of precision.

The United Nations conference on desertification held in Nairobi, KENY (1977) was pointed out that desertification is ranging between four degrees: Slight, moderate, severe and very severe desertification. The desrtification map was created using five layers: land use, soil moisture, rainfall, erosion susceptibility and soil salinity. All of these layers were geocoded to the same coordinate system, to be overlayed and by analyzing vertically these layers we find out:

1- slight desertification : the vegetation cover composed from afforestation, tree crops, annual crops, grassland and reserved areas was intersected with the moist area, area with rainfall higher than 250mm and the stable area.

2- moderate desertification: grassland area was intersected with the moist and semi-arid area, area with rainfall between 150mm and 250mm and the low and medium erosion susceptibility.
3- severe desrtification: the dry land area obtained from land use map was intersected with arid area, rainfall below 150mm and high erosion susceptibility area.
4- very severe desertification: this degree of desertification was composed from saline soil, degradation soil (eroded area), the expansion of urban area and the vegetation cover below 25%.

6.0 -Conclusions and Recommendations

In conclusion of this study .Remotely sensed data can be considered an efficient tool for assessing and monitoring land resources, and it is evident that an "integrated approach" in solving specific problems such as erosion, desertification and land suitability is absolutely necessary. Based on a set of scenarios embodying present and future populations, food and agriculture demands and socio-economic development needs, a range of policy issues for development planning could be addressed. Finally we suggest the following recommendations:
1-Updating the dynamic parameters of study such as land use, desertification and erosion.
2-Relating to irrigation-saline problems, reclamation of soil will be necessary, one common technique is deep plowing in order to break an impervious layer, washing and leaching of salt is required .
3-Application of manure is always recommended to increase the fertility infiltration rate of soil.
4-Build up a basic land suitability map for each region to be introduced in development planning.
5-Giving support projects of water resources management.
6- Giving support projects of afforestatin and soil conservation.
7-Increase the numbers of reserved rangelands.
8-Organize of overgrazing and plowing in marginal areas.

7.0 - References:

-Arnaldo, M. Tonelli "Soil moisture detection and mapping" remote sensing series 54 Rome, FAO 1989.

-Binkman, R. "Overview of land-resources appraisal and management" R.S series 54 Rome, FAO,89.

-Dhrunba P.Shrestha "mapping and monitoring of irrigated area" and " use of remote sensing techniques in soil mapping " R.S series 54 Rome, FAO. 1989.

-David D. Anthony Y. "Soil syrvey and land evaluation". 1980.

-Ergin .A "Geograhpic information system" R.S series 54, Rome, FAO, 1989

-Gerardo.Bocco "Digital image processing techniques for soil erosion assessement" Sympo on R.S appl in hydrology and natural resources, Amman/Jordan. 1987.

-Langeraar W. D. "Identification of salinity extent in irrigated areas by processing of SPOT data "Sympo on R.S appl in hydrology and land resources, Amman/Jordan. 1987.

-Mitchell, C.W & Howard "Land system classification.A case history: Jordan" "The application of landsat imagery to soil degradation", Rome, FAO. 1978.

-Pietro, D. "Land-resources appraisal using aerial photointerpretation" "Satellite data analysis for soil survey" R.S series 54 ,Rome, FAO. 1989.

Measurement of Bidirectional Reflectance of Sand by a Remote Sensing Simulator

Hiroshi Okayama and Jie Sun

Center for Environmental Remote Sensing, Chiba University
1-33 Yayoi cho, Inage-ku, Chiba 263 Japan

Abstract

In the field of remote sensing, there is a need to correct the intensities of bidirectional reflectance because the satellite data collected in nadir and off nadir directions show different values in spite of the measurement of the same point on the earth's surface.

Then we measured the characteristics of bidirectional reflectance from the coastal sand using a remote sensing simulator. From the results of the measurements, we obtained indicatrices, hence Minnaert constants k's (λ) were calculated. We corrected the reflected intensity by assuming that Minnaert constant k of the same area is equal.

1. Introduction

In the papers on reflection and scattering, Lambertian surfaces are usually assumed , but natural surfaces are generally non-Lambertian and their spectral properties obtained from remote sensing data from aircraft or satellite are dependent on view and sun angles [1, 2, 3]. It is , therefore, necessary to take into account the bidirectional reflectance distribution function (BRDF) [4] of the target to compare quantitatively the measurements acquired under different illumination and observation conditions. Knowledge of the bidirectional properties of natural surfaces are especially important.

In remote sensing field, the researchers are confused at the difference in the data in the nadir and off nadir directions for the observation of the same point on the earth's surface by side-angle imagery sensors such as an Advanced Very High Resolution Radiometer (AVHRR) on board NOAA Satellite, and the High Resolution Visible instrument on board SPOT satellite.

Then in this paper as a fundamental experiment of a bidirectional reflectance, we obtained the bidirectional reflectance characteristics for the sand and we discussed how to correct the reflected intensities observed in different nadir directions. Our correction method has a merit that it can be applied to non-Lambertian surface.

2. Experiments and Results

The experiment was done by using a remote sensing simulator [5] showed in Fig. 1. This simulator has a halogen lamp lighted by a stabilized power supply. The detector of the light is a photomultiplier. The optical source and the detector can move along the guides, and required incident and reflected angles are obtained. The detector can also move in the azimuth direction, enabling the bidirectional reflectance of an object to be measured. The size of the sample stage is 60 cm in diameter. The data are processed by a computer.

The sand collected at the Kujukuri coast in Japan was used for the experiment. To determine the wavelength of experiment, a filter of Wratten No. 25 with the same wavelength band as Landsat MSS (5) was used. In measurement of the reflectance, the white barium sulfate board was used. The reflectance of a sample target is calculated by the following equation :

$$\rho(\lambda) = \frac{I_{target}(\lambda)}{I_{white}(\lambda)} \times \rho_{white}(\lambda), \qquad (1)$$

where $\rho(\lambda)$ is the reflectance of target. $I_{target}(\lambda)$ is the reflected intensity of the measured target. $I_{white}(\lambda)$ is the reflected intensity of the white board. $\rho_{white}(\lambda)$ is the reflectance of the white board. The incident angle, reflected angle and azimuth angle are shown in Fig. 2.

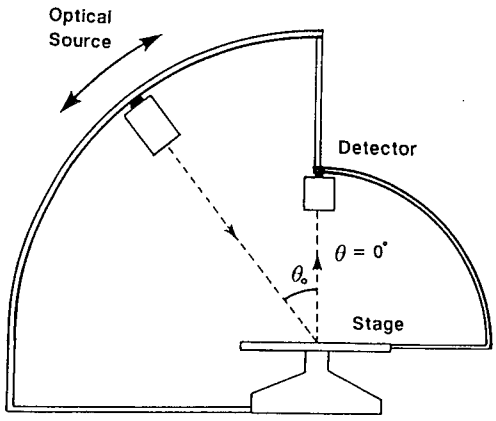

Fig. 1. Schematic diagram of the simulator for remote sensing.

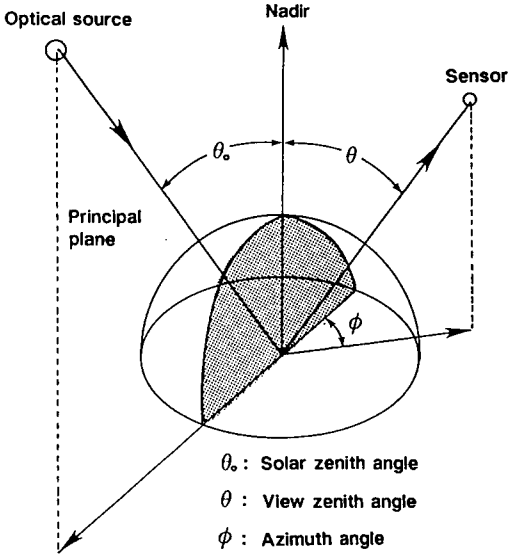

Fig. 2. Geometry of bidirectional reflectance measurements.

First, we measured the reflectance in nadir ($\theta = 0^\circ$) direction and at 0° azimuth angle. The indicatrices of the sand are obtained by changing incident angles. The result in the nadir direction is shown in Fig. 3, and the Minnaert constant obtained from the indicatrix is $k(\lambda) = 1.26$. Next the experiments were made at detection angles ($\theta = 10^\circ$, 20° , 30° , 40° and 50°) . The experimental results at the detection angles 20° and 50° are shown in Fig. 4, and 5, respectively. As is shown in Fig. 3 to Fig. 5, when the detection angle is constant, the indicatrices hardly change by azimuth angle.

The measurement results of the reflectance are shown in Figs. 6 to 8. As is shown in Figs. 6 and 7, where the detection angles are 0° and 20° , respectively, the reflectance distributes between 0.2 and 0.5 with change of the incident angles. When the detection angle is 50° , as is shown in Fig. 8, the reflectance distributes between 0.3 and 0.9 and the distribution depends on the azimuth angle.

Next, the change of Minnaert constants by the azimuth angle is shown in Fig. 9. Minnaert constant (k) is higher when the azimuth angle is larger. In the case of the detection angles

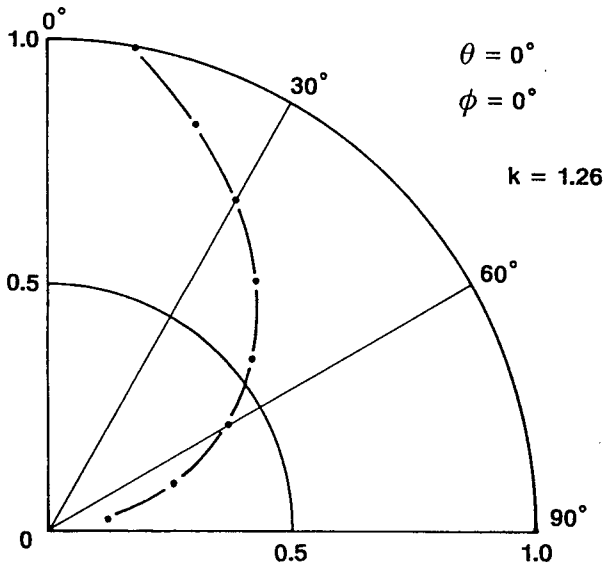

Fig. 3. Indicatrix of sand when the detection angle is 0° and the azimuth angle is 0° .

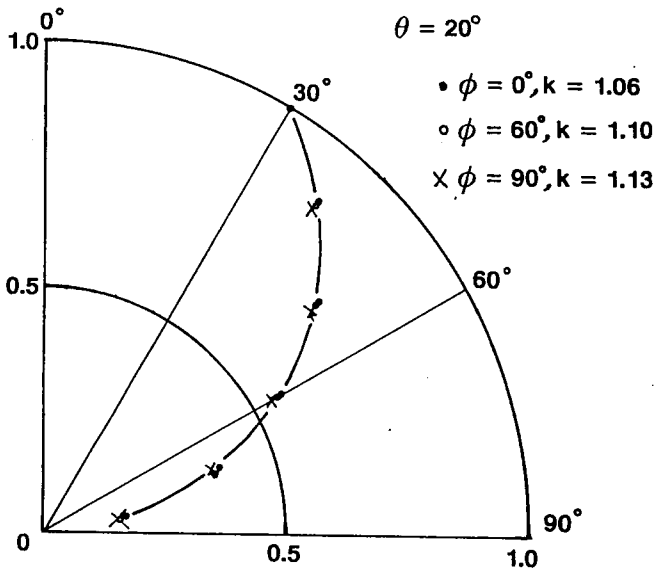

Fig. 4. Indicatrices of sand when the detection angle is 20° and the azimuth angle are from 0° to 90° .

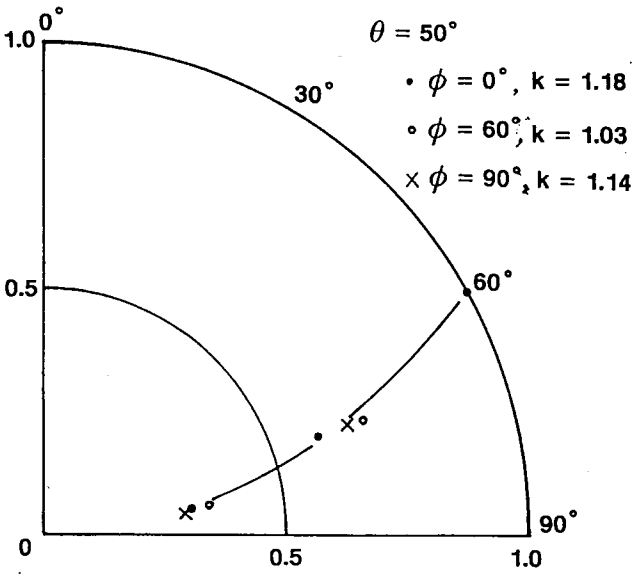

Fig. 5. Indicatrices of sand when the detection angle is 50° and the azimuth angles are from 0° to 90° .

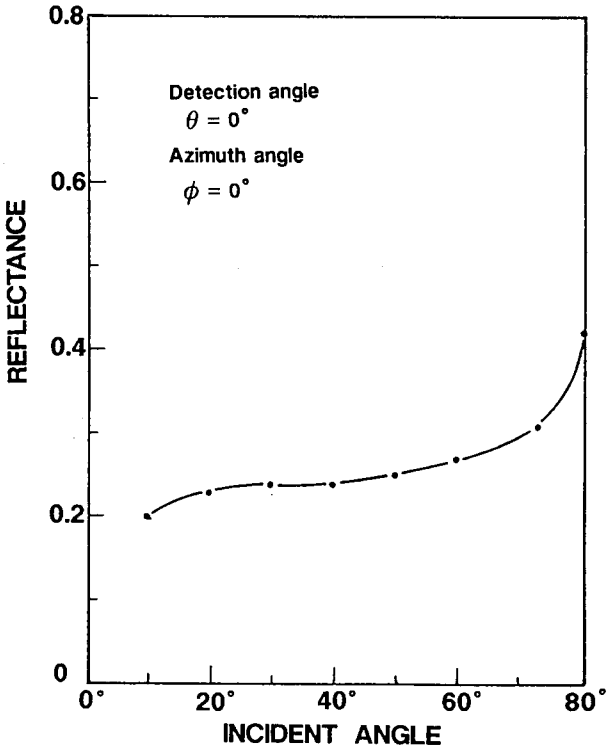

Fig. 6. Reflectance of sand when the detection angle is 0° .

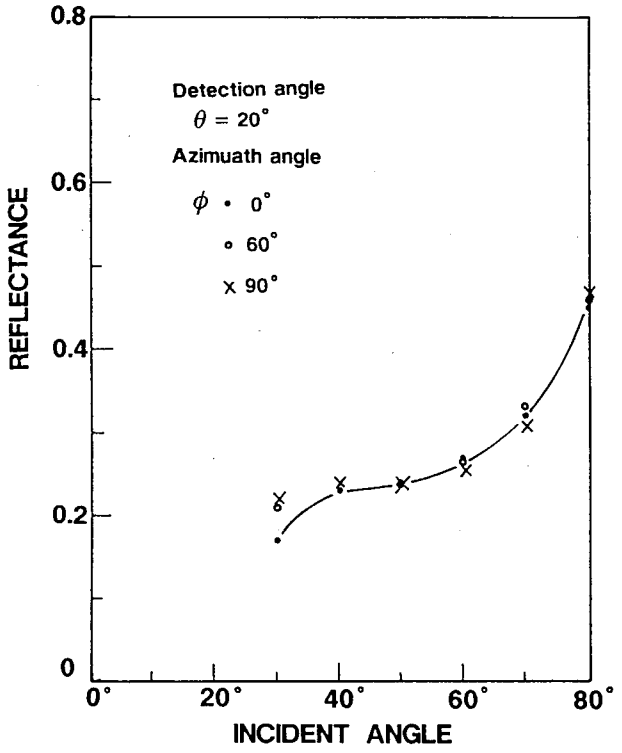

Fig. 7. Reflectance of sand when the detection angle is 20° and the azimuth angles are from 0° to 90° .

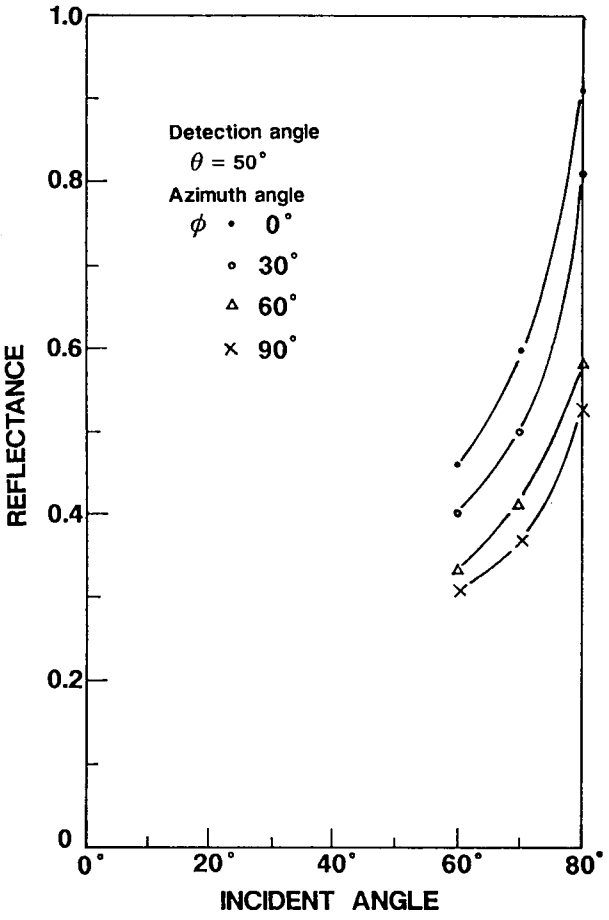

Fig. 8. Reflectance of sand when the detection angle is 50° and the azimuth angles are from 0° to 90° .

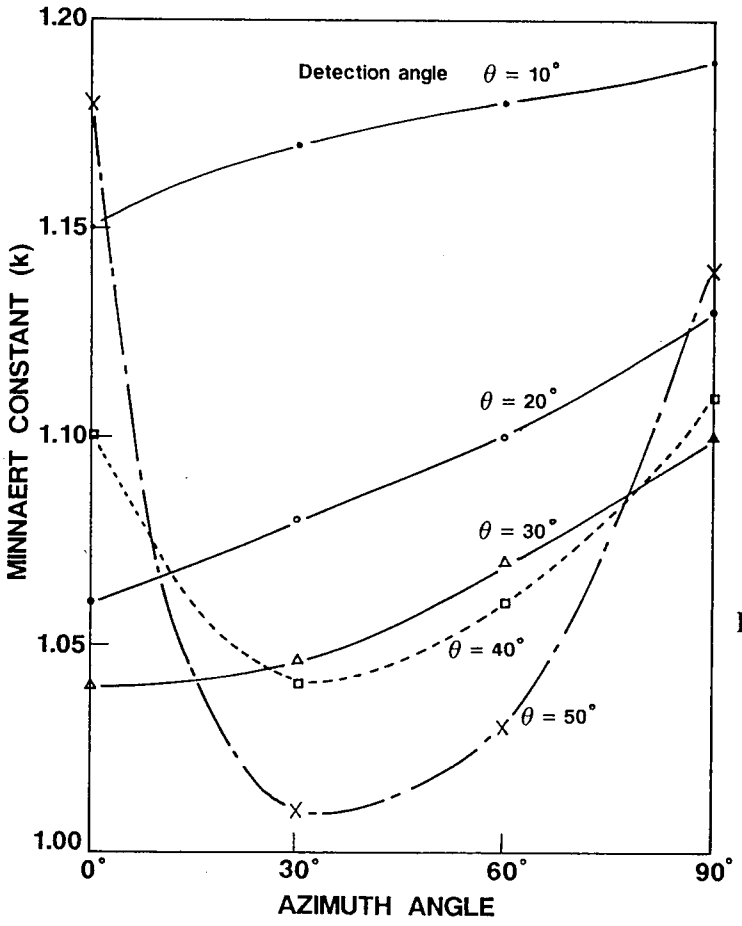

Fig. 9. Minnaert constants of sand when the detection angles change from 10° to 50° .

40° and 50° , when the azimuth angle is 0° , the Minnaert constant shows a large value and when the azimuth angle is 30° , the value becomes minimum and with increase of the azimuth angle the value becomes larger.

3. Correction of Reflected Intensity

The satellite data collected in nadir and off-nadir directions differ in spite of observation at the same point on the earth's surface. Then the correction must be done for these data. To correct them, we measured bidirectional reflectances by a remote sensing simulator. The equation of the reflected intensity $I(\lambda)$ is represented by use of Minnaert constant [6] such as the following :

$$I(\lambda) = I_{\circ}(\lambda)\ \cos^{k(\lambda)}\theta_{\circ} \cdot \cos^{k(\lambda)-1}\theta\ , \tag{2}$$

where $k(\lambda)$ is a Minnaert constant, $I_{\circ}(\lambda)$ is a constant depending on the intensity of incident light and $\theta_{\circ}$ and θ are incident and detection angles, respectively. Since two different Minnaert constants $k_1(\lambda)$ and $k_2(\lambda)$ are obtained from the indicatrices at the same point measured in nadir and off-nadir directions, the two reflected intensities $I_1(\lambda)$ and $I_2(\lambda)$ of nadir and off-nadir direction, respectively, are

$$I_1(\lambda) = I_{\circ}(\lambda)\ \cos^{k_1(\lambda)}\theta_{\circ}\ , \tag{3}$$

and

$$I_2(\lambda) = I_{\circ}(\lambda)\ \cos^{k_2(\lambda)}\theta_{\circ} \cdot \cos^{k_2(\lambda)-1}\theta\ . \tag{4}$$

As these reflected intensities are assumed to be equal, so

$$\cos^{k_1(\lambda)}\theta_{\circ} = \cos^{k_2(\lambda)}\theta_{\circ} \cdot \cos^{k_2(\lambda)-1}\theta\ . \tag{5}$$

Minnaert constants are also assumed to be equal, so

$$k_2(\lambda) \cdot x = k_1(\lambda). \tag{6}$$

From the Equation (5).

$$\cos^{k_2(\lambda)\cdot x}\theta_\circ = \cos^{k_2(\lambda)}\theta_\circ \cdot \cos^{k_2(\lambda)-1}\theta . \tag{7}$$

Hence

$$k_2(\lambda)\cdot x\cdot \log\cos\theta_\circ = k_2(\lambda)\cdot \log\cos\theta_\circ + \{k_2(\lambda)-1\}\cdot \log\cos\theta . \tag{8}$$

Therefore

$$x = \frac{k_2(\lambda)\cdot \log\cos\theta_\circ + \{k_2(\lambda)-1\}\cdot \log\cos\theta}{k_2(\lambda)\cdot \log\cos\theta_\circ} . \tag{9}$$

From Equation (9) x is obtained and $k_1(\lambda)$ in Equation (6) is calculated, but due to experimental errors x must be multiplied a correction coefficient c .
Then,

$$k_2(\lambda)\cdot x\cdot c = k_1(\lambda). \tag{10}$$

This c values are shown in Tables 1 to 4.
The correction of the reflected intensity is possible by substituting $k_1(\lambda)$ into Equation (3). The correction coefficients, c, obtained from experimental results are shown in Tables 1 to 4. These coefficients obtained based on Minnaert constant $k(\lambda) = 1.26$ given by the indicatrix for nadir direction ($\theta = 0^\circ$) and azimuth angle ($\phi = 0^\circ$) for sand. They are not much varied for the same reflected angle.

Table 1. Correction coefficients when azimuth angle is 0° .

θ_s	θ =10°	θ = 20°	θ = 30°	θ = 40°	θ = 50°
30°	1.09	1.17	1.18	0.98	0.73
45°	1.09	1.18	1.19	1.08	0.89
60°	1.10	1.18	1.20	1.11	0.97

Table 2. Correction coefficients when azimuth angle is 30° .

θ_s	θ = 10°	θ = 20°	θ = 30°	θ = 40°	θ = 50°
30°	1.06	1.14	1.17	1.14	1.21
45°	1.07	1.16	1.19	1.18	1.24
60°	1.08	1.16	1.20	1.20	1.24

Table 3. Correction coefficients when azimuth angle is 60° .

θ_s	θ = 10°	θ = 20°	θ = 30°	θ = 40°	θ = 50°
30°	1.05	1.10	1.17	1.08	1.13
45°	1.06	1.12	1.18	1.15	1.18
60°	1.07	1.13	1.18	1.17	1.20

Table 4. Correction coefficients when azimuth angle is 90° .

θ_s	θ = 10°	θ = 20°	θ = 30°	θ = 40°	θ = 50°
30°	1.04	1.06	1.05	0.96	0.80
45°	1.05	1.10	1.10	1.05	0.95
60°	1.06	1.11	1.12	1.09	1.02

4. Conclusions

The experimental results of the bidirectional reflectance have shown that the reflection characteristics differ by the reflected and azimuth angles as represented by use of Minnaert constants. The Minnaert constants are larger when the reflected angles are smaller and when the azimuth angles are larger.

In this paper, we have introduced a correction method, which enables the correction of data from different satellites. Even though observed at the same point, there is a disagreement in the data collected at two different reflected angles, nadir and off-nadir.

In these corrections Minnaert constant obtained from a indicatrix must be used.

References

1. R. D. Jackson, P. M. Teillet, P. N. Slater, G. Fedosejevs, M. F. Jasinski, J. K. Aase and M. S. Moran, "Bidirectional Measurements of Surface Reflectance for View Angle Corrections of Oblique Imagery", Remote Sens. Environ. **32**, 189-202 (1990).

2. A. Royer, P. Vincent, and F. Bonn, "Evaluation and correction of viewing angles effects on satellite measurements of bidirectional reflectance", Photogramm. Eng. Remote Sens. **51**, 1899-1914 (1985).

3. P. N. Slater, and R. D. Jackson, "Atmospheric effects on radiation reflected from soil and vegetation as measured by orbital sensors using various scanning directions", Appl. Opt. **21**, 3923-3931 (1982).

4. Fred E. Nicodemus,"Reflectance Nomenclature and Directional Reflectance and Emissivity", Appl. Opt., **9**, No. 6, 1474-1475 (1970).

5. Hidesaburo Genda and Hiroshi Okayama, "Estimation of soil moisture and components by measuring the degree of spectral polarization with a remote sensing simulator", Appl. Opt., **17**, No. 21, 3439-3443 (1978).

6. M. Minnaert, "The Reciprocity Principle in Lunar Photometry", Astrophys. J. **93**, 403-410 (1941).

Crude oil contamination of soil and groundwater in Kuwait

Hiroyuki II*, Masato KAWAGUCHI**, Masakazu IWABUCHI***,
and Shinobu YABU*

*Faculty of Systems Engineering, Wakayama University
930, Sakaedani, Wakayama-city, Wakayama 640, Japan
Fax:+81-734-54-0134
Email:hiro@sys.wakayama-u.ac.jp

**Institute of technology, Shimizu corporation
3-4-17, Etchujima, Koto-ku, Tokyo 135, Japan
Fax:+81-3-3643-7260
Email:kawaguchi@sit.shimizu-u.ac.jp

***Engineering division, Shimizu corporation
1-2-3, Shibaura, Minato-ku, Tokyo 105-07, Japan

Abstract

During the Gulf war seven hundreds of oil wells were destroyed by the retreating armies of Iraq. In particular, the Burgan oil field suffered heavy damage. Over 50millions of crude oil spilled out flooding the desert and as a result, extensive contamination of desert soils occurred. Field investigations indicated that crude oil penetrated the desert soils under the newly formed oil lakes to a depth of 150 cm for the 5 years following the Gulf war. The calculated penetration of this oil into the soil over the next 100years is determined to be approximately 10 meters. At the Burgan area groundwater was not contaminated because the upper aquifer was at a depth of more than 100 meters.

Key words:Kuwait, oil contamination, oil pollution, crude oil

1. Introduction

Kuwait is a small country located in the northern edge of the Arabian peninsula, bordered by the Arabian Gulf in the east. The total area of Kuwait is 18000km^2 and the rainfall is about 120 mm/yr mainly during winter. Drinking water is desalinated from sea water and brackish water. The Gulf war led to the contamination of air, water and soil in Kuwait. About 700 oil wells were set on fire. Oil well fires also damaged well heads and hence free flowing oil from these resulted in the formation of large oil lakes. Figure 1 shows the distributions of groundwater field and oil contaminated soil. The total amount of crude oil in these lakes was estimated to be about 50 million barrels (Al-Sulaimi 1993). The total area of oil lakes was 49 km^2 and the total amount of oil contaminated soil was 40 million m^3. Groundwater pollution may result from any of the following mechanisms : (1) direct penetration of oil from oil lakes ; and (2) penetrating rainwater can leach some of the products of combustion deposited at ground surface level.

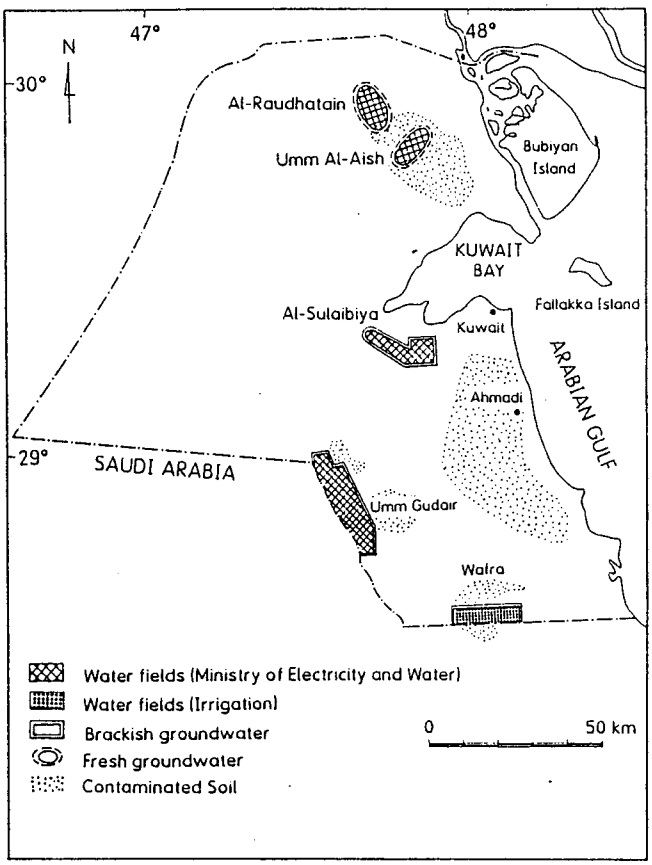

Figure 1 Distribution of groundwater field and oil contaminated soil (Al-Sulaimi et al., 1993)

2. Groundwater contamination in Kuwait

There are three aquifers in Kuwait. The first aquifer which is shallow and fresh is distributed only in northern Kuwait. At Al-Raudhatain and Umm Al-Aish, there are large drainage basins. Although average rainfall is only about 120 mm/yr, the geomorphology is conducive to the formation of large fresh-water lenses over brackish and saline groundwater (Sulaimi et al., 1993). However after oil the fires, these large catchment areas, covered with the products of combustion, contributed to the pollution of groundwater because runoff generated by rainfall dissolved some of the products of combustion. Figure 2 shows the first aquifer which was contaminated by rain water passing through oil contaminated soil. The

concentrations of vanadium and nickel in Kuwait crude oil were about 22.5 and 1.0 ppm, respectively. As a result, the concentration of vanadium, nickel, and total carbon in the groundwater reached 400, 100, and 200 ppb.

The second and third aquifer which are both deep and brackish to saline are distributed all over Kuwait. At the Burgan oil field area, a lot of oil escaped and four fifths of the total number of oil lakes (250) were found there. Therefore, groundwater pollution of the second and third aquifer had to be considered at the Burgan area.

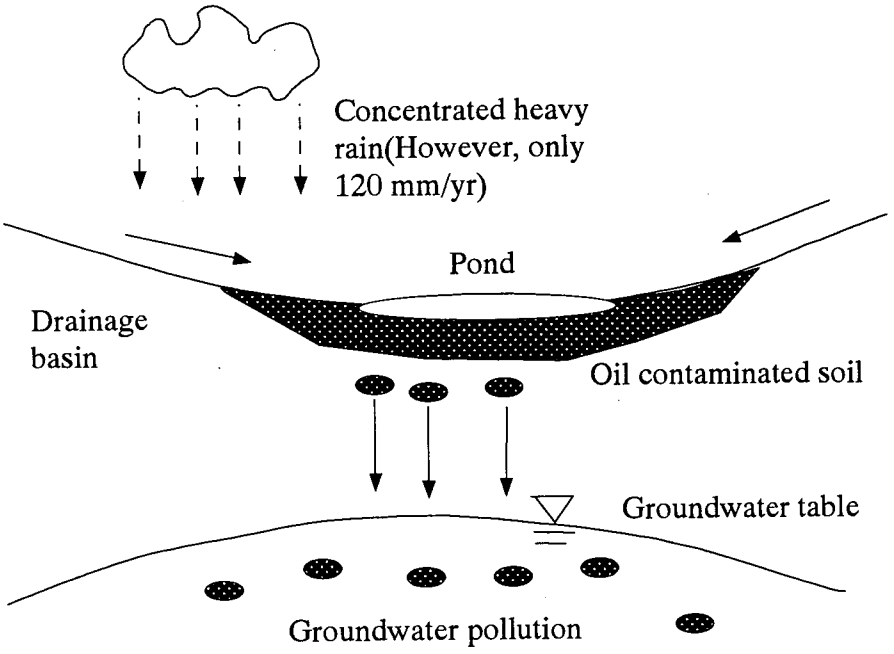

Figure 2 First aquifer which was contaminated by rain water passing through oil contaminated soil

We performed field investigation in September 1995 and oil penetration tests in sand columns in order to analyze oil penetration into the aquifer.

3. Study area and method

3.1 Sampling

Figure 1 shows the study area which is the Burgan oil field south of Kuwait city. The total amount of oil deposits in the Burgan oil field is the second largest oil field in the world. Surface sediments in the area are composed of fine gravel and coarse sand cemented by gypsum.

Around the No.105 oil lake, the oil penetration depth was measured at 150 cm on average by digging pits before our investigation. Three sampling points (AP-1, AP-2 and AP-3) were set around the No.105 oil lake after confirming the absence of mines and ammunitions. Uncontaminated soil was sampled from three pits in order to measure the physical properties of soil and to perform oil penetration tests in a laboratory. Undisturbed soil samples were used for measuring dry density. Disturbed soil sample was used for measuring water content, hydraulic conductivity

and oil penetration tests.

3.2 Physical properties

Water content was measured instantly on the spot. Table 1 shows water contents. Surface soil was very dry and water content increased with depth. Since water content 150 cm in depth was less than 8 %, oil was assumed to penetrate into dry soil. Dry density values were measured at 1.8g/cm^3 on an average from 9 undisturbed block samples.

Table 1 shows the hydraulic conductivity values. At the condition of 1.8g/cm^3 dry density measured for the undisturbed block samples, hydraulic conductivity values were 1×10^{-2} to 1×10^{-1} cm/sec.

Table 1 Water content and hydraulic conductivity values at each depth

	Depth(cm)	Hydraulic conductivity (cm/sec)	Water content (%)
AP-1	10	0.015	0.43
		0.014	
	30	0.021	1.49
		0.024	
	60	0.029	3.04
		0.025	
	100	0.009	3.83
		0.009	
	110	0.016	
		0.004	
	130		4.49
	150	0.035	
		0.009	
	160		4.23

	Depth(cm)	Hydraulic conductivity (cm/sec)	Water content (%)
AP-3	10	0.098	0.23
	30	0.061	0.86
	40	0.033	1.66
	60	0.074	2.80
	100		2.73
	150		7.76
	180		8.26

	Depth(cm)	Hydraulic conductivity (cm/sec)	Water content (%)
AP-2	10	0.086	0.22
		0.070	
	30	0.073	0.61
		0.026	
	50	0.038	2.16
	70	0.041	2.34
	80	0.039	
	100	0.012	3.61
	130		3.41
	170		3.51

3.3Oil penetration test

Figure 3 shows the experimental apparatus for the oil penetration test. An oil head was fixed to be 5 or 10 cm. Dry soil was compacted till the dry density reached 1.8 g/cm^3 because at the oil penetrated depth, water content was very low. Figure 4 and 5 show examples of oil penetrated results at the condition of oil head 5 and 10 cm. For both conditions, oil penetrated depths were 15 to 20 cm for 10 days. According to Philip's moist equation, oil penetrated depth and elapsed time were shown as follows (Kayane、1980) :

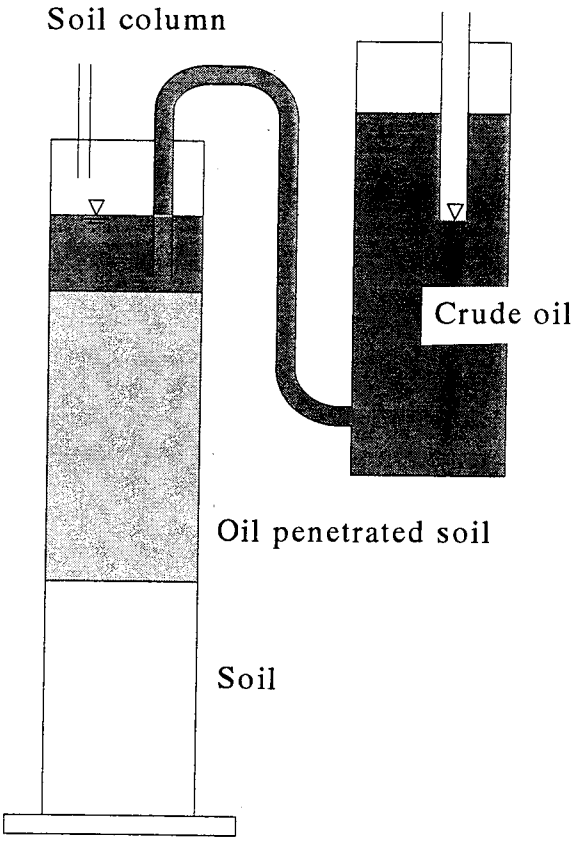

Figure 3 Experimental apparatus for the oil penetrating tests

$$I(T)=AT+BT^{0.5} \qquad (1)$$

Where I(T) is an oil penetrated depth;T is an elapsed time; A is a coefficient of oil conductivity; B is a coefficient of absorption.

Oil penetrated depth is not due to the oil head according to Philip's equation. Oil penetrated depths calculated from the experimental results were 200 to 1500cm for 5 years after the Gulf war ended. Oil penetrated depth within oil lakes was about 150 cm which was smaller than the minimum of calculated oil penetrated depth. Oil compositions of the oil penetrated soil was measured by gas chromatography before extracting oil from samples using diethyl ether as a a solvent. Figure 6 shows examples of oil compositions of each penetrated depth. The X axis shows an intensity measured by gas chromatography per soil weight. The Y axis shows carbon numbers. Surface sand contained more oil than the deeper sand. However, oil composition at each depth was the same. Oil composition did not change during oil penetrated into sand.

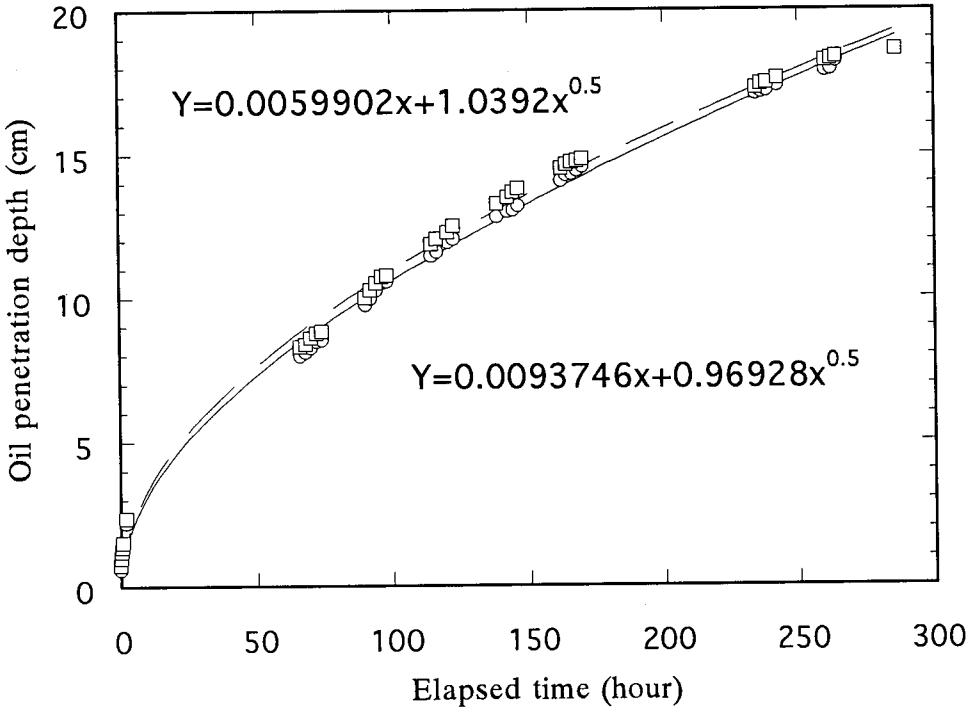

Figure 4 Oil penetration results at the condition of oil head 5 cm (Soil sample derived from the AP-1 pit 60 cm in depth)

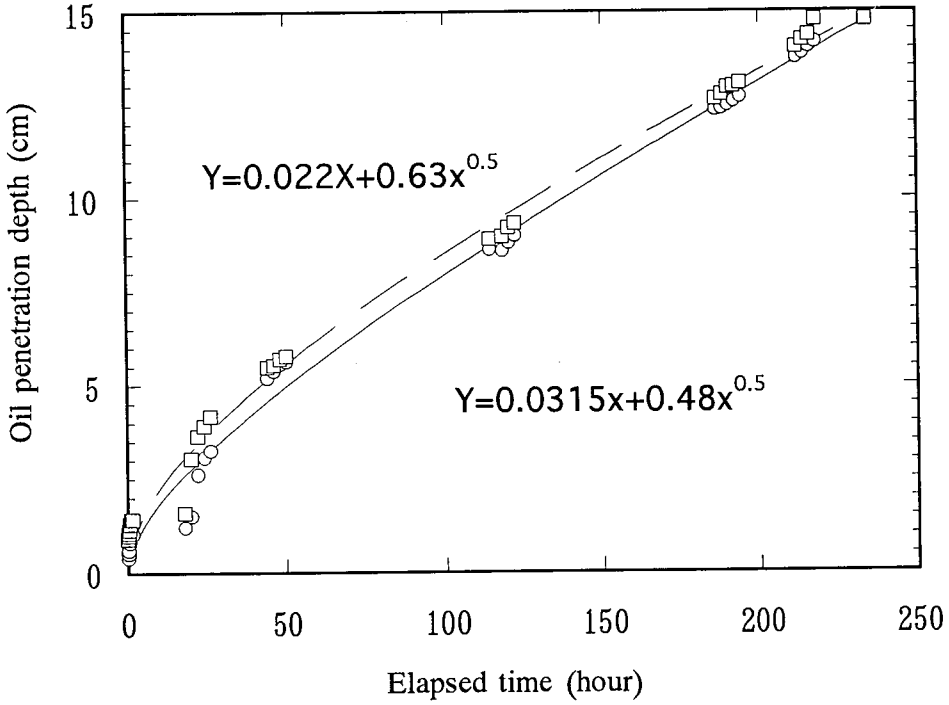

Figure 5 Oil penetration results at the condition of oil head 10 cm (Soil sample derived from the AP-1 pit 10 cm in depth)

4. Discussion and Conclusion

Oil penetration laboratory tests using Kuwait crude oil and the sampled soil were performed in Japan. As a result, penetrated depths were 15 to 20 cm for 10 days

and oil penetrated depths calculated from the experimental results were 200 to 1500 cm for 5 years after the Gulf war ended. Oil penetrated depth within oil lakes in the Burgan area was about 150 cm which was less than the calculated minimum values. The minimum values of calculated penetrated depths for 10 and 100 years were 3 and 10 m and the second aquifer at the Burgan area was 100 m in depth. The second aquifer was not thought to have not been contaminated directly by oil penetration because the calculated minimum depth was larger than the actual depth and the viscosity of oil became smaller with time by reason of volatilization.

In northern Kuwait, rain water penetrated through oil contaminated soil into the first aquifer and the first aquifer was thus contaminated by oil laden rain water. Therefore, in the Burgan area, the second and third aquifer had to be considered to have been contaminated by oil containing rain water which had penetrated through oil contaminated soil and oil lakes.

5. Reference

Al-Sulaimi, J., Viswanathan, M.N. and Szekely, F. (1993) Effects of oil pollution on fresh groundwater in Kuwait. J. Environmental Geology. 22 pp 246-256

Fritz, P. and Fontes, J.Ch. (1980) *Handbook of environmental isotope geo-chemistry*, 2. Elsevier.

Ii, H. (1996) Oil contamination of soil and groundwater in Kuwait and Tracer tests in the Matsumoto Jyoyama tunnel. Soil Phys. Cond. Plant Growth, Japan, 74 (in press)

Kayane, I. (1980) National Geography 3、Hydrology、

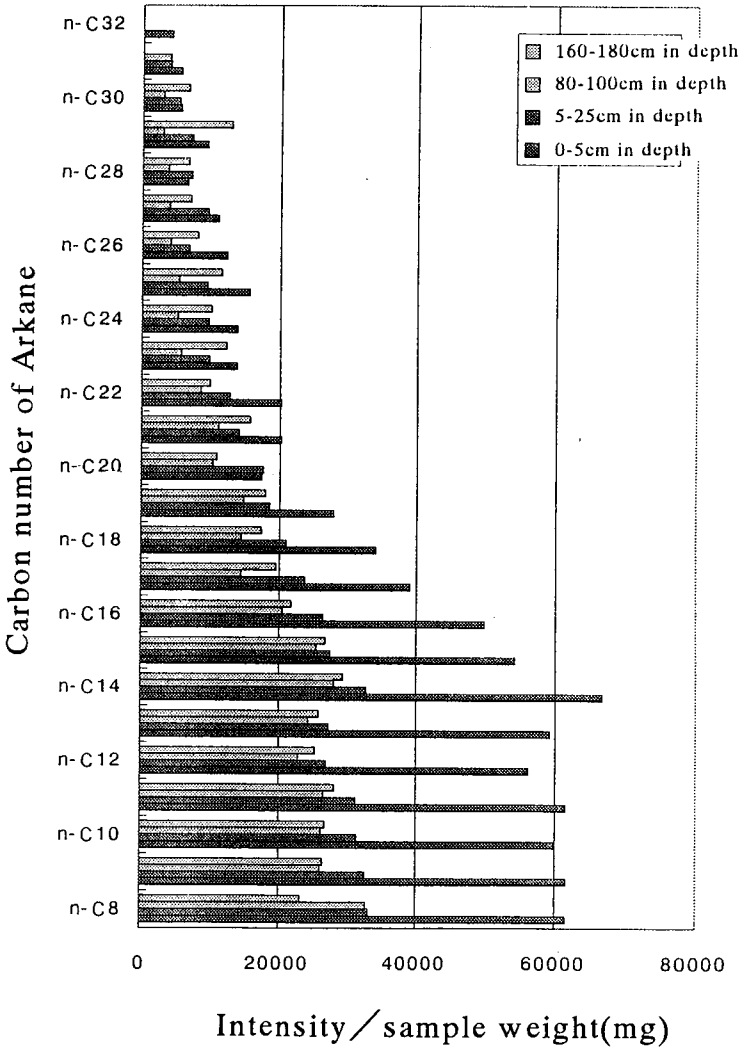

Figure 6 Oil compositions of penetrated soil at each depth
(Soil sample derived from the AP-1 pit 30 cm in depth)

Daimyodo.

Siwek, Z., Hamdan, L. and Amer, A. (1988) An overview of groundwater development in Kuwait. Kuwait Institute for Scientific Research, Kuwait. Report No. KISR 2931.

Seasonal Monitoring of Paddy Cultivation by Landsat TM data in Chiba, Japan

L. Kithsiri Perera(*), Hiroyoshi Ishibashi(*), and Ryutaro Tateishi(**)

(*)**Weathernews Inc.**, D21, 1-3, Nakase, Maihama-ku, Chiba-shi, Japan. *Fax: +81-43-274-3916*

(**)**CEReS**, Chiba University, 1-33, Yayoi-cho, Inage-ku, Chiba shi, Japan. *Fax: +81-43-290-3857*

1. Introduction

According to general terms "Paddy" cultivation is referred as wet rice(un-husked state is known as paddy) cultivation. It ranks second among various crops and cultivated about 145 million ha(1986) globally, following the area of wheat cultivation. In Asia, paddy is the most important crop, and rice is the staple food of almost total Asian population. China and India are the leading producers of rice with total of 56% of world rice production and Japan ranks in the 8th place. Japan recorded a striking production after the world war two, and until resent years its production of 632 kg/10a(in un-husked rice) has been the best yield in the world. Climatologically, all parts of Japanese islands are suitable for cultivation, though the cultivated area has slightly changed since Meiji Era(1868-1912) (Hoshikawa, 1989). In many Japanese farms paddy cultivation can be conducted only once in a year from May to October.

Rice production in Japan bears a huge importance since nearly 100% of the local consumption has to be supplied with local production due to market trends and demands. Japan's very sensitive rice consumers make a big market impact for even a slight change in production. This situation creates inter-prefectural competition for a better yield of rice by the means of quality, quantity, time and other phenological fact.

Therefore; paddy area monitoring, yield forecasting, and natural disaster mitigation are timely important topics not only for Chiba, but also for other parts of Japan. Satellite remote sensing gives a low cost and relatively accurate data source for such studies. This study mainly focus on practical applicability of Landsat TM satellite data with 30m resolution to map the paddy land and possible better ways of data interpretations.

2. Study area and data

Selected study area locates in north eastern Boso peninsula or within Chiba prefecture of Japan(figure 1). Geographically, this is a flat land which is located close to

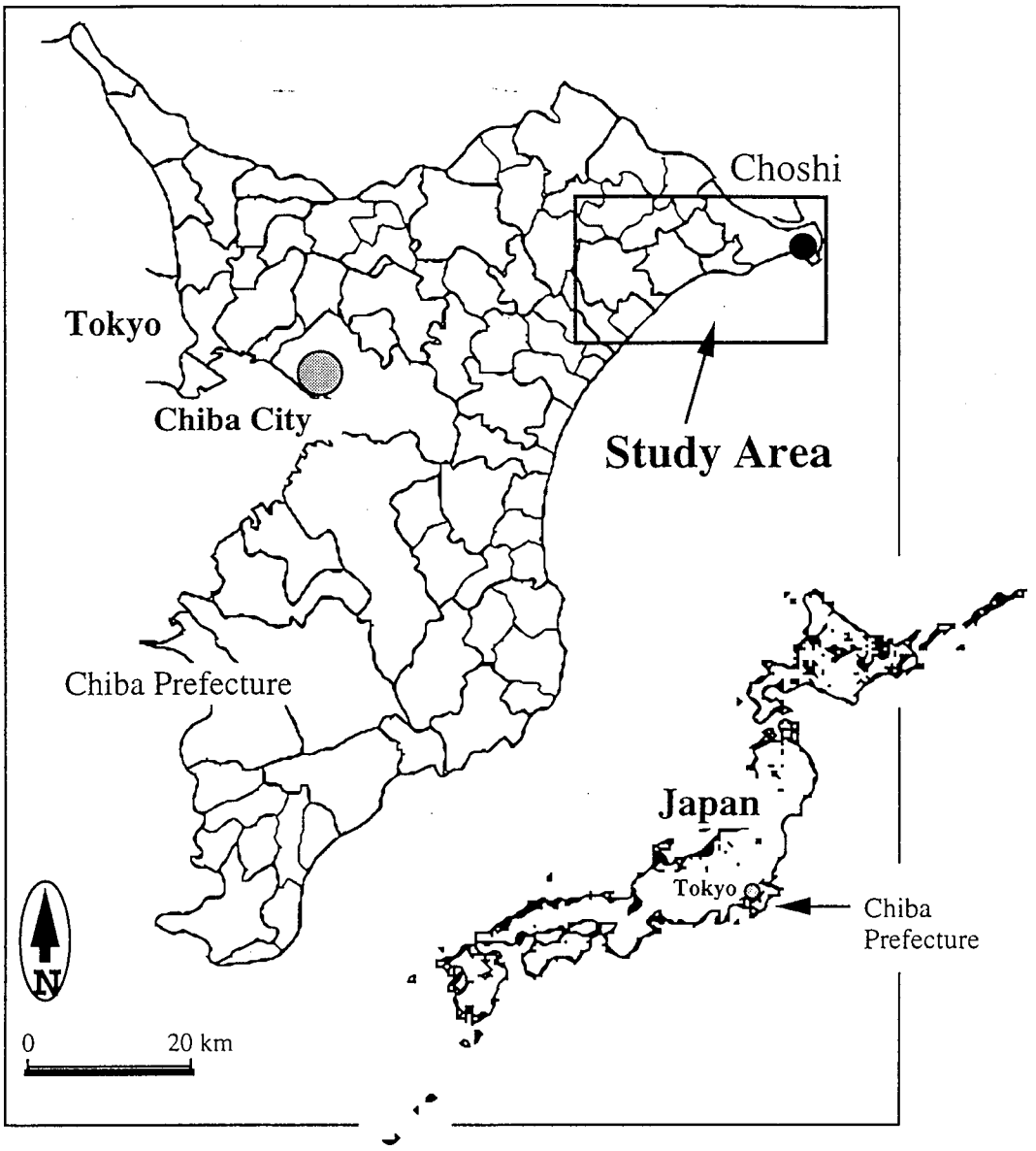

Figure 1. Location of the study area. Chiba city located in the east end of Tokyo metropolitan area.

Date	Cloud cover	Used in present study	Recorded rain fall of Choshi for seven days ending image date in mm.						
			6 days before	5 days before	4 days before	3 days before	2 days before	1 day before	Image date
93.01.29	10	not used			not used				
93.03.18	10	○	-	-	-	19.0	6.0	-	-
93.04.19	0	○	0.5	-	-	-	-	-	-
93.05.21	0	○	-	-	-	-	-	-	-
93.10.28	10	○	0.5	-	-	-	-	-	-
93.11.29	10	○	0.5	-	-	-	-	-	-

Table 1. Collected Landsat TM data and rain fall data respective to each image date.

greater Tokyo urban area. Due to this attractive market potential, paddy cultivation is conducting at very high level in study area. Crop cycle of paddy in Chiba starts with field preparation in May and ends in September-October with the harvest. Over 70% of Chiba paddy lands cultivates the *"Koshihikari"* variety of rice, which is highly popular in Japan.

Application of satellite data for paddy area studies has many advantages associated with the general merits of such data, such as multi-temporal and multi-spectral characters. One significant barrier is lack of cloud free data to cover total growing period with a fair time interval(see table 01). All available TM data of the study area with less than 10% cloud cover in a single year(1993) were collected together with a old crop map and 1:50,000 topographic maps.

3. Data analysis

3.1. Vegetation observation by spectral data

One of the main benefits of earth observation satellites is the periodical monitoring(multi-temporal) capability of vegetation. In the early history of Landsat satellites, multi-spectral data have been used to observe vegetation characteristics under different environmental conditions(Jenson, 1986). In reality, the spectral response patterns from these surface categories as well as others vary due to natural random variations, systematic seasonal causes, atmospheric haze, etc. Light reflectance from plant canopies is an integrated response to various plant structures, soil background, and surface adherents to plants' vegetative and reproductive appendages(American Society of Photog. 1983).

Due to rapid surface changes with respective to different growing stages of rice plant; paddy cultivation receives a special place among other plant community. Such surface changes in crop cycle render advantages and disadvantages regarding satellite data application in studies of this field(Perera *et al.*, 1993). Spectral characteristics in different band data of satellite images make easy to identify vegetation with great details. In the near infrared region of the electromagnetic spectrum, reflectance of green vegetation is considerably high. Dead or senescent vegetation reflects a greater amount of energy throughout the visible spectrum(0.4 - 0.7 *um*). Non-vegetated lands, water or concrete commonly have similar reflectance at visible and near infrared wavelengths(Harris, 1987). Based on such information many vegetation indices have been produced to analyze vegetation types and *Normalized Difference Vegetation Index*(NDVI) is widely used in many studies.

3. 2. NDVI images

Landsat TM data of the study area were geographically rectified with 1:50,000 topographic maps. Then, with Band 3 and 4 of TM data, NDVI images were produced for

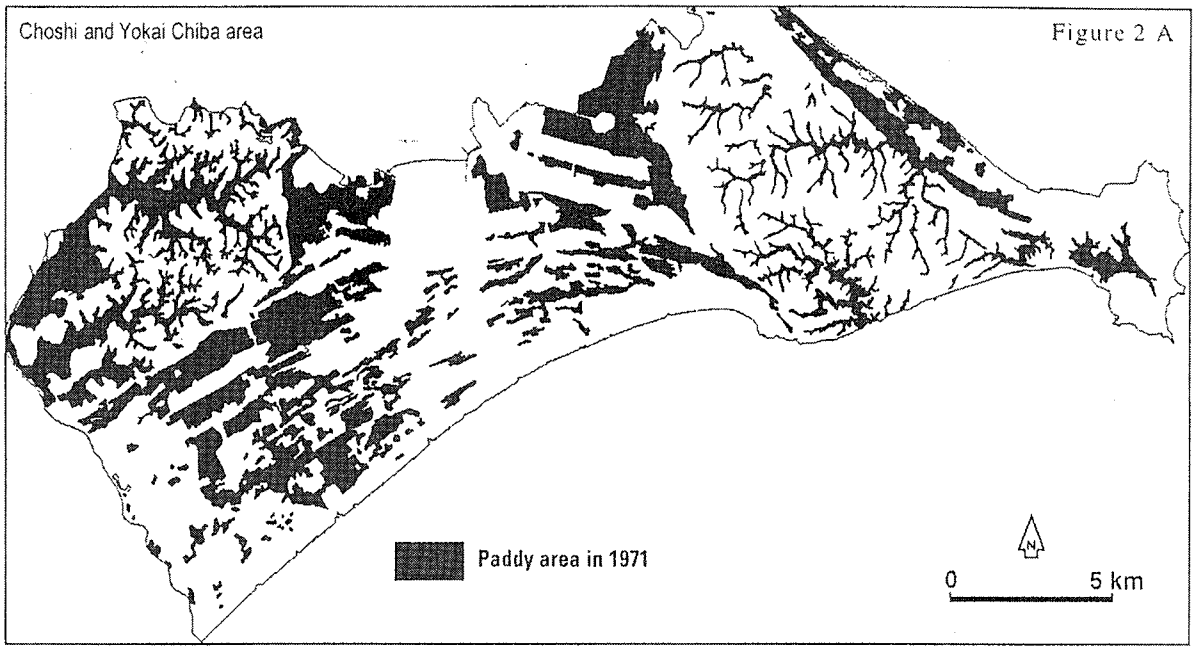
Choshi and Yokai Chiba area
Figure 2 A
Paddy area in 1971
N
0
5 km

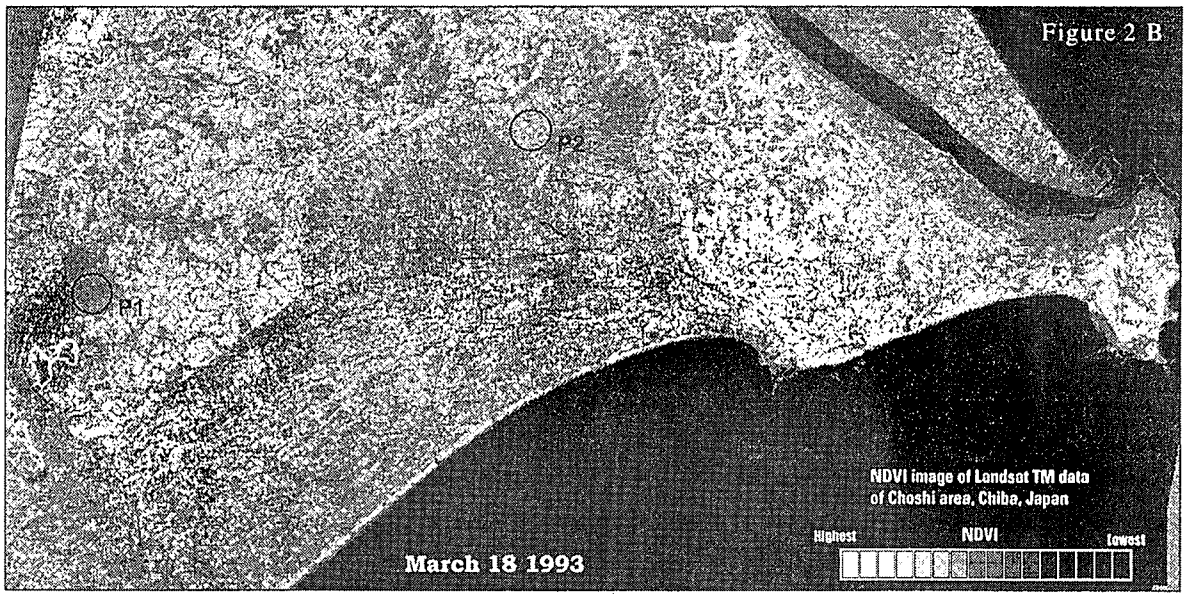
Figure 2 B
P2
P1
NDVI image of Landsat TM data
of Choshi area, Chiba, Japan
Highest
NDVI
Lowest
March 18 1993

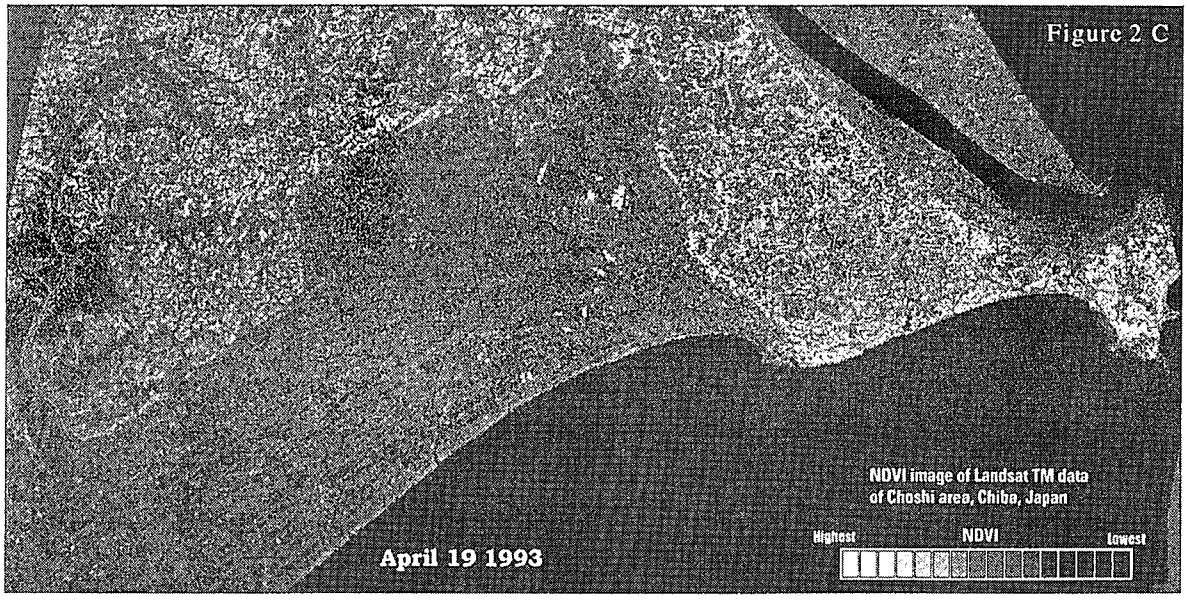
Figure 2 C
NDVI image of Landsat TM data
of Choshi area, Chiba, Japan
Highest
NDVI
Lowest
April 19 1993

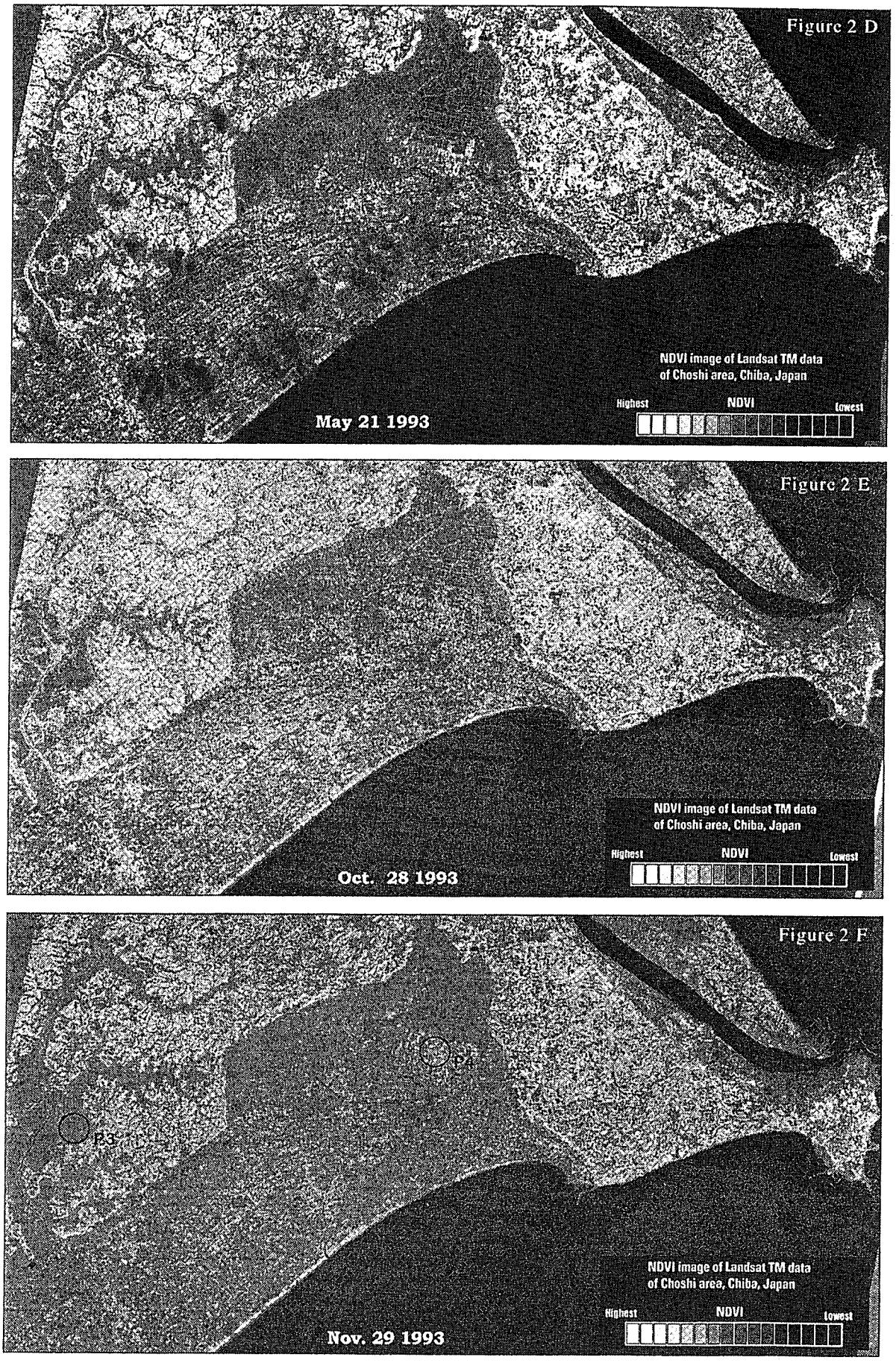

Figure 2 A - F. Paddy area map produced from 1971 crop map and calculated NDVI images(stretched in to few classes).

all images of study area using following equation;

$$NDVI = \frac{TM\ B4 - TM\ B3}{TM\ B4 + TM\ B3}$$

In the resulted NDVI images, values are ranging from -1(desert, water, concrete surfaces, etc.) to +1(optimum green surface). For easy handling purposes, original values of NDVI were converted into 0 - 255, or 8 bit image mode and both of original and 8 bit images were used to analyzed the NDVI characteristics. In figure 2 A - F, resulted NDVI images are presented followed by a manually prepared paddy area map of Choshi area which was created with the best available crop map printed in 1971. This manually prepared paddy area map can be used as ground truth data for identification of paddy in NDVI images. Mid-grown season images of 1993 were not available for the study. All images are relatively away from the influence of wet soil caused by rain fall, which may gives misleading information for paddy area identification(see rain fall data in table No. 1). NDVI images are showing possible paddy areas with different qualities. Compare with the old map, there are two or more different NDVI classes in paddy area of many images.
e.g.;

1. P1(NDVI is -0.01) and P2(NDVI is 0.2) in March image(figure 2 B) and
2. P3(NDVI is 0.03) and P4(NDVI is 0.30) in Nov. image(figure 2 F).

This situation was analyzed in-detail using a sample plot from March, May, and October NDVI images. The sample plot is located within a pre-identified paddy land(also see figure 2 A) and is shown in figure 3 A with a location map and some statistics. A great homogeneity condition was directed in May image, the time that field is filled with water. It has the lowest standard deviation value and low NDVI values representing water. In histograms of these selected three sample plots also show the homogeneity character of May image as presented in figure 3 B. March sample represents rather disturbed texture and October plot shows much green due to fresh open land with grass after harvesting. In these images, similar NDVI values can be found with other vegetation types too.

The significant point with May sample is the areas those are preparing for paddy cultivation is covered with water which makes identification more easy. But, there are bright line features on water in May image which show foot paths or small roads that will lead to make separate classes within paddy lands in a digital analysis. Also surface water area may hidden in paddy lands, due to quite similar NDVI values. Both of these problems can avoid by using visual interpretation and GIS(Geographical Information Systems) technology. The main attention of the present study was given to analyze NDVI values of

Location of the sample area

March

Min. NDVI = -0.1154
Max. NDVI = 0.3832

Mean = 0.0922
St. deviation = 0.0770

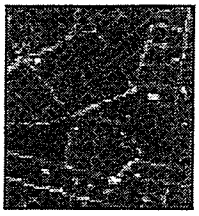

May

Min. NDVI = -0.2055
Max. NDVI = 0.3374

Mean = -0.0144
St. deviation = 0.0578

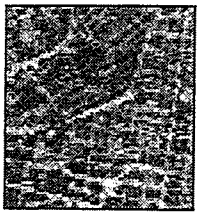

October

Min. NDVI = -0.1364
Max. NDVI = 0.4167

Mean = 0.1447
St. deviation = 0.0639

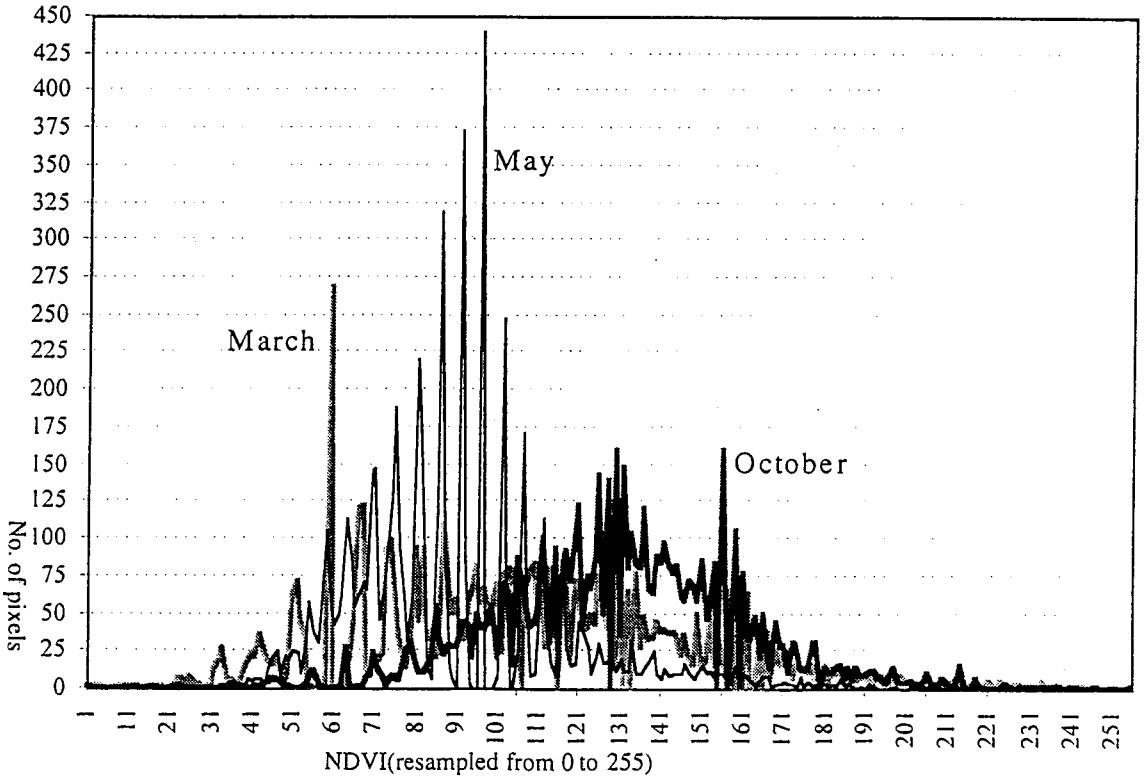

Figure 3 A(Upper). Comparison between NDVI image samples of selected paddy plots.
Figure 3 B(Lower). Histograms of selected paddy plots.

multi-temporal images. This is the first half of a detail study on Chiba paddy lands and resulted paddy area map is not included here. Furthermore, it is very important to carry out field investigations for the verification of final paddy area map.

4. Concluding remarks

There is a high demand for monitor and map paddy areas in Japan to obtain up to-date facts about the crop. Such information can be used for yield forecasting, damage assessments, and other planing purposes. Satellite data associated with GIS technology will give a valuable approach for these kind of studies. As presented in this study, NDVI calculations of multi-temporal satellite images were analyzed to identify the paddy area for mapping purpose.

Although it is needed to analyze mid-growing time images, "fallow" period of paddy field image or May season image gives best information. For the production of map of paddy area, visual interpretation methods can be utilized to avoid discrimination difficulties of paddy land through digital classification methods. This study only deal with experimental level research objects, and more field checks also need for the completion of usable level results.

Acknowledgments

Authors are grateful to Remote Sensing Technology Center(RESTEC), Japan, for providing Landsat TM satellite data and Dr. T. Anzai and Mr. A. Yamaki of Chiba prefectural agriculture experiment station, Chiba, Japan, for valuable data and field information.

References

Harris, R. 1987, *Satellite Remote Sensing*, Routledge & Kegan Paul Inc., USA.

Hoshikawa, K.(1989): *The Growing rice plant; An anatomical monograph*, Nbunkyo, Tokyo, Japan.

Jensen, R. J. 1986, *Introductory Digital Image Processing, A remote Sensing Perspective,* Prentice-Hall, USA.

American Society of Photo. (1983), *Manual of Remote Sensing.,* The Sheridan Press, USA.

Perera, L. K., Kajiwara, K., Tateishi, R.(1993): *Application of Landsat MSS data for paddy area estimation in Sri Lanka.* Annual symposium of Japan Society of Pho. & RS, 1993, Tokyo, Japan, pp. 159-64.